Ecole doctorale : Sciences de la Matière, du Rayonnement et de l'Environnement

THESE

Pour obtenir le grade de **Docteur de l'Université de Lille**

Spécialité : Science des Matériaux

Soutenue le 11/12/2020

Shanshan XU

Intitulée

Influence of macromolecular orientation on mechanical behavior of glassy polymers

(Influence de l'orientation macromoléculaire sur le comportement mécanique de polymères vitreux)

Composition de Jury

Pr. Noëlle BILLON	Professeur- CEMEF-MINES ParisTech	Rapporteure
DR. Didier LONG	Directeur de recherche- LMPA-CNRS/Solvay	Rapporteur
Pr. Cyrille SOLLOGOUB	Professeur- PIMM - CNAM	Examinateur
Dr. Anne RUBIN	Maître de conférences- Institut Charles Sadron- Université de Strasbourg	Examinatrice
DR. Jean-Marc LEFEBVRE	Directeur de recherche émérite- UMET- Université de Lille	Examinateur, **Président**
Dr. Grégory STOCLET	Maître de conférences- UMET-Université de Lille	Co-encadrant
Pr. Valérie GAUCHER	Professeur- UMET-Université de Lille	Directrice

Acknowledgement

Three years of PhD have passed like a wind and I have encountered so many people that I would very much like to say thank you. The work cannot be only credited to one person.

First I would like to thank my two supervisors: Valérie and Greg, for giving me this precious entrance ticket into the world of research. For me they are the first-class guides for beginners: good temper, always patient, full of inspirations and never said no to my questions or requests for help. Every meeting we had together was efficient and productive. I've learnt incredibly much from these two, not only research skills but also the spirit of exploration and never cease learning new things. They showed me every quality to be a good researcher& educator: patience, encouragement, communication…which I'll always keep in mind for my future career.

Year 2020 is to remember. It is and will be, I think, the closest thing I experience to a war. And I cannot survive this complicated period all by myself. I thank Valérie and Greg for their encouragements and checking-ups, especially Valérie who tried her best to stay contact with me every day just to let me feel being cared for. After all, being stuck with her thesis every day in a small apartment is not so idyllic thing as one can imagine….

As for daily research work I should thank Adeline, Isabelle and Jean-François who have taught me so many skills and techniques that would be surely useful in future work. Also, my dear colleagues of laboratory, I thank their company for these three years and those moments of sharing ideas and pieces of life, always full of laughter and passion.

Eight years living in France is brilliant. I have met so many dear friends, some of which I have spent a short time with, some I shall keep as life-long relationships. In either way, I thank them for giving me such the good memories in a foreign country and will look forward to the next encounter.

Last but not least, I thank my parents, my family and friends in China who have supported me no less than friends in France for always being there, even so far away. There is not a single second that I doubt their unconditional love and support, which I will always be grateful for the rest of my life.

Résumé

Cette thèse porte sur l'étude de l'influence de l'orientation macromoléculaire sur le comportement mécanique de polymères amorphes vitreux. Ces travaux ont principalement été menés sur deux grades de Polylactide (PLA), un non cristallisable et un autre capable de cristalliser sous étirage, afin de séparer l'effet de l'orientation macromoléculaire de celui de la cristallisation induite sous étirage sur le comportement mécanique final obtenu.

Les deux types de PLAs étudiés présentent à l'état isotrope un comportement fragile en traction uniaxiale à température ambiante. En revanche, un comportement ductile avec des taux de déformation pouvant dépasser les 100% est observé sur des échantillons ayant subi une pré-déformation à l'état caoutchoutique que ce soit en mono- ou bi-étirage. Afin de mieux comprendre l'origine de cette transition Fragile-Ductile (F-D), une caractérisation structurale approfondie des films pré-orientés a été entreprise. Celle-ci a permis de montrer que ce n'est pas la présence d'une phase cristalline mais plutôt l'orientation de la phase amorphe qui est le paramètre clé gouvernant cette transition F-D. En l'occurrence, ce travail a permis de révéler qu'il existe un taux d'orientation moléculaire critique de la phase amorphe f_c au-delà duquel le comportement du PLA est ductile. Cette valeur critique f_c est similaire quel que soit le grade de PLA.

Les analyses in situ par diffusion des rayons X réalisées lors de l'étirage d'échantillons pré-orientés ou non, combinées à des observations morphologiques, ont montré que la transition F-D correspond à un changement de mécanismes élémentaires de plasticité : le craquelage, prédominant dans le cas des échantillons fragiles, laisse progressivement place au développement de bandes de cisaillement.

Des analyses post-mortem complémentaires par diffusion des rayons X ont par ailleurs mis en évidence que l'orientation macromoléculaire n'a pas d'influence sur la géométrie des craquelures mais induit une diminution de la densité de craquelures formées lors de l'étirage. À partir de ces analyses, la contrainte critique de nucléation des craquelures en fonction du degré d'orientation a pu être déterminée. Il a ainsi été montré que le changement de mécanismes de déformation est dû à l'augmentation de la contrainte d'amorçage des craquelures σ_{cr} avec l'orientation macromoléculaire. Cette contrainte σ_{cr} devient, pour des taux d'orientation supérieurs à f_c, plus élevée que la contrainte de formation de bandes de cisaillement qui, quant à elle, est peu dépendante de l'orientation. Par analyse théorique, l'évolution de σ_{cr} avec l'orientation a été attribuée en partie à l'augmentation de la distance entre enchevêtrements.

Des résultats similaires ont été obtenus pour deux autres polymères amorphes vitreux, le polystyrène et le poly (éthylène 2,5-furandicarboxylate). La seule différence mise en évidence entre les 3 matériaux étudiés étant le degré d'orientation critique à atteindre pour observer la transition F-D.

Ainsi ces travaux de thèse ont permis d'expliquer la transition fragile ductile induite par orientation dans le cas des polymères amorphes déformés à l'état vitreux. De plus, ils suggèrent le caractère universel de cette transition induite par l'orientation macromoléculaire

Abstract

This PhD thesis focuses on the study of the influence of macromolecular orientation on the mechanical behavior of glassy amorphous polymers. This work was mainly carried out on two grades of Polylactide (PLA), one non-crystallizable and another one able to crystallize under stretching, in order to separate the effect of the macromolecular orientation from that of the crystallization induced by stretching on the resulting mechanical behavior.

The two grades of PLAs exhibit, in their isotropic state, a brittle behavior upon uniaxial stretching at room temperature. By contrast, a ductile behavior with elongation at breaks above 100% is observed on samples which have undergone a pre-deformation in the rubbery state, whether upon uniaxial or bi-axial stretching. In order to better understand the origin of this Brittle-to-Ductile (B-D) transition, an in-depth structural characterization of the pre-oriented films was carried out. Results clearly show that it is not the presence of a crystalline phase but rather the orientation of the amorphous phase that is the key parameter which governs this B-D transition. More precisely, this work revealed the existence of a critical molecular orientation degree of the amorphous phase f_c above which the behavior of PLA becomes ductile. This critical value for f_c is similar regardless the grade of PLA investigated.

The in-situ analyses carried out by Small Angle X-ray Scattering (SAXS) during the stretching of pre- or non-oriented samples, combined with morphological observations, showed that the B-D transition corresponds to a change of the elementary plastic deformation mechanisms involved: crazing, predominant in the case of brittle samples, gradually turns to the development of shear banding.

Additional post-mortem SAXS analyses also showed that the macromolecular orientation has no influence on the geometry of the crazes but induces a decrease in the crazes density involved during stretching. From these analyses, the critical stress of crazes nucleation as a function of the orientation degree has been determined. It has thus been highlighted that the change of mechanisms is explained by the increase of the craze initiation stress σ_{cr} with the macromolecular orientation, which becomes higher than the stress of formation of shear bands when chain orientation is higher than f_c. The increase of σ_{cr} with the increase of orientation has been analyzed from a theoretical point of view. From this analysis it could be assumed that the increase of the end-to-end distance between entanglements is one of the elements which contribute to the increase of σ_{cr} with orientation.

Similar results were obtained for two other glassy amorphous polymers, i.e. polystyrene and poly (ethylene 2,5-furandicarboxylate) suggesting the common behavior for amorphous polymers regarding the effect of orientation on occurrence of B-D transition. The only difference highlighted among the three studied materials is the critical orientation degree value required to observe the B-D transition.

In summary, this PhD work allows to explain the origin of the brittle-to-ductile transition induced by orientation in the case of amorphous polymers deformed in their glassy state.

Table of Contents

Symbols & Abbreviations

σ_{cr}	Craze initiation stress
σ_y	Yield stress
σ	Stress
d	End-to-end distance between entanglements
ε_e	Elastic deformation
$\dot{\varepsilon}$	Initial strain rate
λ	Draw ratio
χ_c	Crystallinity
χ_{meso}	Mesophase content
2θ	Bragg's angle
Γ	Surface energy
γ	Surface free energy
ϑ_e	Entanglement density
ρ	Density
B-D	Brittle-to-Ductile
BO	Bioriented
C-PLA	Crystallizable PLA
D_o	Fibril diameter
DSC	Differential Scanning analysis
DMA	Dynamic Mechanical Analysis
E	Young's modulus
E'	Storage modulus
E''	Loss modulus
f_{ij}	Orientation function
FTIR	Fourier Transform Infra Red

G	Shear modulus
L_o	Interfibrilar distance
MD	Machine Direction
M_e	Molecular weight between entanglements
M_n	Number-average molecular weight
M_w	Weight-average molecular weight
NC-PLA	Non Crystallizable PLA
ND	Normal Direction
PC	Polycarbonate
PEF	Poly (ethylene 2.5-furandicarboxylate)
PEN	Polyethylene naphthalate
PET	Polyethylene terephthalate
PLA	Polylactide
PMMA	Polymethylmethacrylate
PS	Polystyrene
q	Scattering vector
SAXS	Small Angle X-ray Scattering
TEM	Transmission Electron Microscopy
TD	Transversal direction
T_d	Drawing temperature
T_c	Crystallization temperature
T_{cc}	Cold crystallization temperature
T_g	Glass transition temperature
T_m	Melting temperature
WAXS	Wide Angle X-ray Scattering
UO	Unioriented

General introduction

For the past century, the global population has been expanding continuously which is not without consequences on the world's natural resources. As can be seen in *Figure 1*, the primary forms of energy that we relied on the most, the fossil fuels (oil, gas and coal), will start a long decline from year 2025 and probably run out in merely a few decades.
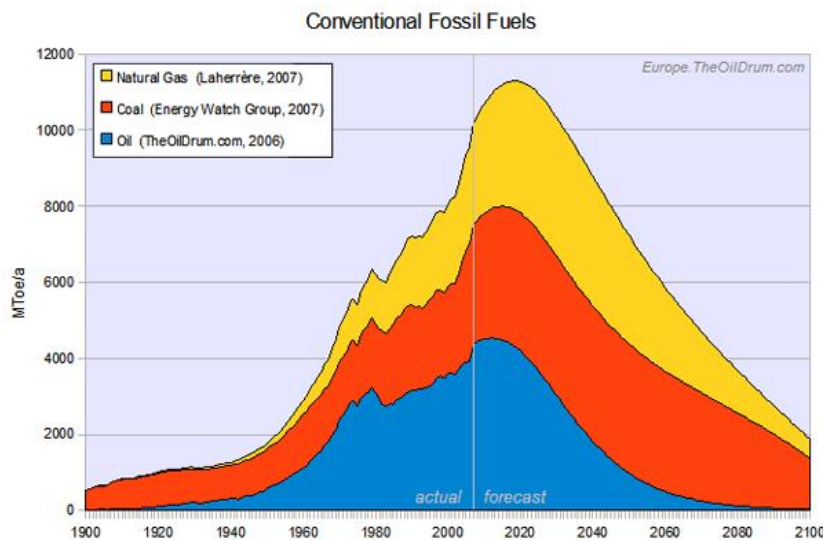
Figure 1. Forecast of conventional fossil fuels per capita according to the studies posted by the oil drum: Europe (http://theoildrum.com/node/3565).

The overwhelming exploitation of these resources have brought along a great number of environmental concerns such as global warming, air pollution, plastic waste in landfills and water bodies…. These escalating problems have driven a thriving awareness of improving sustainability both in energy and material sectors to limit the use of available carbon resources. In the latter case, especially regarding the polymer industry, polymers issued from the biomass represent currently a rapidly growing market aiming at substituting petrochemically-sourced polymers. In addition to their environmental friendliness, biopolymers can also be competitive with both technical and economic interests that bring about new hopes facing the increasing scarcity of fossil resources.

Among all biopolymers that are actually commercialized in industry, Polylactide (PLA), a purely biodegradable and bio-based aliphatic polyester derived from renewable sources such as corn and sugar, has become one of the most promising candidates to replace fossil-based polymers thanks to its excellent combination of properties. Nova-institute has reported a rapid annual growth of

production of PLA for the past decade and estimated that by 2020, the total production capacity should reach around 800,000 t/year (*Figure 2*).

Figure 2. Evolution of worldwide production of PLA in the period of 2011-2020 (Nova-institute: https://www.bioplasticsmagazine.com/en/news/meldungen/PLA_Growth.php).

PLA exhibits comparable optical, mechanical, thermal, and barrier properties when compared with some commercially available commodity polymers such as polypropylene (PP), poly(ethylene terephthalate) (PET), and polystyrene (PS). Beginning with applications focused on packaging industry, PLA is now enlarging its commercialization fields by entering in new domains such as biomedical, electronics, smart textiles…etc.

Since a couple of years, a new bio-based polymer is emerging and is foreseen as another serious candidate for the substitution of PET: the poly (ethylene 2,5-furandicarboxylate) (PEF) which presents outstanding barrier properties. Many companies have paid much research efforts regarding the synthesis of PEF during the past years and an industrial scale production could be expected in the coming years.

Regarding the packaging application field, one of the most commonly applied processes for the elaboration of PLA-based films or bottles is biaxial stretching. This method has been identified to effectively improve mechanical properties of glassy polymers such as polystyrene (PS). Recently, it has been shown that biaxial stretching of PLA allows to greatly improve its stretchability, which is of prime interest in the packaging field. However, the origin of this improvement of mechanical

2

performance induced by macromolecular orientation has not yet been fully understood in literature. Indeed, even if reported decades ago for PS, to the best of our knowledge, former work have mostly focused on description of phenomenon rather than in-depth investigation of the origin.

In such context, this thesis aims at a better understanding of the influence of molecular orientation on the mechanical properties of PLA through a multi-scale investigation of structure-property relationship especially in case of a biaxial sollicitation. In addition, two other glassy amorphous polymers, i.e. PEF and PS, will be studied in the same manner of PLA in order to try to find a generalized explanation to this unique transition behavior.

The Chapter I of the manuscript is a literature review summarizing the important findings and discussions concerning the mechanical properties and deformation mechanisms of amorphous polymers. The materials of this PhD work and the associated research activities are exposed in details along with the description of the main objectives and the methodology used to carry out this research work.

Next, the Chapter II describes the materials used in this study and their elaboration processes. This is followed by a detailed presentation of the techniques and methodologies used in this work.

The three following chapters report the main results of this PhD work. The Chapter III mainly focuses on the study of structure-mechanical property relationships of PLA through a comparison between two grades: one non-crystallizable and one crystallizable in order to separate the influence of molecular orientation from the effect of the induced ordered phase on the properties of stretched films. First, thermal and mechanical behaviors of the initial films are investigated, then oriented films obtained under various stretching conditions will be characterized in terms of thermal, mechanical and structural properties. Finally, the influence of physical aging on mechanical behavior of stretched film will also be evaluated.

To characterize the plastic deformation mechanisms involved during stretching of isotropic and oriented PLA, investigations concerning the influence of molecular orientation on the initiation of elementary deformation mechanisms were carried out in order to determine the origin of transition of macroscopic mechanical behavior discussed in the previous chapter. These results are shown in Chapter IV.

The final chapter, the <u>Chapter V</u>, illustrates studies on two complementary materials, poly(ethylene 2,5-furandicarboxylate) and polystyrene using the same approaches as applied in former chapters in the spirit of confirming the important conclusions drawn from structure-property study on PLA. Discussions based on theoretical reflections will also be developed in order to bring some final answers to the main problematic of study.

Finally, a general conclusion will be found at the end of manuscript summarizing the important findings and conclusions of all chapters. The perspectives of this research will also be presented.

Chapter I
State of art: a literature review

This chapter presents a literature review summarizing the important findings and discussions concerning the mechanical properties and deformation mechanisms of amorphous polymers. First of all the macroscopic mechanical behavior is described both in glassy and rubbery states, followed then by a review of general characteristics of the elementary plastic deformation mechanisms involved during the sollicitation process. Then potential factors that influence the competition between these elementary deformation mechanisms will be discussed, especially regarding the effect of macromolecular orientation on the ultimate properties of glassy polymers. Finally the polymers studied in this PhD work and the relative research activities are exposed in details, along with the description of the main objectives and the methodology of this research work.

I.1. Mechanical behavior of amorphous polymers

Thermoplastic polymers are large molecules or macromolecules consisting of repetitive monomer units. In their equilibrate configuration in the bulk, these chains are arranged in form of entangled statistic coils. Among thermoplastics, two main polymer families have been extensively studied. On the one hand amorphous polymers, for which material chains are randomly coiled without regular arrangement. These polymers are characterized by a glass transition temperature (T_g) which is the critical transition point from glassy state to rubbery state. The other family is semicrystalline polymers. For these materials, in addition to amorphous regions, lamellar crystalline regions are also formed due to regular arrangement of the macromolecules. These materials present, besides T_g, two other characteristic temperatures related to the crystalline phase: the crystallization temperature(s) and the melting temperature(s). Note that under appropriate cooling conditions, it is possible for most of these polymer, to avoid crystallization. Consequently these crystallizable materials can also be found in a fully amorphous state.

With this thesis mostly focused on amorphous materials, only the state of art concerning the mechanical behavior of amorphous polymers both in glassy and rubbery states will be presented.

I.1.1. Deformation behavior below glass transition temperature

Studying and understanding the mechanical behavior of a polymer is of prime interest and this topic has been the subject of numerous studies.

Focusing on initially amorphous polymers, the understanding of mechanical behavior below and above their T_g is fundamental to optimize their end-use performances. Indeed these materials are generally used in their glassy state but elaborated and transformed in their rubbery state. Consequently the mechanical behavior of these polymers stretched in this two regions will be detailed in the next sections.

I.1.1.1.   Stress-strain curve upon uniaxial stretching

Uniaxial stretching test is a widely applied characterization method to study the mechanical behavior of polymers. An example of typical engineering stress- strain curve encountered for a ductile polymer is presented in *Figure I. 1* and the different characteristic stages observed during the deformation are discussed.

Engineering stress (MPa)

(1) (2) **(3)**   **(4)**

σ_y

Engineering strain (%)
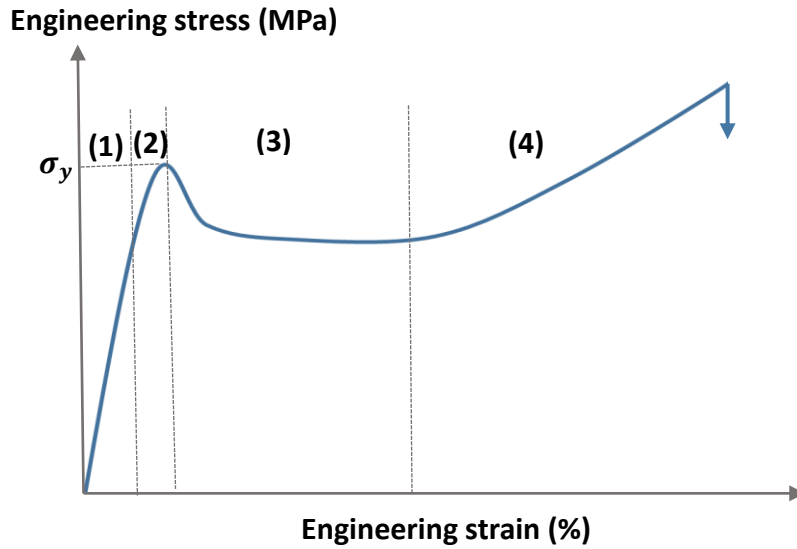
Figure I. 1. Engineering stress-strain curve of a ductile polymer.

Four regions are identified from this figure corresponding to different steps of deformation:

(1) The elastic deformation region. At low strains, the deformation is reversible (elastic deformation) and the recovery is instantaneous. The elastic deformation ε_e is linearly related to the stress σ by Hooke's law:

$$\sigma = E. \varepsilon_e \tag{I.1}$$

With E the slope of the elastic region, commonly known as Young's modulus or elastic modulus. For amorphous polymers the value of E is in an order of several GPa.

(2) The nonlinear viscoelastic deformation region. This region concerns the end of linear domain due to the viscous character of polymers. At this stage the deformation is still reversible but the recovery to the initial state depends on time due to the viscoelastic behavior of polymers.

(3) <u>The plastic deformation region.</u> In this region, which starts from the yield point, σ_y, the deformation is irreversible. From this critical point, a stress drop can be observed related to a geometric change caused by the emergence of necking, as shown in *Figure I.* 2. Indeed, if one studies the true stress-train curve, this stress drop observed in engineering stress-strain figure may no longer be present and the true stress would increase continuously with strain even during necking. Although for some polymers, for instance the polycarbonate, a stress decrease will still be detected upon true stress-strain plot. This phenomenon is called stress (strain) softening (G'Sell et al., 1992).
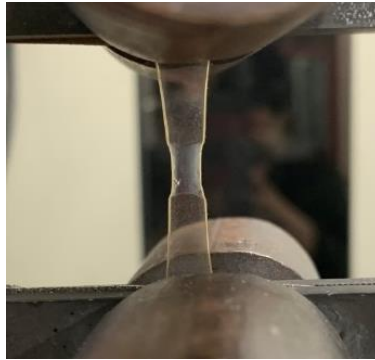
Figure I. 2. A photograph taken during the propagation of necking upon stretching of a ductile sample.

Unlike the behavior observed in region (1)&(2) where the deformation is homogenous, necking is associated with a local stress concentration that makes the strain field non-uniform within the sample causing a non-homogenous deformation behavior. If failure does not happen in the necked region, necking can propagate in a stable mode throughout the useful length of specimen. This domain is called the plastic flow regime and is characterized by a constant plateau of stress level (Halary et al., 2011).

(4) <u>The strain-hardening region</u>. From a molecular architecture point of view, in the plastic deformation region (domains 3 & 4), the polymer chains begin to orient and unfold gradually along stretching axis direction. This chain orientation, originating from the network extension at large strains, often involves a distinct reinforcement of stress level with the increasing of strain. Such strain-hardening regime has been widely observed and studied for glassy polymers possessing generally large molecular weights such as polystyrene (PS), polymethylmethacrylate (PMMA) and polycarbonate (PC) (Hasan & Boyce, 1993; Haward,

1993; Van Melick et al., 2003; Wendlandt et al., 2005; Senden et al., 2012). Note that depending on sollicitation conditions a mesomorphic could be induced during stretching of some crystallizable polymers, as will be discussed later in details.

Finally, the rupture of sample occurs at the ultimate extension level of the macromolecules.

I.1.1.2. Deformation behavior of glassy polymers

The behavior illustrated in *Figure I. 1* is of ductile nature, for which large plastic deformation is observed prior to failure. In opposition, for some polymers, breaking occurs fast, before the yield point. In other words, the material is not able to deform plastically. Such behavior is characteristic of brittle materials.

Regarding glassy amorphous polymers, polystyrene (PS) or poly(methyl methacrylate) (PMMA) are known to be brittle under certain loading conditions whereas polycarbonate (PC) is generally considered as a ductile material with a stable necking formed shortly after the yield point.

The characterization and understanding of these two opposite behaviors has been extensively studied since the 1960s. Besides, these studies have demonstrated that the mechanical behavior observed, i.e. brittle or ductile, largely depends on the sollicitation parameters (stretching/ compression, temperature, strain rate…). As an example, *Figure I. 3* shows a comparison of the mechanical behavior of the previously mentioned glassy polymers sollicited under tension and compression modes (Van Melick et al., 2003).
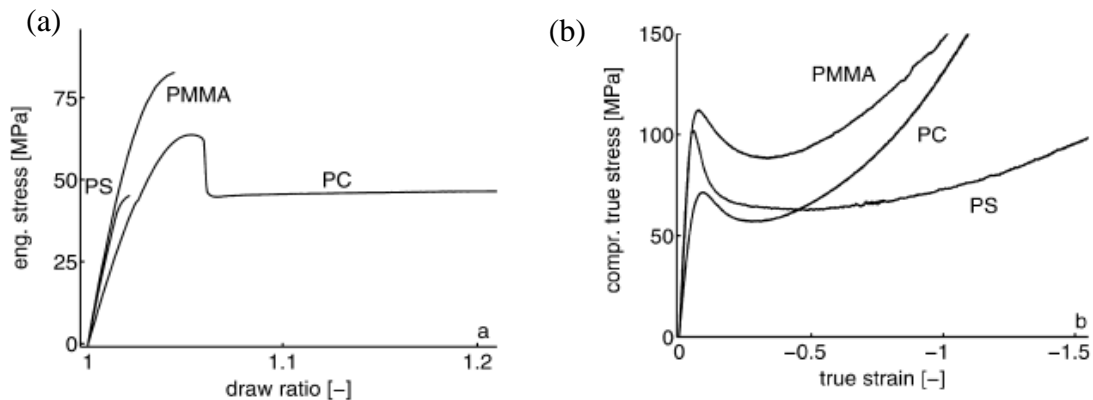
Figure I. 3. Deformation behavior of PS, PMMA, PC upon (a) tension and (b) compression at room temperature   (Van Melick et al., 2003).

It is observed that while PS and PMMA are rather brittle in tension mode, they could exhibit a ductile behavior upon compression (Cavrot, J.P., Haussy, J., Lefebvre, J.M., Escaig, 1978). On the other hand, PC depicts a ductile behavior in both tension and compression.

This clearly demonstrates that the brittle/ ductile behavior of materials relies on the sollicitation conditions (as extrinsic factors). However, former works have also highlighted that intrinsic aspects linked to polymer structure also have to be taken into account as influencing factors (molecular weight, crystallinity, morphology, entanglements…). It is consequently the combinations of these intrinsic and extrinsic parameters that will define the final ultimate behavior of material, which is in fact the result of different plastic deformation mechanisms involved.

I.1.2. Deformation above glass transition temperature

In this section the deformation behavior of polymers uni- or biaxially drawn above T_g will be shown. *Figure I. 4* illustrates a typical stress-strain curve obtained by drawing a polymer in its rubbery state.
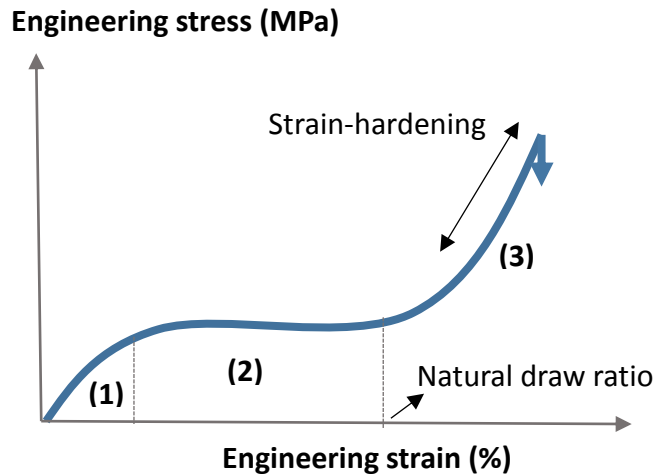
Figure I. 4. Engineering stress-strain curve for an amorphous polymer at temperatures above T_g(Ward, 2012).

When processing amorphous polymers above their glass transition temperature, the chain network is close to that of a rubber and the interpretations of the elongation behavior using the rubbery elastic theory are quite successful in literature (Cansfield et al., 1993; Gordon et al., 1994; Kahar et al., 1978; Perena et al., 1980a; Rietsch et al., 1979). This rubbery-like behavior displays three main regions:

11

(1) <u>The quasi-linear region.</u> In this region the stress increases almost linearly with stretch ratio, which presents an "elastic" drawing behavior. The value of modulus depends on sollicitation rate/ temperature.

(2) <u>The constant plateau region.</u> The increase of stress reaches a certain point and then shifts to a viscous flow where the stress stays at nearly a constant level. Unlike the drawing behavior below T_g where a yield point is systematically detected, for deformation above T_g yield could only be observed under lower temperatures/high strain rates. In addition, if high drawing temperature is applied, relaxation or even disentanglement should be considered as competing processes to chain orientation.

(3) <u>Strain-hardening region.</u> At large deformation levels a strain-hardening stage is sometimes observed where stress rises at a steady rate with draw ratio. According to (Bonnebat et al., 1981) the extension ratio at the onset of strain-hardening is called the natural draw ratio. The value of the natural draw ratio depends upon stretching parameters such as temperature and strain rate. The origin of such phenomenon is closely linked to high level of chain orientation and sometimes to an induced process: the strain-induced crystallization. Both aspects will be presented in details later.

In order to go further regarding the mechanical behavior of polymers stretched above T_g, two typical well-studied materials will be discussed: polystyrene and polyethylene terephthalate (PET).

I.1.2.1.   <u>Polystyrene: competition between orientation and relaxation</u>

Atactic polystyrene remains amorphous during stretching, making this material a good example to understand the evolution of the molecular network upon stretching. A number of former studies carried out on PS have reported the effect of extrinsic parameters (stretching temperature, strain rate) as well as intrinsic aspects (molecular weight) on the chains orientation induced by stretching or other forming methods (De Francesco & Duckett, 2004; Faivre et al., 1985; Lefebvre et al., 1983, 1984; Shimomura et al., 1982; Tassin & Monnerie, 1988). As shown in these studies, low temperature & high strain rate is the most favorable combination to enhance the orientation kinetics upon stretching. In addition, uniaxial elongation strongly aligns the chain segments along the stretching axis, while in the case of biaxial stretching, chains rather depicts an in-plane orientation.

The degree of orientation achieved during drawing is directly dependent to the chain relaxation kinetics that takes place at the same time. Strongly related to the imposed experimental temperature, chain relaxation can be divided into three steps for an amorphous polymeric material (Doi & Edwards, 1986): rouse-like motions of segments between entanglement points, retraction of chain length towards its non-stretched state and finally the total chain disengagement via reptation. The characteristic times of these three relaxation steps can be determined using the Doi-Edwards model (Doi & Edwards, 1986).

(De Francesco & Duckett, 2004) proposed that the final level of orientation is the result of two competing processes: the alignment of chains along the sollicitation direction and the tendency of chains to return to their non-constrained state, governed by relaxation processes. When relaxation becomes dominant like at high drawing temperature ($T \gg T_g$), the stretching can be seen as proceeding in a polymer "melt" for that chains are not actually oriented despite the macroscopic deformation of the bulk material.

Strain-hardening can be observed in PS both upon stretching and compression. During the stretching, chains gradually orient along sollicitation axis especially at high level of extension. This extension of the chains contributes to stiffness of the overall network that presents eventually a hardening stage (Vorselaars et al., 2009).

I.1.2.2. PET: strain-induced crystallization

It is of great interest to go through former studies performed on drawing of PET since this polymer is on some aspects similar with polylactide (PLA), the main material studied in this thesis. PET and PLA are comparable especially in terms of morphology and crystallization behavior. PET is often semi-crystalline, yet it can also be easily quenched to get an amorphous material. In case of uniaxial deformation of amorphous PET, molecular chains gradually orient along the sollicitation axis accompanied often by a strain-induced crystallization process due to its crystallizable nature. Numerous former studies have discussed the effects of draw ratio, temperature, and strain rate on the orientation and strain-induced crystallinity of stretched PET samples (Allison & Ward, 1967; Cansfield et al., 1993; Heffelfinger & Schmidt, 1965; le Bourvellec et al., 1987; Lindner, 1973; Perena et al., 1980b; Schmidt, 1963). According to these studies a few key points can be concluded as below:

(1) Influence of the solicitation parameters:

- For a certain range of strain rates and favorable temperatures, a strain-induced crystallization process is able to occur at relatively large draw ratios (λ>200%) and the value of induced crystallinity increases steadily with draw ratios.

- When the stretching takes place at fast rates and low temperatures, stain-induced crystallization could be no more observed. Instead, it is a transient mesomorphic phase which can be formed (Mahendrasingam et al., 2000). In the work of (Kawakami et al., 2005), this nematic-ordered phase can also be induced during stretching below T_g of PET. The characteristics of such phase will be discussed later in details.

- When drawing temperature becomes too high with quite slow strain rate, no strain-hardening and consequently no strain-induced crystallization can be observed.

(2) The modulation of the crystallization behavior by different combinations of strain rates/ temperatures is in fact linked to the different orientation state and mobility kinetics of the macromolecules under various testing conditions. This relation between orientation and induced crystallization has been summarized by (le Bourvellec et al., 1987; Mahendrasingam et al., 2000). These authors suggested that the onset point of crystallization can be directly correlated to a critical orientation degree of the macromolecules. Under different combinations of stretching conditions, the crystallization process only occurs when this critical level of orientation is reached.

Two major factors should be considered to explain the origin of strain-hardening observed for PET:

- The first factor concerns the role of macromolecular orientation. Upon stretching, alignment of the polymer chains can result in a high degree of orientation in the direction of deformation.

- In case of PET, the alignment and orientation of chains lead also to strain-induced crystallization. Consequently the induced crystallinity, besides molecular orientation, should also contribute to the significant stress increase of strain-hardening stage. However it should be noted that to initiate hardening regime, perfect and large crystals are not

14

necessarily required. (Gorlier et al., 2001) have shown that hardening can be already observed before crystalline structure is totally developed.

Evolution of the macromolecular network upon stretching

As an overview, *Figure I. 5* shows a schematic representation of the evolution of the molecular network during uniaxial stretching in the case of an initially amorphous but crystallizable material.
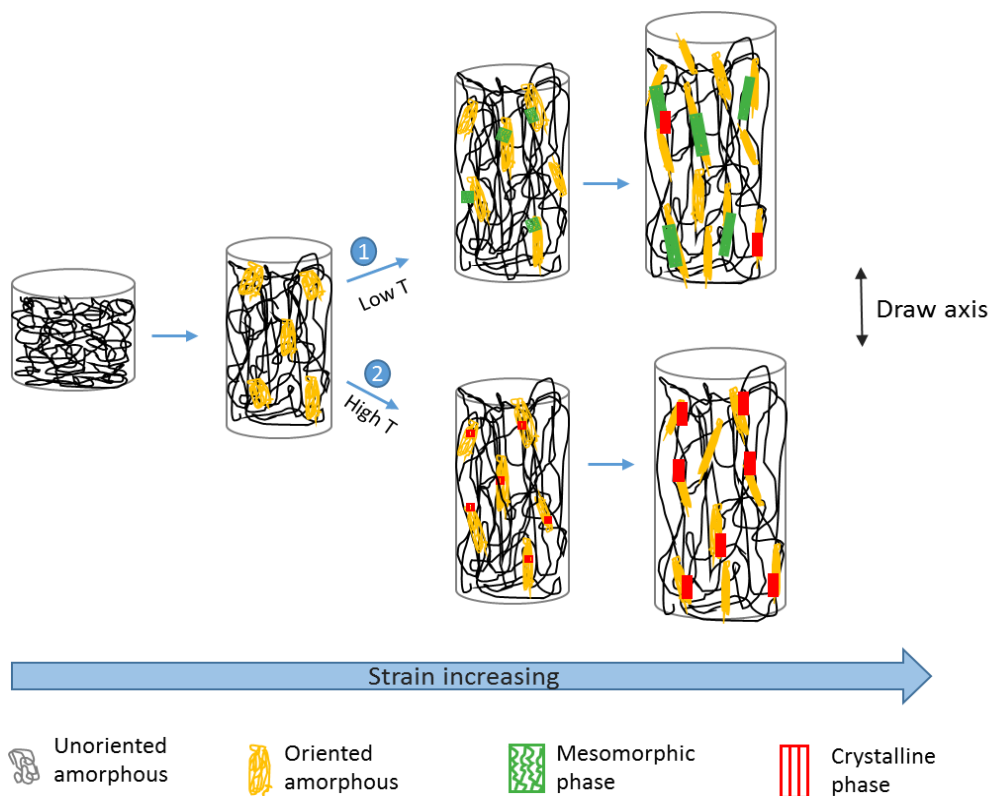
Figure I. 5. Schematic illustration of evolution of molecular network structure as function of strain during uniaxial sollicitation of a crystallizable amorphous polymer (Kawakami et al., 2005).

Starting from an isotropic state, the macromolecules gradually extend upon drawing and regions containing oriented amorphous material begin to appear locally with a preferential order of orientation along stretching axis. Then when strain continue to increase, the arrangement of these oriented amorphous chains in some regions becomes more regular. When a critical level of orientation is reached, strain-induced ordering takes place with the formation of two possible ordered phases depending on stretching parameters: one is the transient mesomorphic phase (route1) and the other one is the highly-oriented crystalline phase (route2). These ordered regions may serve

as entanglement points to enhance the rigidity of the network. Finally upon further extension, a perfection of the structure of mesomorphic/crystalline phase is observed. In addition a mechanically-induced transition from mesomorphic to crystalline phase at very important deformation level is also sometimes observed, as pointed out by (Kawakami et al., 2005).

Chain orientation resulting from stretching leads to anisotropic materials with enhanced properties in the orientation direction (Ge & Robbins, 2010). For instance (Arruda et al., 1993) have shown in their work that the pre-oriented materials presented a more significant strain-hardening modulus. The influence of orientation on mechanical properties of glassy polymers will be discussed later.

I.2. Elementary plastic deformation mechanisms involved below Tg

Brittle failure of polymers generally involves the propagation of a crack through the material. The resistance to this crack propagation is mainly governed by localized plasticity when deforming a polymer below its glass transition. There are mainly two micro-mechanisms of deformation: one rather without change of volume corresponding to shear banding and the other one causing a volume increase (i.e. voids formation) named as crazing.

I.2.1. Shear banding

Shear bands are localized regions in which the material has undergone shear deformation. Appearing at around 45° with respect to stress direction, shear bands represent one mode of non-elastic response of the material to mechanical loading. This type of mechanism is not only often detected for metals and semi-crystalline polymers but also for amorphous polymers, for instance in the case of conventionally-considered ductile materials such as PC (W. Wu & Turner, 1973). Polystyrene, even though often presents brittleness in many loading conditions, can also deform by shear bands for instance under compressive stress (Kramer, 1975).

A series of former studies were conducted to characterize the properties of shear bands by Wu & Li (J. C. M. Li, 1984; J. C. M. Li & Wu, 1976; J. B. C. Wu & Li, 1976). These authors proposed two slip processes for the deformation by shear bands:

(1) A diffuse "coarse band" process, which leads to the formation of shear zones, usually observed under optical microscopy. Such bands propagate rapidly along a localized path inclining at less

than 45º with the stress axis, which produces progressively chain deformation that contributes to plastic strain.

(2) A "fine band" process rather detected by electron microscopy. It concerns very fine and short shear bands arranged in a grid work of two mutually perpendicular sets. These bands spread by multiplication mainly along shear stress direction, contribute largely to the macroscopic strain and cause shape changes of the specimen, but do not induce shear fracture.

Examples of these two types of slip processes are shown in *Figure I. 6(a)*. Note that the shear band morphology depends on the sollicitation parameters (temperature, strain rate) as well as thermomechanical treatment of the polymer (Quinson et al., 1997).

Figure I. 6. Optical microscopy observations of shear bands of various polymers under plain strain compression tests: (a) PS deformed at 20ºC (b) PS at deformed 90ºC and (c) PC deformed at 20ºC (Quinson et al., 1997).

Shear bands are generally observed under compressive stress, but they can be also detected under tensile deformation. In that case the initiation and propagation of the bands is often accompanied by necking. The classical yielding theories such as the Tresca and Von Mises Criterions are usually applied to study the critical shear stress and the critical distortional strain energy respectively. Finally it is noted that shear band is a thermally activated mechanism without volume variation during deformation, which means that no internal surfaces are created (Kramer, 1975).

I.2.2. Crazing

I.2.2.1.   Generalities

"Crazing" is a plastic deformation mode activated under a tensile stress. Crazes are formed perpendicularly to the principle stress axis. Regarding geometric characteristics crazes are ellipsoidal heterogeneities with two decohesion surfaces bridged by many fibrils of small diameter, ranging from 5 to 30 nm, and of average thickness along stress direction from 5nm to 10µm (Kramer, 1983).

For typical "standard" crazes, the fibrils consisting of highly oriented polymeric material show an almost periodic mode arrangement with microvoids developed in between, occupying 30% to 50% of total craze volume. In addition to classical crazes, homogeneous crazes can also be observed and due to their specific morphology they have been called homogenous deformation zones (G. H. Michler, 1989). Inside these craze-like zones, there is only homogeneously stretched material without fibril/voids structure. A schematic representation of both types of craze structure is shown in *Figure I. 7*.
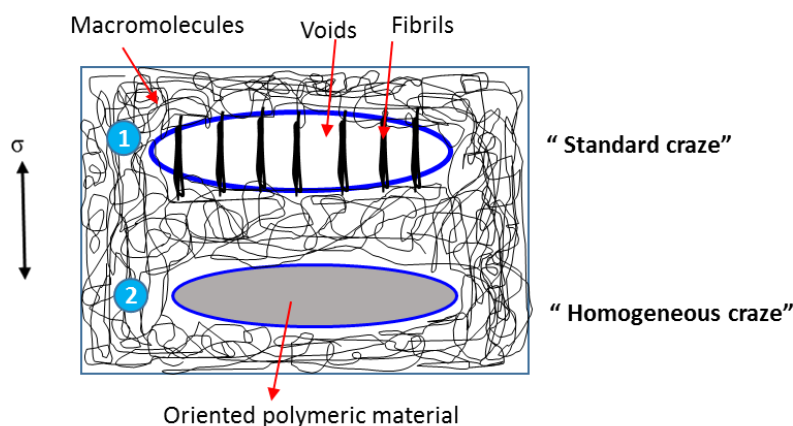

Figure I. 7. Schematic presentation of fibrilled/ homogeneous craze structure.

Different craze fibril morphologies have been reported depending on the deformation parameters and the chain architecture. *Figure I. 8* illustrates three types of craze interior structure observed with High Voltage Electron Microscopy (HVTEM) (Goerg H Michler, 2008).
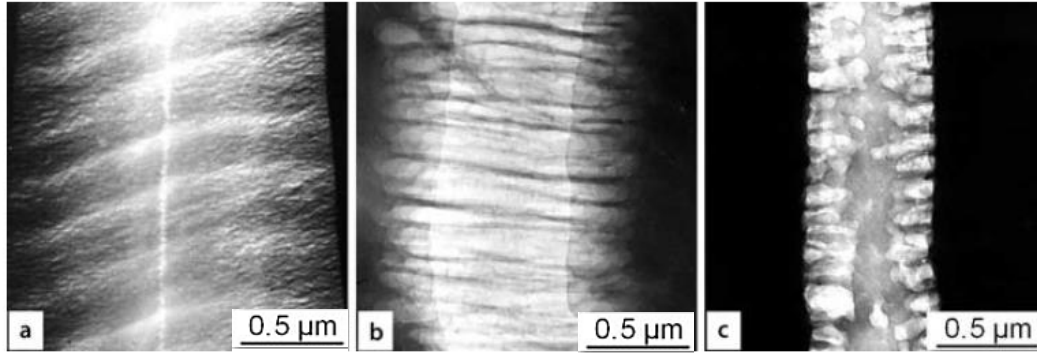
Figure I. 8. HVTEM observations of crazes with different inside structures in case of PS: (a) fine network fibrils (b) coarse fibrils (c) microvoid concentration at the craze boundaries (Goerg H Michler, 2008).

A large number of studies devoted to understand the craze structure in unreinforced polymers are carried out using Transmission Electron Microscopy (TEM). Even if this technique permits a direct observation of the fibrillar structure of craze, some drawbacks could not be ignored when studying crazing in bulk materials. Usually samples prepared for TEM analysis have to be very thin (around tens of nanometers) to reduce overlap problem during image recording. However crazing is a deformation mode involving voiding in the plane perpendicular to the stretching direction, consequently the effect of sample thickness must be taken into account into craze initiation and propagation. Consequently the observed phenomenon on thin films are probably different from the ones occurring in bulk samples. Also, to obtain information on the crazes geometry it is most tedious work to measure enough crazes in order to get good statistics. Thus electron microscopic methods are better suited for observing the fibrillar structure in a small region of a single craze.

Another commonly applied method to characterize crazes is Small Angle X-Ray Scattering (SAXS), which possesses many advantages as compared to TEM when the purpose is to analyze crazes in bulk materials. Being able to provide information such as shapes of scatterers as small as a few nanometers, SAXS allows a fine analysis of the material in transmission mode. Moreover, since the sample is no longer limited in terms of thickness, crazes could be initiated of important density so that the results obtained from SAXS analysis is of statistic interest. Finally with specific configurations, in-situ analysis of crazing during deformation is achievable through SAXS without disturbing the propagation of crazes. However, as a drawback, SAXS gives a representation of crazes in the reciprocal scape and the collected pattern results in the sum of the contribution of all

19

the individual crazes. In other words it is not possible to "look at a single craze" but only to the mean structure.

Typical SAXS patterns of a crazed structure consist in two long streaks nearly perpendicular to each other, as shown in *Figure I. 9* (H. R. Brown et al., 1985; Hugh R Brown & Kramer, 1981; Lode et al., 1998; Mills et al., 1985; Salomons et al., 1999). More precisely, the horizontal streak with high intensity originates from the scattering from the crazes walls while the more diffuse vertical scattering arises from the crazes' fibrils into the crazes.

The analysis of the intensity profiles extracted from horizontal/ perpendicular streaks give access to the geometric parameters of craze envelopes and craze fibrils respectively.
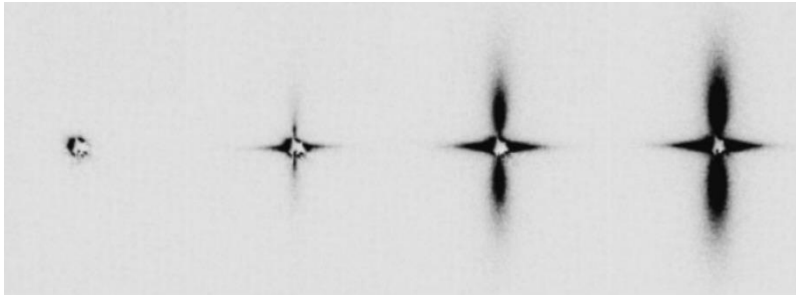
Figure I. 9. The evolution of SAXS images of craze as a function of strain (Zafeiropoulos et al., 2006).

I.2.2.2.   Craze initiation, growth and breakdown

Three main steps have to be considered when studying the mechanism of crazing: the initiation, the growth process and the final rupture of internal structure.

Craze nucleation is possible when the hydrostatic component (often noted as -p) is negative or null (Kramer, 1983). Lots of studies on the nucleation and growth of crazes were carried out by Kramer and his coworkers who proposed several steps for the formation of craze: first a localized plastic zone is formed under stress field, then voids begin to nucleate. With the increase of deformation, oriented polymeric materials between voids serve as ligaments that connect individual voids one to another to form a "mature" periodic fibrillar structure (*Figure I. 10*). A "standard" craze is then well formed.

σ

D   D   D'   Craze tip

Elongated fibrils with mature network   The initiation of crazes: primitive fibrils   Nucleation of voids
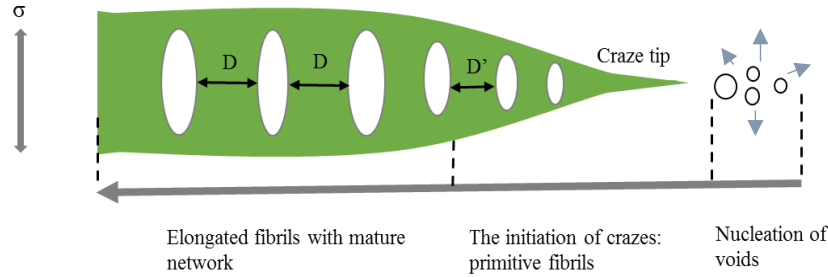
Figure I. 10. Schematic presentation of initiation of a craze.

Even if a few decades has passed since the earliest work studying the mechanism of crazing, there are still some remaining questions regarding this initiation step which is still not well understood. The model proposed by (Argon & Hannoosh, 1977) suggested that the critical event in craze nucleation is the formation of pores by some unstable shear patches and the effort is to separate molecules against their intermolecular van der Waals attraction. When dealing with high-molecular-weight glassy polymers however, the model reported by (Kausch, 1978) is more adapted. In this model, authors associated the formation of cavitation to the presence of heterogeneities of entanglement. Particularly regions where the entanglement density is low can been seen as impurities that could generate important stresses concentrations which favors the nucleation and development of microcavities. Recently (Goerg H Michler, 2008) has proposed a new model for craze initiation which is linked to the formation of a localized "plastic deformation zone". The development of this zone leads to the increase of the hydrostatic stress and voids began to form when the stress level reaches a critical value.

The second stage, the crazing growth, has to be considered in terms of two processes: craze-tip advancement and craze thickening. The most accepted concept for craze-tip growth is the "meniscus instability". This model was first proposed by (Taylor, 1950) and later summarized in (Kambour, 1973; Kramer, 1983). Through an action of stress gradient in the craze propagation direction, the craze tip is considered as a melt-like material and is separated into single polymer fibrils driven by surface energy as schematically presented in *Figure I. 11*.
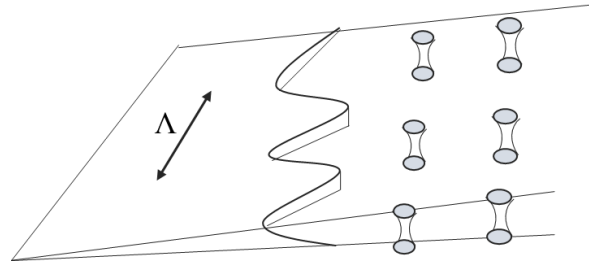
Figure I. 11. Stress-induced melt transformed into fibril fingers via a surface tension driven Taylor meniscus instability (Kramer, 1983).

After evolving into "mature" ones, the elongation of fibrils takes place between voids. In fact, a localized stretching leads to the formation of a stress-activated zone near from the craze/ polymer glass boundary. New polymeric materials are drawn into fibrils from this active zone leading to a conservation of the extension ratio of fibrils under a certain stress on the craze surface. Finally the craze microstructure consist in fibrils containing highly oriented material. Arranged in periodic mode, it is accepted that fibrils keep a constant diameter during stretching. A schematic representation is depicted in *Figure I. 12* (Kramer & Berger, 1990).
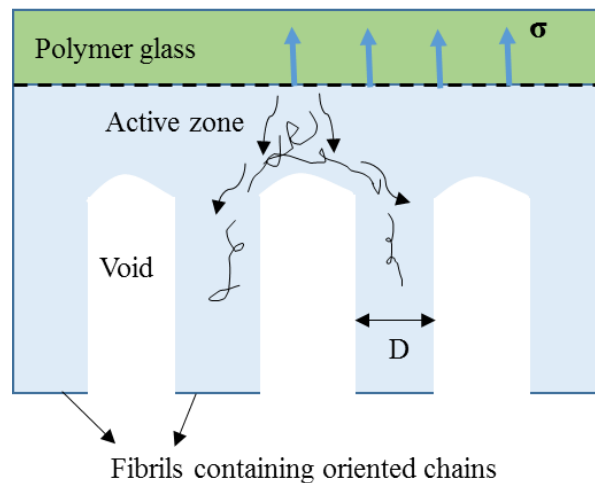
Figure I. 12. Schematic illustration of craze growth (Kramer & Berger, 1990).

The larger the fibril extension ratio, the higher the stress level on craze surface, favoring fibrils to break down. A craze-to-crack transition then happens and the further propagation of the crack generally leads to the failure of the material. The fibrils' failure conditions depends on loading conditions (strain rate, temperature…) and also very largely on the molecular environment of the polymer (Hui et al., 1992; Kramer & Berger, 1990). Two modes of failure of fibrils are identified:

one is through chain scission at low temperatures/high strain rates and the other one concerns a failure mechanism governed by disentangling chains at high temperatures/low strain rates.

I.2.3. Competition between shear bands and crazing

As mentioned previously, during plastic deformation two types of behavior are observed: brittle or ductile. The macroscopic mechanical behavior is in fact the results of the competition between two different elementary deformation mechanisms:

- For brittle behavior: crazing is responsible for the brittle failure of sample after only a few percentage of strain due to the rapid propagation of crazes and an eventual craze-to-crack transition.

- For ductile behavior: large plastic stain is achieved through formation and propagation of shear bands and the final failure of sample also involves propagation of a major crack in deformed zone.

The activation of one mechanism not the other depends on both intrinsic/experimental factors.

Influence of entanglement density

The first intrinsic parameter to discuss is the role of entanglements. As reported by (Athene M. Donald & Kramer, 1982a), a limited degree of chain scission/ slippage must occur to generate the void-fibril network, or in other words, the capacity of initiating crazing depends on how chains could be rapidly disentangled and pulled into fibrils as oriented polymeric material. (Sauer & Hara, 1990) summarized that the increasing of entanglement density is not favorable for crazing, making shear bands an "easier" mode of deformation for polymers possessing high entanglement density. For example PC has an entanglement density (ϑ_e) around 28.95×10^{25} chains/m^3 and it usually behaves like a ductile material with shear bands involved as deformation mechanism. On the other hand, PS is usually seen as brittle material due to rapid development of crazes since its ϑ_e is around 3.28×10^{25} chains/m^3, which is much lower than that of PC (A M Donald, 1985).

Influence of molecular weight

Another important intrinsic parameter concerns the molecular weight of polymer. It has already been mentioned previously that the required work modification for crazing could occur either via

chain scission or disentanglement. (A M Donald, 1985) pointed out that for scission crazing occurring at low sollicitation temperature, the effect of molecular weight is rather modest whereas when it comes to crazing by disentanglement at high sollicitation temperature the molecular-weight- dependence must be considered. These authors reported that in case of high molecular weight polystyrene at high temperature crazing is difficult to initiate and develop due to an increasing barrier for chain disentanglement.

Influence of experimental conditions

The effect of the deformation conditions has largely been studied by (A M Donald, 1985; O'connell et al., 2002; Ward & Sweeney, 2012). For instance the general evolution of critical stress level of crazing/ shear bands with temperature in case of uniaxial stretching is depicted in *Figure I. 13*.
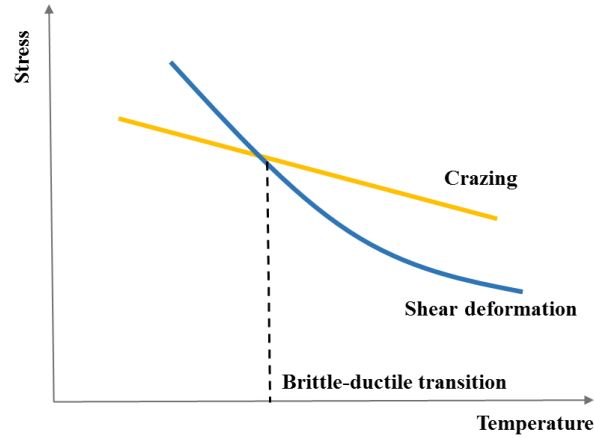
Figure I. 13. General influence of craze initiation stress& yield stress as a function of temperature (redrawn from (A M Donald, 1985; O'connell et al., 2002).

From the figure it can be concluded that the shear bands is more sensitive to temperature and strain rate changes than crazing, so that the latter tends to be suppressed at high temperature. The intersection of the curves indicates that beyond critical points a possible transition from brittle to ductile failure can occur. This behavior is often noted at brittle-to-ductile transition (B-D transition). The effect of strain rate on B-D transition can be analogized from effect of temperature through time-temperature principle. Note that this B-D transition point is also molecular-weight dependent, for longer chains T_{trans} takes place earlier due to important influence of molecular weight on chain disentanglement at high sollicitation temperature   (A M Donald, 1985).

Besides sollicitation parameters, other experimental parameters have to be considered such as the presence of solvents. (Andrews & Bevan, 1972) studied craze propagation over a range of temperature in PMMA immersed in a variety of liquids (methanol, isopropanol…). Authors have found that the critical criterion for craze formation as well as craze development depends on the solubility parameter of polymer in different solvents.

It should be also marked that under certain conditions, it is possible to observe a coexistence of these two elementary mechanisms, as shown in former studies (Athene M. Donald et al., 1982; Athene M. Donald & Kramer, 1982b; Goerg H Michler, 2008; Wellinghoff & Baer, 1978). *Figure I. 14* shows an example of coexistence of shear bands and crazes.
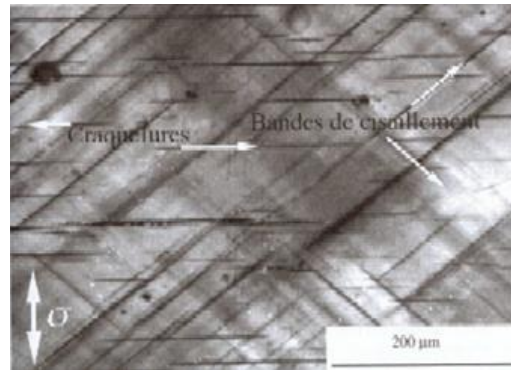
Figure I. 14. Examples of coexistence of shear bands and crazes in case of uniaxial deformation of PC at ambient temperature.

To summarize, with different combinations of factors discussed above, crazing or shear bands will play the dominant role during the deformation. That is to say, if the critical stress to initiate crazes is higher than the one for shear bands, the latter would take place as the more favorable mechanism for energy dissipation resulting in formation of yield point. Inversely if craze stress is lower than yield stress it would be crazing that occurs upon deformation.

In addition, it is worth noting that although crazing usually leads to brittle fracture, it has also been seen in rubber-toughened glassy polymers that when crazing occurs under well-controlled conditions, multiple crazes are formed to effectively absorb energy permitting the overall toughness of material, suggesting it is not always necessary to deform by shear bands to achieve ductile failure (Bucknall, 1997).

I.3. Brittle-Ductile transition induced by macromolecular orientation

As reviewed in previous sections, under appropriate stretching conditions, stretching amorphous polymers above T_g allows to induce molecular orientation along the sollicitation axis. It is of great interest to study this effect of macromolecular orientation on the mechanical behavior of glassy polymers.

I.3.1. Case of Polystyrene

While isotropic polystyrene is known to be quite brittle upon tensile drawing at room temperature, an increase of stretchability can be observed when the films are initially pre-oriented. This observation was first reported in the 1950s (Nielsen & Buchdahl, 1950). These authors have pointed out that, contrary to isotropic PS sample, the pre-oriented PS showed a well-defined yield point upon stretching and was able to strain around 10% before rupture. (Tanabe & Kanetsuna, 1978) have carried out an extensive work studying the effect of pre-orientation induced by processing at different temperature and strain rates (uni-orientation) on various mechanical properties such as tensile properties, relaxation modulus and impact behavior. Regarding tensile properties, authors concluded that the stress and strain at break of samples upon stretching are dependent on the pre-orientation level. Generally for the same tensile test conditions, the increase of the orientation involves an increase of the toughness. However this mechanical toughening is only observed in the pre-orientation direction.

The pre-orientation can be induced by either uniaxial or biaxial stretching process. In particular, the latter is considered as a common deformation route to improve the brittle behavior of PS films. Several investigators have reported the observations of Brittle-Ductile (B-D) transitions in amorphous PS films thanks to biaxial orientation (Choi et al., 1989; Matsumoto et al., 1981; Thomas & KJ, 1972; Xiaomin Zhang & Ajji, 2003). Contrary to uniaxially stretched samples, balanced biaxially oriented (BO) films exhibit ductile yielding in all directions in the plane of film regardless of sampling directions. Generally speaking an improvement of stretchability to 5-10% can already be seen as evidence of ductile failure in case of PS. However an increase up to 100% has also been reported by (Choi et al., 1989) (*Figure I. 15*).
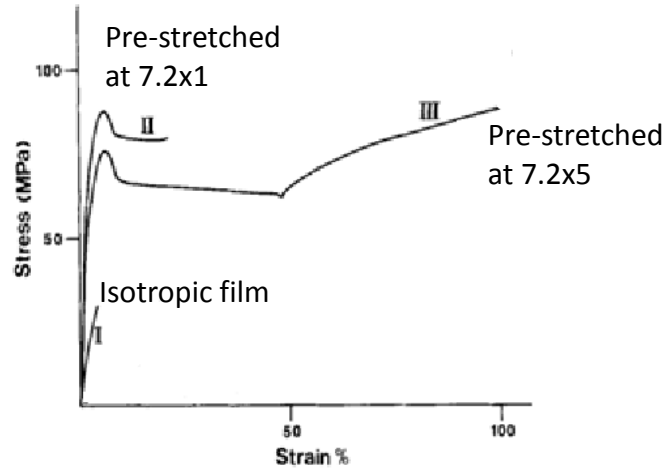
Figure I. 15. Stress- strain curves of isotropic and pre-oriented polystyrene films upon uniaxial stretching at room temperature (Choi et al., 1989).

I.3.2. Case of PLA

Similar to the case of PS, isotropic PLA is known to be brittle below T_g . However, macromolecular orientation can induce a ductile behavior for this eco-friendly polymer (Sarasua et al., 2005a).

For instance, uniaxial stretching has been proved to be efficient in improving the tensile properties of PLA. (Oh & Kim, 2014; Velazquez-Infante et al., 2013) have reported that pre-stretched PLA films are well reinforced in terms of yield stress and ultimate properties. For instance an improvement of strain at break values over 100% was already reported for a pre-oriented sample upon tensile deformation at ambient temperature. However, similar to case of PS, the improvement of such mechanical properties can only be detected when sampling along uniaxial orientation direction.

Biaxial stretching process is also of prime interest as it allows to simulate industrial processes such as bottle stretch-blow molding, biaxial film drawing or thermoforming. Its influence on the mechanical behavior and the associated structural evolution has been largely reported in case of PET (Bonnebat et al., 1981; Hassan & Cakmak, 2013; Maruhashi & Asada, 1996; Rao et al., 2008). In the case of PLA, former studies on biaxial stretching mainly focused on the structure development of the material during orientation and the influence of stretching conditions on end-use properties of drawn films (Al-Itry et al., 2015; Chapleau et al., 2007; Ou & Cakmak, 2008,

27

2010; Tsai et al., 2010). Here authors paid most attention to the positive effect of pre-orientation on tensile properties of stretched films as explored by a few authors (Jariyasakoolroj et al., 2015; Z. Li et al., 2017; J. H. Wu et al., 2013) and also in a recent work of laboratory (Ouchiar et al., 2016). This previous work has illustrated that it is possible, thanks to biaxial stretching, to get access to a super-tough PLA with over 100% of strain at break, suggesting the possibility to induce a B-D transition in oriented materials.

I.3.3. Major question: Origin of B-D transition

As previously discussed, an initially brittle polymer may present a ductile behavior depending on various factors such as stretching conditions and molecular parameters like entanglement density. Generally speaking, the brittle/ ductile behavior of a polymer during deformation mainly depends on whether crazing or shear bands is "easier" to be induced.

Concerning B-D transition, one could imagine that the induced molecular orientation affects the deformation mechanism that takes place, however the topic is complex and has not yet been clearly understood in literature. For instance in the case of PS it has been widely accepted that the brittle failure results from the fast propagation of craze-crack mechanism and the development of such process is considered to be suppressed or even stopped in oriented samples (Jones, 2013; Tanabe & Kanetsuna, 1978).

The situation for crystallizable materials like PLA is more complicated. This polymer is able to form a crystalline phase during the orientation process if stretching conditions are favorable, in others words strain-induced crystallization is often involved. Particularly, in the work of (Jariyasakoolroj et al., 2015) authors ascribed the impressive mechanical behavior improvement to the formation of crystalline lamellae during biaxial stretching. Quite recently (Razavi & Wang, 2019) have also highlighted the critical role of these induced "nanocrystals" in inducing B-D transition observed with uniaxially stretched PLAs.

These assumptions, however, contradicts a previous work carried out in our research group where authors suggested that is still quite possible to observe ductile behavior in BO PLA that remains globally amorphous after stretching (Ouchiar et al., 2016). These results are in agreement with former conclusions drawn in the case of PS, allowing to wonder if the formation of a crystalline structure is after all a necessary condition to induce a B-D transition. Regarding the potential

influence factors, besides strain-induced crystallization process, one should also consider the role of macromolecular orientation.

In short, the present PhD study aims at determining the origin of B-D transition that has been observed for glassy polymers, especially in the case of PLA. A few other polymers will also be studied to complete the observations. The detailed objectives of research will be presented in last section of this chapter.

I.4. Materials of study

I.4.1. Polylactide (PLA)

Among the various polymers produced from renewable resources in the aim of reducing the use of traditional petroleum-based polymeric materials, poly (lactic acid) or polylactide (PLA) has received the most attention in recent decades. As a thermoplastic aliphatic polyester, PLA has interesting properties such as transparency, high strength and high modulus required for large number of industrial applications.

Moreover, due to its non-toxicity and its biocompatible/ bioresorbable nature, PLA is generally recognized as a safe material by the United State Food and Drug Administration (FDA) for all food packaging applications *(FDA notification no.178, 2002)*. Since the FDA approval, researches focused on applications for biomedical applications such as prosthesis or disposable products have been widely reported for the past decades. Besides packaging and biomedical industries, many other uses of PLA have also been extensively explored for instance in the field of textile, automobile, electronics as reviewed in (Farah et al., 2016). A summary of applications of PLA-based polymers is available in *Figure I. 16*.
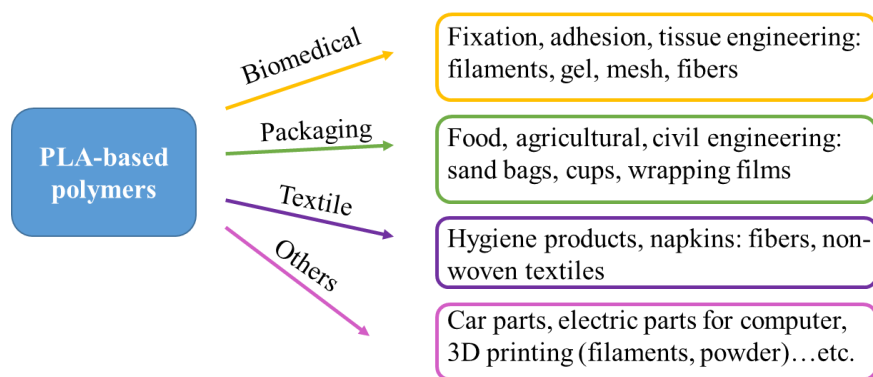
Figure I. 16. General application fields of PLA-based polymers. Summarized from (Di Lorenzo & Androsch, 2018).

PLA is the main material of this thesis study. The following sections will give a review of the principle characteristics and properties of PLA.

I.4.1.1.   Synthesis of polylactide

Poly (lactic acid) is a linear aliphatic polyester with a repeating unit $(C_3H_4O_2)_n$. The monomer, the lactic acid, is generally issued from fermented starch rich plants such as corn, sugarcane or cassava. Lactic acid has a chiral carbon, leading to the presence of two stereoisomers consisting of enantiomeric D- and L-lactic acid units in different ratios, as presented in *Figure I. 17*.
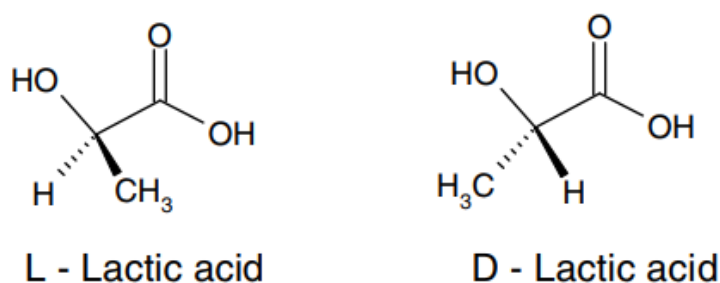
Figure I. 17. Different isomeric forms of lactic acid (Gupta & Kumar, 2007).

There exist two main routes to synthesize PLA polymers from lactic acid (Garlotta, 2001):

- Direct polycondensation of lactic acid. This process yields a low molecular weight leading to a brittle polymer with poor mechanical properties which is not suitable for many applications such as packaging.

- The depolymerization of lactic acid into lactide (a cyclic diester of lactic acid) and the polymerization of lactide by Ring Opening Polymerization (ROP). This method permits the synthesis of high-molecular-weight PLA ($M_w >$ 100,000g/mol), which is adopted by most of PLA manufactures.

The synthesis routes of PLA are schematically presented in *Figure I. 18* (Lunt, 1998).
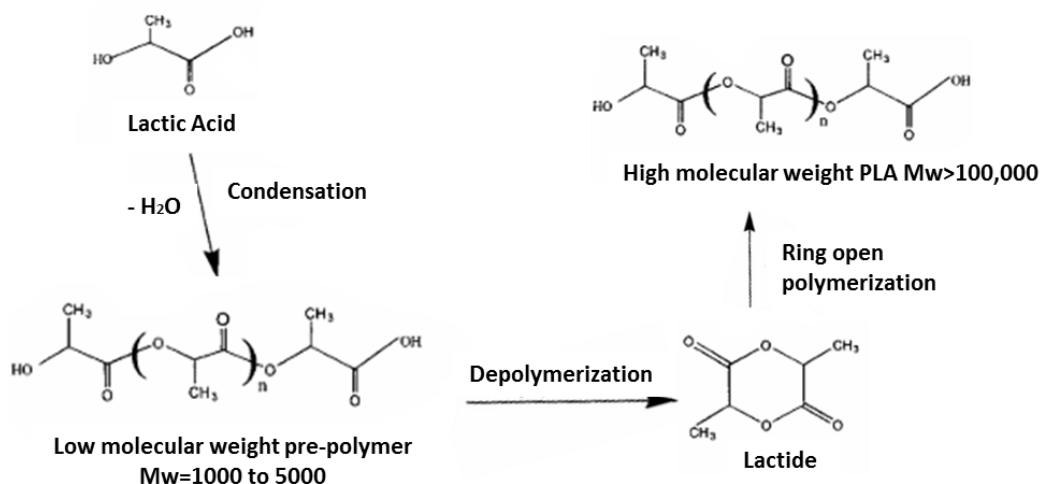
Figure I. 18. Manufacturing routes to polylactic acids (Lunt, 1998).

As shown before, lactic acid possesses asymmetric carbons which brings lactide to a chiral diester. It is then possible to obtain 3 different stereoisomeric forms of lactides: DD-, LL-, and DL-lactides (meso-lactide), as shown in *Figure I. 19*.
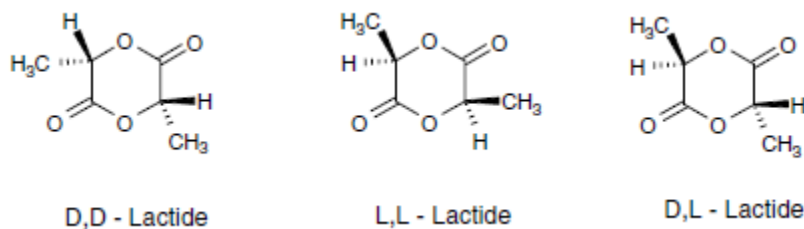
Figure I. 19. Different forms of lactide isomers(Gupta & Kumar, 2007).

Because of the stereoisomeric nature of lactides, different polylactides are obtained by ROP:

- Homopolymers poly(L-lactide) (PLLA) and poly(D-lactide) (PDLA) synthesized from pure enantiomers.

31

- Random copolymers PDLLA issued from synthesis of a mixing of L-lactide and D-lactide or meso-lactide. These materials are classified into different grades according to the different L/D isomer ratios.

The polylactides of this PhD work are PDLLA copolymers containing different contents of D-isomer as minor units. For sake of simplification these copolymers will be noted only as PLA.

I.4.1.2.   Principle structures & properties

High-molecular-weight PLA is a colorless and stiff thermoplastic polymer with mechanical properties similar to the ones of PET. The amorphous PLA is soluble in most organic solvents such as tetrahydrofuran (THF), benzene and chlorinated solvents (Garlotta, 2001). PLA presents good resistance against grease or oil whereas its water or oxygen barrier properties are poor as compared to PET for example (R. Auras et al., 2004).

PLA crystalline structures

PLA can be initially fully amorphous or semi-crystalline. Besides semicrystalline PLA is polymorphic with different crystalline structures depending on the thermomechanical treatment history. The PLLA homopolymer is able to crystallize under four distinct crystalline phases as follow:

- The α -form. This is a crystalline phase formed upon "standard" conditions of crystallization. This phase presents a pseudo-orthorhombic crystal lattice in which helixes adopt a 10_3 helical conformation.

- The α′-form. This phase is often considered as a disordered α-form with similar chain conformation as the α-form consisting of 10_3 helical chains.

- The β -form. This crystalline phase is obtained by stretching fibers under specific conditions, usually under high temperature and important strain rate (Eling et al., 1982). This phase adopt an orthorhombic lattice containing distorted 3_1 helical chains

- The γ-form. This peculiar formed was reported by (Cartier et al., 2000) in their work on epitaxial crystallization of PLA on a hexamethylbenzene substrate. The unit cell is built up

by two macromolecular chains based on helix conformation forming also an orthorhombic lattice.

It should be noted that the α'-form crystalline phase is metastable and can transform into the α-form upon heating. (J. Zhang et al., 2008) have reported the formation of the α′-form for crystallization temperatures below 120°C. When heated above 130°C a α′-to-α phase transition can be observed. Both phases are characterized by a main peak at 2θ∼16.8° (with Kα=1.54Å) corresponding to the (200)/(110) crystallographic planes.

The last crystalline phase reported is the stereo-complex form. (Ikada et al., 1987). This crystalline form is encountered in the case of PLLA and PDLA blends and arises from the crystallization of PLLA macromolecules with PDLA macromolecules which generate the so-called "stereocomplex" crystals.

This phase has a triclinic lattice and exhibits a fairly larger melting point, around 230°C, than the other crystalline forms of PLA (melting point around 150-180°C).

The mesomorphic phase

During stretching above T_g, amorphous polymer chains orient and can be able to crystallize if the stretching conditions are favorable. However when stretched near T_g, PLA can form a mesomorphic phase upon stretching. This metastable phase exhibits an intermediate degree of ordering between the amorphous and crystalline phases (*Figure I. 20*). The conformation adopted by the macromolecules in the mesomorphic phase is close to that of crystals but without regular 3D arrangement.

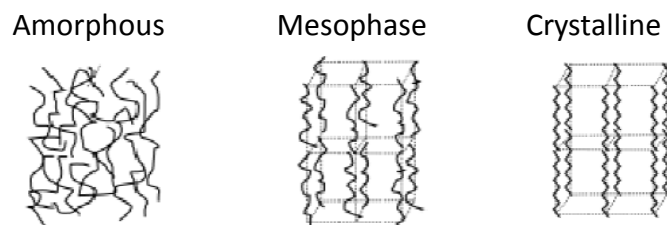Amorphous   Mesophase   Crystalline

Figure I. 20. Schematic presentation of mesomorphic phase compared to amorphous and crystalline phase (Grégory Stoclet, 2009).

This mesophase was first reported by (Mulligan & Cakmak, 2005) as a "nematic" ordering containing highly oriented chains. Stoclet and coworkers carried out extensive studies on uniaxially drawn PLA by means of *ex situ* (G. Stoclet, Seguela, Lefebvre, Elkoun, et al., 2010) and *in situ* diffraction analysis (G. Stoclet, Seguela, Lefebvre, & Rochas, 2010). According to their characterizations, mesophase exhibits a poor thermo-mechanical stability since this phase was detected to melt at low temperature (~70°C). Depending on drawing conditions, the melting behavior of the mesophase may significantly be affected by the occurrence of the cold-crystallization upon heating beyond T_g.

A mesophase- to- crystal transformation can be mechanically achieved upon stretching. (Hu et al., 2012) reported in their work of uniaxial stretching of PLA where a mesophase is first induced at lower level of strain. Then upon large strain this induced mesophase transfers to disordered crystalline phase due to a more compacted chain packing with increasing of strain. Such observation is also confirmed by (Zhou et al., 2016),who proposed that mesophase first forms into "meso crystals" then into well-ordered crystals under favorable conditions.

The strain-induced mesophase of PLA is similar to the one of PET or polyethylene naphthalate (PEN) (Carr et al., 1997). For these latters, (Abou-Kandil et al., 2007) explains that the stacking of planar aromatic rings in these polymers contributes to the mesomorphic ordering. However, such rigid groups are absent in case of PLA consequently the physical origin of mesophase in this polymer remains still unclear.

Thermal properties

The L/D ratio affects the thermal properties of PLA. For instance, (Urayama et al., 2001) observed the glass transition T_g decreases with the increase of the D-isomer content. They noticed that T_g varies in a range of [55-65]°C for most of the PLA grades while a particular low value around 50°C can be obtained for PDLA containing over 70% of D-isomer. In the same way the melting temperature (T_m) is determined at 180°C for pure PLLA and goes down to around 155°C with a few percent of D-isomer. For D-isomer contents above 8-10% the material is no more able to crystallize and is this still amorphous.

Regarding thermal stability, PLA polymers start to thermally degrade above 200°C and completely decompose at 400°C when tested under dried nitrogen environment. Thermal decomposition is independent of the L/D isomer ratio.

Mechanical properties

The mechanical properties of PLA have been studied by many investigators. Among different commercial grades of PLA, the ones with D-isomer as minor unit are the most available grades at large scales (types used in thesis). Some characteristic tensile properties upon uniaxial stretching of PLA are summarized in *Table I. 1* and compared to those of PS and PET (R. Auras et al., 2003).

Table I. 1. Mechanical properties of a classical PLA film compared to PS and PET.

Mechanical property	PLA (2% of L-lactide)	PS	PET
Yield stress (MPa)	65-70	55-80	275
Elastic modulus (GPa)	2.1-2.8	3.2	2.8-4.1
Elongation at break (%)	3-10	2	60-165

It can be seen that the mechanical properties obtained for PLA are generally within the range of values determined for PS when the same testing conditions are used. However when compared to PET, amorphous PLA has a lower stretchability.

As previously discussed, the intrinsic brittleness of PLA consists in a major drawback that limits a wider application of PLA in various fields. This is mainly due to the fact that this polymer tends to deform by crazing when stretched in its glassy state, as reported in (G. Stoclet et al., 2014). The characteristics of crazing/ shear bands as elementary plastic deformation mechanisms have already been discussed in I.2. In section I.3 authors have reviewed a possible transition from brittle to ductile behavior of PLA induced by molecular orientation through processing above glass transition temperature.

I.4.1.3.   Crystallization kinetics: influence of the D-isomer content

PLA is a slow-crystallizing material similarly to PET. The fastest rates of isothermal crystallization for pure PLA are found in the temperature range [110-130]°C and crystallization from the melt

leads to a spherulitic crystalline morphology. The rate and extent of crystallization depends on numerous factor such as temperature, molecular weight and the presence or not of nucleating agents…etc. Typically a maximum crystallinity in an order of 30–50% can be developed (Garlotta, 2001).

Here authors would like to highlight the influence of the D-isomer content on the crystallization kinetics of PLA. (Huang et al., 1998) reported that a copolymer containing 0.4% of D-isomer crystalize over 40 times faster than the one containing 6.6% of D-isomer. Recently (Tábi et al., 2019) also demonstrated that the decrease of the D-isomer content induces a shift of cold crystallization towards lower temperatures, which promotes the formation of α' crystals. (Saeidlou et al., 2012) summarized in their review that the increase of the minor unit, no matter L or D-lactide, decreases the crystallization rate which results in a limitation of maximum achievable crystallinity. It was also pointed out that for PLAs with D-contents above 10%, crystallization is suppressed, leading to non crystallizable amorphous materials.

Besides D-isomer content, the way that D-unit is introduced into the PLA chain should also influences the spherulit growth, as reported by (Huang et al., 1998). These authors suggested during synthesis of PLA containing D-units as impurity, using D,D lactide allows higher maximum crystallinity than using meso-lactide.

In conclusion, the increase of the D-isomer content results in a severe slowing down of isothermal crystallization kinetics. However worth noting is that the D-isomer content has no influence on strain-induced crystallization kinetics but only on the maximum crystal content achieved at the end of drawing, as reported in (G. Stoclet et al., 2011).

I.4.1.4.   The physical ageing of PLA

It is well known that the amorphous polymers below T_g are in non-equilibrium state, so the driving force of ageing is in fact to approach towards equilibrium through a change of properties of material. Depending on different thermal history, the state of the polymer glass will strongly influence both the physical and thermomechanical properties of the bulk material (specific volume, enthalpy….) (J. M. Hutchinson, 1995).

(Celli & Scandola, 1992) investigated the influence of the ageing conditions on thermal properties of PLA. They reported an increase of the relaxation enthalpy at glass transition, a gradual increase of T_g with the increase of the aging time and a faster aging rate when T_{ageing} is closer to T_g as already shown for other amorphous polymers. (Pan et al., 2007) investigated the influence of ageing on the viscoelastic properties and tensile mechanical behavior of PLA. Particularly authors observed that physical ageing favors a reinforcement in terms of both yield strength and tensile modulus at the expense of an embrittlement of the material.

Later these authors carried out analyses to evaluate the effect of physical ageing at a molecular scale(Pan, Zhu, et al., 2008). In fact, at temperature below T_g the chain movements are restricted so that the molecular reorganization towards the equilibrium state is extremely slow, which makes an *in situ* analysis quite difficult. Nevertheless by comparing aged/unaged sample these authors reported a conformational variation, particularly the high-energy *gg* conformers rearrange into the low-energy *gt* counterparts during physical ageing. This conformational change was later correlated to the crystallization behavior of PLA by (Pan, Liang, et al., 2008). It was surprisingly found that aged samples required less time to crystallize as the nucleation ability and crystal growth rate were favored by the presence of localized "ordered" domains resulting from the chain rearrangement which occurred during ageing.

Note that the physical ageing phenomenon is actually a "reversible" process in the sense that it is possible to rejuvenate an aged sample by simply heating the samples onto equilibrium state, i.e. above T_g. Despite the numerous former work in literature, the intrinsic mechanism of physical ageing is still a complicated topic. Further relations still need to be established linking the macroscopic properties with microstructure and chain conformation for polymeric materials.

I.4.2. Poly(ethylene 2,5-furandicarboxylate)

Poly(ethylene 2.5-furandicarboxylate) or poly(ethylene 2.5-furanoate), generally abbreviated as PEF, is a newly-emerging bio-based polymer foreseen as a potential candidate to replace PET. Among numerous polyesters synthesized from 2.5-furandicarboxylic acid (FDCA), PEF has received much recent attention due to improved performances as compared to PET for instance in terms of superior gas barrier properties. Nevertheless at present the commercialization degree of this polymer is still in pilot stage compared to PLA and far from that of PET (Eerhart et al., 2012).

Synthesis

PEF is an aromatic polyester that can be produced by polymerization of FDCA with ethylene glycol (EG). In fact, the process is quite similar to the production of PET where terephthalic acid (TA), a petrochemical-derived monomer, is used to polymerize with EG. Then if the TA is replaced by FDCA, the polymerization result with EG gives PEF, as schematically presented in *Figure I. 21* (Gomes et al., 2011). The resulting PEF can be fully bio-sourced since FDCA is a renewable building block that can be obtained from sugar and EG can also be bio-based.
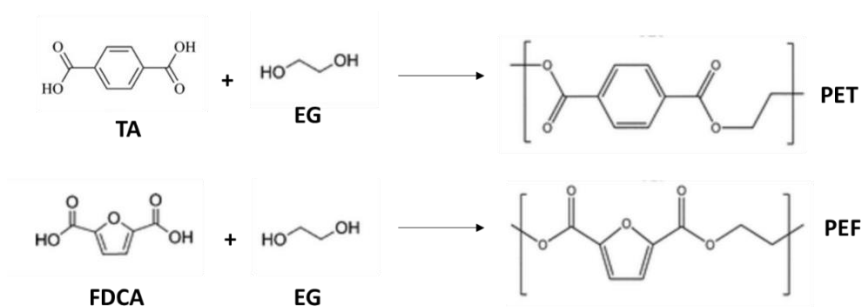
Figure I. 21. Schematic illustration of polymerization processes of PET and PEF(Gomes et al., 2011).

Due to the striking similarities of FDCA to TA, PEF is seen as the direct furan analogue to PET. Still differences are detected in terms of ring size, polarity and linearity leading to difference performances of the two polymers (Burgess et al., 2014).

Crystalline structure

The crystal structure of PET consists in a triclinic unit cell with one monomer along c-axis. While the structure of PET is extensively studied, the same is not for PEF as only few papers have been published reporting its crystalline structure (Maini et al., 2018; Mao et al., 2016) and crystallization behavior (Guigo et al., 2017; G. Stoclet et al., 2015; Tsanaktsis et al., 2015). According to these authors a maximum crystallinity around 40% is obtained in the optimum conditions.

According to these studies, in the case of bulk crystallization (melt-crystallized), a defective crystal structure in α'-form is generated at low temperatures (< 170ºC). Upon crystallization above this temperature, the process often involves the formation of a more perfect structure, the α-form. A α'-

to-α transition can be observed if one continues heating (over 190ºC) due to a reorganization and perfection of crystalline structure, a similar process has already been discussed in case of PLA.

Recently (Maini et al., 2018) has proposed a complete structural characterization of crystalline forms in PEF: the triclinic α-form, the monoclinic α′-form and the monoclinic β-form (crystallization in solvent). In all cases PEF chains adopt an almost planar configuration.

Thermal properties

the comparison of thermal properties between, PEF, PET and PEN was reported by (Papageorgiou et al., 2014). It was determined that the T_g of PEF (~85ºC) is slightly higher than the one of PET (~80ºC) but lower than the one of PEN (~123ºC) and that the melting temperature of PEF is around 200-220ºC which is lower by 30ºC and 50ºC than the ones of PET and PEN, respectively. As for thermal stability, these authors have indicated that PEF is thermally stable up to 325ºC, which is slightly lower than for PET or PEN.

Mechanical properties

Regarding mechanical properties of PEF, (Knoop et al., 2013) showed that amorphous PEF exhibits a similar Young's modulus than PET, but fails in a brittle manner with only a few percentage of elongation at break. This is quite different from PET that generally displays ductile behavior. Besides, no yielding is detected upon tensile drawing of PEF.

Recently (G. Stoclet et al., 2018) reported to observe crazing upon deformation of glassy PEF which should be the origin of the brittle fracture of this polymer. These authors carried out a structure-property study of PEF upon uniaxial drawing and reported a similar strain-hardening behavior as observed for PET. The occurrence of a hardening stage is linked to a strain-induced crystallization but not necessarily, since a mesomorphic phase can be induced when stretching at low temperature around T_g, as previously discussed for PLA.

Biaxial orientation behavior of PEF was explored by (van Berkel et al., 2018). In their work authors highlight that strain-hardening and strain-induced crystallization for BO PEF appeared at higher stretch ratios than for PET (for similar molecular weights). However, the maximum crystallinity reached upon biaxial stretching for PEF is relatively less significant that for PET. Regarding BO

films, oriented PEF has shown a higher modulus and better barrier properties against oxygen and carbon dioxide as compared to BO-PET.

To summarize, PEF will be studied as a complementary materials using the same methodology as applied for PLA in order to test the generalization of the method and confirm the most important observations since the two materials exhibit similar properties.

I.4.3. Polystyrene

Since its first commercial production in 1931 by BASF, polystyrene has become one of the most widely-used thermoplastic polymer that is produced at a scale of millions of tons per year (Scheirs & Priddy, 2003). Typically, PS is a transparent, rigid and rather brittle polymer fabricated in form of either solid or foam. Common applications of PS include packaging cases (CD, DVDs), containers, bottles, films and disposable products. As a non-biodegradable polymer, the accumulation of the use of PS has become a major source of pollution of waterways and oceans especially in its foam form.

In this study PS will not be studied as much extensively as PLA but rather investigated as a reference material since it is a well-known polymer in literature and it has similar properties as PLA. This section presents synthetically the general characteristics and most important properties of this material.

Synthesis

Polystyrene is synthesized by polymerization of styrene. One of the most applied polymerization processes to synthesize typical linear PS is through free radical polymerization (Mayo, 1943). An initiator   (often noted as R·) such as benzoxyl starts the process, then the propagation begins by adding one after another new styrenes to the chain and the reaction will be terminated once a desired molecular weight is reached. The process is schematically presented in *Figure I. 22*.
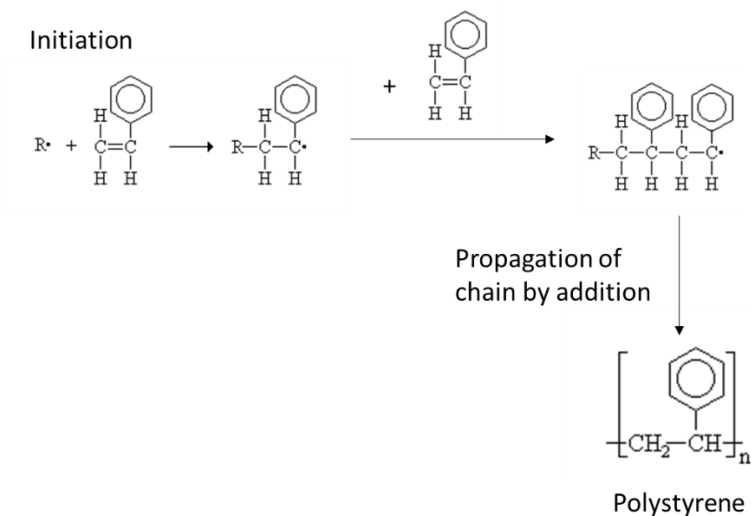
Figure I. 22. A schematic presentation of free radical polymerization of synthesis of polystyrene (Mayo, 1943).

Typically a few thousands monomers are polymerized to form the principle chain, resulting in a polymer possessing M_w=100,000- 400,000 g/mol for commercialized grades.

Structure

It is observed that the carbons on the PS backbone attached with a phenyl group are stereogenic. If the backbone is considered as a flat elongated zig-zag chain, each phenyl group would be tilted forward or backward compared to the plane of the chain. The different stereochemical structure of consecutive phenyl groups determines the tacticity, which has an effect on various properties of the material. Standard PS, as used in this thesis work, is atactic where phenyl groups are randomly distributed on both sides of the main chain. Other diastereomers include isotactic PS and syndiotactic PS, where for the former all phenyl groups positioned on one side of backbone and for the latter the distribution of phenyl groups is alternative (*Figure I. 23*).

Figure I. 23. Illustration of PS of different tacticity.
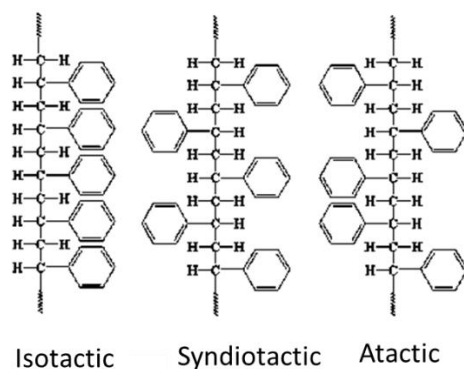
Atactic PS is the most found form for commercial uses. The random distribution of phenyl groups prevents the chains to align in regular arrangement, which results in a polymer that does not crystallize even upon stretching or isothermal conditions. Other two forms of PS are often semi-crystalline. In this thesis only atactic PS will be studied.

Thermal properties

Atactic polystyrene is an amorphous material which has low shrinkage and is easy to process. Commercially speaking high-molecular-weight grades (M_w=100,000- 400,000 g/mol) are usually used. Due to its atacticity, only a glass transition is detected upon heating scan due to its amorphous nature. The dependency of T_g on molecular weight was investigated by (Claudy et al., 1983), and it was observed that for M_w above 50,000 g/mol the determined T_g is roughly constant at around 100°C. Though molecular weight seems to have little effect, other molecular-structure-related factors such as entanglements can still influence the glass transition stage. For instance (Rong et al., 2005) has reported a depression of T_g with a reduction of entanglements through analysis a series of freeze-dried samples from diluted solution of atactic-PS.

Mechanical properties

As previously discussed, amorphous PS is brittle upon uniaxial tension with a strain at break of only 2-3% which occurs even before yield point. Apart from sollicitation parameters, molecular weight appears to be an intrinsic factor that influences the failure behavior. For instance (Nunes et al., 1982) reported in their review work that the increase of molecular weight favors the deformation at rupture, even so the improved value is still low (10-15%) and the yield stage is less

well-defined as compared to ductile polymers. The main deformation mechanism involved in failure of PS is crazing.

Briefly, PS has similar properties with PLA and has the major advantage of being always amorphous even upon thermal mechanical treatment due to its atactic nature. It is a well-known polymer which has been already widely analyzed. Therefore this polymer will be studied as a reference material in this thesis in order to compare with the findings of research on PLA.

I.5. Objectives of the PhD work

Polylactide (PLA) is currently one of the most promising polymers issued from renewable resources with a great industrial potential. However its intrinsic brittleness at room temperature was found to be a major limit to a wider range of application. Upon various physico-chemistry methods aiming at improving this drawback, mechanical deformation such as stretching above glass transition can be seen as a "green" route to overcome the PLA brittleness, which draws much attention of research interest.

Generally speaking the macroscopic mechanical behavior of glassy polymers is closely linked to the elementary plastic deformation micro mechanisms (crazing vs shear bands) involved during its stretching. Activation of one mechanism relative to the other depends on various factors, which leads to the different failure manner of the target polymer.

The main goal of this PhD thesis is to understand the influence of molecular orientation on mechanical properties of glassy polymers, especially in case of PLA. Indeed, at favorable stretching conditions, oriented PLA is able to display a B-D transition at ambient temperature. However the origin of this transition has not yet been well explained in literature since controversial suggestions have been identified. Thus, a macro-to-micro analysis will be carried out in order to better understand the relations between orientation-induced B-D transition and involved deformation mechanisms.

Two grades of PLA will be targeted in a first place: one crystallizable and one stays always amorphous, even during stretching. The investigations on these two types of PLA aims at separating the respective effects of strain-induced crystalline structure and macromolecular orientation on the mechanical behavior. Two complementary materials with similar properties of

PLA will also be explored: PEF, a newly-thrived material with great potential and PS, a well-studied historic material studied as reference material in the spirit of examining the applicability of the methodology for other biopolymers.

The experimental approach adopted during this PhD study is presented in *Figure I. 24*.
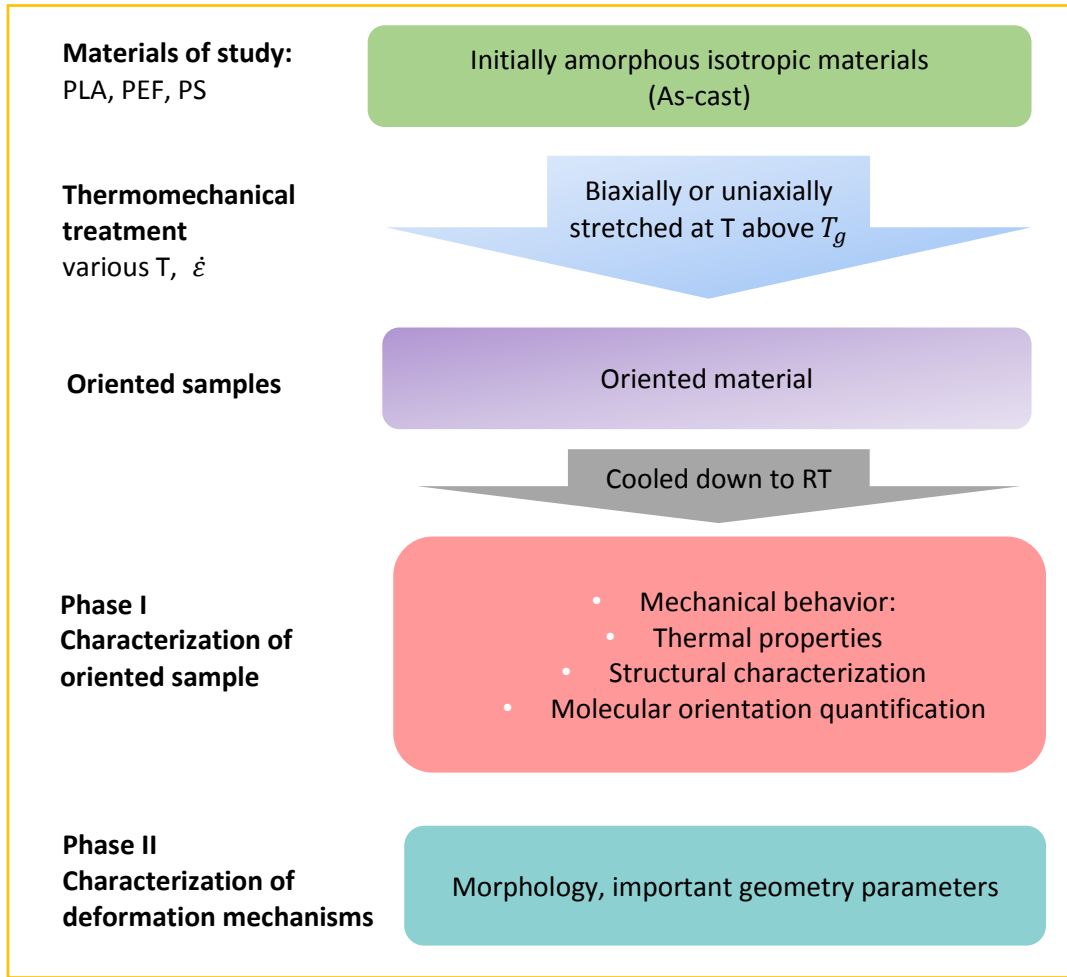

Materials of study: PLA, PEF, PS	Initially amorphous isotropic materials (As-cast)
Thermomechanical treatment various T, $\dot{\varepsilon}$	Biaxially or uniaxially stretched at T above T_g
Oriented samples	Oriented material
	Cooled down to RT
Phase I **Characterization of oriented sample**	• Mechanical behavior: • Thermal properties • Structural characterization • Molecular orientation quantification
Phase II **Characterization of deformation mechanisms**	Morphology, important geometry parameters

Figure I. 24. Schematic presentation of methodology of thesis.

First of all the films will be stretched above T_g at various stretching conditions in order to induce various orientation degrees. Then these stretched films of different orientation status will be characterized in terms of thermal, mechanical and structural properties. The relative investigations concerning two grades of PLA will be reported in Chapter III.

In a second step, the deformation mechanisms will be investigated both for isotropic and oriented PLA. The main result will be summarized in Chapter IV

Finally, PEF and PS will be studied through the same methodology applied for PLA in order to confirm the most important conclusions. Then the results obtained from three materials will be summarized to provide some answers for the main problematic of thesis. Discussions and elements of theoretical reflections will be developed in Chapter V.

Chapter II
Materials & experimental techniques

This work deals with the influence of molecular orientation on the mechanical behavior of PLA films. The role of strain-induced phases as well as chain orientation in the ductility improvement will be carefully investigated. Two PLA grades, a crystallizable and a non crystallizable one, will be compared in order to separate the respective effects of crystalline structure and macromolecular orientation on the mechanical behavior.

In addition of PLA which will be the main studied material, two other glassy polymers, Poly (ethylene 2.5-furandicarboxylate) (PEF) and Polystyrene (PS) films will also be investigated as complementary materials. The purpose of studying these materials is to highlight a common effect of chain orientation on mechanical behavior of glassy polymers upon tensile test.

In this chapter, a description of the materials used in this study and their elaboration processes will be firstly presented. This will be followed by a detailed presentation of the techniques and methodologies used in this work.
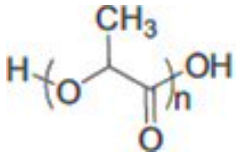
II.1.   Materials of study

II.1.1.   The Polylactide: PLA

The main material investigated in this study is PLA. Pellets of PLA used in this study are purchased from NatureWorks LLC. Two grades of PLA are used: a crystallizable grade 4043D noted as C-PLA and a non- crystallizable grade 4060D noted as NC-PLA.

Material characteristics

PLA used in this thesis is a copolymer PDLA containing D-isomer as the minor unit. Some molecular characteristics of the two PLAs used in this study are summarized in *Table II. 1*.

Table II. 1. Molecular characteristics of the two grades of PLA used in thesis.

Chemical form	Characteristics	PLA 4043D	PLA60D
$(C_3H_4O_2)_n$.	M_n (kDa)[1]	75	61
	M_w (kDa)[1]	124	104
	Density(g/cm^3)[2]	1.24	1.24
	D-isomer content[2]	~10%	~2%
	T_g (°C)[2]	55-60	

[1]determined by means of GPC on PLA films   [2]provided by Natureworks

It is well known that the crystallization ability of PLA is modulated by the content of D-isomer. The different crystallization behavior of the two PLAs will be studied in chapter III.1 through isothermal crystallization analysis.

Film extrusion

Both materials were elaborated using a cast extrusion line type LE25-30/C (Figure II.1): the extrusion temperature was fixed at 190°C; then films were casted on a chill-roll at room temperature, as presented in *Figure II. 1*. Before casting, the pellets of PLA were dried overnight at 60ºC under vacuum. Note that the roll speed was adjusted in order to prevent or at least minimize any orientation into the film. For each grade of PLA, two film thicknesses of 100 and 500µm respectively are prepared in order to fulfill different requirements of the characterization methods presented in the next sections.

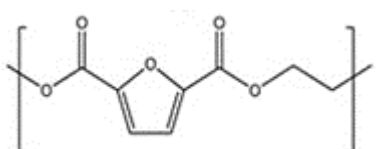*Figure II. 1. Extrusion processing line used for film elaboration.*

II.1.2.   Complementary materials of study: PEF& PS

In order to generalize the observations made in the case of PLA, a similar approach has been applied to other glassy polymers and the results have been compared with those obtained for PLA. In our study, two materials were chosen as additional materials: polyethylene 2,5-furandicarboxylate (PEF) and polystyrene (PS).

II.1.2.1.   Polyethylene 2,5-furandicarboxylate

Among all the emergent bio-based polymers, Polyethylene 2,5-furandicarboxylate (PEF) is one of the most interesting and promising biopolymers. It is foreseen as a potential alternative material to replace the use of traditional petroleum-based polyethylene terephthalate (PET). The PEF film studied in this thesis are synthesized and kindly provided by Corbion LLC. The material characteristics are available in *Table II. 2*.

Table II. 2. Macromolecular characteristics of the PEF resins.

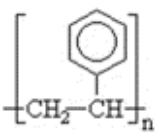| Chemical form	Characteristics[1]	PEF
$(C_8H_6O_5)_n$	M_n (kDa)	26
	M_w (kDa)	46
	Density(g/cm^3)	1.43
	T_g (°C)	85

[1]provided by Corbion

Resins were first dried before extrusion below a moisture content of 50 ppm. Extruded cast film was elaborated using as single screw extruder at 255 °C. The obtained cast was cooled using a 30 °C cooling drum. The average obtained sample thickness was around 350µm.

II.1.2.2. Polystyrene

Polystyrene is selected as the reference material. Indeed, the pioneering studies dealing with the topic of this PhD thesis were carried out on PS. In addition, PS is often mentioned as a reference material regarding the crazing mechanism and the B-D behavior.

Pellets of PS used in this study, grade Styron^{TM} 685D, are purchased from Trinseo LLC. The chosen grade of PS is inspired by the work of (Choi et al., 1989). A few material characteristics are summarized in *Table II. 3*.

Table II. 3. Molecular characteristics of polystyrene used in thesis.

Chemical form	Characteristics	PS
$(C_8H_8)_n.$	M_n (kDa)[1]	121
	M_w (kDa)[1]	232
	Density(g/cm^3)[2]	1.04
	T_g (°C)[2]	90-95

[1]determined by means of GPC   [2]provided by Trinseo

Film extrusion is carried out on a cast-extrusion line type LE25-30/C with extrusion temperature set at 220 °C. As proceeded in extrusion of PLA, films are casted to chill-roll at room temperature with adjusted roll speed preventing orientation into the extruded sheets. Two film thicknesses of 100 and 500µm are prepared for different characterization techniques.

II.2.   Elaboration& Characterization techniques

II.2.1.   Mechanical tests

II.2.1.1.   <u>Stretching above glass transition temperature</u>

In order to induce uniaxial or biaxial orientation into the materials of this study in a controlled manner, a biaxial stretcher, type Karo IV (Brückner), has been used. The equipment, as illustrated in *Figure II. 2*, consists in a first zone (marked by the red square) where the sample is loaded and released and two separate ovens where stretching and post- stretching treatments can be performed according to the parameters previously entered in the control panel.

Figure II. 2. A photo of biaxial stretcher with zoom of central film stretching zone.

Samples are fixed by seven pneumatic clamps on each side and can be stretched until a maximum draw ratio (λ) x (λ) of 7x7 ($\lambda = \frac{Final\ stretched\ length}{initial\ length}$). The stretching speed can be chosen from 1 to 500mm/s. In addition two stretching modes are available:

1) Simultaneous mode: the sample is stretched simultaneously along machine direction (MD) and transversal direction (TD). (MD, TD and ND direction are depicted in *Figure II. 2*).

2) Sequential mode: the sample is stretched first in one direction (MD) and then in the transverse direction (TD).

In our study, sample of 120 x 120 mm^2 squares were cut from film rolls and placed into the clamps. The final useful length of each side is 100 mm. On each sample, a grid is printed with ink in order to confirm the homogeneity of the deformation during stretching.

Note that in any case, the sample was placed into the stretcher with the extrusion direction parallel with respect to MD.

Biaxial stretching

In order to obtain biaxially oriented samples, draw ratios λ_{MD}xλ_{TD} up to 4.5x4.5 were performed at draw temperatures T_d ranging from 70 to 110°C (the temperature range choice will be discussed in chapter III.1) with stretching rates ($\dot{\epsilon}$) varying from 0.01 to 5/s.

For each test, samples are preheated at T_d during 60s in order to reach thermal equilibrium before being stretched. Only simultaneous stretching mode is applied in this study and the forces applied along both MD and TD are recorded. In order to freeze the microstructure in its stretched state, the BO films were directly quenched to room temperature under tension at the end of biaxial stretching and then unloaded from the stretcher. Then they are carefully stored at room temperature (around 23°C) before characterizations. A schematic illustration of the biaxial stretching process and an example of stretched film are available in *Figure II. 3*.
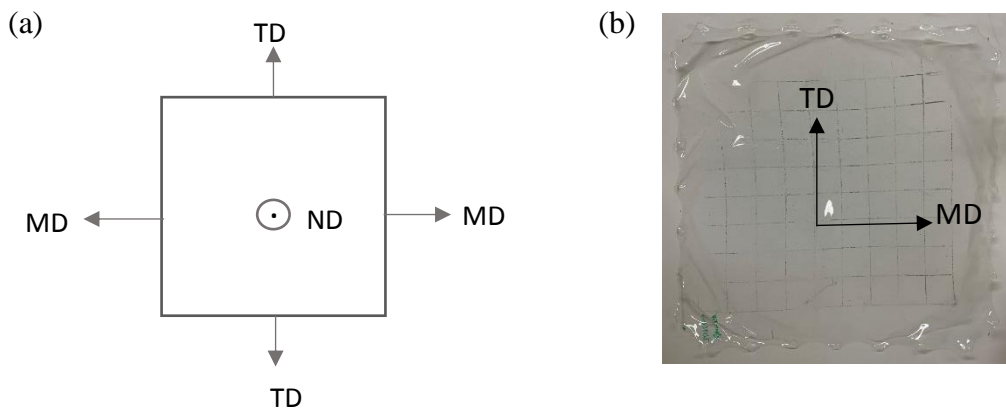

Figure II. 3. (a) Schematic illustration of a film being biaxially stretched (b) An example of BO film.

The film thicknesses of stretched films are summarized in *Table II. 4*.

Table II. 4. Average thickness of biaxially stretched films of various draw ratios (measured with a micrometer).

λ_{MD} x λ_{TD}	Average film thickness (µm)		
	PLA	PS	PEF
As-cast	~500	~500	~350
2x2	~125	~125	~85
2.5x2.5	~90	~90	~60
3x3	~55	~55	~40
3.5x3.5	~40	~40	~30
4x4	~30	ND	~22
4.5x4.5	ND	ND	~18

Uniaxial stretching

To produce uniaxially oriented samples, the stretching process can also be carried out in the same equipment. Sample of 120 x 100 mm^2 (MDxTD) were prepared and loaded to the stretcher. In this study the stretching direction is parallel to MD (useful length=100mm) and along the transversal direction, TD, the film is non-clamped and free to contract. A schematic illustration of uniaxial stretching is presented in *Figure II. 4*.
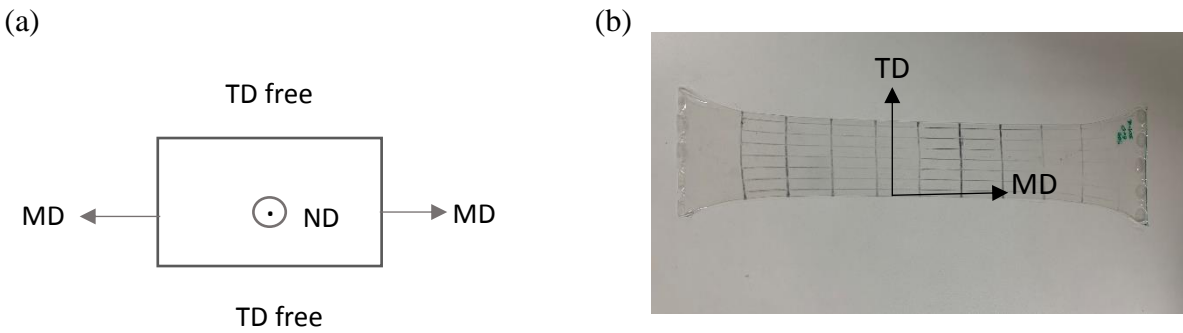

Figure II. 4. (a) Schematic illustration of a film being uniaxially stretched (b) An example of UO film.

The conditions used for uniaxial stretching are:

- A stretching temperature selected in the 70 to 110°C range (i.e. above the glass transition temperature of the materials)

- A stretching rate from 0.1 to 1/s.

Except for the study of the physical ageing effect on mechanical properties of BO samples, all types of films, whether the as-cast or stretched, have undergone the same period of physical ageing (at room temperature) before being characterized. Particularly for uniaxial tensile test at room temperature, all tests were conducted only few hours after the stretching process.

II.2.1.2. Uniaxial tensile test at room temperature

Tensile testing is a fundamental testing method for analyzing mechanical properties of materials. A sample is fixed between two clamps and elongated uniaxially until failure. The necessary force used to deform sample and real- time displacement will be recorded during the test. Finally, an engineering stress- engineering strain curve will be plotted using equations:

$$\text{Engineering stress } \sigma = \frac{F}{S_0} \tag{II.1}$$

$$\text{Engineering strain } \varepsilon = \frac{\Delta L}{L_0} = \frac{L - L_0}{L_0} \tag{II.2}$$

With F the recorded force during the test, S_0 the initial cross-section, L_0 the initial length of the sample and ΔL which correspond to the displacement of the clamp.

Uniaxial stretching was performed on an Instron 4466 apparatus. Tests were carried out at 23±2°C (i.e. far below the glass transition temperatures of the materials) using an initial stretching rate $\dot{\varepsilon} = 4 \times 10^{-3} \text{ s}^{-1}$ ($\dot{\varepsilon} = \frac{V_{transversal}}{L_0}$). For each type of sample, either oriented or not, at least five dumbbell specimens with 28 mm and 5 mm in gauge length and width respectively were tested.

II.2.1.3. Dynamic Mechanical Analysis

Viscoelastic properties of materials were studied by means of Dynamic Mechanical Analysis (DMA), which is a technique that is widely used to characterize the material's properties as a function of temperature, time, frequency, stress or a combination of these parameters. DMA

experiments consists in applying a controlled sinusoidal sollicitation (stress or strain) to a sample. The experimental conditions are such that the sample is sollicited in its linear viscoelastic domain. In this context, the response is also sinusoidal with a shift depending of the contribution of the viscous and elastic part.

In this study the DMA measurements were performed on a strain-controlled apparatus type RSA3 (TA instruments) according to different test methodologies described below.

DMA analysis in tensile mode

As sinusoidal deformation is applied to the sample:

$$\varepsilon(t) = \varepsilon_0 \sin(\omega t) \tag{II.3}$$

The measured stress, which is shifted to an angle of δ compared to the strain signal can be presented as:

$$\sigma(t) = \sigma_0 \sin(\omega t + \delta) \tag{II.4}$$

The ratio between the response and the solicitation gives access to the complex modulus defined by

$$E^* = \frac{\sigma^*}{\varepsilon^*} = E' + iE'' \tag{II.5}$$

With

- $E' = \frac{\sigma_0}{\varepsilon_0} \cos(\delta)$ as the storage modulus representing the elastic part of the response.
- $E'' = \frac{\sigma_0}{\varepsilon_0} \sin(\delta)$ the loss modulus measuring the energy dissipated as heat, i.e., the viscous part of the response.
- $\tan \delta = E'/E''$ the tangent of the loss angle, also called damping factor.

During this study, samples of 5mm width and of 15mm of gauge length are solicited with a constant strain $\varepsilon_0 = 0.01\%$. A frequency of 1Hz is used within temperature range 20-110°C. Few tests have been carried out with different testing conditions. This will be detailed in the text when needed.

Determination of the relaxation time of molecules: the Doi-Edwards model

Doi and Edwards suggested that the relaxation process of polymers is the sum of three distinct processes: relaxation, retraction and reptation (Doi & Edwards, 1986). At each process, a specific characteristic time can be associated. In this context, the relaxation time τ_a can be written as a function of repeat units number n_e as the equation

$$\tau_a = \frac{a^2 \xi (M_e/M_0)^2}{6\pi^2 kT} \tag{II.6}$$

Where M_e is the molecular weight between entanglements, M_0 the repeat unit molecular weight, a the characteristic length of the repeat unit, ξ the friction coefficient, k the Boltzmann constant and T the temperature.

The retraction time, τ_b, is proportional to the square of the chain molecular weight as the equation:

$$\tau_b = 2\tau_a (n/n_e)^2 \tag{II.7}$$

Where n the number of repeat units per chain defined by M_n/M_0, n_e the number of repeat units between entanglements defined by $n_e = M_e/M_0$, M_n the number-averaged molecular weight. Finally, the reptation time τ_c, is proportional to the cube of the chain molecular weight as the equation:

$$\tau_c = 6\tau_a (n/n_e)^3 \tag{II.8}$$

The determination of τ_a, τ_b, τ_c using the Doi-Edwards model requires the knowledge of M_e, a and ξ. These parameters can be determined from rheological measurements.

a) The determination of M_e

The entanglement molecular weight, M_e , was determined from the DMA viscoelastic measurements for both types of as-cast PLA using the following relation:

$$G_n^0 = \frac{\rho RT}{M_e} \tag{II.9}$$

Where ρ is the material density (equals to 1.24 g/cm^3 (Sin et al., 2013) for both types of PLA), T the temperature, R the perfect gaz constant, and G_n^0 the value of storage modulus taken when loss modulus reaches its minimum after the principal relaxation stage.

Note that the shear modulus G can be deduced from the Young modulus E through the relation

$$G = \frac{E}{1+2\vartheta} \tag{II.10}$$

With ϑ the Poisson's ratio. Particularly ϑ has been taken equal to 0.5 as soon as the material is in the rubbery state. The value of elastic modulus E_n^0 was taken on the rubbery plateau at the temperature where the minimum of tanδ is observed, as shown in the *Figure II. 5*.
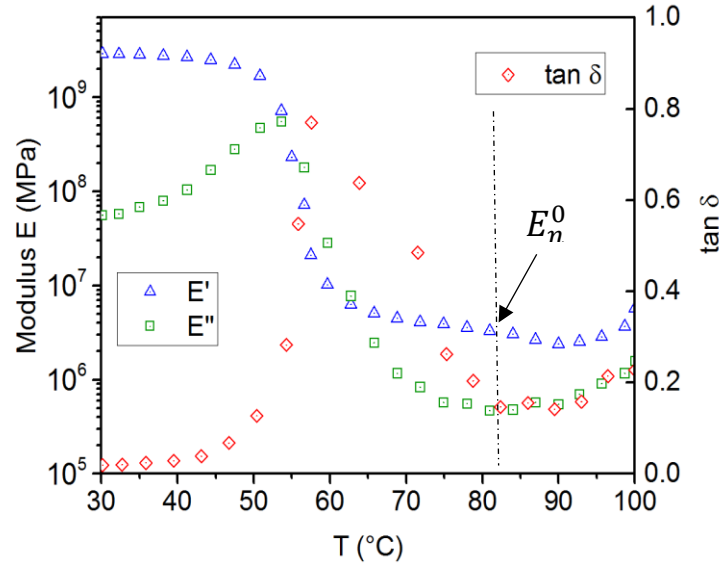

Figure II. 5. Evolution of E', E'' as a function of temperature for as-cast C-PLA.

b) <u>The determination of $a^2\xi$</u>:

It is possible to determine the value of $a^2\xi$ from the master cuves built at a given reference temperature T_{ref} using the time- temperature superposition principle (Ferry, 1980). The relaxation times will be calculated at this reference temperature.
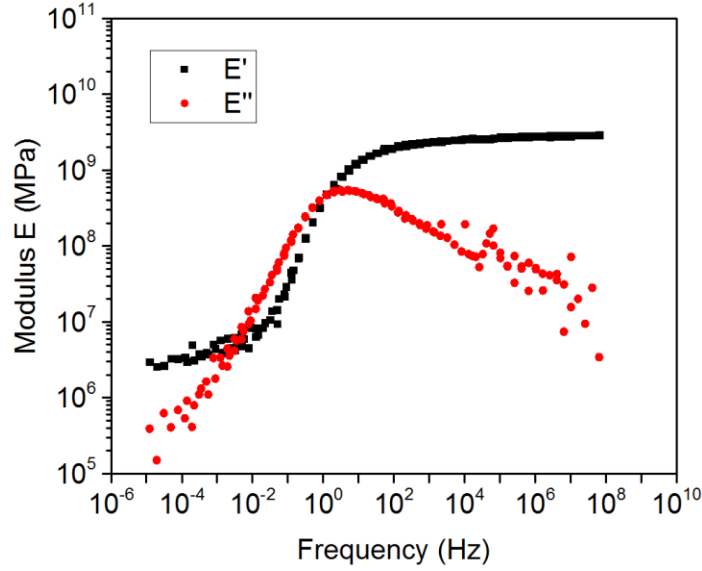
Figure II. 6. Master curves build at $T_{ref} = 55°C$ for an as-cast C-PLA

using the time-temperature superposition principle.

Figure II. 6 illustrates the master curve of E' and E'' at T_{ref} equals to 55°. It can be seen from this figure that there exists a small range of frequency where E' equals to E'', both are proportional to the square root of frequency f. According to the Rouse theory, the relaxation times are sufficiently short to allow the following expression

$$G' = G'' = \left(\frac{a\rho N}{4M_0}\right)[\xi kT/3]^{1/2}f^{1/2} \tag{II.11}$$

Where N the Avogadro number and other parameters already been defined. With the knowledge of the values of E' and E'' and with relation (II.10), it is possible to deduce the value of $a^2\xi$.

Finally with the determination of M_e and $a^2\xi$, the charactersitic relaxation times can be calculated using equations mentioned in (II.6), (II.7) and (II.8) according to each reference temperature. In this study the T_{ref} is tested from 30 to 80°C. Above 80°C the status of PLA film becomes too viscous to proceed accurate measurement.

II.2.2.   Thermal properties analysis

Thermal properties of samples were analyzed by differential scanning calorimetry (DSC), which is a common thermal analysis in which the difference in the amount of heat required to increase the temperature of a sample and reference is measured as a function of temperature. The basic

principle of this technique is to always maintain the temperature measured in sample pan equals to the one of reference pan. When the sample undergoes phase transitions, more or less heat will be needed to keep the same temperature as reference. The increase or decrease of heat flow depends on whether the process is exothermic (such as crystallization) or endothermic (such as melting). In addition, the variation of calorific capacity during glass transition will also be recorded.

In this study DSC measurements were performed on a Perkin Elmer Q20 apparatus. Samples of about 10 mg were placed into aluminum pans and heated at 10°C/min on the temperature range: 20-180°C under a nitrogen atmosphere. The temperature and heat flow were calibrated using a high purity indium sample according to standard procedures.

Characteristic thermal properties are determined from the obtained thermograms. The glass transition temperature T_g is defined as the temperature at the half value of step change of heat capacity (C_p). Cold crystallization T_{cc} and melting temperature T_m were taken at the maximum of the corresponding peaks. The standard melting enthalpy ΔH_m^0 has been taken equal to 93J/g for PLA (Arnoult et al., 2007).

Reference samples (as-cast)

Note that the thermograms obtained for unstretched films (as- cast) were measured on isotropic films that have undergone the same thermal treatment (temperature, duration) as the highest biaxially drawn films. These thermally treated unstretched samples will be considered as reference samples.

II.2.3.   **Structural characterization**

II.2.3.1.   2D WAXS analysis

Wide Angle X-ray Scattering (WAXS) is one of the main method to characterize the structure of solid materials. When an X-ray beam is send on matter, photons interact with the internal structure of the material and the re-emitted waves scattered by atoms can result in diffuse scattering as well as constructive or destructive interferences. Particularly, the interferences are constructive when Bragg condition is satisfied:

$$2d \sin \theta = n.\lambda \qquad\qquad (II.12)$$

with n=1, 2, 3…the order of interference, d the interplanar distance of the considered (hkl) plane, 2θ the Bragg angle and λ the wavelength used.

In our study, WAXS experiments were carried out owing to a Xeuss apparatus (XENOCS). The equipment is composed of a microsource using the Cu Kα radiation (λ= 1.54 Å), collimated and monochromatized by a FOX3D optic. 2D WAXS patterns are collected on a Pilatus 200k hybrid pixel detector (Dectris). The sample-to-detector distance is precisely determined using reference sample (AgBe powder).

1D intensity files are computed using the Foxtrot® software by radial integration of the 2D WAXS/SAXS patterns. Standard corrections, such as dark current and background removal, were applied before analysis. Note that for bi-oriented samples, diffraction patterns are recorded along M, T, N directions and average diffractograms were calculated from extracted intensity profiles. A schematic presentation of collection of 2D image is presented in *Figure II. 7*.
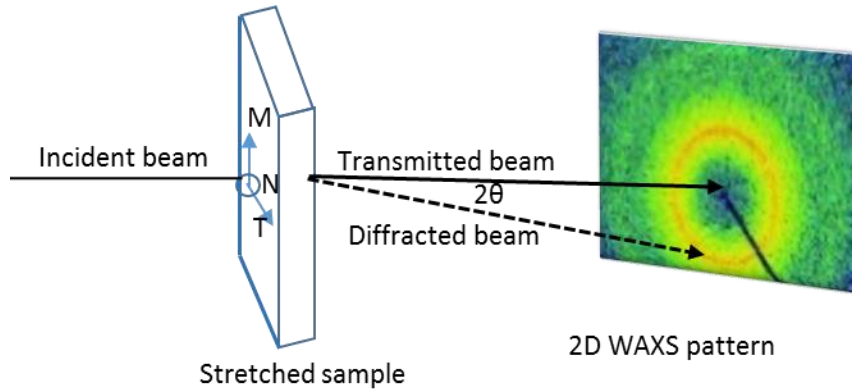

Figure II. 7. Example of 2D WAXS pattern obtained for a biaxially stretched PLA (MT plane).

The determination of the phase(s) content(s) is proceeded by deconvolution of the average intensity profile $I = f(2\theta)$ using the Peakfit® software. Gaussian functions are used in a fitting process as previously used in literature (Mano, 2007). A Gaussian function can be expressed by

$$I(x) = I° \times e^{-0.5 \times \left[\frac{x-x°}{\Delta x}\right]^2} \tag{II.13}$$

with $x°$ the central peak position, Δx the full-width at half-maximum (FWHM) value and $I°$ the maximum peak intensity.

Deconvolution is performed in the 2θ range: 2° - 58°. The profile for as- cast, i.e. fully amorphous PLA, was deconvoluted into four components with 2θ≈ 15.5°, 2θ≈ 21.7°, 2θ≈ 30.4° and 2θ ≈ 43.8° as proposed in (G. Stoclet, Seguela, Lefebvre, & Rochas, 2010). An example of deconvolution of cast PLA can be seen in *Figure II. 8*. For each simulation the four representative components of amorphous phase were fixed in terms of peak position and FWHM values.
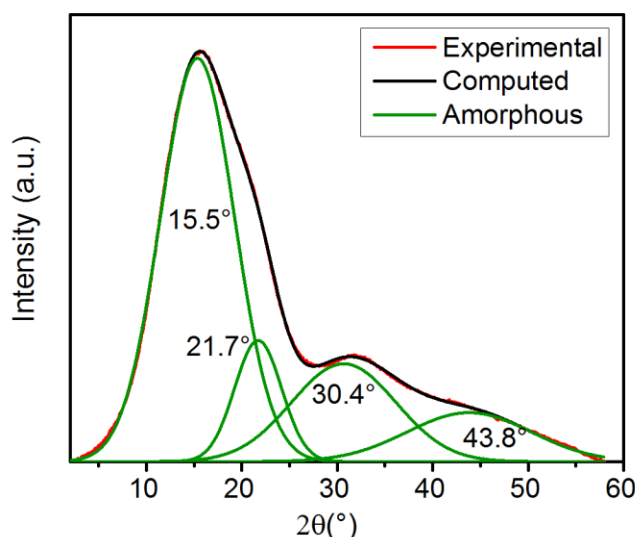

Figure II. 8. Example of the deconvolution profile of an as-cast C-PLA.

After stretching, it is possible that other phases are present into the sample. In this case, the corresponding WAXS patterns require the addition of new Gaussian functions apart from those defined for the amorphous phase in order to achieve a proper fitting.

During this work, two cases have been identified:

   Deconvolution of the intensity profile of PLA containing mesophase

Figure II. 9 depicts an example of deconvolution of a PLA where mesophase is induced. It is found that two new peaks at 2θ≈ 16.2° and 2θ≈ 32.8° have to be added to the profile in order to properly deconvolute the intensity profile. These functions are characterized by FWHM values (typically around 2°) intermediate between the FWHM of amorphous peaks (typically 5°) and the FWHM of crystalline peaks (typically 0.5°).
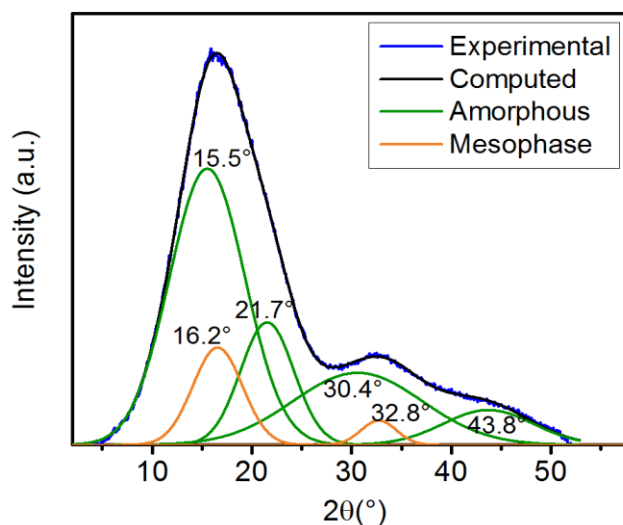
Figure II. 9. Example of deconvolution profile of a C-PLA biaxially stretched at 3.5x3.5 at 70°C.

<u>*Deconvolution of the intensity profile of PLA containing a crystalline phase*</u>

Figure II. 10 shows an example of deconvolution of a semi-crystalline PLA sample (in this case the α' crystalline form is involved). It is observed that, by adding Gaussian functions of peaks at $2\theta \approx 14.8°$, $2\theta \approx 16.5°$, $2\theta \approx 18.5°$ and $2\theta \approx 32.5°$ to the formerly defined functions for amorphous phase, the fitting is satisfying. The new peaks are functions with small FWHM values (usually ≈0.5°) characteristic of long range order.
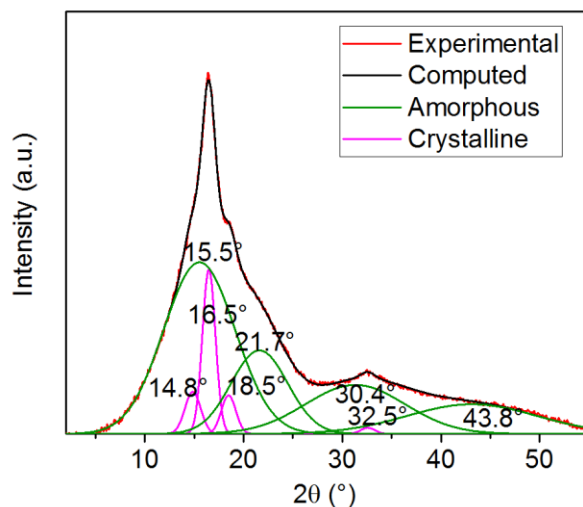

Figure II. 10. Example of the deconvolution of a profile of a C-PLA biaxially stretched at 3.5x3.5 at 80°C.

63

Note that the positions of the peaks characteristic of the mesomorphic or crystalline phases, were found to be in agreement with what has been reported in (Oh & Kim, 2014; G. Stoclet, Seguela, Lefebvre, & Rochas, 2010).

From these deconvolutions, the proportion of the different phases can be calculated by dividing the area of the peaks characteristic of the phase by the total area scattered. The obtained values will be compared to the quantification results determined by means of DSC.

II.2.3.2. Trichroic FTIR

The quantification of chain orientation in BO films is complex and only a few analyses techniques allows it. In order to calculate the orientation function of molecular chain along M, T and N directions, trichroic FTIR methodology has been applied. Spectrum S_M, S_T are directly measured with polarization along M, T directions respectively. The third spectrum, S_N, is accessed through a trichroism configuration which has already been used in (Cole et al., 2004; Fereydoon et al., 2014; Sallem-Idrissi et al., 2009). After the measurement of S_M, S_T, the film is tilted at 45° around T axis in the plane MN, as presented in *Figure II. 11*. Then two new spectrum S_{MN}, S'_T are measured with polarization perpendicular and parallel to T axis, respectively.
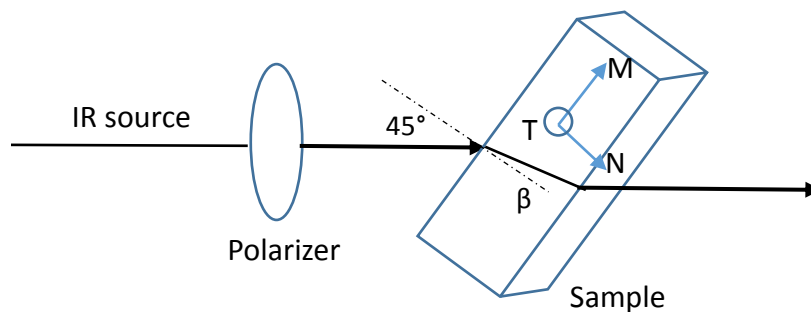

Figure II. 11. Schematic presentation of the principle of "tilting" sample measurement.

The refracted ray makes an angle of β with the normal of sample plane according to the law of Snell- Descartes:

$$\sin \beta = \frac{\sin 45°}{n} \tag{II.14}$$

With n the refractive index of polymer which equal to 1.46 for PLA (M. H. Hutchinson et al., 2006).

Then the two new spectrum, S_{MN}, S'_T can be written as

$$S_{MN} = \frac{S_M \cos^2 \beta + S_N \sin^2 \beta}{\cos \beta} \tag{II.15}$$

$$S_T' = \frac{S_T}{\cos \beta} \tag{II.16}$$

Spectrum S_N is then deduced from equations (II.14, II.15, II.16)

$$S_N = \frac{\cos \beta}{\sin^2 \beta} (S_{MN} - S_M \cos \beta) \tag{II.17}$$

Or more precisely,

$$S_N = (2n^2)\sqrt{1 - \frac{1}{2n^2}} \times S_{MN} - (2n^2 - 1) \times S_M \tag{II.18}$$

The structural factor S_0 (or the average spectrum) is calculated by

$$S_0 = \frac{1}{3}(S_M + S_T + S_N) \tag{II.19}$$

For a certain vibration mode, the orientation function can be calculated using

$$f_{ij} = \frac{1}{2}(3\cos^2 \theta_{ij} - 1) \tag{II.20}$$

Where f_{ij} is the Hermans function, corresponding to the orientation function of axis i of molecular chain with respect to considered direction J. When transition moment is along axis i, the expression of f_{ij} becomes:

$$f_{ij} = \frac{1}{2}(D - 1) \tag{II.21}$$

With D the trichroic ratio

$$D = \frac{A_J}{A_0} \tag{II.22}$$

Where A_J, A_0 the absorbance in J (J=M, T, N) and S_0 spectra respectively.

In an orthogonal system,

$$f_{iM} + f_{iN} + f_{iT} = 0 \tag{II.23}$$

According to expression (II.21), f_{ij} varies from minimum value of -0.5 when axis i is perpendicular to direction J and to a maximum value of 1 when axis i is parallel to J. *Table II. 5* summarizes the ideal situation for uniaxial and biaxial orientations.

Table II. 5. Orientation factors in the case of perfect uniaxial and biaxial orientations.

Orientation function	f_{cM}	f_{cT}	f_{cN}
Perfect uniaxial orientation	1	-0.5	-0.5
Perfect biaxial orientation	0,25	0,25	-0,5

One way to present the orientation functions is to use a Wilchinski diagram (*Figure II. 12*). For this triangular plot, each apex represents a perfect orientation in one direction J (J=M, T, N), in this case f_{ij} =1. The center of triangle stands for isotropic status where f_{ij} =0. Each side of plot corresponds to f_{ij} =-0.5, meaning an axis i is perpendicular to the direction J which is the apex opposite to the considered side.
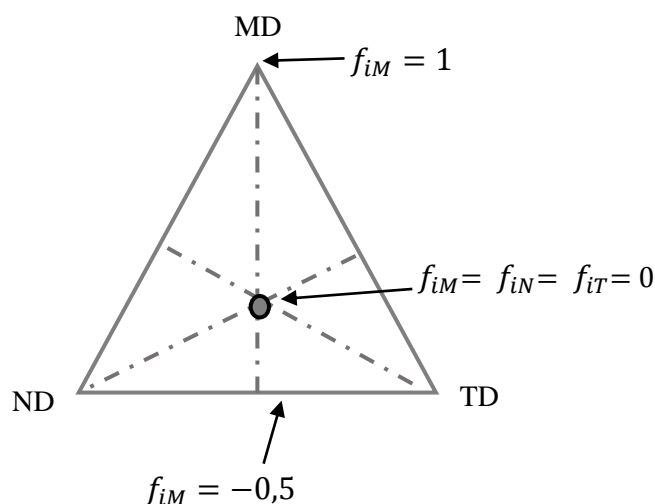

Figure II. 12. Description of molecular orientation in a Wilchinski diagram.

In our study, FTIR spectra were collected in transmission mode on a Bruker VERTEX 70v spectrometer equipped with a DTGS detector and a rotating wire grid polarizer. Every FTIR spectrum consisting of 64 scans was recorded over the wavenumber range 370–3500 cm^{-1} with a resolution of $2cm^{-1}$. Note that before computing any calculations, all obtained spectra were first

of all proceeded with background subtraction and baseline correction. A typical non- polarized spectrum obtained for a biaxially stretched PLA is shown in *Figure II. 13*. Band assignment is summarized in *Table II. 6*.
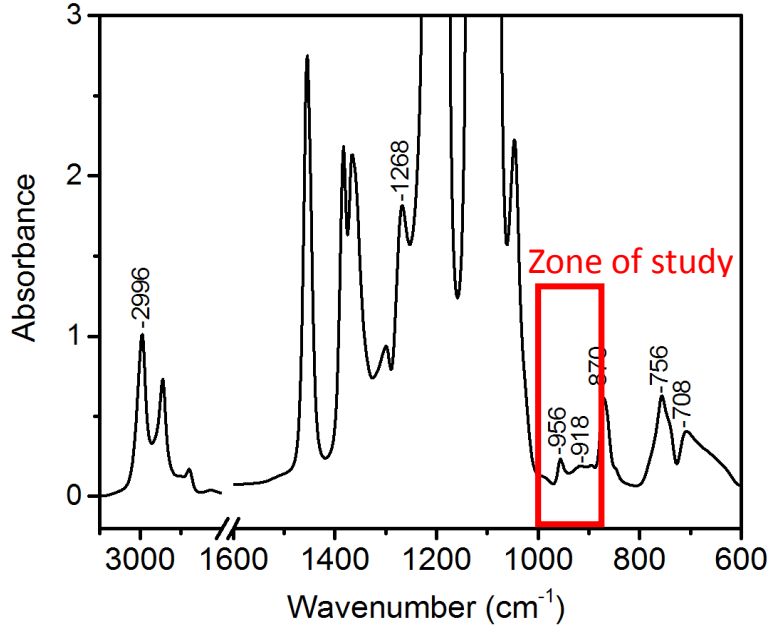

Figure II. 13. Typical non-polarized FTIR spectrum obtained for BO C-PLA stretched at 70°C.

Table II. 6. Band assignment for characteristic bands of PLA (Hu et al., 2012; Meaurio et al., 2006; J. Zhang et al., 2005).

IR frequency (cm^{-1})	Polarization	Assignment	Phase
2996	-	$\vartheta_{as}(CH_3)$	Internal band
1268	⊥	δ (CH) + ϑ (COC)	Amorphous
956	∥	$r(CH_3)$ + ϑ (C-C)	**Amorphous**
918	⊥	/	**Mesophase**
922	⊥	ϑ (C-C) + $r(CH_3)$	**α/ α'**
871	⊥	ϑ (C-C OO)	α/ α'/ Mesophase
757	⊥	δ (C=O)	α/ α'/ Mesophase
708	∥	r (C=O)	Mesophase

The backbone vibration of PLA refers to absorbance in the wavenumber range 975-825 cm^{-1}.In our work this region is specifically chosen as principal zone of study as the band at 956 cm^{-1} and the bands at 918/922 cm^{-1} are distinct bands characterizing amorphous and crystalline/mesomorphic phase respectively. These bands are sensitive to conformational change and interesting to study since the band intensities are relatively low so that problems like band saturation can be well avoided during calculations. The band at 2996 cm^{-1} is not sensitive to conformational change, which can be used as reference band when normalization of spectrum is required.

II.2.4. Characterization of plastic deformation mechanisms by means of Small Angle X-ray Scattering analysis

Small Angle X-ray Scattering analysis is particularly well adapted to the analysis of crazing mechanism. In this thesis SAXS is used as main characterization technique to study the elementary deformation mechanism upon uniaxial stretching. Both in-situ test and post-mortem scanning experiment configurations are applied, as will be presented in details later in this section.

II.2.4.1. Analysis of a typical SAXS pattern of crazing

A typical SAXS pattern representing scattering from "standard" crazes with regular fibrillar internal structure is shown in *Figure II. 14*.
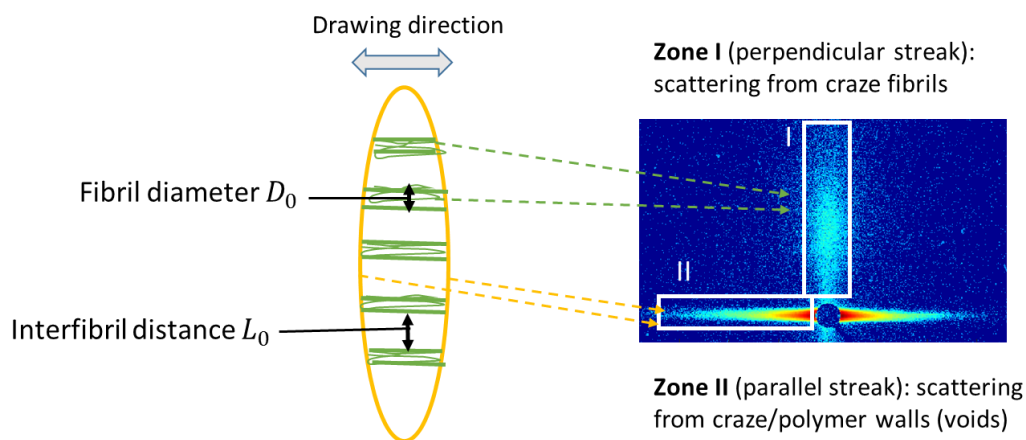

Figure II. 14. Schematic presentation of scattering from crazes and a typical pattern obtained during deformation of a cast PLA.

The collected SAXS patterns were corrected as done for diffraction analysis and the azimuthal integrated profiles are presented as a function of the scattering vector ($q = \frac{4\pi\sin(\theta)}{\lambda}$). It is well accepted in literature that the streak perpendicular to draw axis (zone I) stands for scattering from fibrils while the streak parallel to draw axis (zone II) stands for scattering from the craze/polymer walls (voids). The intensity profiles extracted from zone I and zone II give access to the craze fibril geometry structure and craze density respectively.

Analysis of zone I: craze fibril structure

The modeling of the intensity profile extracted from zone I can give access to the quantification of the internal structure of the craze, i.e. to the geometry of the fibrils. In this work, a cylindrical model has been used as form factor to describe the shape of fibrils. The scattering curve of a cylinder is depicted in *Figure II. 15.*
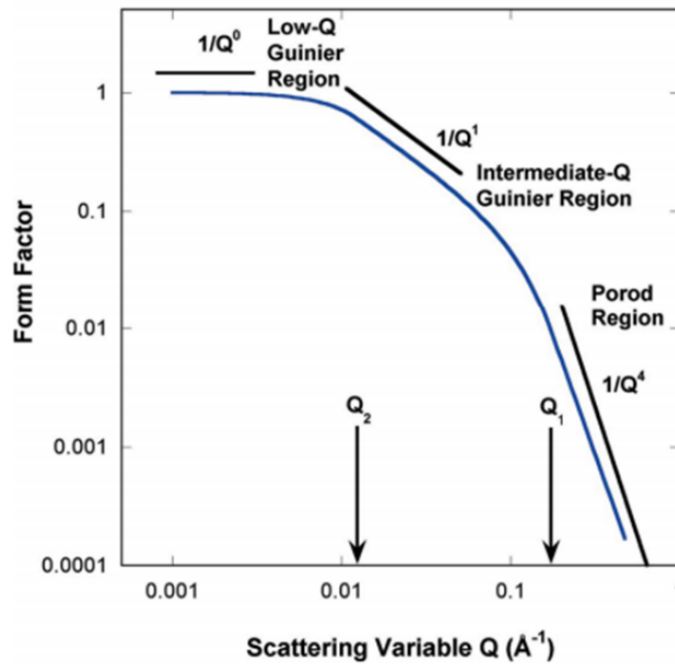

Figure II. 15: Typical scattering curve of a cylinder plotted using the Guinier-Porod model (Hammouda, 2010).

According to the Guinier-Porod analysis three distinct regions can be highlighted:

- The low q region, which corresponds to the Guinier region. The fact that the Guinier region is observable on a scattering profiles indicates that "the whole object is being analyzed".

- The intermediate q region which gives information about the shape of the scatterer. Particularly, in the case of a cylinder, a -1 slope is observed on a log(I)-log(q) representation.

- The high q region corresponds to the Porod region. This part is characterized by a -4 slope on a log(I)-log(q) representation.

Between each region, a slope change occurs at a specific q. The q position is proportional to a characteristic length of the scatterer. In our case, i.e. a cylinder, Q_1 is proportional to the radius R of the cylinder and Q_2 is proportional to its length L.

In addition to this form factor an interference function has been used as structure factor in order to take into account the fact that, inside the craze, fibrils are separated from each other at a roughly regular distance (L_0).

Based on this model, the fitting of intensity profile of craze fibril was done using the Irena macro which is a tool suitable for modeling and analysis of small angle scattering (Ilavsky & Jemian, 2009). An example of an intensity profile recorded in the zone I of a craze and the corresponding modeling is presented in *Figure II. 16*.
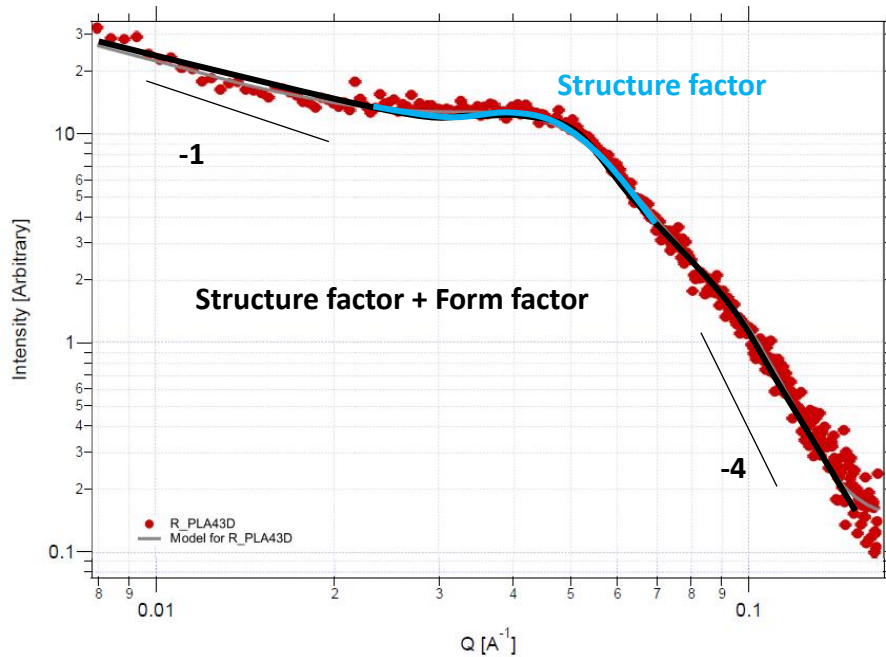

Figure II. 16. Fitting example of intensity profile obtained from integration of zone I using SAS^{TM} of an as-cast C-PLA.

As can be seen, the form factor (dark line) of the modeling curve is the same as illustrated in *Figure II. 15*. However, one can observe that the Guinier region is not observed here. Only the end of the -1 slope region and the Porod region are accessible in the SAXS range investigated. This indicates that the fibrils length are high leading to a transition region at very low q.

On this figure, a broad correlation peak (blue part) is also identified in the intermediate-q region superimposing with the form factor function (dark line). Consequently, from this modeling only the mean fibril diameter D_0 and the mean interfibrilar distance L_0 can be determined.

Analysis of zone II: craze density

Regarding the scattering in zone II, no quantitative information regarding the size of craze/polymer walls (or called as craze envelopes) could be obtained. Indeed, in the same manner as discussed for the fibrils length, craze envelope sizes are large leading to slope transitions in ultra-low q region which is not accessible using conventional SAXS.

Nevertheless, it is still interesting analyze the intensity profiles of zone II for that the scattering intensities at low q values are proportional to initiated craze density. For sake of accuracy the profiles obtained for as-cast and BO films will be first normalized with respect to film thickness and then analyzed as function of BO draw ratio.

II.2.4.2. Deformation mechanism study in Synchrotron

The in-situ study of the deformation mechanism was proceeded by recording the real-time SAXS patterns in order to determine the plastic deformation mechanisms involved during the uniaxial stretching at room temperature. Thanks to the in-situ character, the effects of relaxation on the characterization of the deformation mechanisms can be neglected.

In-situ SAXS analysis in this thesis was carried out in The European Synchrotron Radiation Facility (ESRF) located in Grenoble (France). A detailed introduction of this facility is exposed in Appendix-II. SAXS experiments were carried out at ESRF on the D2AM-BM02 beamline. A monochromatic beam at an energy of 10 keV (i.e. λ=1.26514 Å) was used with a sample to detector distance of 1.20 m. Mechanical tests have been performed thanks to a portable homemade stretching device designed so as to adapt on the beamline and allowing symmetrical stretching, as shown in *Figure II. 17*. Tests are performed at room temperature at a strain rate $\dot{\varepsilon} = 4 \times 10^{-3} \text{ s}^{-1}$.

(a)

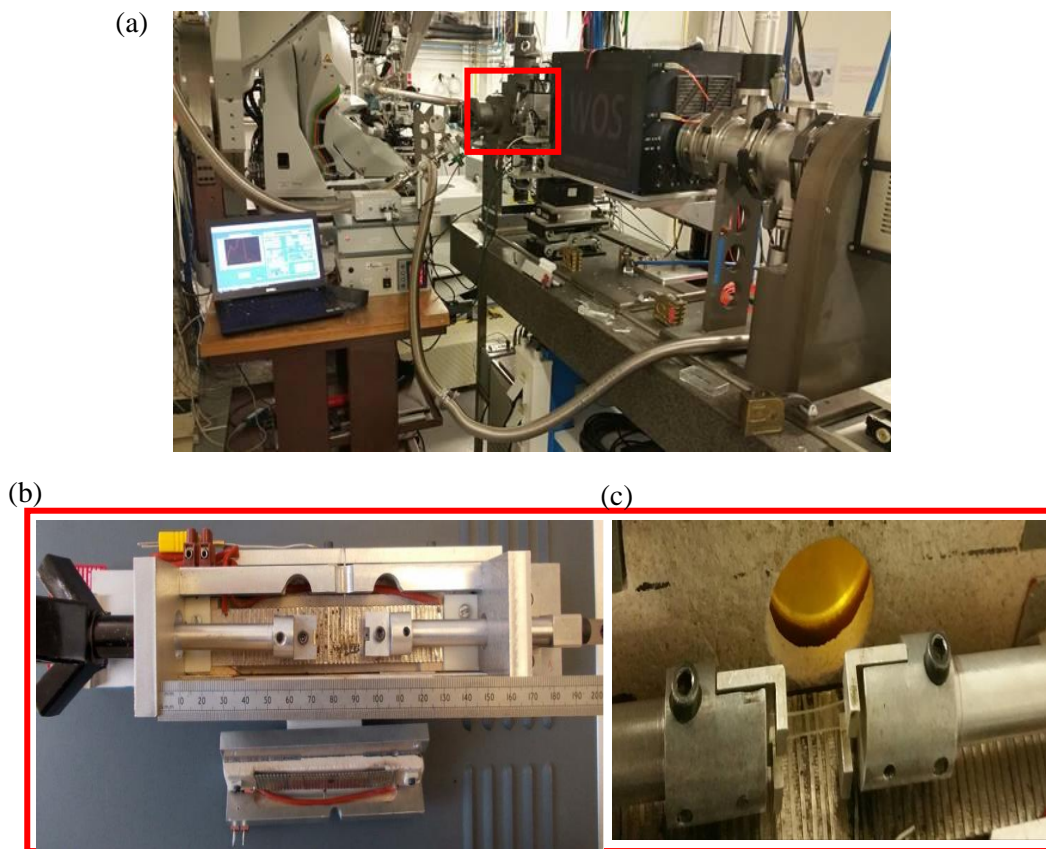(b)   (c)

Figure II. 17. (a) Photo of the experimental setup used during the experiments at ESRF and of the home-made stretching device (the drawing axis is horizontal): (b) top view and (c) front view with sample.

Unfortunately, due to the technical characteristics of the SAXS detector used (hybrid pixels D5 detector), the collected images will only be analyzed qualitatively. Indeed this kind of detectors has "dead zones" between the detection regions which involves missing q ranges, as shown in *Figure II. 18(a)*. The according log(I)-log(q) intensity profile extracted from scattering of fibrils (zone I) is presented in *Figure II. 18(b)*.
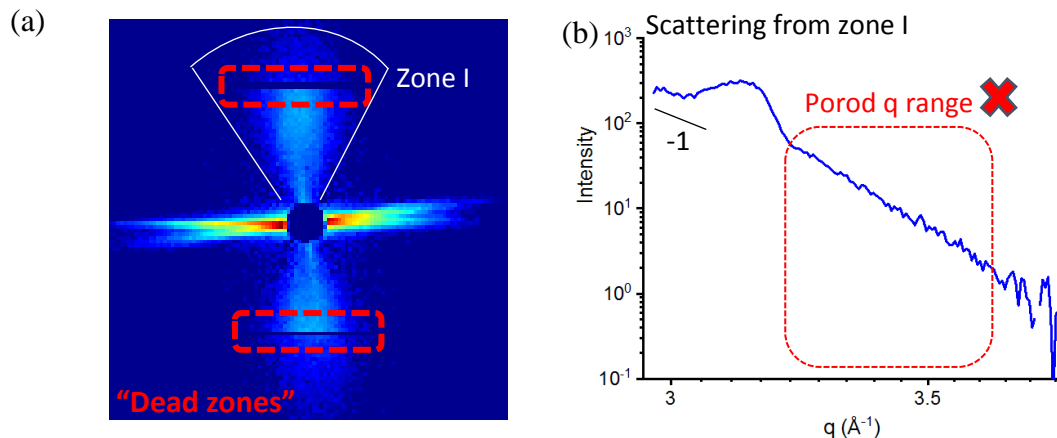
Figure II. 18. (a) A typical SAXS pattern containing "dead zones" obtained for an as-cast C-PLA during in-situ experiment in ESRF (b) The corresponding intensity profile of scattering from craze fibrils (zone I).

As can be seen from the figure, the "dead zones" are the thin black zones that cut horizontally the scattering region from craze fibrils (zone I). Consequently the according integrated intensity of zone I is incomplete for that the Porod-q region is missing so that no transition of slope can be observed when compared to previous examples shown in *Figure II. 15* and *Figure II. 16*. Therefore the modeling analysis on these profiles failed to provide any quantitative results related to craze fibrils. Similar problems were also encountered during the study of NC-PLA.

Considering such circumstances, the results of in-situ experiment carried out in ESRF experiments will only be analyzed qualitatively providing some preliminary understanding of the deformation mechanisms involved during stretching. A further quantitative estimation of craze-related geometric parameters was proceeded through a SAXS study using laboratory equipment that will be presented in the next section.

II.2.4.3. Deformation mechanism study on a laboratory equipment

"Pseudo in-situ" test

As previously discussed, the experiments conducted in ERSF allows a preliminary qualitative analysis of deformation mechanism. In order to extract quantitative information on the craze internal structure, complementary "pseudo in-situ" laboratory experiments have been carried out (*Figure II. 19(a)*). Unlike the real in-situ analysis formerly presented, the sample is "paused" under tension during the stretching in order to have enough time for the image recording *(Figure II. 19 (b))*. The same homemade stretching device as the one previously presented for synchrotron

experiments was used. The Cu Kα radiation (λ= 1.54 Å) was maintained and the sample- to-detector distance was set to 2.3 m (maximum available distance on our laboratory X-ray equipment) corresponding to the q range from 4.10^{-3}… to 0.13 Å^{-1}.
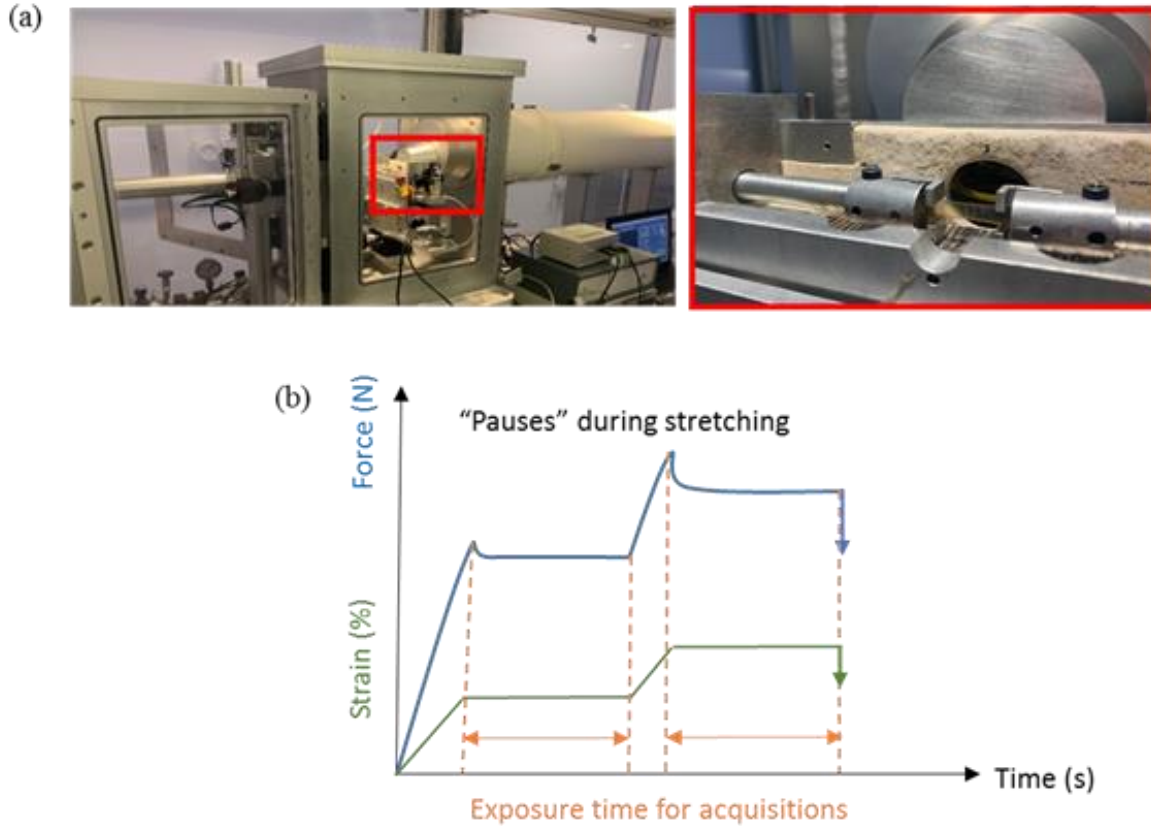

Figure II. 19. (a)"In-situ" SAXS experiment set-up in laboratory (b) Schematic illustration of a stress-strain curve with pauses during stretching.

Scan of post- mortem samples

Post- mortem SAXS scans were also carried out on the laboratory equipment using the same experimental parameters as chosen for "pseudo in situ" analysis in order to precisely determine the critical stress for craze initiation.

The detailed experimental steps are described as below:

1) Firstly the samples were stretched until breaking on the tensile test machine using always the same stretching conditions previously shown (23ºC, $\dot{\varepsilon} = 4 \times 10^{-3} \text{ s}^{-1}$).

2) Then the broken sample was examined post-mortem by means of according to a "scanning" method. Particularly, starting from the break point (white point), samples are scanned all along the useful length with the X-ray beam diameter set at 800µm. Successive acquisitions are performed for each 200µm (red points), as presented in *Figure II. 20*. For each step, a SAXS pattern is recorded and the according intensity profile is analyzed. A few patterns at critical positions (start point, a middle point, final point) are chosen to be illustrated.

3) Among the exhaustive SAXS patterns collected for the same sample, the objective is to find out and mark the first position where the scattering from craze is no more observed, i.e. the first position where a pattern of isotropic nature is detected (final point in *Figure II. 20*).
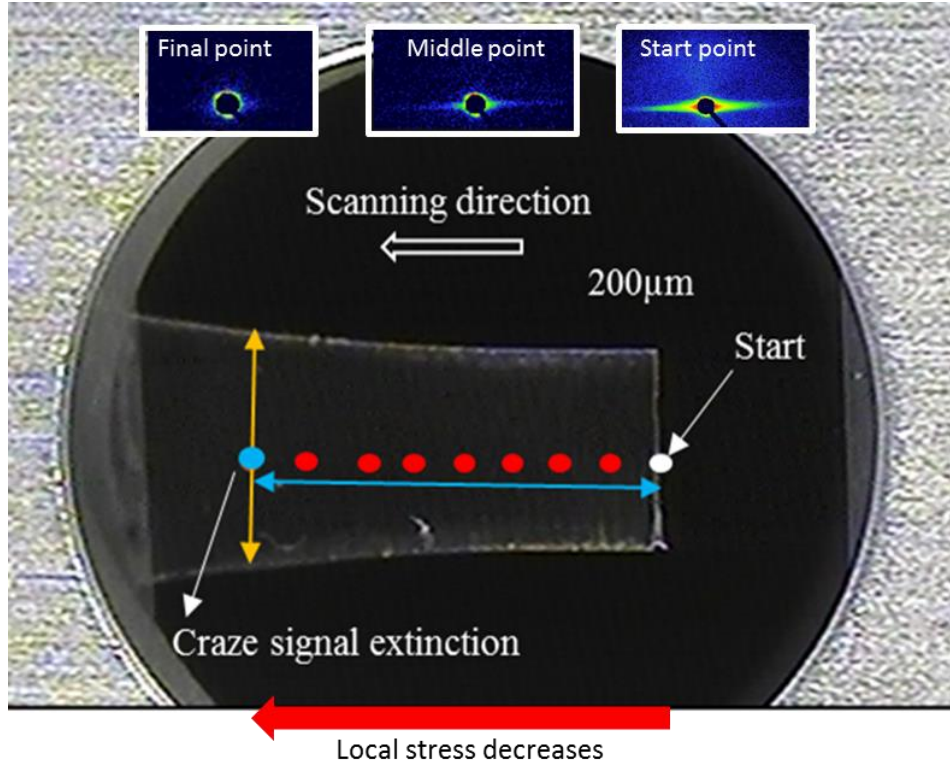

Figure II. 20. Schematic illustration of post-mortem scanning analysis.

This specific position can be considered as the one where craze where are first initiated. Consequently the critical macroscopic stress σ_{cr} applied to initiate crazing mechanism can then be deduced by the expression:

$$\sigma_{cr} = \frac{F_r}{S_c}$$ (II.24)

75

Where:

- F_r the fore at break measured from tensile test.

- S_c the sample section at craze signal extinction point which equals to L_c (the sample width at blue point) x Sample thickness (measured with a micrometer).

In particular, L_c is measured under microscopy with knowledge of length of blue arrow as reference thanks to analytical tools associated to microscope, as presented in *Figure II. 21*.
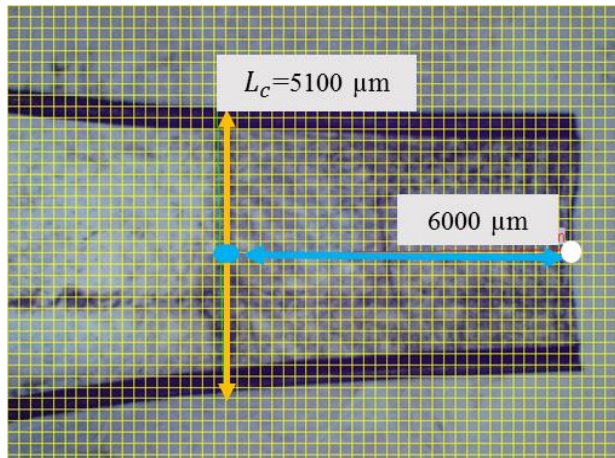

Figure II. 21. An example of dimension measurement (with help of a 200µmx 200µm grid).

II.2.5.   Surface energy measurement

Surface free energy (SFE) quantifies the disruption of intermolecular bonds that occurs when a surface is created. In the physics of solid materials, the surface energy is defined as the excess energy at the surface of a material compared to the bulk, or it is the work required to build an area of a particular surface. The surface energy of a polymer influences its adhesive properties and is important for processes such as printing and heat sealing.

In this thesis, the effect of biaxial stretching on surface energy of polymer films is accessed through contact angle measurements, which is also one of the most commonly applied techniques used to determine the SFE due to its simplicity and applicability to polymeric material surfaces.

The Owens-Wendt method is used to determine SFE as usually applied for solids with low surface energies such as polymers (Awaja et al., 2009). The Owens-Wendt theory divides the surface

energy (γ_s) into two components: surface energy due to dispersive interactions (γ_s^d) and surface energy due to polar interactions (γ_s^p). The relation can be written as:

$$\gamma_s = \gamma_s^d + \gamma_s^p \tag{II.25}$$

These can be determined from contact angle, θ, data of polar and no-polar liquids with known dispersion (γ_L^d) and polar (γ_L^p) parts of their surface energy using (II.25) (Awaja et al., 2009)

$$\gamma_L(1 + \cos\theta) = 2\sqrt{\gamma_L^d \gamma_s^d} + 2\sqrt{\gamma_L^p \gamma_s^p} \tag{II.26}$$

Where γ_L is the liquid surface tension.

In this study the apparatus used for contact angle measurement is model Kruss-DSA100. Three different liquids namely water, diiodo-methane and formamide were used for measurement. During each test a sessile drop of liquid (~2µl) was placed on the film surface and the geometry of the droplet was evaluated with CCD camera. The measurements were taken after the droplet had stabilized and no significant changes in contact angle values were observed in consecutive images. For each type of liquid, the contact angle measurements are repeated at least three times (for each measurement a new spot was selected) and the average values are calculated. An example of contact angle measurement is shown in *Figure II. 22*.
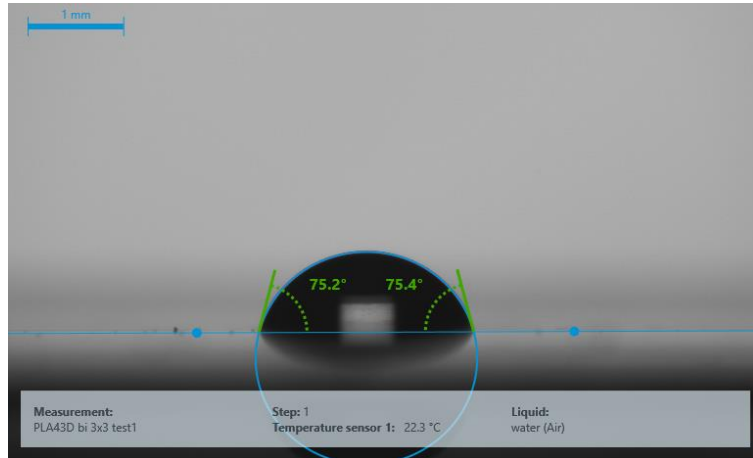

Figure II. 22. An example of contact angle measurement with a BO C-PLA film using water as liquid for sessile drop (blue line is baseline for angle measurement).

For each type of material, after one serie of measurements (3liquids x 3droplets), the value of SFE is calculated automatically thanks to model OWRK (short for Owens-Wendt method) as proposed in software linked to apparatus.

Appendix-II

Presentation of ESRF synchrotron facility

Since their invention, synchrotron radiation sources across the world provide exciting and various opportunities to researchers in studying various materials in many branches of science such as biology, chemistry, physics and material engineering. Concerning SAXS analyses, the synchrotron radiation source is particularly suited for in-situ experiments, for that only such kind of facility is able to provide an extremely intense, accelerated narrow X-ray beam to analyze the real-time kinetics of deformation mechanism with stretching.

In-situ SAXS analyses carried out during this PhD thesis were carried out at The European Synchrotron Radiation Facility (ESRF) located in Grenoble (France), which is one of the the most intense source of synchrotron-generated light around the world. ESRF generates X-rays with exceptional properties giving opportunities in the exploration of materials and living matter. These X- rays are produced at the ESRF by the high energy electrons 100 billion times brighter than the X-rays used in hospitals. The principle of producing synchrotron light is shown in *Figure AII. 1 (ESRF1)*. First of all, electrons are generated and accelerated in the LINAC (LINnear ACcelerator). Then bunches of electrons are injected into the booster synchrotron, which is a 300-metre-long pre-accelerator where the electrons are accelerated to an energy of 6 billion electron-volts (6 GeV) before being finally injected into the storage ring. After injection, electrons race around the storage ring, a circular tunnel measuring 844 meters in circumference, for hours at a speed close to the light one.
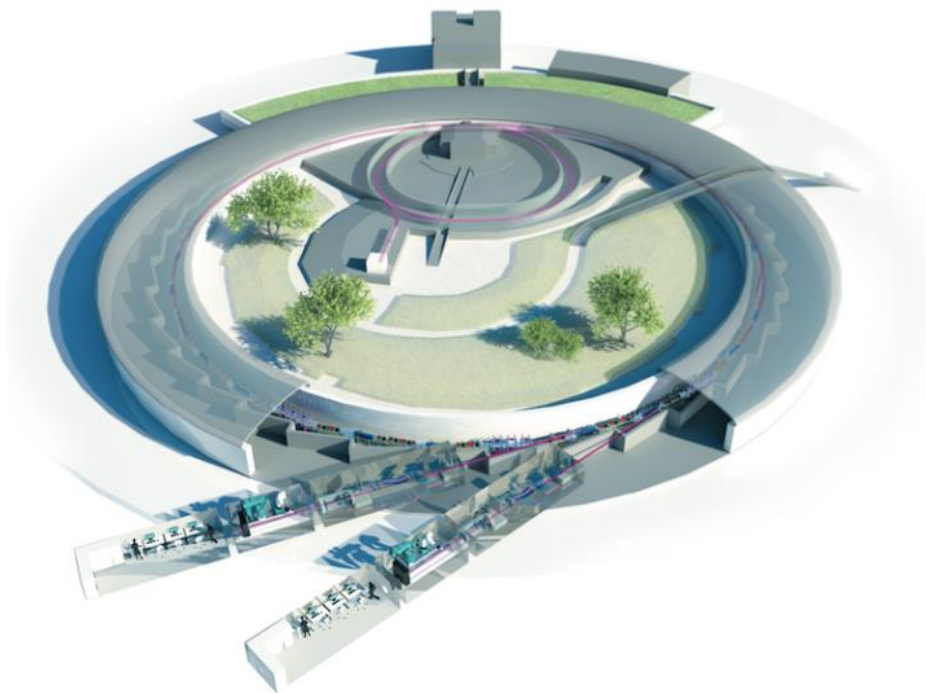
Figure AII. 1. Scheme of a Synchrotron machine.

The storage ring, as schematically illustrated in *Figure AII. 2*, includes straight and curved sections in alternating order. In each curved section, two large bending magnets force the path of the electrons into a racetrack-shaped orbit. In each straight section, several focusing magnets ensure that the electrons remain close to their ideal orbital path. The straight sections also host the undulators, where the intense beams of X-rays are produced. These magnetic structures, made up of a complex array of small magnets, force the electrons to follow an undulating trajectory. The radiation emitted at each consecutive bend overlaps and interferes with that from other bends, generating a much more focused beam of radiation than that generated by a single magnet.
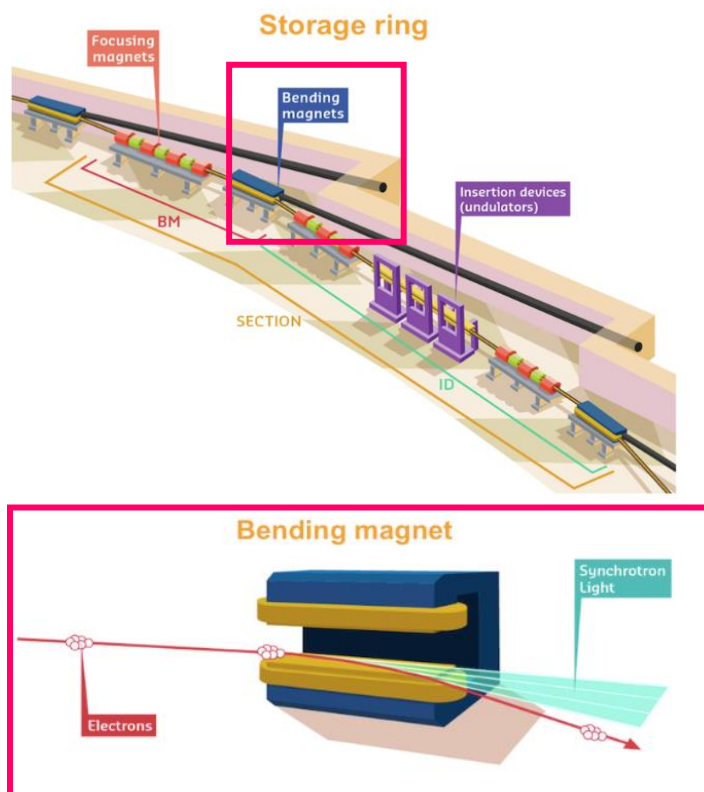
Figure AII. 2. Schematic illustration of storage ring and emission of the synchrotron light from a bending magnet.

Moreover, the gap between the rows of magnets can be changed to fine-tune the wavelength of the X-rays in the beam. The synchrotron light from a bending magnet covers a wide and continuous spectrum, from microwaves to hard X-rays, which are directed along different beamlines fulfilling the requirements of various fields of scientific researches. A beamline as shown in *Figure AII. 3* consists of an optics cabin, an experimental cabin and a control cabin, aligned in a row *(ESRF2)*.
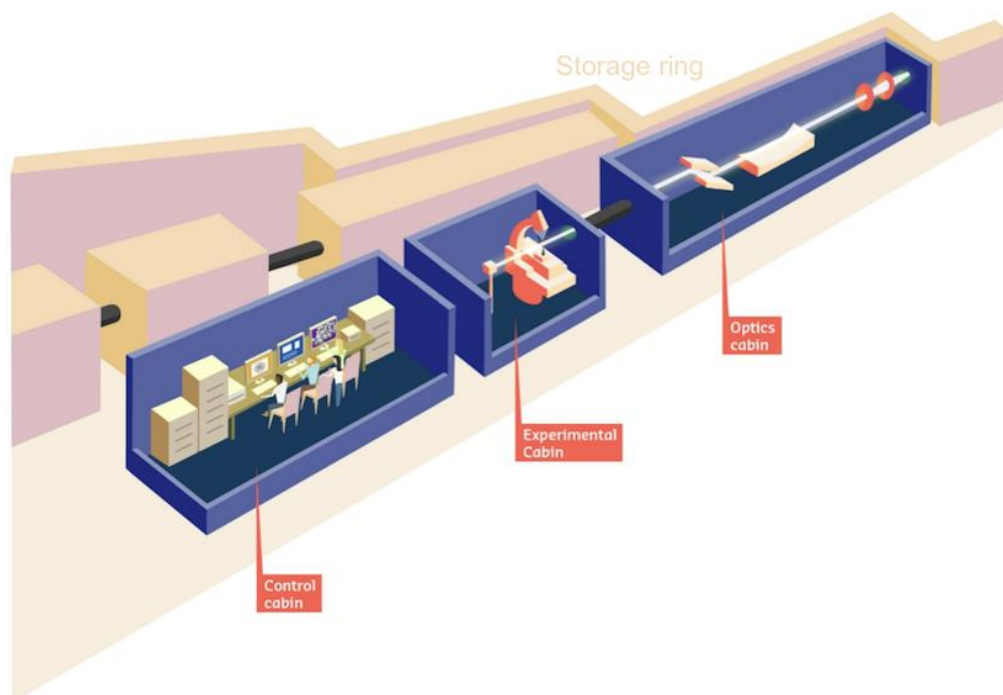
Figure AII. 3. Scheme of a typical Beamline in Synchrotron.

Chapter III
A macroscopic scale
study of structure-mechanical properties of PLA

This chapter mainly focuses on the study of structure-properties relationships of the crystallizable and non-crystallizable grades of PLA used in this work. First of all, the properties of the as-elaborated films are characterized, followed by the study of two grades of PLA biaxially stretched under the same conditions. The characterizations in terms of thermal, mechanical and structural properties are discussed and compared between these two grades. The influence of stretching parameters such as stretching temperature and strain rate on mechanical properties of the stretched films are also discussed since different molecular orientation degrees and phase compositions were induced. Complementary experiments carried out using uniaxial stretching are also studied and compared with results of biaxial stretching. Finally, the effect of physical aging on mechanical properties is illustrated for pre-oriented samples.

III.1.   Characterization of cast films

III.1.1.   Thermal properties

The thermal behavior of as-cast PLAs films of both grades (reference samples described in II.2.2) is illustrated in *Figure III. 1.*
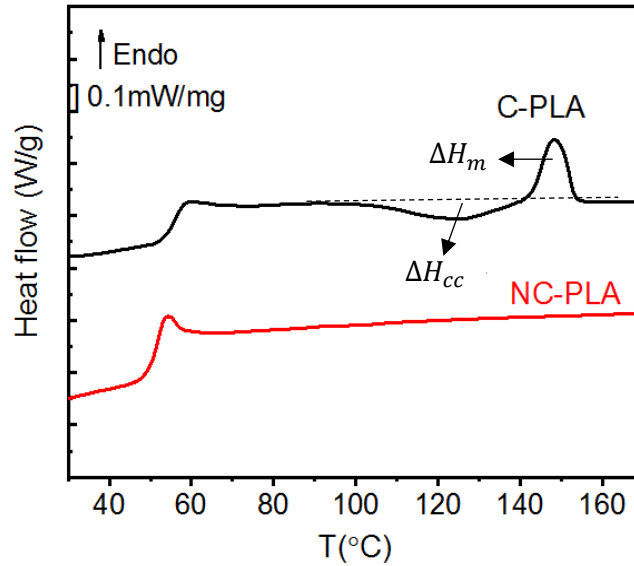

Figure III. 1. Thermal behavior of non-stretched reference C-PLA and NC-PLA upon DSC heating scan at a heating rate of 10°C/min.

It is observed that the C-PLA exhibits three thermal events: a glass transition around 55°C, a cold crystallization peak around 125°C and a melting peak around 148°C. Also, the difference between the two enthalpies ($\Delta H_m - \Delta H_{cc}$) is determined to be around 0 (taking into account of experimental errors), indicating that C-PLA is initially amorphous. As expected these two peaks are not observed for the NC-PLA during heating considering the non-crystallizable nature of this type of PLA. Only a glass transition around 52°C was observed for the NC-PLA cast film, i.e. at slightly lower temperature compared to C-PLA. This difference could be related, on the one hand to a lower molecular weight determined for NC-PLA and, on the other hand, to the higher content of D-isomer for this type of PLA (10% of D component). As reported in former studies (Gogolewski et al., 1993; Perego et al., 1996) that have investigated the thermal properties of PLAs of different stereochemical   architectures, PDLLA generally has a lower T_g than PLLA with an overall average difference ranging from 5-10°C.

85

Crystallizability of the two PLAs during isothermal crystallization

Thermograms presented above have indicated that NC-PLA was, as expected, non-crystallized. To confirm that NC-PLA was a non-crystallizable grade (and does not have a slow crystallization kinetic), isothermal crystallization experiments under optimal conditions were conducted for C-PLA to be fully crystallized. The same cycle of experiment was also applied to NC-PLA to compare the two polymers. According to this procedure, samples of 10 mg are first annealed at 130°C for 12h and then quenched to 20°C. A heating cycle at 10°C/min from 20 to 180°C is then performed and the resulting thermograms are depicted in *Figure III. 2*.
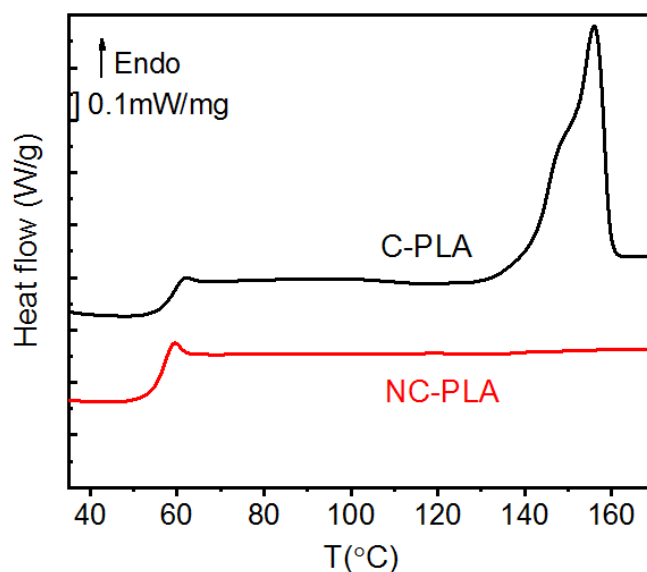

Figure III. 2. Thermal behavior of reference non-stretched PLAs after isothermal treatment at 130°C for 12h from the molten state (heating rate: 10°C/min).

It appears that C-PLA is able to be fully crystallized as confirmed by the absence of cold crystallization peak and a distinct melting peak at 158°C with a small shoulder detected at 148°C. In addition C-PLA exhibits a "multiple" melting peak which should be ascribed to a melting-recrystallization process as reported in (J. Zhang et al., 2008). The crystallinity obtained for this optimum crystallization condition is around 35%. As for NC-PLA, under the same isothermal conditions this type of material remains always fully amorphous: 10% of D-lactide isomer in the chain should introduce conformational defects that prevent any crystallization.

86

III.1.2. Viscoelastic properties

The viscoelastic properties of the cast PLA films were investigated by means of DMA and the comparison between the two grades in terms of evolution of storage modulus E' as a function of temperature is depicted in *Figure III. 3*.
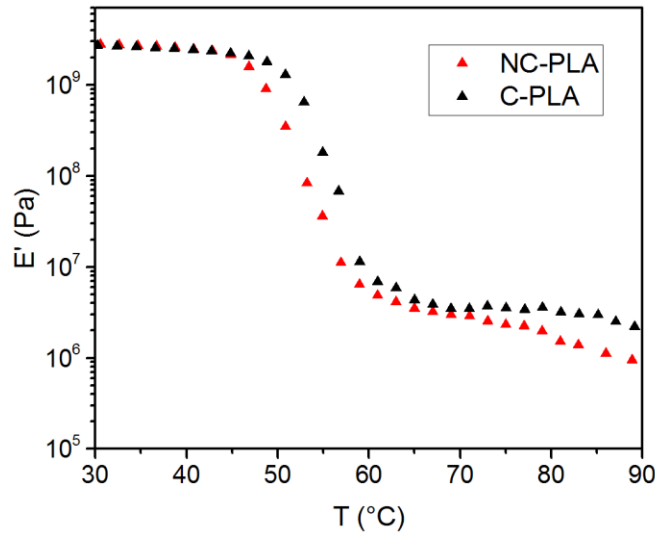

Figure III. 3. Evolution of the storage modulus E' as a function of temperature at 1 Hz, heating rate 2°C/min.

In their glassy state, the two polymers present similar modulus, around 2.8 GPa. Then E' decreases drastically up to 3-4 MPa. This sharp decrease is characteristic of the α-relaxation of an amorphous polymer. It can be observed that the decrease of modulus for NC-PLA takes place about 2-3°C before the one of C-PLA, which is in good agreement with previous results obtained by DSC analysis.

In addition, both materials are in the rubbery state from around 65°C, with C-PLA showing a rubbery plateau in the temperature range of [70-85]°C while the NC-PLA starts to present viscous behavior at around 75°C as indicated by the drop of the modulus. This should be linked to the fact that NC-PLA has a lower molecular weight than C-PLA (cf II.1.1).

Determination of the stretching temperature range

The characterizations presented previously allow to choose a suitable stretching temperature for biaxial stretching process where two main factors have to be considered:

1) Stretching should be carried out in the temperature range where the material is fully in its rubbery state in order i) to allow homogeneous deformation and ii) to reach sufficiently high elongation ratios to induce macromolecular orientation.

2) Thermally- induced crystallization has to be avoid in the timescale of the biaxial stretching process in order to determine solely the effect of stretching.

As a result, combining the thermomechanical properties formerly presented, the biaxial stretching range is carefully chosen to be 70°C for NC-PLA and 70°C-85°C for C-PLA as the most suitable processing temperatures.

III.1.3.   Structural characterization

The 2D-WAXS patterns of both types of as-cast films of PLA are illustrated in *Figure III. 4.* For each type of PLA, all the MT, MN and TN patterns exhibit a uniform broad halo indicating the isotropic and amorphous nature of initial samples.
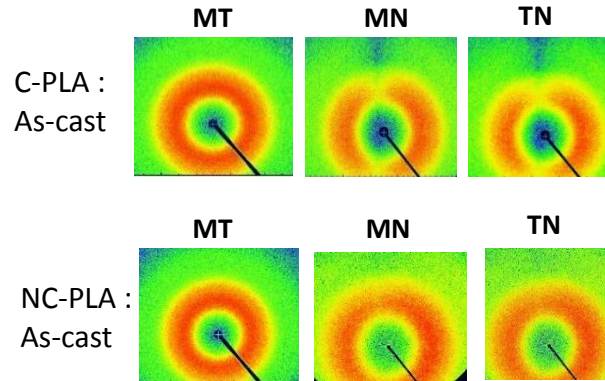

Figure III. 4: In-plane (MT) and profile (MN & TN) WAXS patterns of the two grades of PLAs.

Trichroic FTIR analysis has also been applied to non-stretched cast films to validate the methodology and confirm the isotropic nature of initial films. An example of resulting trichroic spectra of an as- cast C-PLA film can be seen in *Figure III. 5.*
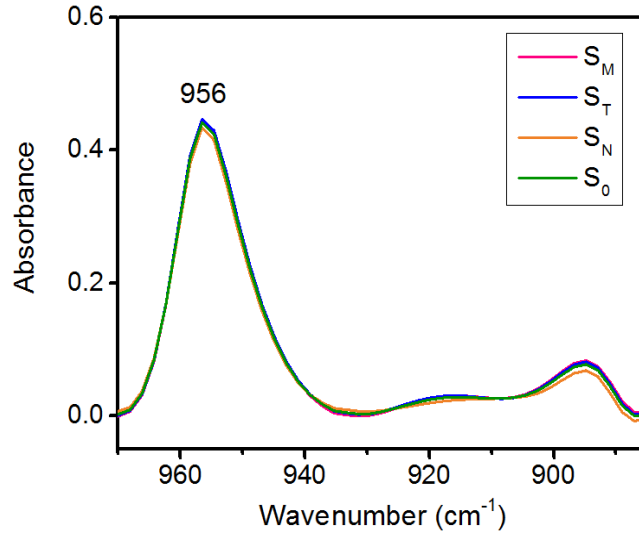
Figure III. 5. Trichroic spectra obtained for an as-cast C-PLA.

The overlap of S_M, S_T, S_N with S_0 suggests that no trichroic behavior has been detected for band at 956 cm^{-1} which proves once again, the isotropic nature of unstretched film.

III.2. Biaxial stretching of PLA films at 70°C

This section deals with the biaxial stretching behavior of the two grades of PLA drawn at $T_d =70$°C and at an initial stretching rate $\dot{\varepsilon}=0.1$/s. Particularly, a detailed comparison of C- and NC-PLA samples biaxially stretched at different draw ratios in terms of thermal, mechanical and structural properties is presented and discussed.

III.2.1. Mechanical behavior during biaxial stretching

The mechanical behavior upon biaxial stretching of C-PLA and NC-PLA cast films is presented in *Figure III. 6.* It is observed that both materials exhibit a rubbery-like behavior, consisting of first of all a non-linear increase of stress as a function of draw ratios, then a short plateau at intermediate draw ratios finally followed by a strain-hardening domain at high strains before rupture. C-PLA breaks at λxλ= 3.5x3.5, which is slightly lower than NC-PLA, i.e. 4x4. This rubbery behavior which was already reported in (Delpouve et al., 2012; Ouchiar et al., 2016) could be expected considering that both amorphous PLA films are stretched above their glass transition temperature which is around 55°C, as shown previously.
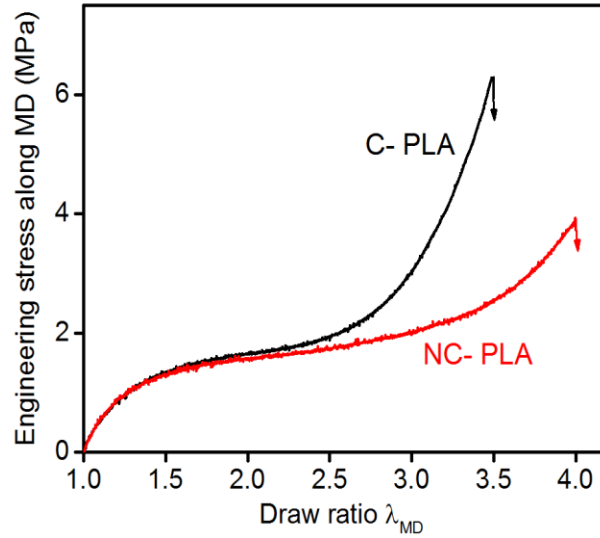
Figure III. 6. Engineering stress versus draw ratio curve of C-PLA and NC-PLA during biaxial stretching at 70°C at $\dot{\varepsilon} = 0.1 \ s^{-1}$ (only behavior along MD is plotted for sake of clarity).

The stress levels of both PLAs nearly superimpose until the onset of the strain-hardening stage. Note that the onset of strain hardening occurs earlier for C-PLA (λxλ= 2.5x2.5) than for NC-PLA (λxλ= 3x3) and the strain hardening is more pronounced for C-PLA. The origin of the strain-hardening stage has been largely debated in the literature, especially in the case of uniaxial stretching. It turns out that two effects could be addressed to its origin:

1) A highly extended macromolecular network induced by chain orientation as observed for polystyrene (Hasan & Boyce, 1993).

2) The occurrence of strain- induced crystallization during stretching as reported, for example, for PET (Chandran & Jabarin, 1993; Gorlier et al., 2001) or PLA (Ouchiar et al., 2016; Xiuqin Zhang et al., 2011).

Structural characterizations on BO films in the following sections will provide some answers regarding the origin(s) of the difference of hardening between the two PLAs.

III.2.2. Mechanical behavior of BO films at room temperature

The influence of macromolecular orientation on the mechanical behavior of BO samples, both in linear viscoelastic domain and plastic deformation domain has been investigated.

III.2.2.1. Viscoelastic properties

The effect of macromolecular orientation on storage modulus in the linear viscoelastic domain has been investigated through DMA analysis by recording E' as a function of time (30°C, 1Hz, strain fixed at 0.01%, relaxation during 1h). Samples have been taken along the machine direction. As a result, it was observed for both PLAs that the storage modulus remains constant during the test period without any sign of relaxation decay. Also, the average values of E' obtained from E'(t) curves of various draw ratios of both grades are summarized in *Table III. 1*.

Table III. 1. Storage modulus E' of BO films of C-PLA and NC-PLA stretched at various draw ratios.

λ_{MD} x λ_{TD}	Elastic modulus E' (GPa±0.1)	
	C-PLA	NC-PLA
As-cast	2.6	2.4
2x2	2.7	2.5
2.5x2.5	2.9	2.8
3x3	3.2	3.3
3.5x3.5	3.9	3.8
4x4	ND	4.1

The table above shows that for both PLAs the storage modulus increases with the draw ratio and the relative increase percentage (compared to as-cast samples) was plotted as draw ratio *Figure III. 7(a)*). For highest stretch ratio the increment reaches nearly 60% of the value of cast samples.
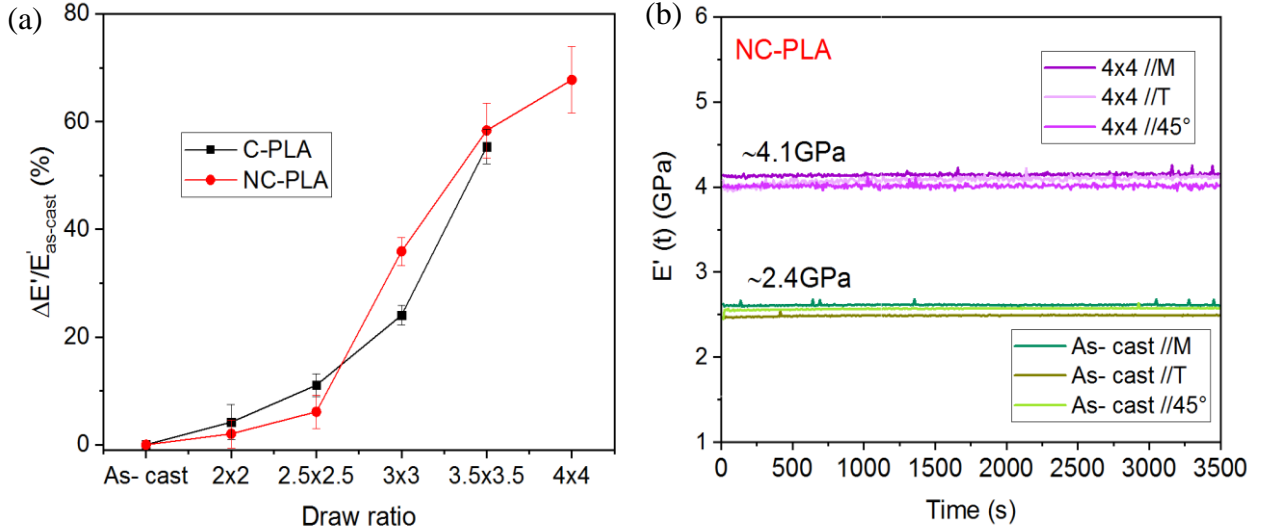
Figure III. 7. (a) E' versus time curves with samples cutting along different axes presented for sample of NC-PLA stretched at 4x4 (b) the increase of modulus ΔE' as function of draw ratios of two grades of PLAs.

In order to check that this behavior is observed whatever the sampling direction, the modulus has been measured along the two biaxial drawing axes and a third direction of 45° with respect to one of the drawing axes. An example of E'(t) curves obtained for as-cast and BO sample in case of NC-PLA is depicted in *Figure III. 7(b)*. As can be seen from the figure, E'(t) curves superimpose for samples taken along different directions both for as-cast and BO samples. These results are in line with the structural characterization previously presented showing the isotropic structure of cast films. Plus, for BO films this is an evidence of the isotropic nature of mechanical properties in the stretched film plane.

III.2.2.2. Mechanical behavior upon tensile test

In addition to viscoelastic properties, a particular attention has been paid to the effect of biaxial stretching on the deformation behavior upon uniaxial tensile of PLA films at room temperature. The engineering stress- strain curves of as- cast and BO samples of the two PLAs are reported in *Figure III. 8.*
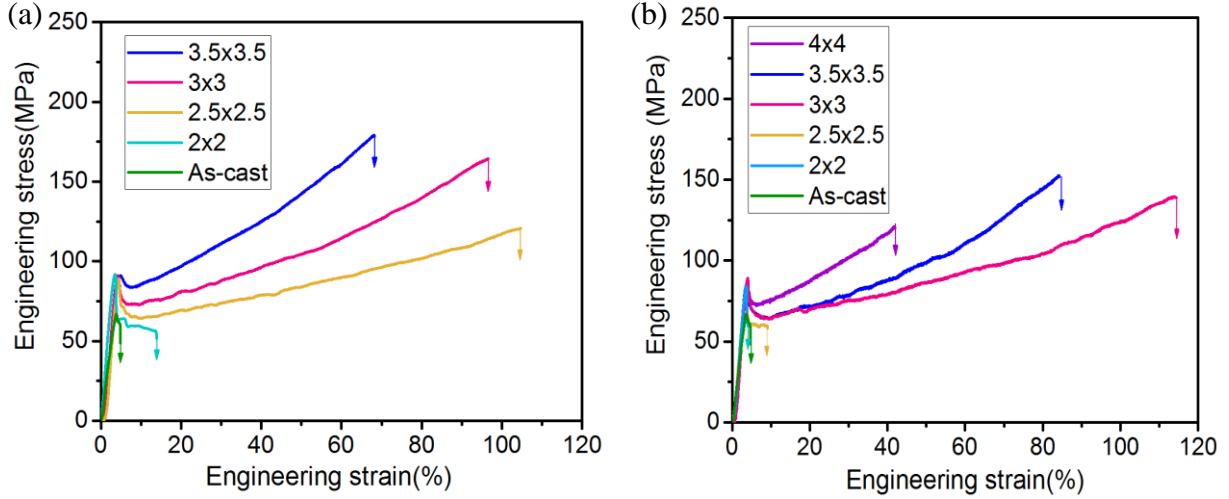
Figure III. 8. Engineering stress-strain curves of as-cast samples and BO samples stretched at various draw ratios of (a) C-PLA and (b) NC-PLA. Tensile test conditions: 23°C, $\dot{\varepsilon} = 4x10^{-3}s^{-1}$.

First of all it is noticed that the unstretched (isotropic) samples are very brittle as already reported in (Sarasua et al., 2005b), which endure rupture very quickly even before having a proper yield point.

For BO samples, a yield point is observed whatever the draw ratio sample, which is different from the stretching behavior above glass transition temperature. Yet the yield stress remains nearly unchanged (around 80MPa) even along the increase of stretch ratios. Thus, a particular attention has been paid to the evolution of strain at break as a function of draw ratio, as depicted in *Figure III. 9(a)*. As a result, a ductile behavior is observed for the C-PLA samples as soon as the biaxial draw ratio is above 2x2. A similar evolution is observed for NC-PLA except that the transition occurs for a slightly higher critical draw ratio, i.e. 2.5x2.5. These results confirm the thermomechanically induced B-D transition in both PLAs.
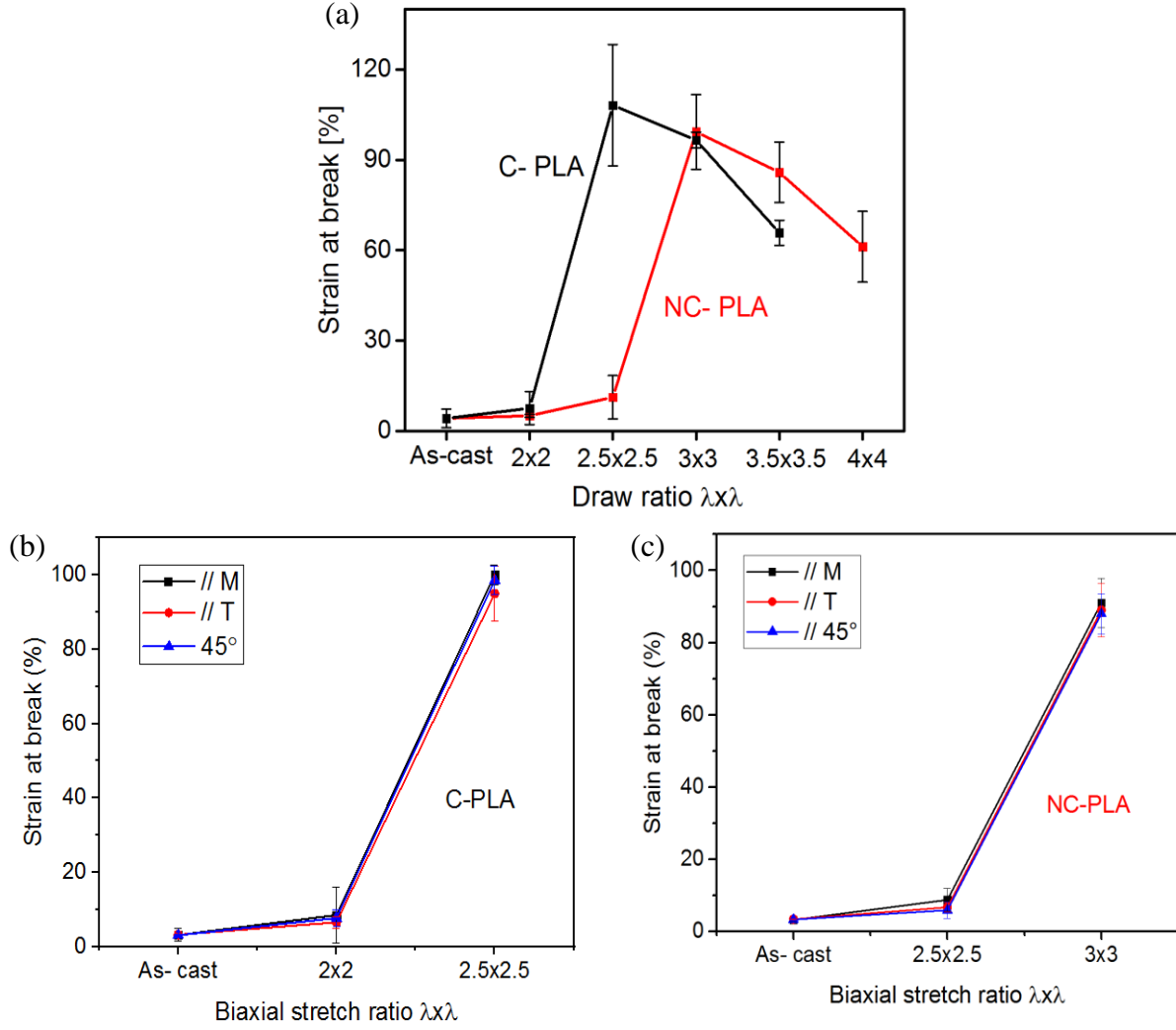
Figure III. 9. (a)Strain at break as a function of draw ratios of as cast and BO films of two grades uniaxially drawn at $\dot{\varepsilon} = 4 \times 10^{-3} \, s^{-1}$, 70°C and comparison of results when sampling along different axes in the plane of film at characteristic draw ratios in the case of (b)C-PLA (c) NC-PLA.

In addition, this gain in terms of strain at break reaches an optimum value of over 100% for C-PLA stretched at 2.5x2.5 and for NC-PLA stretched at 3x3. Note that this gain remains the same whatever the cutting angle of the samples tested: along MD, TD or 45°C, as presented in *Figure III. 9(b)&(c)* for the critical draw ratios formerly discussed. Again, these results illustrate the isotropic nature of mechanical properties in the BO film plane.

One should also note that these optimum ratios correspond to the onset ratio of strain -hardening previously determined on biaxial stretching behavior. As soon as the most optimized ratios are attained, the strain at break values steadily decrease with the increase of the biaxial draw ratio. This

can be explained by the fact that at high stretch ratio macromolecular chains are already extremely oriented during biaxial stretching so that the aptitude to deform during the uniaxial test should be less significant. The improvement of ductility through biaxial stretching will be further interpreted with complementary structural characterizations.

III.2.3.   Thermal properties

The thermal behavior of BO samples are shown in *Figure III. 10*. Note that the 1x1 samples in both figures correspond to the as-cast samples that were thermally treated (i.e. annealed at T_d) with the same duration than the most stretched samples and then tested on DSC analysis (cf reference samples described in II.2.2).
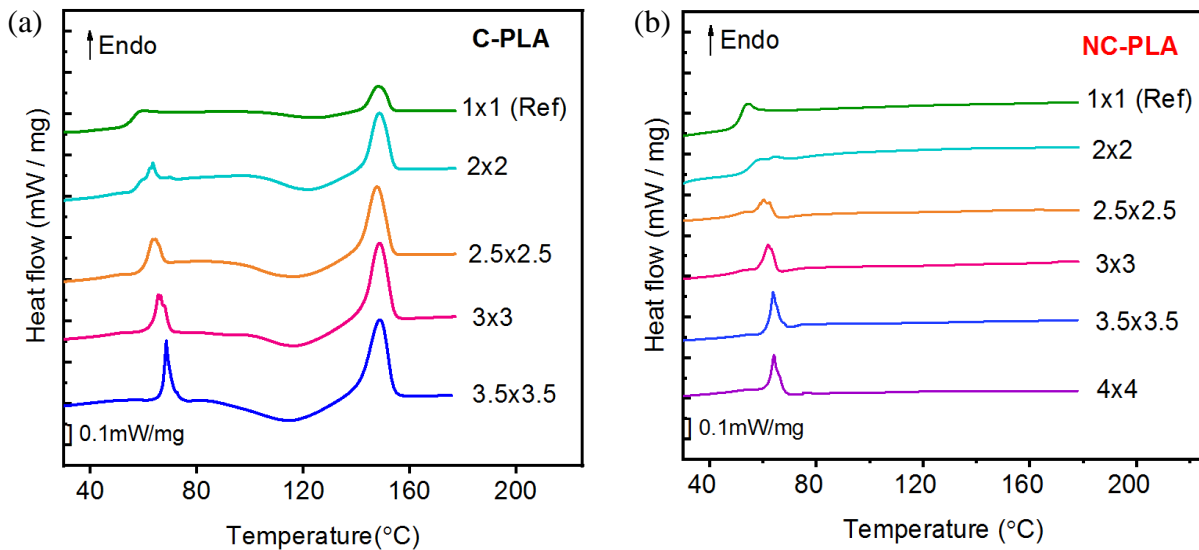

Figure III. 10. Thermograms heating at 10°C/min for non-stretched and BO samples of various draw ratios of (a) C-PLA (b) NC-PLA.

For C-PLAs, with the increase of draw ratio, the crystallization temperature decreases slowly and gradually while the area of the exothermic peak steadily increases. This observation indicates that the increase of the macromolecular orientation degree favors the crystallization of PLA. Similar beneficial effect of orientation on crystallization kinetic has been reported for uniaxially stretched PET films (Chang et al., 1993; LeBourvellec et al., 1986; Terada et al., 1982). The area of the cold crystallization endotherm ΔH_{cc} and melting exotherm ΔH_m has been measured for BO films of various draw ratios and the values of $\Delta H_m - \Delta H_{cc}$ are reported in *Table III. 2*. It can be concluded from the table that no strain-induced crystals are present in the oriented films since the difference

95

of enthalpy $\Delta H_m - \Delta H_{cc}$ is negligible whatever the achieved elongation ratio. In addition to cold crystallization, an endotherm occurs immediately after the glass transition around 65-70°C, which is ascribed to the signature of the melting of an intermediate mesomorphic phase formed upon stretching (G. Stoclet, Seguela, Lefebvre, & Rochas, 2010). As the draw ratio increases, the peak intensity steadily becomes more important and then completely merges with the glass transition. The increase of this strain-induced "ordered" phase content should be taken into account as a parameter contributing to the hardening process.

For NC-PLA samples, neither crystallization nor melting was observed upon heating. Nevertheless, a similar endothermic peak near glass transition temperature is detectable for stretch ratio higher than 3x3, afterwards the area of peak seems to remain unchanged. Such particular thermal behavior suggests that even for PLAs unable to crystallize, the chain orientation induces the formation of mesophase when a critical stretch ratio is reached. Similar thermal behavior has been reported by (Lee et al., 2013) for a PLA containing 10% of D-isomer that has been previously uniaxially stretched at various ratios.

The ratio of the mesomorphic phase was estimated from the area of post-T_g endothermic peak using Equation (III.1):

$$X_{meso} = \frac{\Delta H_{meso}}{\Delta H_{meso}^0} \qquad (III.1)$$

Where ΔH_{meso} is the area of post-T_g endothermic peak and ΔH_{meso}^0 refers to specific melting enthalpy of mesophase with a value equals to 70 J/g reported in (G. Stoclet, Seguela, Lefebvre, & Rochas, 2010). The results are summarized in *Table III. 2*.

Table III. 2. Thermal characteristic values determined for biaxially stretched C-PLA and NC-PLA at various ratios at 70°C.

λ_{MD} x λ_{TD}	$\Delta H_m - \Delta H_{cc}$ (J/g ±2)	X_{meso} (% ±1)	
	C-PLA	C-PLA	NC-PLA
2x2	0	2	0
2.5x2.5	0	4	1
3x3	1	6	2
3.5x3.5	1	8	4
4x4	ND	ND	4

It seems that C-PLA tends to form more mesophase than NC-PLA when biaxially stretched, though the weight fraction of this phase remains relatively low for both types of BO PLAs. Considering the fact that the melting peak of mesophase is superimposed with glass transition, the quantification of mesophase from DSC results should be taken with caution. In that case the quantification of the mesophase content will also be proceeded through 2D WAXS experiments and the results will be reported in the next section.

III.2.4.   Structural characterization by WAXS

In order to analyze the structure, and to determine the phase composition of BO films, *ex situ* WAXS measurements were carried out in both in-plane (MT) and profile (MN, TN) configurations. 2D WAXS patterns and the averaged intensity profiles computed from these patterns are depicted in *Figure III. 11*.
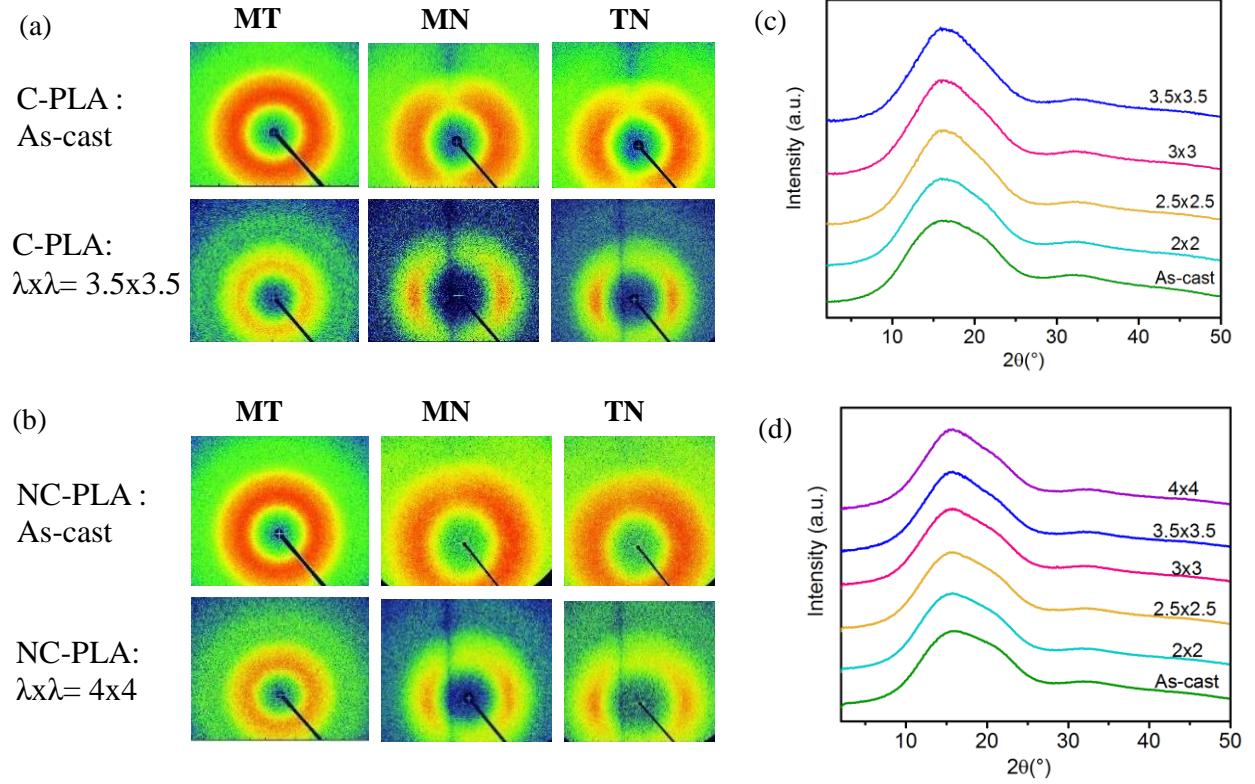
Figure III. 11. In-plane & profile WAXS patterns of (a) as-cast; C-PLA stretched at 3.5x3.5 (b) as-cast; NC-PLA stretched at 4x4 and average diffractograms of as-cast and BO films drawn at various ratios of (c) C-PLA (d) NC-PLA.

As-cast samples are isotropic and amorphous as already discussed in section III.1. For BO samples, the broad amorphous halo observed on MT patterns remains unchanged in comparison with that of cast samples for both materials indicating that samples are not textured in (MT) plane.

By contrast, along MN and TN, the initial halo turns into a pair of equatorial arcs with the increase of the biaxial stretch ratio, revealing preferential chain orientation parallel to the film plane with drawing.

In addition, no clear diffraction spots or fine rings were detected confirming that no strain-induced crystallization occurs. This is not surprising since the stretching temperature is relatively low (near T_g), which tends to induce a phase with less ordering than crystalline phase, the mesomorphic phase (cf I.4). MT WAXS pattern indicates that this mesophase is randomly dispersed in the MT plane, however in NT plane a preferential order of distribution along stretching axis should be considered

(*Figure III. 12*), which is in accordance with the model proposed by (Ou & Cakmak, 2008). This suggestion of mesophase structure will be later confirmed by FTIR experiments in the next section.
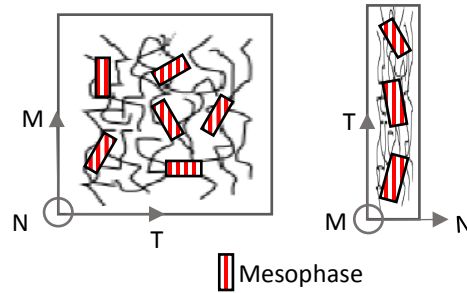

Figure III. 12. Schematic representation of the distribution of mesophase in BO PLA films.

Regarding the average diffractograms in *Figure III. 11(c)&(d)*, the absence of distinct sharp peaks proves once again the lack of well-defined three-dimensional crystalline order in the biaxially stretched films. Yet the presence of a second phase apart from amorphous has also been clearly revealed by the emergence of two new peaks around $2\theta \approx 16.2°$ and $2\theta \approx 32.8°$ when deconvolving profiles of BO samples, attributed to the formation of mesophase as already presented in II.2.3 *(cf Figure II. 9)*.

The quantification of this mesophase content as a function of deformation is summarized in *Table III. 3*. It was found that the determined quantity of mesophase is in agreement with former DSC results. The difference of mesophase portion of the two PLAs should contribute to the different hardening behavior formerly discussed since C-PLA presents a higher strain-hardening slope than NC-PLA, for the latter the mesophase quantity is barely traceable even at high stretch ratios. More importantly, considering the low content of induced mesophase, one can conclude that it is the molecular orientation which mainly governs the hardening process as well as the reinforcement of elastic modulus formerly presented for both PLAs.

Table III. 3. Mesophase content quantified by deconvolution method for C-PLA and NC-PLA.

λ_{MD} x λ_{TD}	Xmeso (% ±2)	
	C-PLA	NC-PLA
2x2	2	0
2.5x2.5	3	0
3x3	5	1
3.5x3.5	7	1
4x4	ND	2

III.2.5.   Orientation characterization by FTIR

2D WAXS results allow to characterize the "ordered" structure involved and to qualitatively assess the amorphous macromolecular orientation in BO films. In order to complete the characterization of the amorphous phase, trichroic FTIR analysis was performed so as to obtain the chain orientation functions along the three mutually orthogonal axes of the film: M, N and T directions.

III.2.5.1.   <u>Chain orientation in amorphous phase</u>

The spectra obtained along the three axis for BO films are presented in *Figure III. 13*. The characteristic bands detected at 956 cm^{-1} and at 918 cm^{-1} are ascribed to the amorphous phase and the mesophase respectively (II.2.3.2). The emergence of the band at 918 cm^{-1} for C-PLA and NC-PLA samples drawn at 3.5*3.5 and 4*4 respectively confirms once again the presence of mesophase.

The superposition of S_M and S_T spectrum clearly indicates that the film is equally oriented along M and T directions, while the S_N spectrum exhibits a decrease of the band at 956 cm^{-1} combined with the increase of band at 918 cm^{-1}, for instance as illustrated in *Figure III. 13(a)* for BO C-PLA. This observation of trichroic behavior of both 956 and 918 cm^{-1} bands suggests that the stretched film is textured with a planar orientation in both phases. It is also noticed that the absorbance of the band at 918 cm^{-1} is extremely low and barely oriented especially in the case of NC-PLA (*Figure III. 13(b)*), which is in agreement with the previous WAXS analysis.
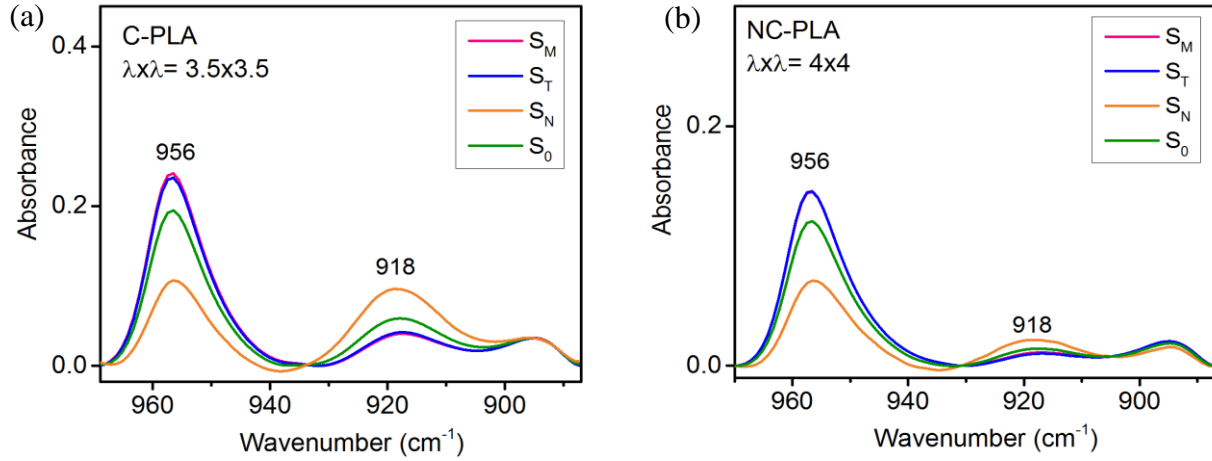
Figure III. 13. Trichroic spectra obtained for (a) C-PLA stretched at 3.5x3.5 and (b) NC-PLA stretched at 4x4.

The orientation functions of chain axes in the amorphous phase are summarized in *Table III. 4*. For sake of clarity, only selected orientation functions are represented in the Wilchinski diagram (*Figure III. 14*).

Table III. 4. Orientation functions of chain axis of amorphous phase obtained from the trichroic spectra with band at 956 cm^{-1}.

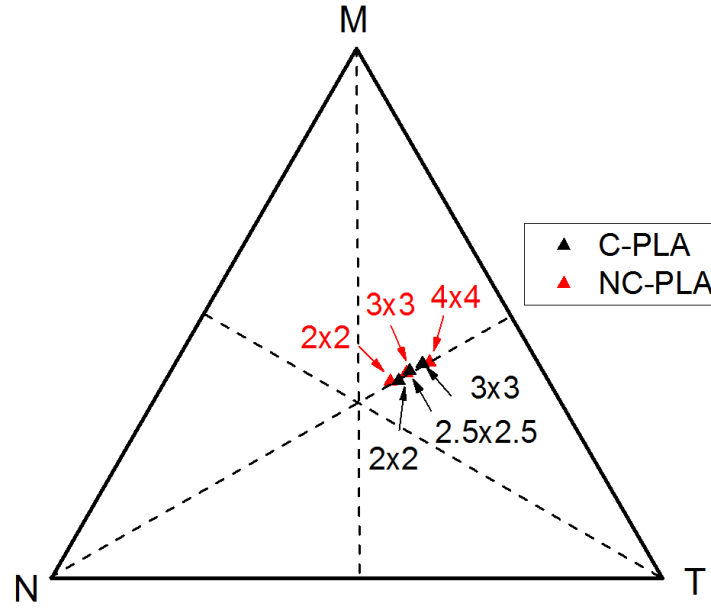| Chain orientation functions of amorphous phase							
C-PLA				NC-PLA			
$\lambda \times \lambda$	f_{cM}	f_{cT}	f_{cN}	$\lambda \times \lambda$	f_{cM}	f_{cT}	f_{cN}
2x2	0.069	0.067	-0.137	2x2	0.055	0.059	-0.115
2.5x2.5	0.085	0.087	-0.178	2.5x2.5	0.072	0.071	-0.142
3x3	0.106	0.108	-0.215	3x3	0.081	0.082	-0.163
3.5x3.5	0.128	0.131	-0.261	3.5x3.5	0.107	0.101	-0.207
				4x4	0.121	0.118	-0.237

Figure III. 14. Wilchinski diagram of the f_{ij} orientation functions of the c axis in the amorphous phase as a function of biaxial draw ratios ($\lambda_{MD}x\lambda_{TD}$) for C-PLA and NC-PLA.

All measured points are located upon the median of the MT plane confirming that the polymer chain axis is equally oriented along M and T directions. As expected, for both PLAs the evolution tendency of orientation functions indicates that the chain axis in the amorphous phase progressively orients towards the MT plane when increasing draw ratios. However, one can notice that for the same draw ratio, the orientation functions are slightly different between the two materials with, a higher value measured for C-PLA.

One explanation of the result could be related to the difference between the glass transition temperatures of the two PLAs as indicated by thermal characterization. The T_g of NC-PLA is 2°C lower than the one of C-PLA. Consequently, as both polymers are stretched at the same temperature (70°C), chains of NC-PLA could be expected to relax slightly faster, which would explain the observed slower orientation kinetics for this polymer.

In order to confirm this point, the characteristic relaxation times were determined for both PLAs at various temperatures (both at and above T_g) using the method described in II.2.1.3. The detailed results of calculations can be seen in *Figure III. 15*.
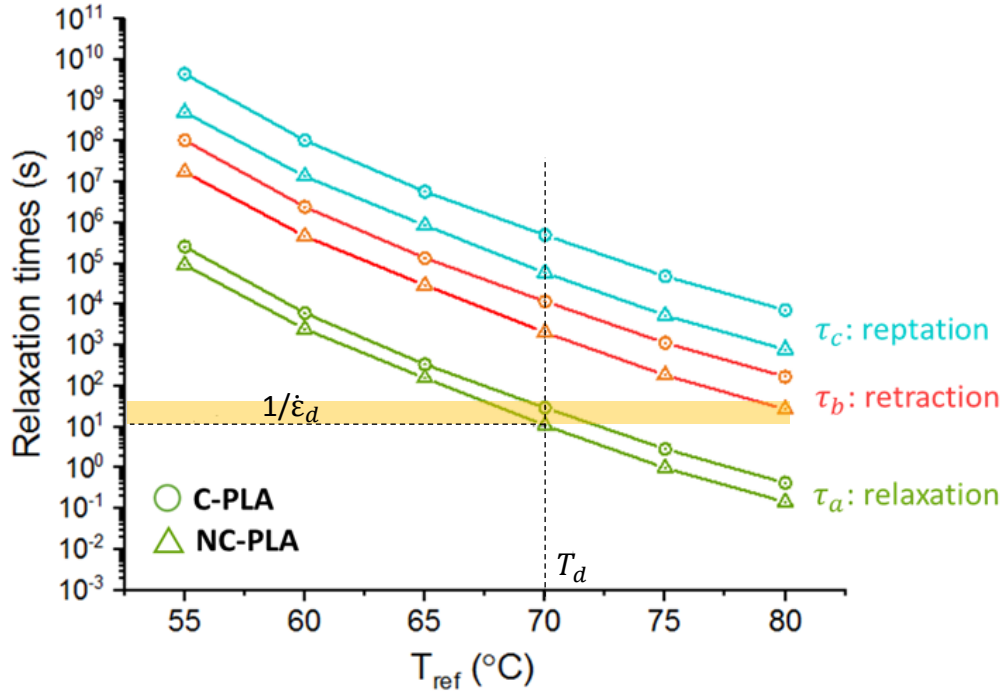
Figure III. 15. Characteristic relaxation times determined at various reference temperatures of as-cast PLAs using method described in chapter II.

It was observed that the relaxation times decrease in the same manner with the increase of the stretching temperature for the two polymers. At each measured reference temperature, the NC-PLA requires less time for all the three relaxation processes than C-PLA. Particularly regarding the biaxial stretching parameters used in this study (the colored region in the figure), among the three relaxation processes considered it is the relaxation time (τ_a) the most relevant time to consider. In that case, *Figure III. 15* shows that NC-PLA exhibits a slightly shorter relaxation time, resulting in lower chain orientation function when stretching at the same draw ratio compared to C-PLA.

The difference of relaxation kinetics in the C-PLA is one element which explains the higher content of the mesophase obtained for this grade in comparison with NC-PLA. Note that, as soon as some mesomorphic domains have been formed, the latter can be considered as physical entanglement points which can also promote chain orientation by restricting molecular mobility.

III.2.5.2. Orientation-mechanical behavior correlation study

Since the quantity of induced "ordered" phase is very low in both materials, one can assume that the most important factor influencing the mechanical properties of BO samples is the macromolecular orientation of the amorphous phase. To test this hypothesis, the mechanical data previously discussed will be analyzed in terms of amorphous chain orientation.

As formerly discussed, the B-D transition occurs at different draw ratios depending on the PLA grade. Thanks to trichroic FTIR analysis a correlation study is now available between the onset of this transition and the macromolecular orientation. The evolution of the strain at break as a function of the orientation function of the amorphous phase has been computed and only the results of correlation with f_{cM} were presented in *Figure III. 16* for the sake of clarity.
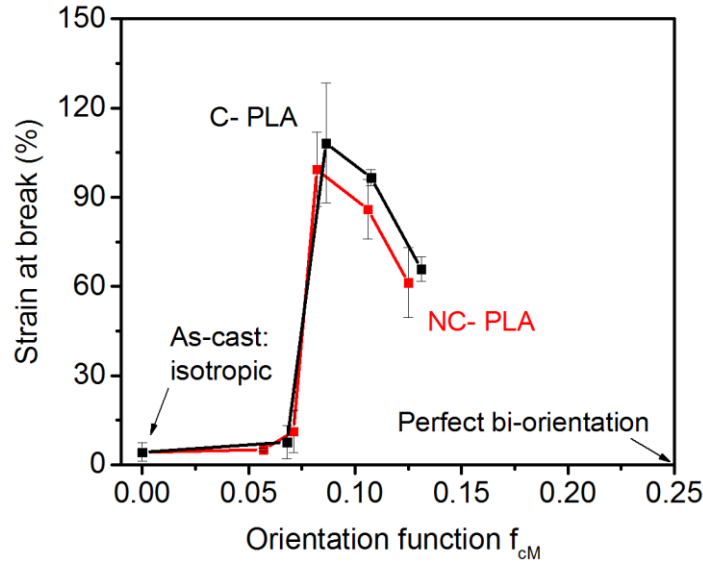

Figure III. 16. Correlation results of strain at break with respect of chain orientation function f$_{cM}$ of the amorphous phase for C-PLA and NC-PLA.

Contrary to the results presented in *Figure III. 9* where the transition from a brittle to a ductile behavior was observed at different stretch ratio for C-PLA and NC-PLA, it appears in *Figure III. 16* that the B-D transition occurs nearly at the same macromolecular orientation degree, i.e. $f_{cM} \approx 0.07$ for both polymers. In addition it is observed that the highest strain at break for both PLAs is obtained for $f_{cM} \approx 0.09$. Note that (Choi et al., 1989) obtained quite similar results when studying BO polystyrene with $f_{cM} \approx 0.09$ (±0.04) determined as optimal orientation factor for a sample strained as much as 100%. This result suggests that **the achievement of a critical value of chain**

orientation in amorphous phase is the key parameter triggering the B-D transition and **confirms the minor role of the mesophase in the contribution of inducing the enhancement of ductility**, which is contrary to what was previously reported in literature (Jariyasakoolroj et al., 2015; Razavi & Wang, 2019).

The correlation between orientation function and strain at break will be deeply studied in the next section using the NC-PLA that forms a negligible mesophase content.

III.3.   Complementary biaxial stretching of NC-PLA at 70ºC

The previous section deals with the critical role of amorphous chain orientation on inducing a brittle-to-ductile transition of PLA. In this section, an in-depth orientation-mechanical behavior study of NC-PLA was carried out to understand the influence of the stretching parameters on the observed B-D transition. NC-PLA is specifically chosen as the material of this study due to the limited mesophase content induced in this material so as to limit the effect of this parameter on the properties of stretched films. Various orientation states were induced by varying the stretching rate. The resulting effect on the mechanical behavior of stretched films will be discussed in details.

III.3.1.   Mechanical behavior during biaxial stretching at various strain rates

As mentioned in section III.1, NC-PLA is most suitable to be drawn at 70ºC. In order to induce different orientation states while maintaining the homogenous nature of the stretched films, 4 supplementary stretching rates $\dot{\varepsilon}$, other than 0.1/s used in section III.2, were applied to obtain BO NC-PLA films. The biaxial stretching behaviors are presented in *Figure III. 17*.
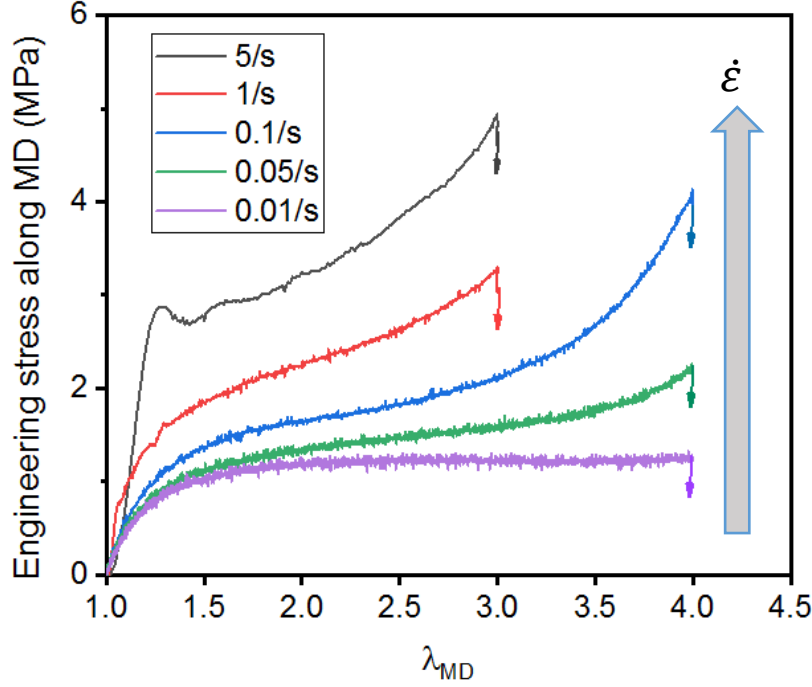
Figure III. 17. Mechanical behavior along MD during biaxial stretching of NC-PLA at T=70°C at various stretching rates.

As presented in the previous section, it is observed from this figure that globally all curves show a rubbery behavior at the beginning of stretching, except for the one stretched at $\dot{\varepsilon}$=5/s showing a yield point, which suggests that the sample is close to its glassy state at this stretching rate. This can be explained by the time-temperature principle: the behavior of stretching at high rate (short time) and high temperature is equivalent to that of stretching at low strain rate (long time) at low temperature. In addition, as expected, the stress level increases when stretching at higher strain rate. The increase of stress level is in the same order with what has been reported in (Xiuqin Zhang et al., 2011) for uniaxially stretched PLA at different strain rates. Meanwhile, the slope in the strain hardening stage systematically decays when the stretching rate slows down. For the lowest strain rate $\dot{\varepsilon}$= 0.01/s, the hardening stage is barely seen at all. This could be related to a less significant molecular chain orientation induced during the stretching.

III.3.2.   Mechanical behavior of BO films at room temperature

The mechanical behavior of each set of different biaxial stretching strain rate has been investigated using the same parameters as in previous section (23ºC, $\dot{\varepsilon} = 4x10^{-3}\ s^{-1}$). To simplify, the exhaustive stress-strain curves of BO films of two representative sets, i.e. biaxially stretched at 5/s and at 0.01/s are presented and in the *Figure III. 18(a)* and *Figure III. 18(b)* respectively.
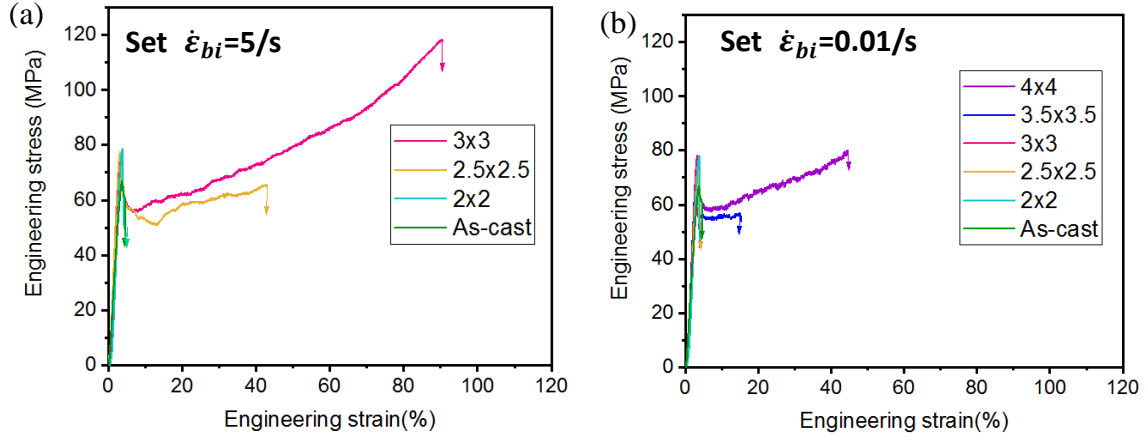

Figure III. 18. Engineering stress-strain curves of BO samples pre-oriented at various ratios and biaxial stretching rates: (a) the set pre-oriented at 5/s (b) the set pre-oriented at 0.01/s.

All sets show a B-D transition behavior whatever the biaxial strain rate $\dot{\varepsilon}_{bi}$. In the case of ductile behavior, the yield stress is rather constant around 80 MPa, which is insensitive to $\dot{\varepsilon}_{bi}$. However it was observed that the onset draw ratio of the B-D transition and the maximum improvement of strain at break of each set depend on stretching rates.

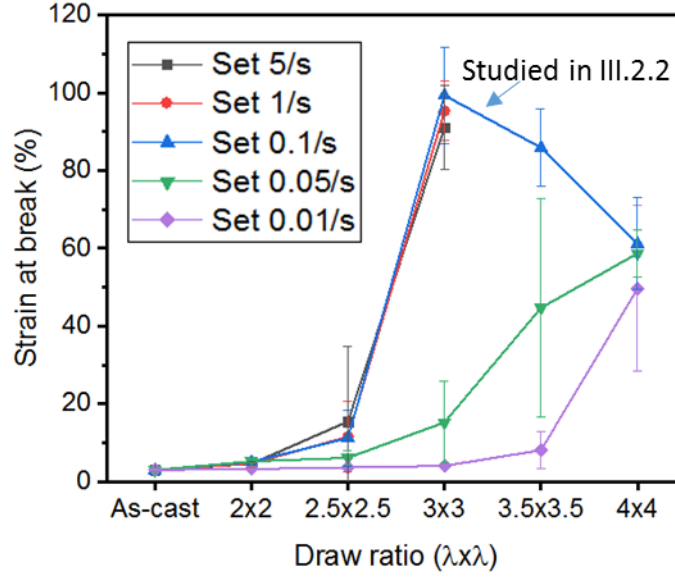A summary of the evolution of the strain at break as a function of draw ratios is presented in *Figure III. 19.*

Figure III. 19. Strain at break values as a function of draw ratios of samples pre-orientated at various strain rates.

Comparisons have been made with the set of NC-PLA stretched at 0.1/s at 70ºC (III.2.2):

1) For sets of $\dot{\varepsilon}_{bi} > 0.1$/s, no obvious shift of onset draw ratio value was seen as the stretched films all begin to show distinct beginning ductile behavior from 2.5x2.5. Similar value of maximum gain of strain at break around 100% is reached whatever the strain rate.

2) For sets of $\dot{\varepsilon}_{bi} < 0.1$/s, a significant shift of the onset value of transition towards higher draw ratio is clearly seen with the decrease of the stretching rate $\dot{\varepsilon}_{bi}$. For instance, this critical draw ratio observed at around 2.5x2.5 for set-0.1/s shifts towards 3.5x3.5 for set-0.01/s. Also, for these low-strain-rate sets, the highest obtained strain at break values were less improved compared to those of high-strain-rate sets.

The orientation function- mechanical behavior correlation study results presented in the next section will explain the different onset values of B-D transition observed for sets stretched at various rates.

III.3.3. Orientation characterization by FTIR

III.3.3.1. <u>Chain orientation in amorphous</u>

The chain orientation in the amorphous phase for different sets has been quantified using the same trichroic method as previously. The corresponding results are presented in the *Figure III. 20* (for sake of clarity only the orientation function along MD, f_{cM}, was plotted as function of draw ratio).
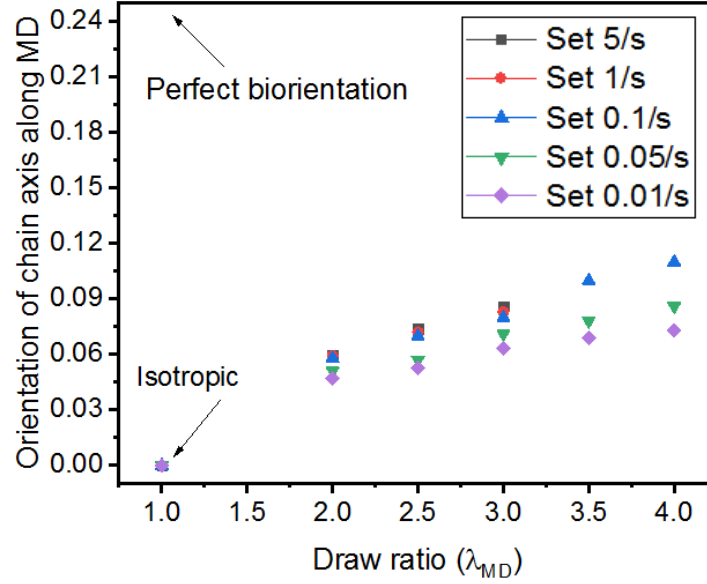

Figure III. 20. Orientation function f_{cM} of amorphous phase as a function of draw ratios of NC-PLA pre-oriented at different strain rates $\dot{\varepsilon}_{bi}$.

As expected, for all sets of strain rates, even for the lowest one, the chain orientation of the amorphous phase increases steadily with the draw ratio. However the orientation function increases faster with draw ratio for higher stretching rates ($\dot{\varepsilon}_{bi}$).

Important to note is that at the same draw ratio, the amorphous chain orientation systematically decreases when the stretching rate $\dot{\varepsilon}_{bi}$ slows down. The difference of orientation function values seems lower for low draw ratios (below 3x3) and appears more and more obvious when stretch ratios increase.

These findings should be explained by the chain relaxation kinetics formerly determined for NC-PLA (cf *Figure III. 15*). In fact, from *Figure III. 15* one could consider that when stretching at 0.1/s, the inverse of $\dot{\varepsilon}_{bi}$ (which corresponds to the experimental time) is in the same order of magnitude

than the relaxation time (τ_a) of NC-PLA measured at 70°C. At strain rates $\dot{\varepsilon}_{bi} > 0.1/s$ the experimental time is shorter than the relaxation time thus chains would have less time to relax, leading to a stronger orientation.

When stretching at rates $\dot{\varepsilon}_{bi} < 0.1/s$, the experimental time becomes longer than the relaxation time, allowing chain relaxation during biaxial stretching which leads to a less important chain orientation. One can imagine that if $\dot{\varepsilon}_{bi}$ continues to decrease, chains could completely fail to orient even at high draw ratios.

In summary, when stretching is carried out in the rubbery state, the chain orientation should be considered as the result of two competing processes: the extension of chain network and the chain relaxation process. Different stretching parameters lead to one of the two mentioned process taking a more "dominant" role, resulting in various orientation states.

III.3.3.2. Orientation - mechanical behavior correlation study

As previously established for the comparative study of the two grades of PLA, the study of the correlation between strain at break and orientation is once again accomplished for sets of pre-oriented samples at various strain rates. The correlation results are presented in *Figure III. 21*.
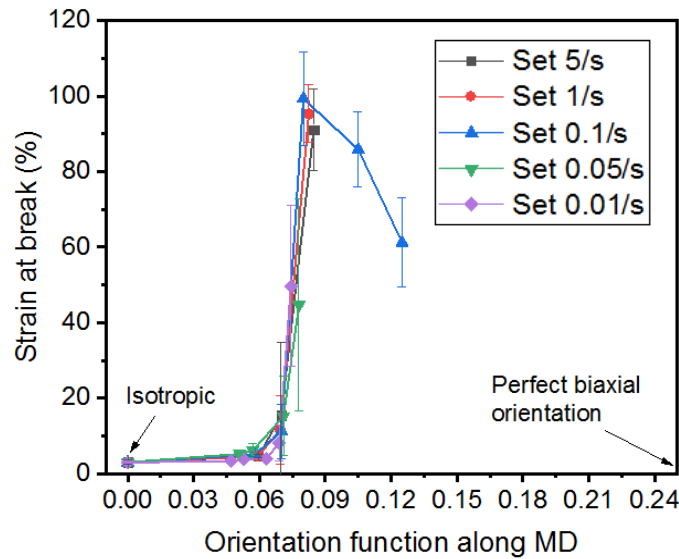

Figure III. 21. Strain at break as a function of orientation function f_{cM} for samples pre-oriented at different strain rates.

110

As observed in section III.2.5, the curves obtained for the different sets perfectly superimpose. Whatever the stretching rate, the critical value of chain orientation function of the amorphous phase that induces the B-D transition is always found around $f_{cM}=f_{cT}\approx 0.07$. Also, an orientation factor $f_{cM}=f_{cT}\approx 0.09$ gives access to the highest improvement of the strain at break value. Both values align perfectly with results previously obtained in the comparative study of the two PLA grades. This clearly highlight once more the key role played by the chain orientation of the amorphous phase in inducing a ductile mechanical behavior of PLA through biaxial stretching.

III.4. Complementary biaxial stretching of C-PLA at 80°C

In previous sections we have shown the crucial role of chain orientation of amorphous phase into the B-D transition. Even so, in this part, we will investigate the potential influence of the crystalline phase on the B-D transition behavior. To achieve this goal a complementary biaxial stretching study was carried out on C-PLA at $T_d = 80°C$. This temperature has been chosen as it is an optimal temperature to promote strain-induced crystallization. The influence of stretching temperature on the final mechanical and structural properties of oriented films will be presented and compared between the two sets of C-PLA drawn at different temperatures. Obviously, only C-PLA will be studied here as the NC-PLA grade is not able to crystallize.

III.4.1. Mechanical behavior during biaxial stretching at different temperatures

The mechanical behavior during biaxial stretching of C-PLA at 80°C is depicted in *Figure III. 22* and compared to the one obtained at 70ºC with the same stretching rate. Only engineering stress-strain curves along MD are presented for sake of clarity.
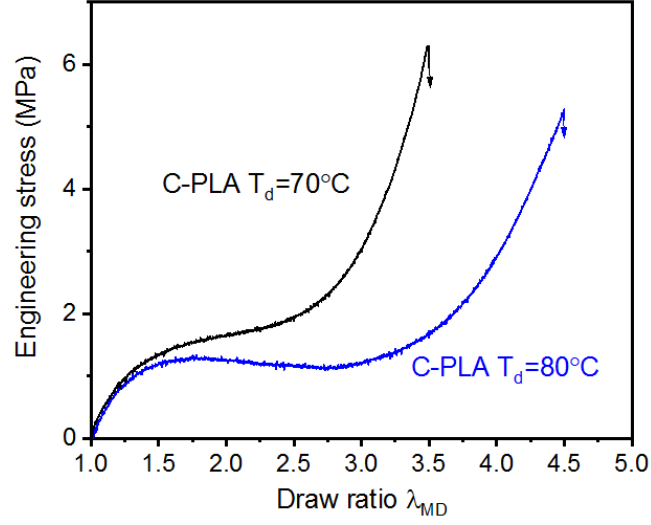
Figure III. 22. Mechanical behavior recorded along MD during biaxial stretching of C-PLA at different temperatures at $\dot{\varepsilon} = 0.1s^{-1}$.

It can be seen from this figure that when stretching at 80ºC, the onset of strain-hardening is around 3x3, that is to say at a higher draw ratio as compared to the value observed for 70ºC. The hardening stage slopes are similar for the two curves. This point will be further discussed along with structural characterization results.

III.4.2.   Mechanical behavior of BO films at room temperature

As done for other sets, the mechanical behavior of BO samples stretched at $T_d = 80°C$ at various draw ratios has been investigated at room temperature and the results were compared to the results obtained for $T_d = 70°C$ are shown in *Figure III. 23*.
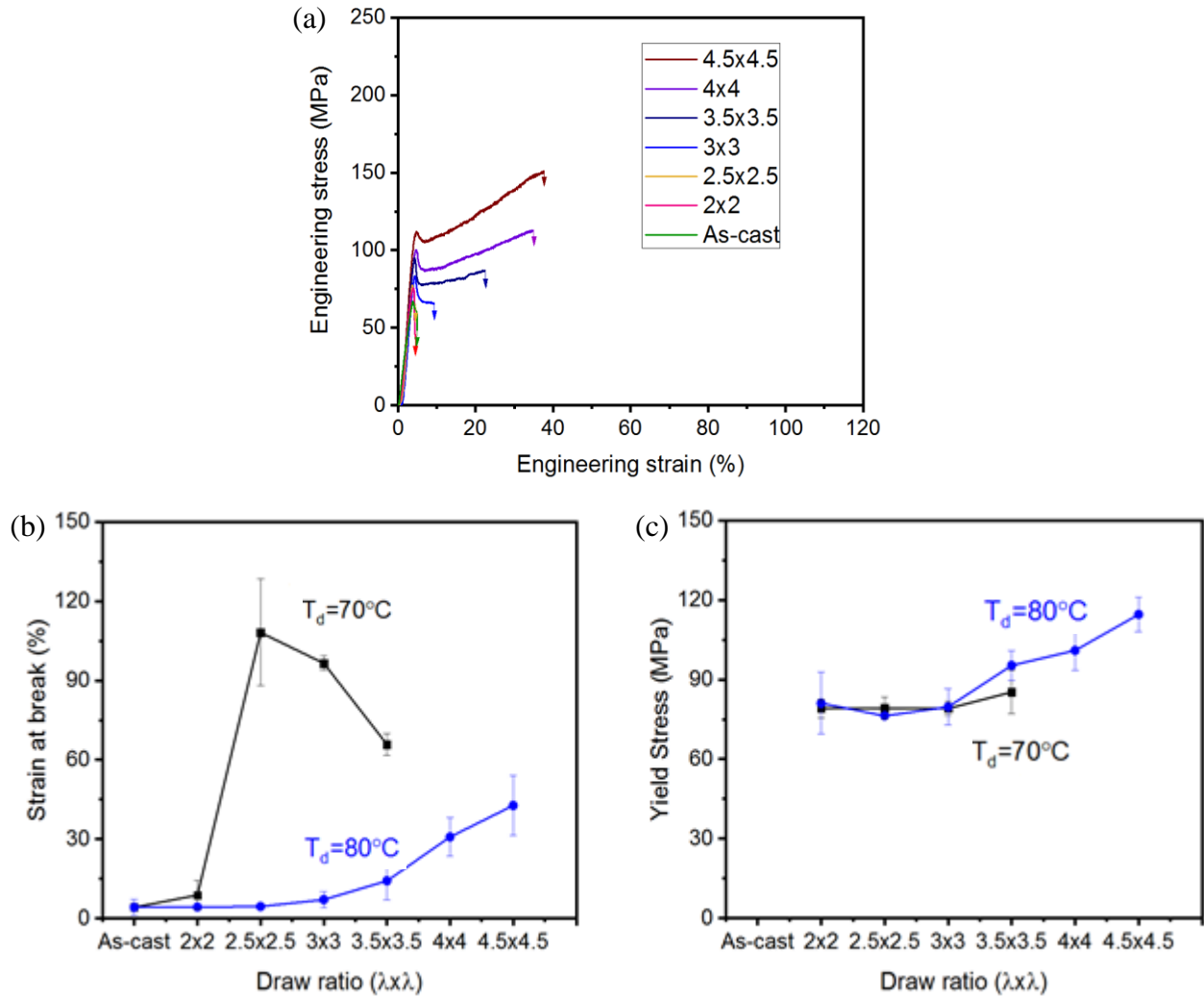
Figure III. 23. (a) stress-strain curves of samples pre-oriented at various ratios at 80°C and comparison with results for $T_d = 70°C$ in terms of (b) strain-at-break (c) yield stress as a function of draw ratios.

From the above figure, it was noticed that a B-D transition is still observed for some of the samples bioriented at 80°C. However when compared to the set of $T_d = 70°C$ the onset draw ratio value of B-D transition has been significantly retarded from λxλ= 2x2 to about λxλ= 3x3 - 3.5x3.5. This shift of critical draw ratio values of B-D transition observed between the two sets is in good agreement with the shift of the onset of strain hardening previously observed (*Figure III. 22*). Even if a B-D transition occurs from 3.5x3.5, it is observed that the maximum improvement for the strain at break value (~50%) is merely half of what was gained for $T_d = 70°C$.

113

Another interesting finding is the enhancement of the yield stress with the increase of draw ratio, from the critical point of B-D transition to the highest draw ratio with a maximum yield stress value of ~120MPa. This improvement of the yield stress was not detected in set of $T_d = 70°C$. The origin of this observation will be analyzed in details in the following sections.

III.4.3. Thermal properties of BO films

The thermal behavior of the reference sample (non-stretched, annealed at 80°C during the same duration than the most stretched BO sample) and BO films stretched at various ratios are depicted in *Figure III. 24*.
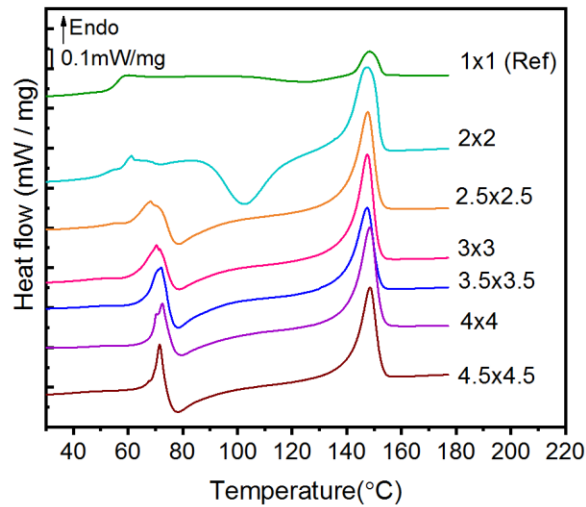

Figure III. 24. Thermograms of samples biaxially drawn at various ratios at 80°C (heating rate 10°C/min).

The non-stretched reference sample does not crystallize at 80ºC, allowing to eliminate the effect of thermally-induced crystallization for stretched films. Regarding the biaxially stretched samples, a remarkable shift of the cold crystallization temperature was observed. Such favorable effect of orientation on crystallization is much more significant than in the case of biaxial stretching at 70ºC.

In addition, for samples at high draw ratios, the endothermic peak attributed to the melting of mesophase was still detected. However the intensity of this peak in case of $T_d = 80°C$ is lower than in the case of $T_d = 70°C$ for sample drawn at same ratio. The presence of this peak may seem surprising considering that the stretching temperature is higher than the melting point of the mesophase.

114

However this could be explained by the fact than the melting temperature measured by DSC is determined on an un-constrained sample which is able to relax/retract upon heating (especially when the temperature becomes close to T_g). During the stretching test, the sample is kept constrained and the amorphous phase remains oriented. Considering the relation $T_m^0 = \frac{\Delta H_m^0}{\Delta S_m^0}$ one can easily imagine that the ΔS_m^0 value could be different in the following two cases: during stretching step where the amorphous phase is oriented and during the DSC analyses where the amorphous phase has, at least partially, relaxed. Consequently the "apparent melting temperature" of mesophase is different and especially higher during stretching than during the DSC analysis. Similar result has been reported on PET by (Jain & Gupta, 1990). Complementary experiments are required to elucidate this phenomenon.

Note that due to the complexity to determine the onset of cold crystallization, crystallinity quantification will not be proceeded from the DSC results.

III.4.4. Structural characterization by 2D WAXS

The 2D WAXS characterizations results of BO samples stretched at 80°C and the comparison with characteristic result of set $T_d = 70$°C are presented in *Figure III. 25*.
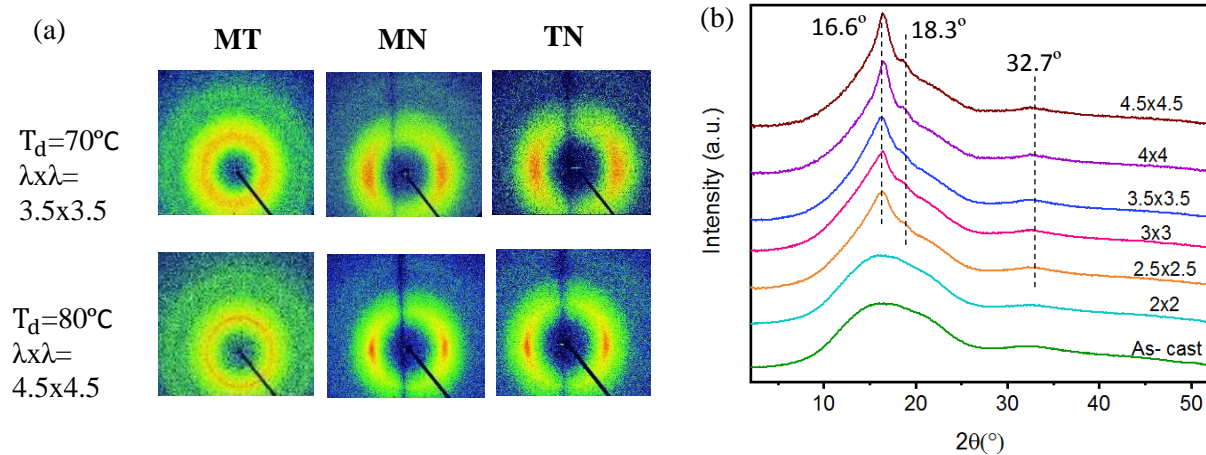
Figure III. 25. (a) in-plane& profile 2D WAXS patterns obtained for sample stretched at highest draw ratio of T_d = 70°C and T_d = 80 °C (b) average diffractograms of samples stretched at various ratios of set T_d =80°C.

The first point to notice from *Figure III. 25(a)* is that the broad ring observed on the MT plane pattern for sample biaxially drawn at 3.5x3.5 at 70°C turned into a thin and well-defined ring for the sample

stretched at 4.5x4.5 at 80ºC. This ring is characteristic of the diffraction from the well-ordered crystallized phase, which clearly appears in *Figure III. 25(b)*. The intensity profiles show, starting from ratio 2.5x2.5, i.e. before the critical onset ratio of strain-hardening stage, the appearance of a sharp peak at $2\theta \approx 16.6º$ which becomes more intense with the increase of draw ratio. Two other peaks at $2\theta \approx 18.3º$ and $2\theta \approx 32.7º$ are also detected, even if their intensities remain quite modest. All these data reveal the formation of the crystalline α' form induced upon stretching.

The crystallinity quantification using the deconvolution method described in chapter II has been performed on these data and is summarized in *Table III. 5*.

Table III. 5. Crystallinity quantification results determined by deconvolution method for samples of the set T_d =80ºC.

Draw ratio	Crystallinity (% ±2)
2x2	ND
2.5x2.5	7
3x3	7
3.5x3.5	9
4x4	12
4.5x4.5	15

From the table it can be concluded that the presence of crystalline phase becomes more important with the increase of stretch ratio and reaches a maximum value of ~15%. This strain-induced crystallization should be the reason of the yield stress increase formerly observed on uniaxial mechanical behavior for BO samples stretched at 80°C.

The structural characterization of the induced crystalline phase is well illustrated by in-plane& profile patterns. As can be seen in *Figure III. 25(a)*, the ring observed on MT patterns indicates the non-textured nature of induced crystallites in the plane of BO film. The same characteristic has already been detected for mesophase induced for films of set T_d =70ºC. As for the pair of arcs detected on profile patterns, they appear to be much more intense and defined for samples of set-

T_d =80ºC than in the case of T_d =70ºC, suggesting strong orientation of molecular chains along the sollicitation axis.

However, the WAXS analysis do not allow easily to distinguish the orientation of the amorphous phase from the one of the crystalline phase. This point will be more clarified with complementary FTIR quantification results.

III.4.5. Orientation characterization by FTIR

III.4.5.1. Chain orientation quantification

FTIR results provided complementary information on the structural properties of BO films at 80ºC. First of all, a comparison of the spectrums obtained for films drawn at the same ratio at T_d = 70°C (where only a mesomorphic phase is formed) and T_d = 80°C (where a crystalline phase is mainly formed) is shown in *Figure III. 26*. It is observed that the characteristic band at $956cm^{-1}$ standing for amorphous phase stays at the same position for the two samples while a clear shift was observed for the band at $918cm^{-1}$ for the sample having mesophase to $922cm^{-1}$ for the sample having crystals. This confirms once again the occurrence of strain-induced crystallization for samples of set T_d =80ºC.
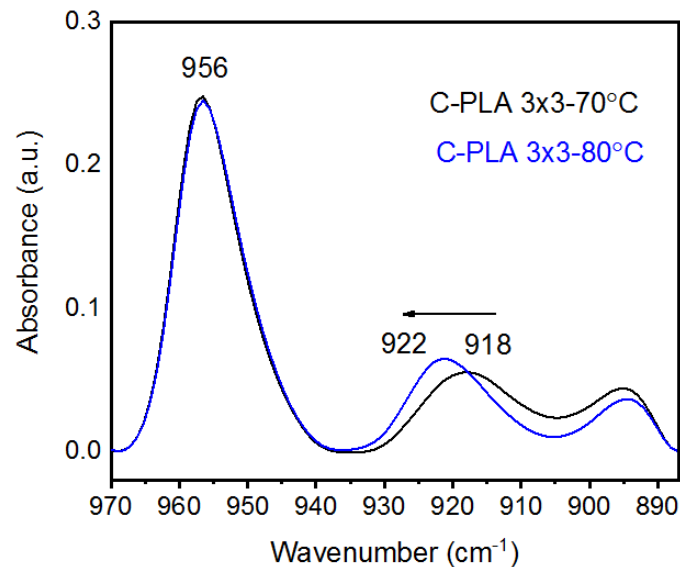

Figure III. 26. Example of spectrum obtained with polarization along MD of samples stretched at 3x3 at 70ºC and 80ºC respectively.

As previously done, trichroic FTIR analysis has been applied in order to quantify the orientation of amorphous phase and this time, of crystalline phase as well using the band at $922 cm^{-1}$ in calculations. The orientation functions along M, T, N directions for some representative draw ratios were selected to be illustrated in Wilchinski diagram (*Figure III. 27*). Globally speaking, the points are located upon the median line of MT plane. For the chain orientation functions of the amorphous phase, the general trend of evolution is towards MT plane with the increasing of draw ratios, indicating that macromolecules tend to orient more and more in the plane of the films for both sets. As for chain orientation in crystalline phase, the functions are observed to locate on the opposite side of MT plane, i.e., facing N direction. This behavior is actually due to the fact that the band at $922 cm^{-1}$ is a perpendicular band (i.e. transition moment perpendicular to the chain axis). Consequently, the more the chain axis is oriented along the sollicitation directions in the film plane (MT plane), the more the corresponding crystalline orientation functions approaches the normal direction ND. In our case the chain orientation in the crystalline phase seems to little evolve with draw ratio.

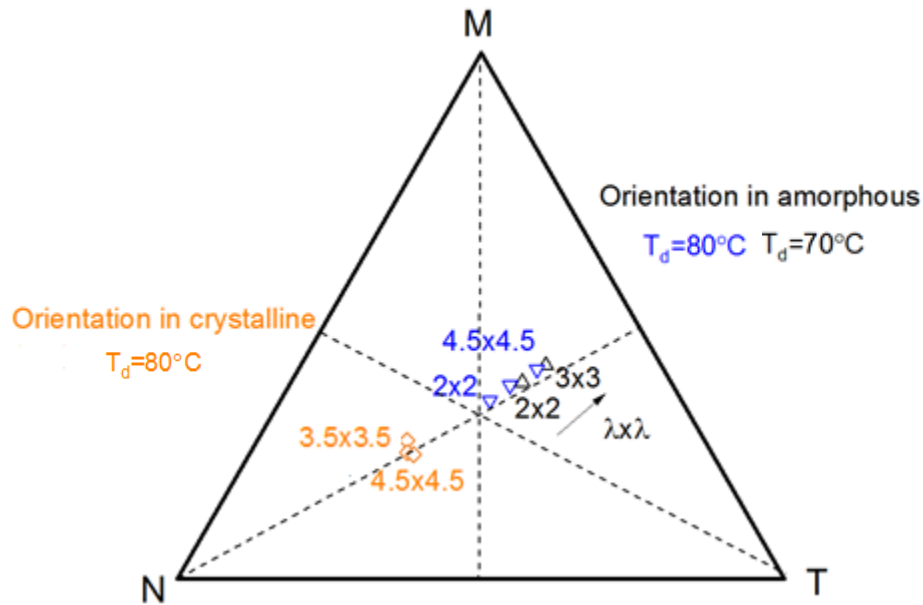

Figure III. 27. Wilchinski diagram of the f_{ij} orientation functions of amorphous and crystalline phases as a function of biaxial draw ratios for C-PLA stretched at various ratios and temperatures.

In order to compare accurately the results between the two sets, the f_{CM} of amorphous and the f_{CN} of crystalline phase were plotted as a function of draw ratios (*Figure III. 28*).
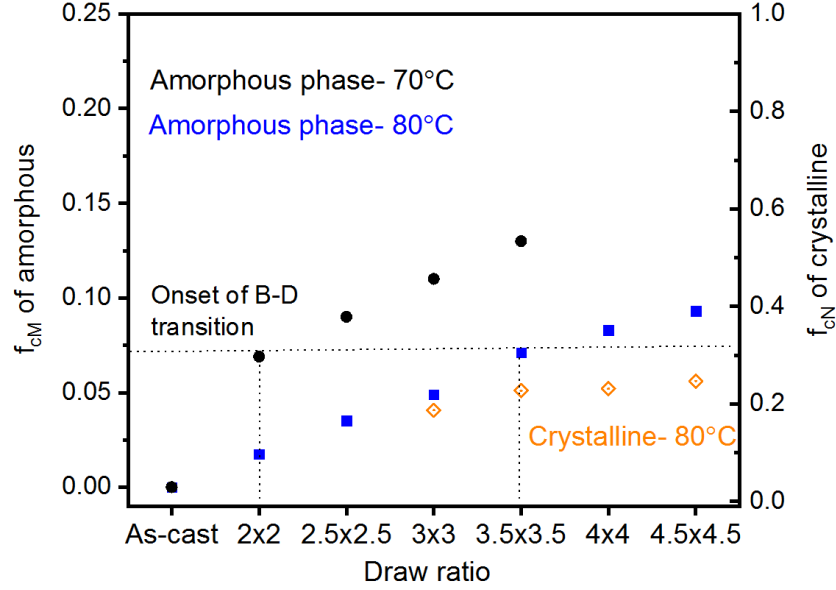
Figure III. 28. Orientation function f_{cM} of amorphous phase of set-T_d =70ºC and T_d =80ºC as a function of draw ratios and function f_{cN} of crystalline phase of set T_d =80ºC.

The above figure shows that the chain orientation in the amorphous phase is proportional to the increase of draw ratios for both sets, though the trend slope for curve at 70ºC seems more important than that of 80ºC. One can notice that at same stretch ratio, the orientation of the amorphous phase strongly decreases with the increase of the stretching temperature. This could be ascribed to the increase of macromolecular mobility at T_d =80ºC since a shorter time is required for relaxation of chain segments between entanglements (τ_a), as previously depicted in *Figure III. 15*. Consequently more rapid chain relaxation at higher stretching temperature leads to less oriented amorphous phase for the same draw ratio.

The gain in molecular mobility, however, makes strain-induced crystallization possible at 80ºC since oriented chain segments have more abilities to perform local rearrangements. Contrary to the evolution tendency the orientation of amorphous phase with draw ratio, for crystalline phase, once crystallites have been formed, the chain orientation seems to stay rather stable.

One can also assume that the less oriented amorphous phase at 80°C (compared to 70°C) could be "balanced" by presence of crystals, resulting in a similar strain hardening slope when stretching at 80ºC as compared to stretching at 70°C (*Figure III. 22*).

III.4.5.2.   Orientation-mechanical behavior correlation study

The study of correlation between amorphous chain orientation and strain at break values is shown in *Figure III. 29.*
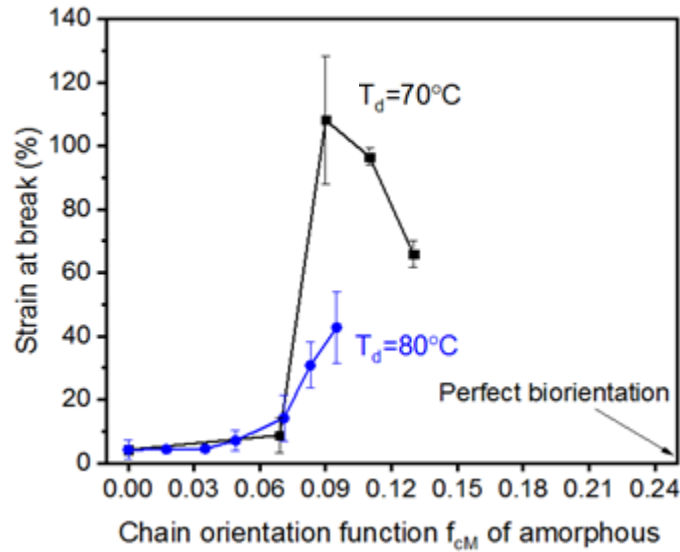

Figure III. 29. Strain at break values as a function of orientation functions of set $T_d = 70°C$ and $T_d = 80°C$.

The first point to notice is that the onset values of orientation function where the B-D transition is observed for both sets are almost the same   ($f_{cM} \approx 0.07$), regardless the presence of crystallites or not. This strongly suggests once again that **it is the achievement of a critical chain orientation level in the amorphous phase that induces the shift from a brittle behavior to a ductile one and not the presence of a crystalline phase**. The role of strain-induced crystallization on the activation of this transition seems unnecessary.

It also seems that the presence of crystals limits the improvement of the strain at break in the ductile domain. Indeed for the same value of chain orientation in the amorphous phase, e.g. $f_{cM} \approx 0.09$, the strain at break obtained around 100% for the sample of set $T_d = 70°C$ drops to 40% for the sample of set $T_d = 80°C$. This behavior can be explained by the induced crystals in the latter which act as supplementary physical entanglement nods, resulting in a lower chain extensibility upon uniaxial stretching.

In summary, a critical orientation factor of the amorphous phase of PLA is required to induce a ductile behavior, while the presence of an "ordered" phase in the material, either mesophase or

crystals, is not a necessary condition. This conclusion is contrary to what was previously reported in literature (Jariyasakoolroj et al., 2015; Oh & Kim, 2014; Razavi & Wang, 2019). The formation of crystals upon stretching will rather play a role on the value of the yield stress at the expense of elongation at break.

III.5. Influence of stretching mode: a study of uniaxial stretching of NC-PLA

Previous sections depicted the results of macromolecular orientation- mechanical behavior of PLA through biaxial stretching. As discussed in chapter I, besides biaxial stretching, uniaxial stretching is also considered as a common deformation route to improve the tensile properties of glassy polymers.

In this section, samples were pre-stretched in only one direction and the mechanical behavior of uni-oriented films was investigated. Results are compared to those obtained from previous biaxial stretching study. The goal is to con firm the important conclusions drawn from former observations, and to assess the role of the sollicitation mode.

For sake of simplification, NC-PLA was chosen for this study and was uniaxially stretched at 70ºC & $\dot{\varepsilon} = 0.1$/s. The stretching axis (MD) was chosen parallel to the extrusion line direction (non-constrained along TD). Pre-oriented samples were then studied in terms of mechanical behavior at room temperature and structurally characterized.

III.5.1. Mechanical behavior of UO films at room temperature

The mechanical behavior of the uniaxially oriented (UO) samples was investigated upon tensile test at 23ºC, $\dot{\varepsilon} = 4. \, 10^{-3}$. Samples are first of all taken parallel to MD, i.e. the stretching direction. The most representative stress-strain curves of each stretch ratio and strain-at-break values as a function of draw ratios are presented in *Figure III. 30*.
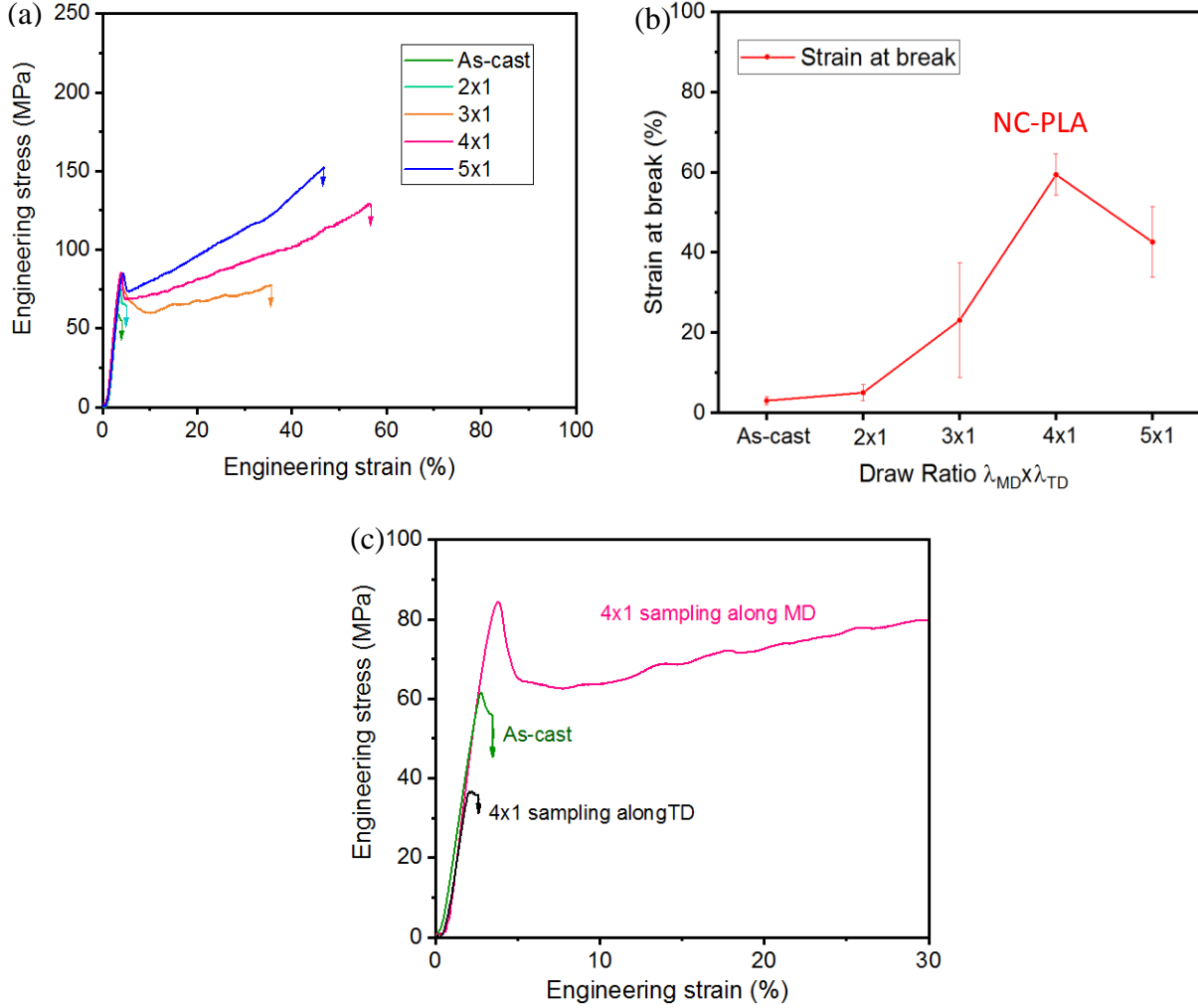
Figure III. 30. (a)Engineering stress-strain curves of pre-unioriented samples at various ratios (b)Strain-at-break values plotted as function of draw ratios (T_d =70ºC, $\dot{\varepsilon}_d$=0.1/s).
(c) Comparison of mechanical behavior at room temperature of specimens cut along different axis of a sample pre-stretched at 4x1 at 70ºC.

The evolution of the strain at break as a function of the elongation ratio for uniaxially stretched samples shows a brittle-to-ductile transition similarly to that has been observed in the case of BO NC-PLA. The transition starts around 3x1 and reaches an optimum at 4x1 with a maximum of strain at break value of 65%. This value is almost 40% lower than what was observed for the sets of bioriented samples. Moreover, unlike in the case of biaxial stretching where the mechanical properties is homogeneous in the plan of stretched film, in case of uniaxial stretching, the improvement of mechanical properties is seen only when sampling direction is along MD as illustrated in *Figure III. 30(c)*. In addition, the behavior of sample cut along TD is even more brittle than that of as-cast sample.

III.5.2. Structural characterization by 2D WAXS

2D WAXS results of UO samples were illustrated in *Figure III. 31* with selected in-plane/ profile patterns at several draw ratios for sake of simplification.
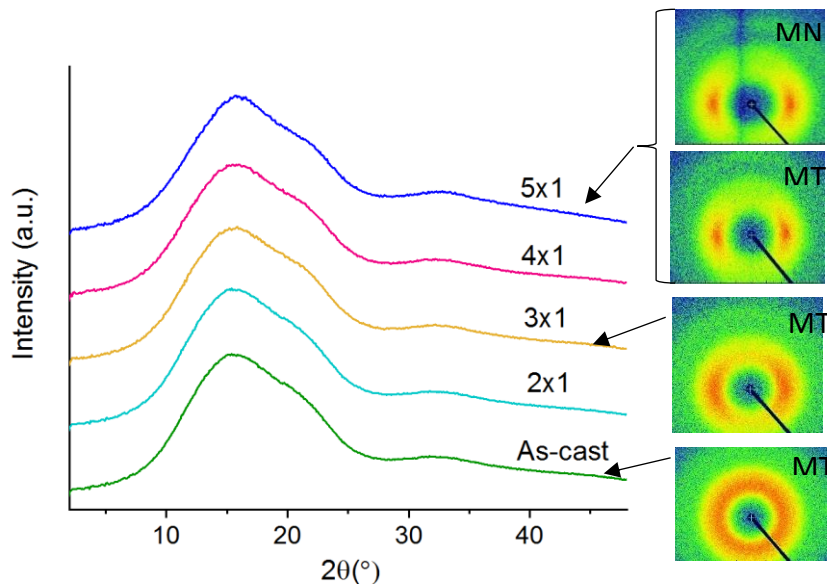

Figure III. 31. Diffractograms obtained for unioriented samples at various draw ratios with a few 2D WAXS in-plane& profile patterns selected at some characteristic draw ratios.

For UO samples, a pair of equatorial arcs were detected on both MT& MN patterns indicating that a chain orientation along the MD axis is induced during the stretching. The similarity of in-plane and profile patterns shows that the induced orientation is of cylindrical nature around the sollicitation axis. The arcs become more and more defined and intense with the increase of draw ratio, which is a sign of a gradually stronger level of orientation which will be quantified. The mesophase content induced during uniaxial stretching has been quantified from deconvolution of the diffractogram profile. *Table III. 6* shows that, similarly with BO, the induced mesophase quantity is very modest even for highest draw ratio, showing that the stretched films stay globally amorphous.

Table III. 6. Mesophase contents obtained for samples unioriented at various ratios using a deconvolution method.

Draw ratio	Mesophase (% ±2)
2x1	0
3x1	0
4x1	3
5x1	5

III.5.3.   Orientation characterization by FTIR

An example of trichroic spectra obtained for a sample stretched up to 5x1 is shown in *Figure III. 32*. The superposition of the spectrums obtained along TD and ND confirms the cylindrical nature of the orientation towards stretching axis MD
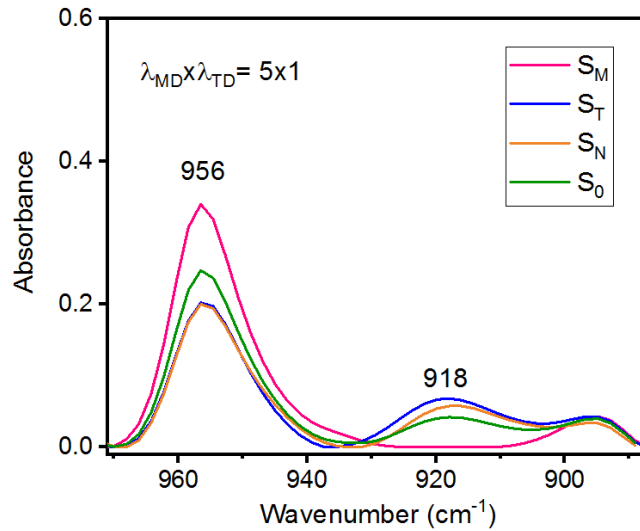
Figure III. 32. Trichroic spectra obtained for a sample unioriented at 5x1.
T_d=70ºC, $\dot{\varepsilon}$=0.1/s).

For the characteristic band at $956 cm^{-1}$ which stands for the orientation of the amorphous phase, the band absorbance in S_M is higher than in S_T and S_N. This indicates that the chain orientation is, as expected, more important along MD, i.e. along the stretching axis. The orientation of the mesophase, illustrated by the band at $918 cm^{-1}$, is hardly observed in S_M while it is clearly

noticeable on the other spectrums. Considering that this band is perpendicular, this observation actually indicates that this strain induced mesophase is strongly oriented along MD, which is in accordance with results previously reported in (Hu et al., 2012).

Since mesophase is present at very low quantity, the quantification of the orientation factor was mainly carried out for amorphous phase and the orientation-strain at break correlation result is presented in *Figure III. 33*. For UO samples a critical orientation $f_{cM} \approx 0.15$ is required to activate the B-D behavior and at around $f_{cM} \approx 0.26$ an optimum gain in terms of stretchability can be reached.
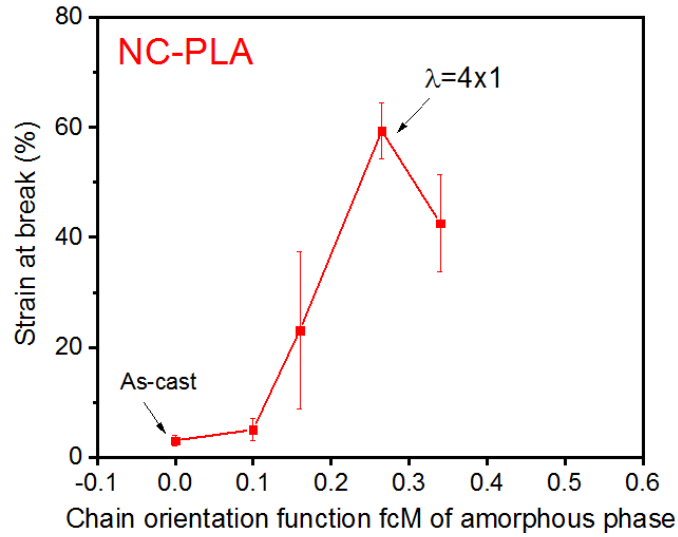
Figure III. 33. Strain at break values of pre-unioriented samples as function of the amorphous chain orientation function f_{cM}.

In summary, in the same manner than for biaxial stretching, uniaxial stretching above glass transition can also induce a B-D transition when a sufficient chain orientation degree is achieved. Nevertheless, the favorable effect of orientation on mechanical properties can only be detected when sampling along the direction of stretching axis. By contrast, biaxial stretching produces thin, non-textured (in-plane) films with more outstanding gain on strain-at-break whatever the sampling angle used, which is a competitive characteristic for applications in domains such as packaging.

III.6.   The effect of physical aging on mechanical properties of BO PLA

The previous results were obtained for "freshly" drawn BO films that are only aged of a few hours at room temperature (cf II.2.1.2) after biaxial stretching. As formerly discussed in chapter I, PLA is a polymer that ages fast with time. Consequently one can wonder if physical aging has an influence on the stretchability improvement gained after BO.

To evaluate the influence of physical ageing on mechanical behavior of this polymer, NC-PLA drawn at 3x3, being globally amorphous and presenting a ductile behavior (strain at break ∼ 100%), is a perfect case of study. Rejuvenated as-cast NC-PLA (sample was heated during 2 min at 70°C) will also be studied as reference sample.

A lot of specimens were cut from a NC-PLA film drawn at 3x3 at the same moment. Then these specimens were stored at temperature-controlled room (23°C) for different periods before being tested on uniaxial stretching. For each ageing period, five specimens were tested and the most representative curve of each ageing conditions is shown in *Figure III. 34(a)*. The ageing time ranges from days to years so only a few typical periods were chosen for sake of clarity.

The influence of ageing on tensile behavior of as-cast NC-PLA is also studied as a reference. Cast films are intrinsically brittle so only a comparison between a "fresh" sample to a well-aged one is presented in *Figure III. 34(b)* for sake of simplification
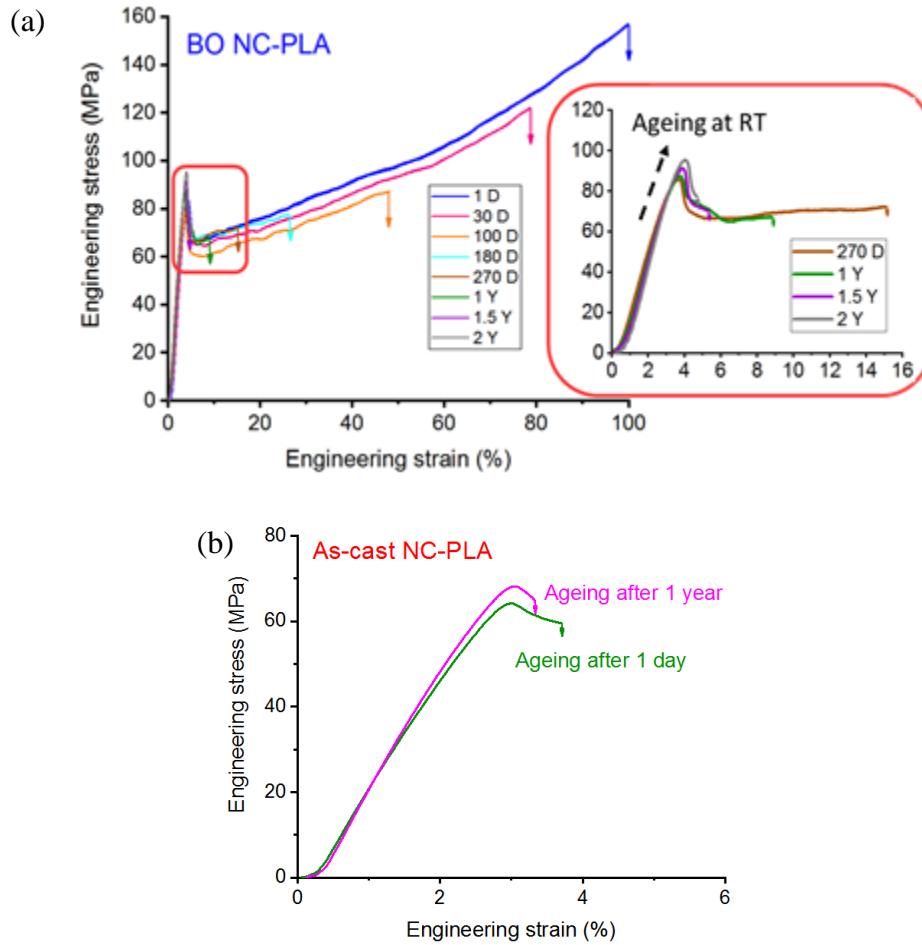
Figure III. 34. (a)Representative engineering stress-strain curves obtained with samples after various ageing times at room temperature (D for days and Y for years). (b)Representative engineering stress-strain curves obtained for as-cast NC-PLA samples after ageing period of 1 day and 1 year.

It can be seen that the improvement of stretchability decreases as the ageing time increases while all the stress-strain curves exhibit a well-defined yield point even for the longest ageing time, i.e. 2 years. For these long aging durations a slight increase of yield stress is observed as compared to unaged sample.

For as-cast samples, there's no significant evolution of the mechanical behavior of NC-PLA between samples during aged one day and one year. A slight increase of the "pseudo" yield stress can still be detected for aged sample, which is similar, though a lot less significant, to observation in case of BO sample. These findings is in agreement with the work of (Pan et al., 2007).

The characteristic tensile properties in terms of strain at break values and yield stress (only for BO sample) are plotted as function of ageing time (days), as shown in *Figure III. 35*.

127
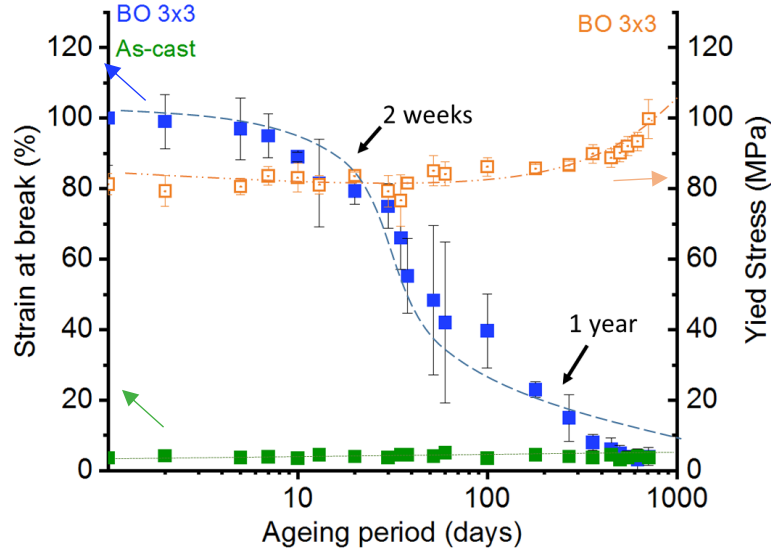
Figure III. 35. Strain at break and yield stress plotted as function of ageing days for BO and as-cast NC-PLA.

The improvement of stretchability, initially around 100%, is still observed within the ageing period of two weeks. Then, the stretchability begins to systematically decrease with ageing time to a minimum value around 10% at the end of one year of storage. After 2 years of ageing, the BO sample nearly loses all the initial improvement of strain at break. At the same time, the yield stress is increased from 80 to around 100MPa with ageing.

Although the improvement of strain at break value of BO film may decay substantially down to the same order of that of a cast sample, the former will not display a completely brittle behavior: a well-defined yield stage is always detected upon deformation even after a significant time of ageing.

Conclusions of chapter

On macroscopic scale: a study of structure-mechanical properties of PLA

⭐ Key conclusions

✧ Chain orientation in the amorphous phase is the key parameter which controls the ductile behavior.

✧ Varying stretching parameters results in different orientation states of the amorphous phase and sometimes modifies the nature of the strain-induced phase (mesomorphic or crystalline).

✧ The same critical orientation function value in the amorphous phase was found to induce the B-D transition whatever stretching conditions in the case of biaxial stretching.

✧ Strain-induced crystals limit the stretchability.

✧ Biaxial stretching is more favorable than uniaxial stretching as a processing route to improve the stretchability of PLA.

✧ The improvement of the strain at break gradually decreases with the increase of the physical aging time, but after two years the samples do not become again, as brittle as the as-cast sample.

Chapter IV

A microscopic study of orientation- deformation mechanisms of PLA

This chapter focuses on the characterization of the plastic deformation mechanisms involved during stretching of PLA in glassy state. Both isotropic and pre-oriented samples were studied in order to investigate the origin of the B-D transition identified in chapter III.

Firstly the qualitative results obtained from in-situ tests carried out at ESRF will be presented. Further investigations concerning the influence of molecular orientation on the initiation of elementary deformation mechanisms were carried out using both a "pseudo in-situ" experimental method and a post-mortem scanning analysis as described in chapter II. Finally, the main parameters which govern the micro-mechanisms determined from the previous analysis will be correlated to the orientation functions measurements, in order to provide some answers regarding the origin of the transition of macroscopic mechanical behavior induced by molecular orientation.

IV.1. In-situ evaluation of deformation mechanisms (ESRF)

It is well-known that amorphous polymers show two main localized plastic deformation mechanisms: crazes and shear bands. The description and characteristics of these two elementary plastic deformation mechanisms have been presented in chapter I. Generally speaking, brittle polymers tend to deform preferentially by crazing while ductile polymers deform rather by shear bands.

In-situ SAXS analyses were carried out to identify the elementary plastic deformation mechanisms involved during uniaxial stretching at room temperature of both isotropic and BO PLAs that have been in depth characterized on a macroscopic scale in chapter III. As previously presented, as-cast PLA samples are brittle whereas the BO ones can exhibit a ductile behavior when a critical orientation factor of the amorphous phase is achieved. *Figure IV. 1* presents some characteristic SAXS patterns recorded during stretching of two samples showing brittle or ductile mechanical response.
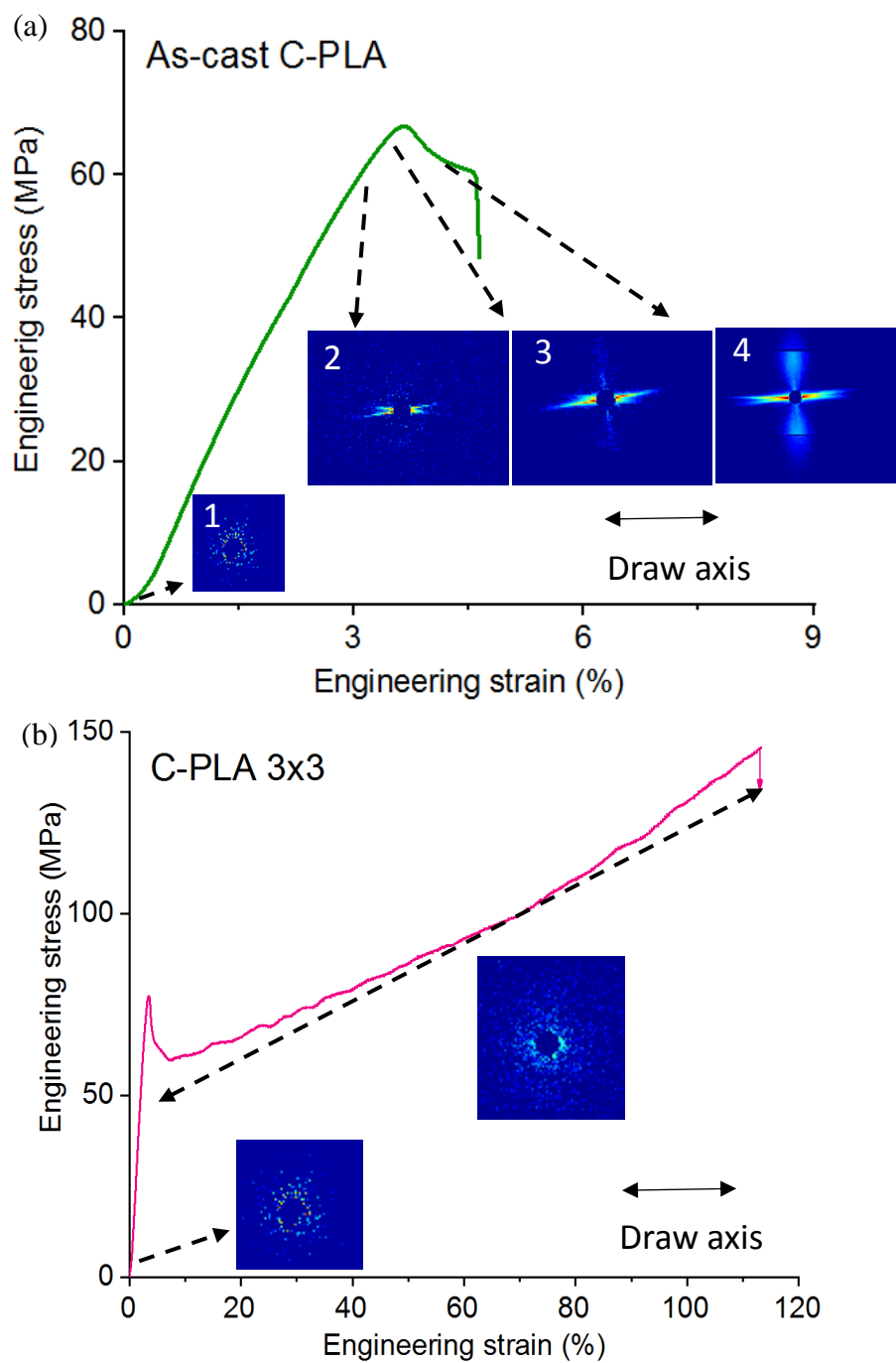
Figure IV. 1. In-situ SAXS patterns recorded during uniaxial stretching of (a) an as-cast C-PLA and (b) a C-PLA biaxially stretched at 3x3.

Different characteristics of deformation mechanisms are observed:

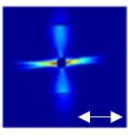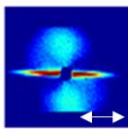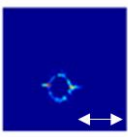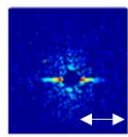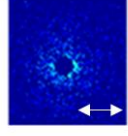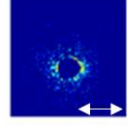(1) For the brittle as-cast sample, the SAXS patterns are characteristics of crazing mechanism.

- Pattern 1 (at the beginning of stretching) shows a central isotropic scattering with very low intensity, illustrating the isotropic and not-ordered nature of the sample.

- Pattern 2 (close to σ_{max}) exhibits intense streaks along the direction parallel to draw axis. These streaks arises from the scattering of ellipsoidal voids created into the polymer matrix. These voids have their main axis perpendicular to the draw direction. This observation reveals the presence of early-initiated localized micro crazes.

- Pattern 3 (at ~ σ_{max}) shows that the intensity of these streaks increases as well as their length suggesting an increase in terms of both density and size of voids. In addition, a vertical diffuse streak appears. This suggests the presence of a periodic arrangement of fibrils within the voids, in agreement with standard structural description of crazes discussed in chapter I.2.

- Pattern 4 (just before failure) becomes more representative of the signature of crazing. The pattern consists in one horizontal long streak related to craze thickness and the two broad ellipsoidal lobes corresponding to the periodic fibrillar structure containing oriented polymeric materials along draw axis.

(2) For ductile samples, on the contrary, only a diffuse isotropic scattering with low intensity is detected during all the experiment (*Figure IV. 1(b))*. This clearly demonstrates that for ductile polymer crazing is not involved as a main deformation mechanism during the stretching.

The observation of the non-occurrence of crazing in oriented samples is in good agreement with previous work carried out in our research group (Ouchiar et al., 2016).

In order to get an overview of the influence of biaxial stretching on the deformation mechanisms involved, the most representative patterns obtained just before failure for have the different BO samples were recorded and associated to their macroscopic deformation behavior. The results for both grades of PLA are available in *Table IV. 1*.

Table IV. 1. A summary of typical SAXS patterns obtained before failure of as-cast and BO samples obtained during in situ ESRF experiments (draw axis horizontal).

	C-PLA			NC-PLA	
$\lambda \times \lambda$	Mechanical behavior	Typical pattern	$\lambda \times \lambda$	Mechanical behavior	Typical pattern
As cast	Brittle		As-cast	Brittle	
2x2	Transition		2x2, 2.5x2.5	Transition	
Beyond 2x2	Ductile		Beyond 2.5x2.5	Ductile	

From this table three types of SAXS patterns can be identified:

- Type 1: Brittle samples.

  The SAXS patterns reveal a high density of crazes as evidenced by the high scattered intensity. The ellipsoidal lobes from the scattering from fibrils are more diffuse and broader in case of NC-PLA, suggesting that the structure of fibrils of the craze initiated in this polymer could be less oriented than in case of C-PLA.

- Type 2: Transition zone.

  The crazing density is strongly decreased for BO samples just approaching the critical orientation factor but the improvement of stretchability is not yet

remarkable. At such stage, a "transient" state is detected: the vertical streak nearly disappears completely while a minor horizontal one is still detectable. This shows that craze formation is extensively suppressed as compared to as-cast samples. Some minor crazes may still be initiated but at a strongly reduced intensity and fail to develop well-fibrilled internal structure.

- Domain 3: Ductile samples.

    Crazing mechanism is completely inhibited for largely strained, ductile samples for BO PLAs of both grades.

Morphology observation

In order to better characterize the deformation mechanism involved for BO samples enduring ductile behavior, morphology observations have been carried out through optical microscopy and a typical obtained image is illustrated in *Figure IV. 2*.
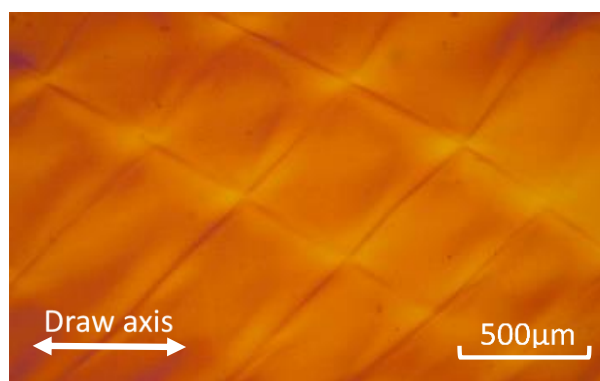
Figure IV. 2.   Optical microscopy image showing shear bands obtained for a post-mortem ductile BO PLA

It can be seen that intersecting bands inclined approximately at 35° about draw axis dominate the deformation mode known as characteristics of shear banding mechanism.

The comparison of the post-mortem morphology observation (optical microscopy) with the in-situ SAXS results allows to drawn the following conclusion: with the increasing of molecular orientation the initial mode of deformation, i.e. crazing, tends to be suppressed for the benefit of shear banding. Such behavior leads to improvement of

ductility. In other words, **the transition of mechanical properties consists in fact in the switch of one deformation mechanism (i.e. crazing) towards another one (i.e. shear banding). This switch is governed by the macromolecular orientation parameter. However a narrow zone in terms of macromolecular orientation exists with the coexistence of these two mechanisms.**

Our in-situ experiments performed at ESRF (D2AM-BM02) did not allow to perform a quantitative analysis due to some missing q ranges located in the area of interest originating from "dead zones" on the detector (cf II.2.4).

In that case, to study in depth how molecular orientation involved the suppression of the crazing mechanism, "pseudo in situ" analysis has been carried out in the laboratory on both grades of PLA in order to determine useful quantitative information related to crazes. Particularly a "semi-quantitative" analysis on craze density and on fibril geometry was carried out in laboratory in order to investigate the effect of macromolecular orientation on these two parameters.
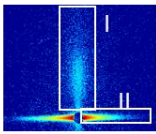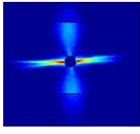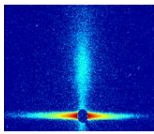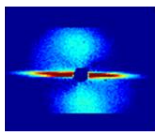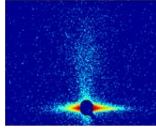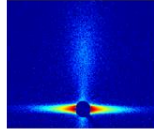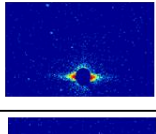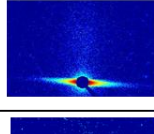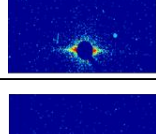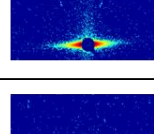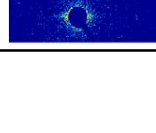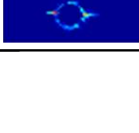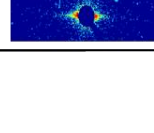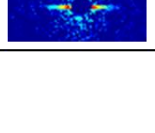
IV.2. "Pseudo in-situ" analysis of deformation mechanisms

As mentioned previously, a transition of mechanism from crazing to shear banding is at the origin of the macroscopic B-D transition. However, the change seems to be rather sudden since crazing was already strongly suppressed even at lowest tested BO ratio, e.g. 2x2. Consequently the qualitative results of ESRF need to be completed to explain how molecular orientation prevent the crazing mechanism.

To address this point, it is essential to investigate the deformation behavior of films having orientation values just below and near the B-D transition. For this purpose, BO films of lower draw ratios than 2x2 (i.e. 1.25x1.25, 1.5x1.5…) of both grades of PLA were prepared (70ºC, 0.1/s) and tested with "pseudo in-situ" SAXS experiments (cf chapter II for detailed experimental parameters).

The characteristic patterns recorded just before sample's breaking during "pseudo in-situ" tests (lab) are summarized in *Table IV. 2*. These results are compared to the patterns recorded just before rupture during real time in-situ experiments (ESRF) for as-cast and BO samples.

Table IV. 2. Comparison of characteristic SAXS patterns recorded just before the sample rupture of as-cast and BO samples of both grades of PLA obtained from "pseudo in-situ" tests (lab) and real-time in-situ tests (ESRF). The draw axis is horizontal.

	C-PLA		NC-PLA	
	Lab	ESRF	Lab	ESRF
As-cast				
1.25x1.25		ND		ND
1.5x1.5		ND		ND
1.75x1.75		ND		ND
2x2				

From the table, one observes a similarity between patterns recorded during "pseudo in-situ" tests and real-time in situ experiments performed at ESRF. This indicates that samples do not relax too much during the "pseudo in-situ" conditions and consequently validates our experimental protocol. Moreover, these experiments allow to complete the observations of in-situ experiments performed at ESRF by characterizing samples with intermediate BO ratios.

All samples tested on "pseudo in-situ" using lab equipment, either non-stretched or pre-oriented with low BO ratios, have shown signature of crazing as main deformation mechanism. When compared to ESRF results where crazing is abruptly suppressed at

2x2, lab results have illustrated for both types of PLA a more gradual attenuation of scattering intensities of zone I (from fibrils) and zone II (from craze voids/polymer walls) with BO ratios increasing.

However, one can notice that, at the same BO ratio, the scattering from both zones is more intense for NC-PLA than for C-PLA suggesting that the crazing density is higher for NC-PLA than for C-PLA. The different chain orientation kinetics determined previously for these two PLAs may explain this observation. Since the amorphous phase of C-PLA tends to be more oriented than that of NC-PLA for the same BO ratios, the preventing effect of molecular orientation on crazing would naturally manifest at lower BO ratios in case of C-PLA.

IV.2.1. The evolution of craze density

In order to go further into the influence of chain orientation on the craze density, the integrated intensity profile extracted from zone II (craze voids/polymer walls) of patterns presented in *Table IV. 2* of both PLAs were computed and are illustrated in *Figure IV. 3*. The intensity profiles are normalized with respect to sample's thickness.
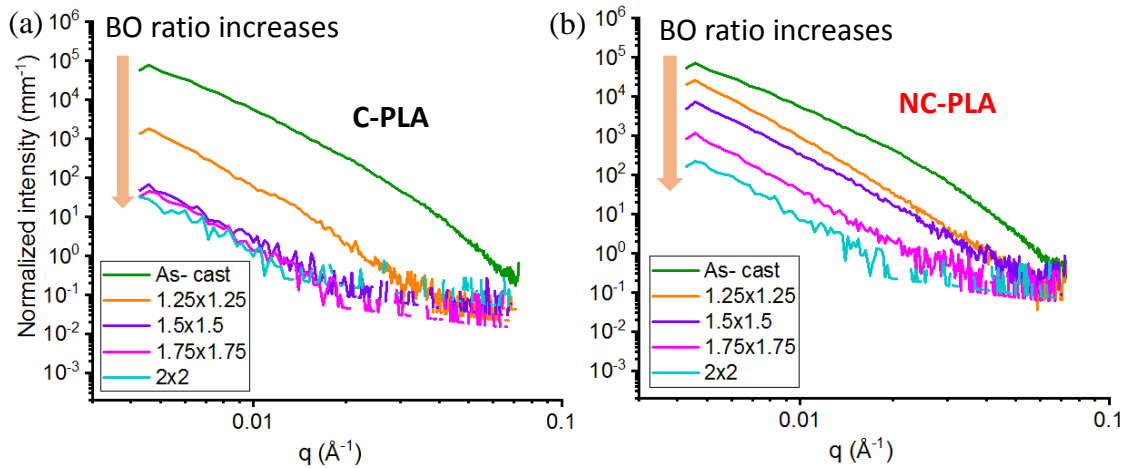
Figure IV. 3. Normalized intensity profiles extracted from zone II of as-cast and BO samples of (a) C-PLA and (b) NC-PLA.

It should be noted that the geometric parameters related to the craze voids (craze thickness, craze length…) are not quantifiable with these intensity profiles because the

size of scattering objects are too large considering the limited accessible q-range in the pseudo in-situ experiments conditions. However, at low-q values, the scattering intensities, that are proportional to initiated craze density, provide valuable information regarding the evolution of craze density as function of BO ratio. In particular, for both grades of PLA, it is observed that the normalized intensity level systematically decreases with the increase of BO ratios: this indicates that the more the samples are pre-oriented, the less the crazes are initiated during deformation.

IV.2.2.   Evolution of the craze fibrillar structure

This section deals with the evolution of the interior craze structure, i.e. of the geometric parameters of the internal fibrillary structure as a function of BO ratios. The intensity profiles extracted from zone I (craze fibrils) of patterns presented in *Table IV. 2* are depicted in *Figure IV. 4*. The intensity profiles are normalized to sample thickness. Note that only samples showing detectable scattering from craze fibrils are illustrated.
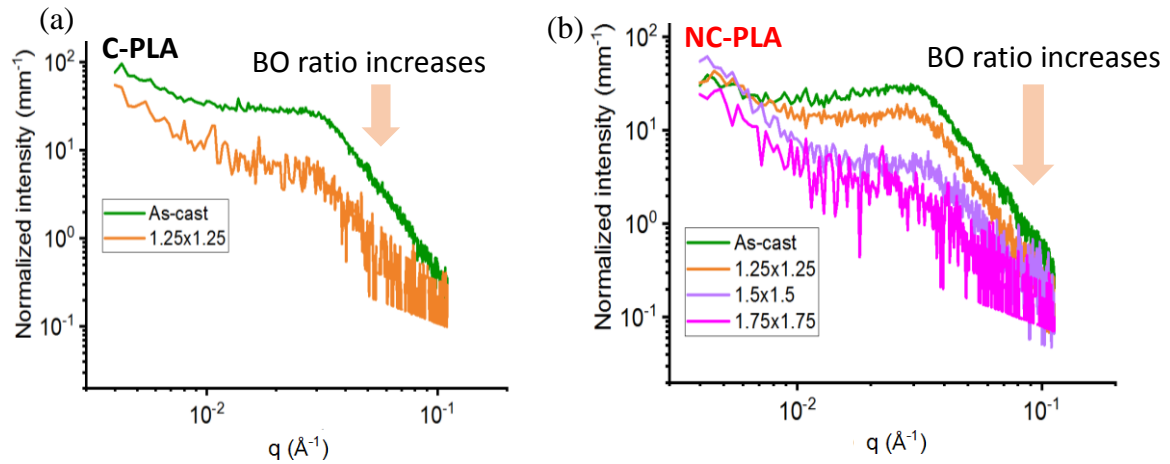
Figure IV. 4. Normalized intensity profiles extracted from zone I of as-cast and BO samples of (a) C-PLA and (b) NC-PLA

The scattering profiles exhibit characteristic of a fibrillar structure, with the presence of a broad peak in the intermediate-q zone indicating that the fibrils are regularly ordered (cf II.2.4). It is observed for both PLAs that the increase of the BO ratio involves a decrease of the intensity of this correlation peak as well as a decrease of the

total scattered intensity. This is correlated to the reduction of the craze density in pre-oriented samples, while not necessarily to a change of the geometry of craze fibrils.

To clarify the latter issue, authors conduct a series of modeling analysis of these curves to estimate the main characteristic parameters of the fibril structure: the fibril diameter (D_0), and the interfibrillar distance (L_0). The modeling method has been described in details in Chapter II.4.1. The results for both PLAs are summarized in *Table IV. 3*. Note that some samples are marked with "not determined" because the scattered intensities of these profiles are too low to be quantitatively analyzed.

Table IV. 3. Summary of the modeling results of the geometric parameters of craze fibrils for the as-cast and BO samples (both C-PLA and NC-PLA).

BO ratio λxλ	C-PLA		NC-PLA	
	D_0 (nm)	L_0 (nm)	D_0 (nm)	L_0 (nm)
As-cast	7	17	7	18
1.25x1.25	6	17	8	17
1.5x1.5	ND		8	16
1.75x1.75	ND		ND	

Table IV. 3 shows that the fibril diameter and interfibrillar distance are similar for both grades of unstretched PLA. The calculated fibril diameter values are in the same order that what was already reported for other glassy polymers, e.g. for PS and PMMA D_0 is in the range of 6-8nm (Berger, 1990; H R Brown et al., 1984; Mills et al., 1985).

As for BO samples, it was noted that the geometric parameters of craze fibril remain almost constant when the BO ratios increase. Along with results of former section, one may conclude that molecular orientation mainly influences the amount of crazes formed during the deformation rather than the internal craze structure which remains rather similar whatever the BO ratio.

The origin of this craze density decrease with the increase of the BO ratio will be discussed in details in next section.

IV.3. Post-mortem scanning analysis

It is observed from in-situ analyses that the increasing of BO ratio tends to suppress the formation of crazes upon deformation. A possible explanation could be that a higher level of energy is required to initiate crazes in pre-oriented samples than in the case of non-stretched ones. In other words one can assume that the "craze initiation stress" increases with the molecular orientation. Consequently this deformation mechanism will be no longer the more "cost effective" above a critical BO ratio.

To clarify this point, post-mortem scanning experiments were carried out to determine the craze initiation stress for the as-cast and BO samples for the two grades of PLA. In this study, samples are stretched up to rupture and analyzed by SAXS, as described in chapter II.4.

IV.3.1. Mechanical behavior of BO films of low draw ratios

The stress-strain curves of BO films of intermediate draw ratios are shown in *Figure IV. 5* for both types of PLA.
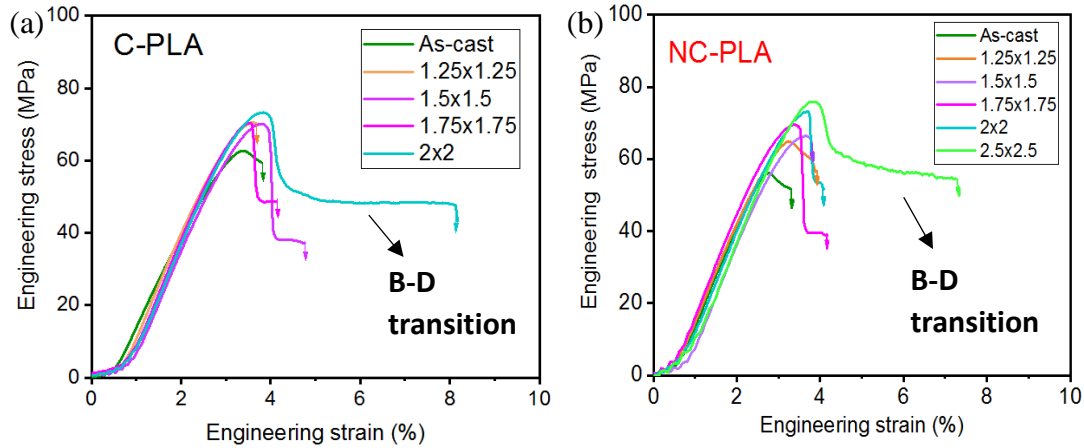
Figure IV. 5. Engineering stress-strain curves of as-cast and BO samples drawn at intermediate ratios of (a) C-PLA and (b) NC-PLA samples. Tensile test conditions: 23°C, $\dot{\varepsilon} = 4x10^{-3}s^{-1}$.

As expected, it can be seen from the figure that all samples with BO ratios lower than the onset value of B-D transitions are brittle. Then, as draw ratio increases, both polymers are able to gradually develop a yield point followed by a progressive

enhancement of stretchability. One can notice that NC-PLA needs to be further pre-oriented than C-PLA to form a well-defined yield point. This observation should be related to the different orientation kinetics of the two grades of PLA, as shown in our previous results. Moreover, for samples whose yield point is clearly detected, the values of σ_y (yield stress) seem to slightly increase with draw ratio. Especially in the case of NC-PLA, σ_y increases from 70 to 80 MPa during the B-D transition and then remains almost constant combined. In the meantime an enhancement of stretchability is observed.

These results, complementary to the former in-situ SAXS analysis, indicate that the change of macroscopic mechanical behavior is closely related to the evolution of microscopic deformation mechanisms. In particular, for films of low BO ratios, such as 1.5x1.5 (C-PLA) and 1.75x1.75 (NC-PLA), crazes are extensively suppressed and the according mechanical behavior of these samples immediately begin to exhibit a ductile behavior indicated by the presence of a yield point. However, it would be more suitable to classify these samples as "transition" samples because they are still far from being truly ductile showing just a modest enhanced stretchability.

IV.3.2. Influence of molecular orientation on the initiation of elementary plastic deformation mechanisms

In order to determine the critical stress of craze nucleation, the broken samples from uniaxial stretching tests were analyzed by SAXS. A mapping of the samples was carried out along all the sample length with a step size of 200μm. An example of scanning is shown in *Figure IV. 6*. Note that only a few representative patterns are presented for sake of clarity.
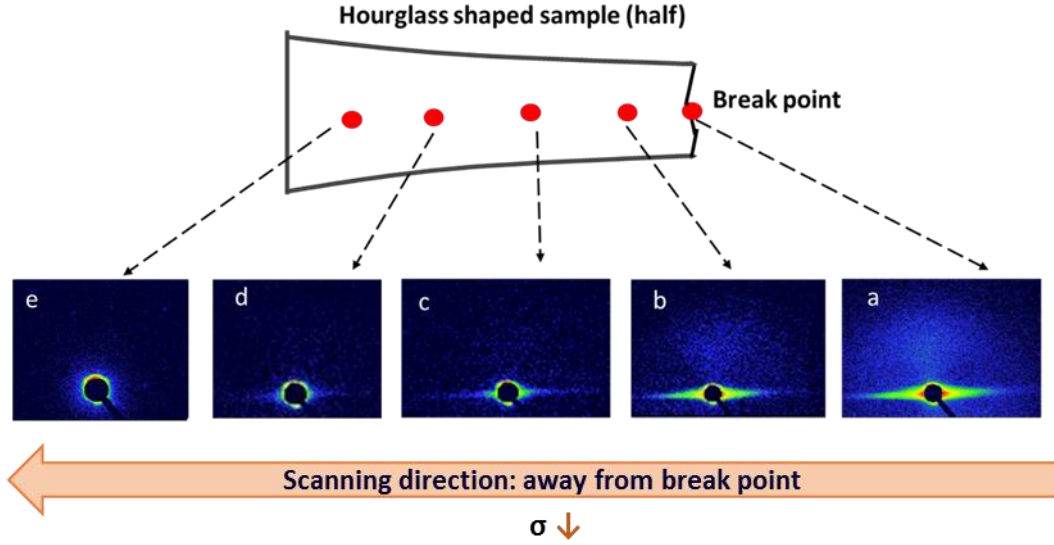
Figure IV. 6. SAXS patterns taken at different distances away from break point during the scanning analysis of a post-mortem as cast C-PLA sample.

Regarding the influence of the scanning position, it appears that the scattered intensity is significantly higher near from the fractured zone (pattern a). This is related to the sample geometry (hourglass shape) which induces a stress concentration in this area.

With the scanning direction going further away from this failure area (i.e. with the decrease of the stress applied), the scattering intensity in both the vertical and horizontal streaks is gradually reduced, indicating the heterogeneous distribution of crazes density along the sample length. As shown by patterns c and d where the vertical streaks characteristic of fibrils are hardly detected, one may suspect that at these positions only some minor, localized crazes are formed but failed to be enough thickened to develop well-fibrilled structure before sample rupture.

Pattern d corresponds to the last position where a signal of craze can be detected. Then, considering the sample geometry as described in chapter II.4, the stress value at this specific position (i.e. σ = Force/ (length*width of the sample at this position)) is calculated and associated to the critical stress of craze nucleation σ_{cr}.

The critical stress of craze initiation deduced from the post-mortem scanning analysis and the yield stress determined from the engineering stress-strain curves (*Figure IV. 5*) were plotted as function of BO ratios for the two grades of PLA (*Figure IV. 7*).
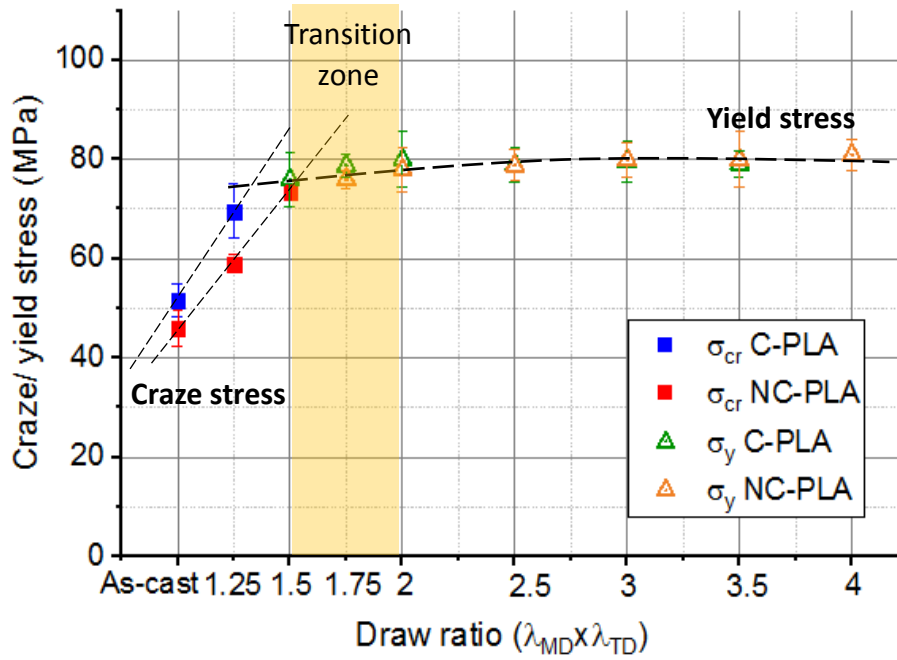
Figure IV. 7. Evolution of craze stress and yield stress as a function of BO ratios for C-PLA and NC-PLA.

For both PLAs, two main evolutions can be distinguished:

- For BO ratios lower than the onset value of B-D transition, the craze initiation stress steadily increases with the BO ratio.

- For BO ratios above 1.5x1.5, the yield stress is almost constant with a value around 80 MPa whatever the draw ratio.

Note that while the yield stress is similar for both PLAs, the value of craze stress is slightly lower for NC-PLA compared to C-PLA at same draw BO ratios. In order to check if it is related to the different macromolecular orientation kinetics, the craze/yield stresses are plotted as function of orientation factor, and some representative

morphology observations are also illustrated for NC-PLA (*Figure IV. 8*). Note that similar results are obtained for C-PLA.
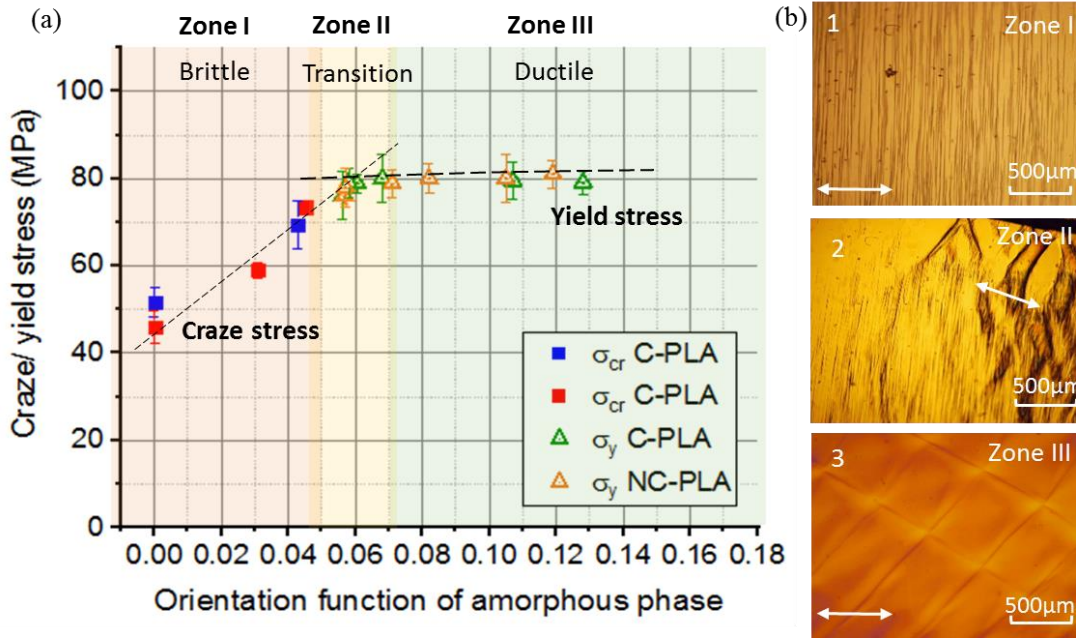
Figure IV. 8. (a) Craze/yield stress plotted as function of the orientation function of amorphous phase and (b) Representative morphology observations of deformation mechanisms of post-mortem samples with different orientation functions (NC-PLA).

These observations reveal that the change of crazing to shear banding with the orientation function increase is accompanied by a transition zone where the two mechanisms coexist. In summary three characteristic domains can be identified:

- Zone 1 ($f_{cM} < 0.05$): in this domain, σ_{cr} is lower than σ_y if one extrapolates the latter considering the constancy of σ_y with the orientation function. In this domain, crazes are the predominant deformation mechanism (image 1) as their stress nucleation is fairly lower than the one of shear bands. Elongated thin craze/cracks are formed perpendicularly to the draw axis. With increasing the draw ratio, σ_{cr} increases systematically, indicating more difficulties for crazes to be initiated. This explains the decrease of the craze density with the increase of the BO ratios previously observed during in-situ analysis. In this domain, samples break in a brittle manner upon stretching.

- Zone 2 ($0.05 < f_{cM} < 0.07$): the level of σ_{cr} begins to intersect with the curve of σ_y at around 75 MPa. In this thin "transition" zone it is possible to detect a coexistence of both elementary deformation mechanisms (image 2). Some minor, short crazes are observed together with a few localized coarse shear bands. As formerly discussed in the previous section, in this zone the mechanical behavior of these "transition" samples begins to change with the observation of a "neat yield point" upon stretching. However the overall improvement of strain-at-break is still quite modest.

- Zone 3 ($0.07 > f_{cM}$): the orientation function still increases and the extrapolation of the σ_{cr} curve leads to higher values than σ_y. This allows shear bands to become the more "cost-effective" deformation mechanism (image 3). In this domain, samples show a ductile behavior characterized by a clear enhancement of stretchability thanks to the stabilized propagation of shear bands.

In conclusion, the craze initiation stress σ_{cr} systematically increases with the increase of molecular orientation. Consequently crazes are more and more difficultly initiated. This explains the former observation of reduction of craze density obtained with samples of increasing BO ratios.

Then starting from a critical orientation value $f_{cM} \approx 0.05$, crazes are largely suppressed and shear bands begin to appear. Samples start to behave as ductile materials while the values of σ_y, seem to remain quasi-constant with the orientation factor increasing, contrary to the evolution of craze stress. The independent nature of yield stress to molecular orientation has been checked by an additional biaxial stretching study performed on polycarbonate which is well known to deform by shear bands (Appendix-IV). Note that (De Focatiis & Buckley, 2011) also reported a similar different "sensitivity" of craze initiation stress/ yield stress to orientation factor in case of stretched polystyrene

Finally, with orientation continues to increase, shear banding becomes the preferential deformation mechanism, which eventually introduces large plastic strain.

In our study, two complementary materials, PEF and PS will be investigated through the same methodology and results for these two polymers will be discussed in next chapter.

Conclusions of chapter

A microscopic study of orientation-deformation mechanisms of PLA

Origin of B-D transition: crazing changes to shear banding with increase of chain orientation

Three characteristic zones are identified:

Zone I	**Zone II**	**Zone III**
Brittle behavior	Transition	Ductile behavior
$\sigma_{cr} < \sigma_y$	$\sigma_{cr} \approx \sigma_y$	$\sigma_{cr} > \sigma_y$
Only crazes are initiated	Coexistence of crazes/ shear bands	Only shear bands are initiated

✧ The macroscopic B-D transition of mechanical behavior is assigned to a change of elementary deformation mechanism from crazing to shear banding. With orientation↑, the change of mechanical behavior is closely linked to an evolution of micro deformation mechanisms.

✧ The initiation stress of crazes/shear bands show different "sensitivity" to the increasing of molecular orientation: the craze initiation stress σ_{cr} increases systematically with greater orientation function whereas the yield stress σ_y is much less affected. This insensitivity of yield stress to orientation has been confirmed by a study on BO polycarbonate films.

✧ As orientation increases, less crazes are initiated (inner fibrilled structure remains unchanged) until reaching a transition zone where crazes& shear bands coexist. Then upon a critical orientation function value, only shear bands will be activated as favorable deformation mechanism which leads to a ductile mechanical response.

Appendix-IV

Complementary study on polycarbonate: influence of biorientation on yield stress

As formerly illustrated in case of PLA, the BO ratio seems to have no major influence on the yield stress upon uniaxial stretching, as long as the stretched films are globally amorphous, i.e. without influence of strain-induced crystals (cf *Figure III-23*).

Since PLA undergoes a change of elementary plastic deformation mechanisms with the increase of the pre-orientation factor, it appears essential for authors to conduct a biaxial stretching study on an amorphous polymer that always deforms by shear bands to confirm that yield stress is not affected by molecular bi-orientation (especially at low draw ratios) to confirm the previous hypothesis.

As a model material, polycarbonate, well-known as a ductile amorphous polymer exhibiting shear bands as main deformation mechanism, has been chosen for this complementary study. Biaxial stretching has been applied to PC films at 170ºC (T_g+25ºC) up to a draw ratio of 2x2 at a stretching rate $\dot{\varepsilon}$=0.1/s.

Mechanical behavior of non-stretched and BO films upon uniaxial stretching is shown in *Figure AIV. 1* (tested under the same parameters used in the study of PLA).
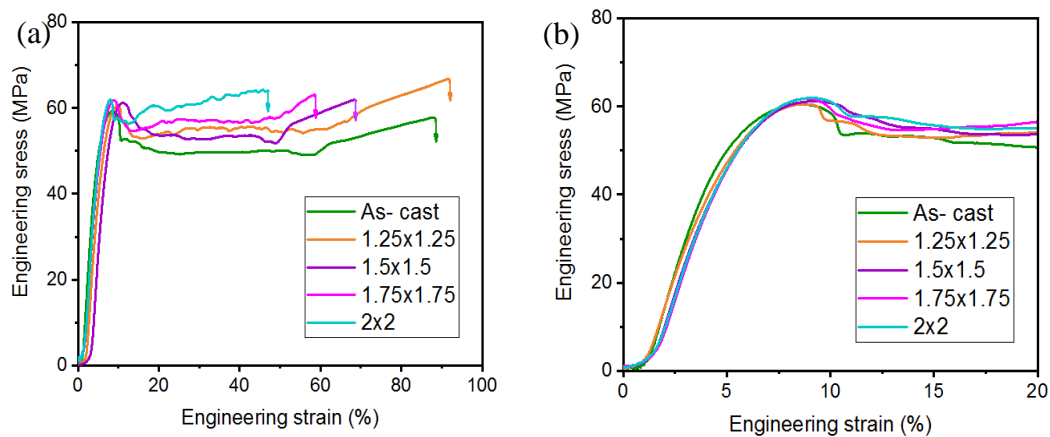
Figure AIV. 1. Engineering strain-stress curves of as-cast and BO polycarbonate films of various draw ratios upon uniaxial stretching at $\dot{\varepsilon}$=4x10^{-3}/s at room temperature: (a) until rupture (b) zoom on yield point.

It can be seen from the figure that all samples, whether pre-oriented or not, exhibit a ductile behavior upon uniaxial stretching. Each sample is able to develop a well-defined yield point where shear bands are initiated and propagate along the overall sample length until breaking with a strain at break detected at an average value over 50%.

Regarding the yield stress, whatever the draw ratios, this one remains nearly constant at around 60MPa, confirming the "insensitivity" of yield stress to draw ratio.

To confirm that macromolecules are oriented in BO PC films and that chain orientation increases with draw ratio (no major chain relaxation during the biaxial stretching), BO PC films are also characterized by trichroic FTIR. An example of trichroic spectra obtained for the most stretched film at 2x2 is available in *Figure AIV. 2(a)*. The wavenumber range of 1450-1350 cm^{-1} probing the backbone vibration of polycarbonate (Lunn & Yannas, 1972) is selected as zone of study.
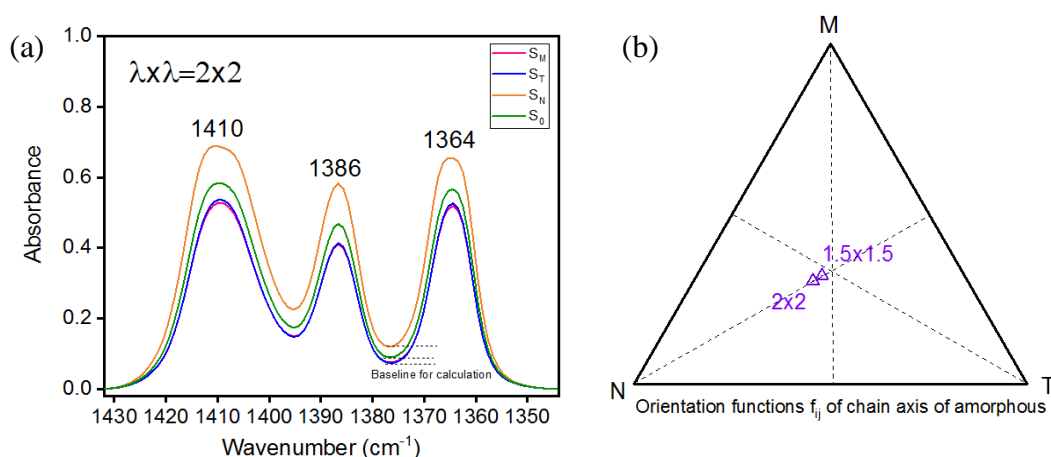
Figure AIV. 2. Trichroic FTIR results obtained for BO PC films: (a) Trichroic spectra obtained for a PC film stretched at 2x2. (b) Orientation functions f_{ij} of a few selected BO PC films presented in a Wilchinski diagram.

For the three IR bands detected in this region, a trichroic behavior is identified as indicated by the spectrum S_N which differs from S_M and S_T. This can be seen as an evidence of chain orientation induced in stretched films. Also, the band intensities in S_N are higher than that of other spectra as they possess a transition vector perpendicular to chain axis (Uchiyama & Yatabe, 2003). The orientation functions calculated from these bands are averaged and presented in *Figure AIV. 2(b)*. With increasing of draw

ratio, the orientation functions tend to approach the N direction, indicating an increasing of planar orientation of molecular chains in MT plane considering the perpendicular nature of bands used for calculations.

In summary, the observation on mechanical behavior of PC films confirmed the conclusions drawn from former studies on PLA: for amorphous materials, the molecular orientation does not significantly influence the initiation stress of shear bands.

Chapter V

Structure-property relationships of polyethylene 2,5-furandicarboxylate and polystyrene

Chapter III focused on the study of the brittle to ductile (B-D) transition in case of PLAs. This work clearly shows that the key point to induce the B-D transition is the achievement of a critical level of molecular orientation of the amorphous phase. Then, chapter IV investigated the origin of this transition which has been found to be originating from a change of the elementary plastic deformation mechanisms involved.

In order to confirm these main conclusions drawn from PLAs, and to better understand the B-D transition, the behavior of two complementary materials are also investigated:

- The first one is poly(ethylene furanoate) (PEF), a newly bio based polymer with properties comparable to the ones of PET.

- The other one is polystyrene (PS), a well-known material for which a B-D transition has also been reported (Choi et al., 1989).

The goal of this additional study is to know if the findings obtained for PLA can be generalized to amorphous polymers which intrinsically exhibit a brittle behavior.

In this chapter the analysis of these two materials will be mainly focused on three aspects to confirm the results obtained for PLA, to know:

- Is a B-D transition achievable through a biaxial orientation process?

- Is there a critical orientation factor linked to this transition?

- Does this B-D transition originate from a transition from crazing to shear banding and what is the link to macromolecular orientation?

In order to achieve these goals, the same experimental approach than the one applied for PLA described in the former chapters will be used.

V.1.   Structure-property relationships of PEF

The PEF films used are initially amorphous and isotropic with a glass transition temperature around 85°C. The first step is to obtain biaxially oriented films through stretching above T_g. The drawing temperature is set at 100°C, i.e. T_g+15°C, which is similar to the one used in the case of PLA. Draw ratios up to 4.5x4.5 were tested at a strain rate $\dot{\varepsilon}=1$ /s.

V.1.1.   Mechanical behavior of BO films

The biaxially stretched films were tested upon uniaxial stretching at room temperature and the results are shown in *Figure V. 1*.
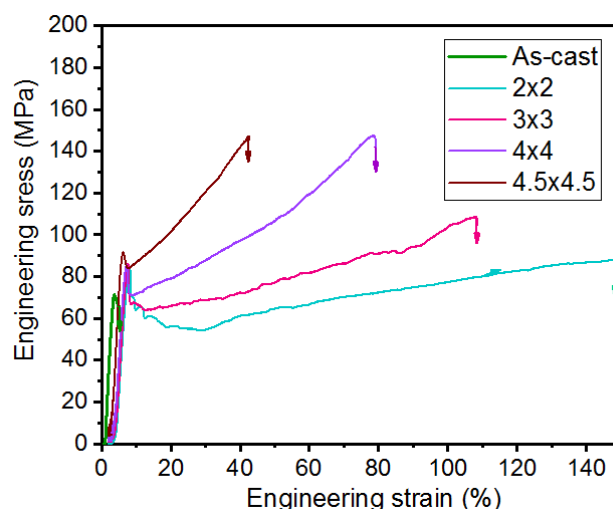
Figure V. 1. Engineering stress-strain curves of as-cast and BO PEF samples of various draw ratios upon uniaxial stretching at room temperature at $\dot{\varepsilon}=10^{-3}$/s.

It can be seen from the figure that, as observed in the case of PLA, as-cast PEF is brittle. Then, from λxλ ≥ 2x2, a remarkable B-D transition occurs with a distinct enhancement of stretchability up to 150%. This increased strain at break is in the same order of magnitude than the one obtained for BO PLA (~120%). Van Berkel et al. have reported a similar stretchability for biaxially PEF and PET films drawn in their rubbery state up to 4x4(van Berkel et al., 2018). It is worth noting that PEF is a biobased polymer able to substitute PET due to their similar properties. Consequently, it is obvious that the

comparison of the impact on biaxial stretching on the end-use properties of PEF as compared to PET is of prime interest, especially from an industrial point of view. This complementary study has been carried out and will be reported in Appendix-V.

It is also noted that even if all samples beyond 2x2 are well stretchable, the maximum strain at break value decreases with the increase of the BO ratio. Consequently a BO ratio of 2x2 is an optimum to obtain the most ductile response. This decrease of stretchability has already been reported by (van Berkel et al., 2018) in case of both BO PEF and BO PET. Also, in chapter III authors has pointed at a similar behavior for PLA. Regarding the evolution of yield stress, as observed for PLA, the increase of draw ratios does not seem to influence its value which remains roughly constant (around 85-90MPa).

In summary, it is here confirmed that it is possible to induce a B-D transition through a pre-orientation process in PEF.

V.1.2. Orientation characterization by FTIR

The quantification of the orientation functions of BO-PEF films was carried out using the perpendicular band at 619 cm^{-1} which is a characteristic band assigned to amorphous phase (Araujo et al., 2018). The orientation functions f_{ij} are plotted as a function of draw ratios in *Figure V. 2*.
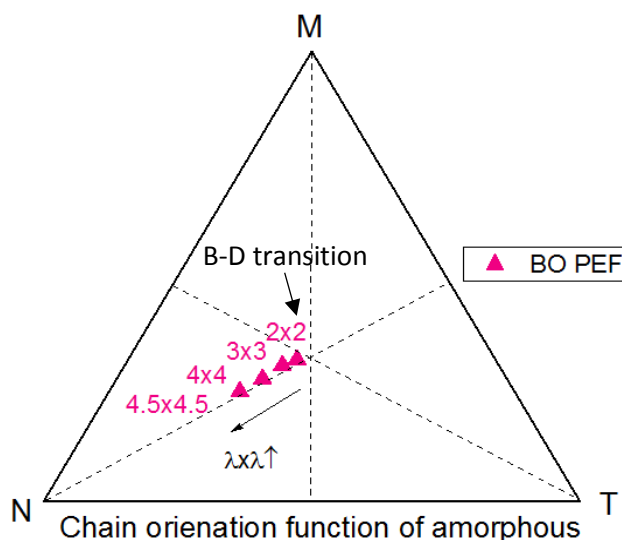
Figure V. 2. Wilchinski diagram representing orientation functions f_{ij} of chain axis c in amorphous phase of BO PEF samples as a function of draw ratios.

All points are localized along the median of MT plane, indicating an equibiaxial chain orientation in the plane (MT). When increasing draw ratio, the orientation functions values increase progressively towards the N direction related to the transition moment of the band at 619 cm^{-1} perpendicular to the chain axis.

Based on these results, a critical level of orientation of the amorphous phase required for inducing the B-D transition can be determined and corresponds to a value around $f_{cN} \approx 0.03$.

V.1.3.   Deformation mechanisms characterization

As shown previously for PLA, a change of elementary deformation mechanisms is at the origin of the B-D transition. To confirm that this phenomenon also occurs in the case of PEF, both "pseudo in-situ" and post-mortem scanning SAXS analyses, have been carried out using the same methodology as in chapter IV.

As shown previously, BO PEF shows a ductile behavior for draw ratios above 2x2. Thus to better investigate the influence of molecular orientation on the deformation mechanisms, films of lower BO ratios, i.e.1.25x1.25, 1.5x1.5 were analyzed.

V.1.3.1. "Pseudo in-situ" SAXS analysis

The characteristic SAXS patterns recorded during the "pseudo in-situ" experiments of as-cast and BO samples are presented in *Figure V. 3*.
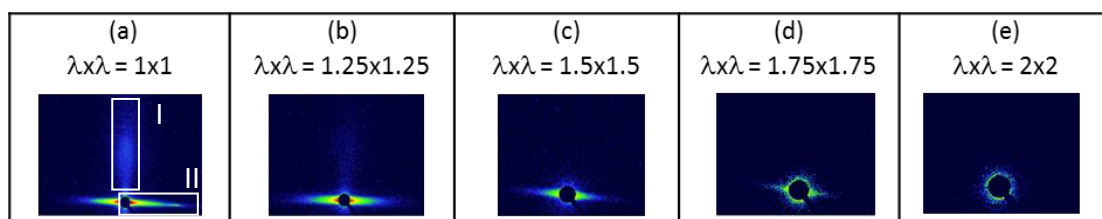
Figure V. 3. Representative SAXS patterns recorded during "pseudo" in-situ test of as-cast and BO PEF samples pre-oriented at various ratios (draw axis horizontal).

In the case of as-cast sample, the SAXS pattern is typical of the occurrence of crazing as shown by the presence of both vertical and horizontal streaks with high intensities indicating a high craze density. For BO samples, as the draw ratio increases, the scattering from crazes is gradually attenuated in terms of both vertical and horizontal streaks. This trend is observed up to $\lambda x \lambda = 2x2$ where no more scattering is observed. This evolution is similar to what was observed for PLA.

The normalized scattering intensities from craze walls (zone II) and from craze fibrils (zone I) are depicted in *Figure V. 4(a)* and *Figure V. 4(b)* respectively.
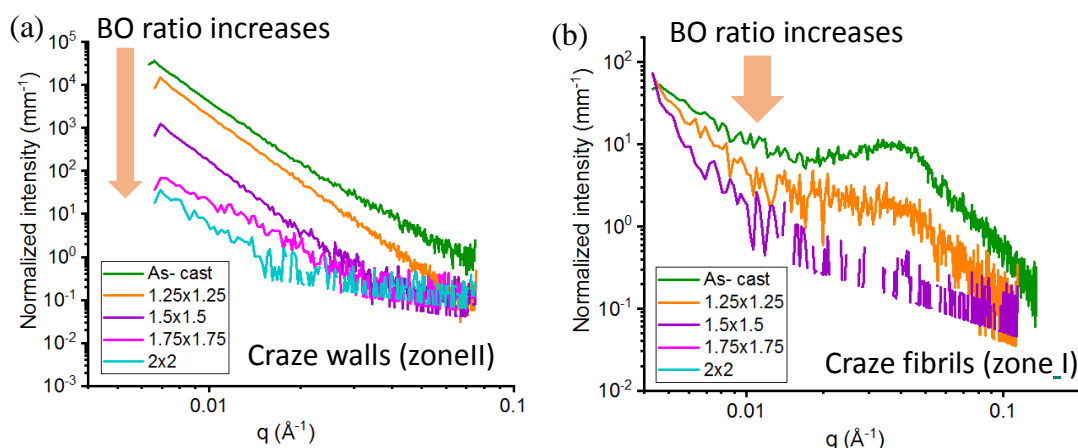
Figure V. 4. Intensity profiles (normalized with respect to sample thickness) extracted from (a) craze fibrils (b) craze/polymer walls of computed from the representative SAXS patterns of as-cast and BO samples of various pre-oriented ratios illustrated in Figure V. 3.

Regarding the evolution of the craze density, as shown in both figures, the scattering intensities from craze fibrils and craze walls decrease steadily with increasing the BO ratios. This indicates a gradual suppression of crazing due to molecular orientation. Such evolution is in good agreement with former results obtained in case of PLA.

Regarding a quantitative analysis of the data, only as-cast PEF (green curve in *Figure V. 4(b))* was successfully modeled. For this sample, a value ~ 5nm and ~ 10nm were obtained for fibril diameter and mean interfibrilar distance respectively. The curves of BO samples, due to a too low scattering, fail to give reliable modeling results.

Morphological observation of post-mortem samples

As carried out for PLA, post-mortem analyses of as-cast and ductile BO samples by means of optical microscopy have been carried out and are presented in *Figure V. 5*.
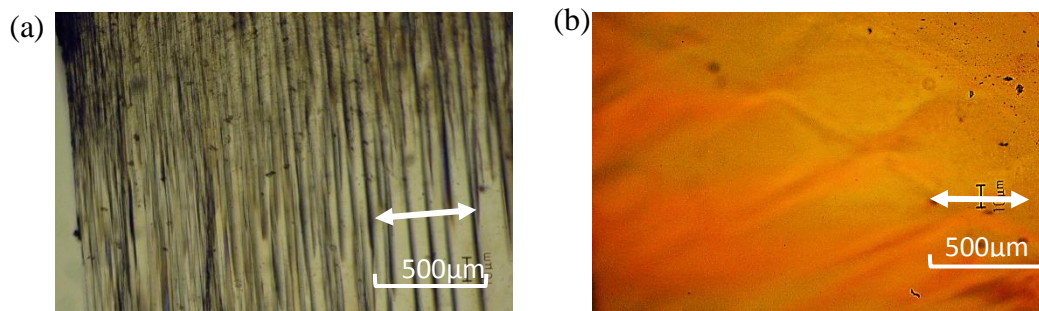
Figure V. 5. Post-mortem optical microscopy observations after rupture upon uniaxial stretching of a (a) as-cast and (b) BO sample pre-oriented at 2x2 (arrows indicate the stretching axis).

For as-cast sample, a large amount of crazes is observed on the surface perpendicularly with the draw axis. By contrast, no more craze but only shear bands are detected for the BO sample exhibiting a ductile behavior. Particularly regular fine slips intersecting at about 35º with respect to draw axis are observed.

The morphological observations confirm thus the change of deformation mechanism from crazing to shear banding with the increase of orientation in the case of PEF which involves the B-D transition.

V.1.3.2.   Post-mortem scanning SAXS analysis

The as-cast and BO PEF samples with low pre-orientation ratios are also analyzed with post-mortem scanning SAXS analyses to investigate the influence of molecular orientation on initiation stress of elementary deformation mechanisms: crazing/shear bands.

Mechanical behavior of intermediate-BO-ratio samples

The samples were uniaxially stretched at room temperature until breaking. Corresponding stress-strain curves are presented in *Figure V. 6*.
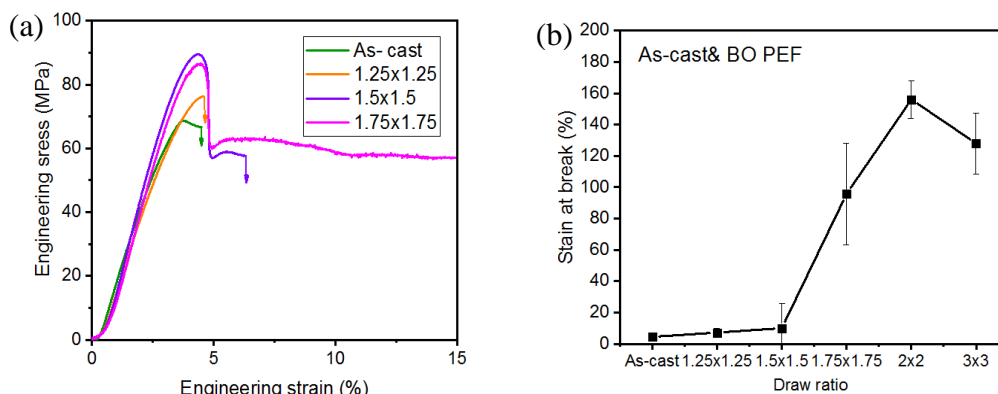
Figure V. 6. (a)Engineering stress-strain curves of BO-PEF films drawn at intermediate draw ratios upon uniaxial stretching at room temperature
(b) strain at break values as a function of draw ratio.

As shown in *Figure V. 6*, the B-D transition occurs at lower draw ratios than 2x2. From 1.5x1.5, a well-defined yield point is observed along with an improvement of stretchability. Then with increasing draw ratio, the strain at break values gradually increases up to an optimum value of 160% for sample drawn at 2x2.

Influence of orientation on craze/yield stress

The fractured as-cast and intermediate-draw-ratio BO samples were then studied by SAXS analyses. The calculated critical craze initiation stress from post-mortem scanning experiment and the yield stress determined from *Figure V. 6* were plotted as function of BO ratios and are presented in *Figure V. 7*.
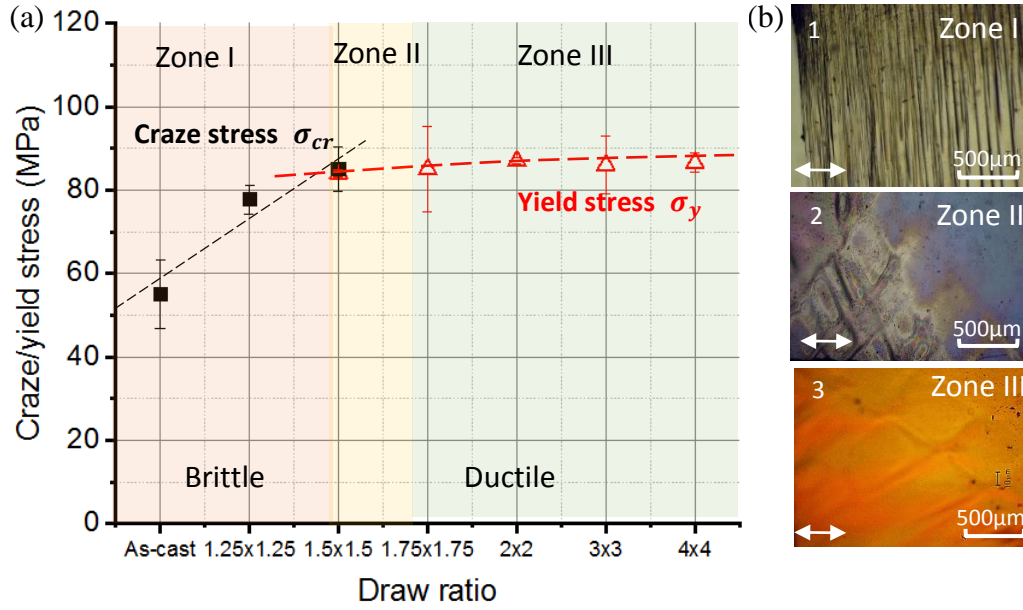
Figure V. 7. (a) Evolution of Critical craze initiation stress (calculated from post-mortem scanning analysis) and yield stress (determined from engineering stress-strain curves) plotted as function of draw ratios for PEF. (b) Optical microscopy observations of characteristic samples (the arrow indicates the tensile axis.

The critical stress to initiate crazes (σ_{cr}) in PEF increases with respect to draw ratios while the initiation stress of shear bands, assumed to be equal to the yield stress, was found to remain roughly constant.

The transition of elementary deformation mechanism from crazing to shear banding can be described as follow:

-   Zone I: brittle behavior. At low BO ratios, σ_{cr} is found to be lower than the extrapolation of σ_y so that crazing is initiated as the dominant deformation mechanism (image 1). With the increase of molecular orientation, σ_{cr} continues to grow up, resulting in a progressive difficulty to initiate crazes. Samples in this zone will always break in a brittle manner.

-   Zone II: transition zone. σ_{cr} and σ_y are similar leading to the coexistence of crazes and coarse, localized shear bands (image 2). Samples begins to show a

ductile behavior. In this zone, a relatively large dispersion of the results regarding the strain at break is observed.

- Zone III: ductile zone. With the increase of orientation, the extrapolated curve of σ_{cr} gives values above σ_y. In other words, the nucleation of shear bands is easier than the nucleation of crazes. Consequently only shear bands will be initiated leading to a remarkable enhancement of ductility.

This scenario of craze to shear transition is similar to the one discussed in the case of PLA. Consequently, it seems that a "universal behavior" may exist regarding the possibility of involving a craze-to-shear band transition by chain orientation.

In order to definitely assess this point, a third amorphous brittle polymer has been studied, the polystyrene (PS).

V.2. Structure-property study of Polystyrene

The polystyrene used for this PhD work is an amorphous grade with a high molecular weight. The films are initially isotropic and exhibit a glass transition temperature around 90°C. As previously done, the first step of the study is to obtain oriented films through biaxial stretching above T_g. The drawing temperature is set at 105°C, i.e. T_g+15°C as for PLA and PEF. Draw ratios up to 3.5x3.5 were tested at a strain rate of 100%/s.

V.2.1. Mechanical behavior of BO films

The as-cast and BO films were tested upon uniaxial stretching at room temperature. Results are shown in *Figure V. 8*.
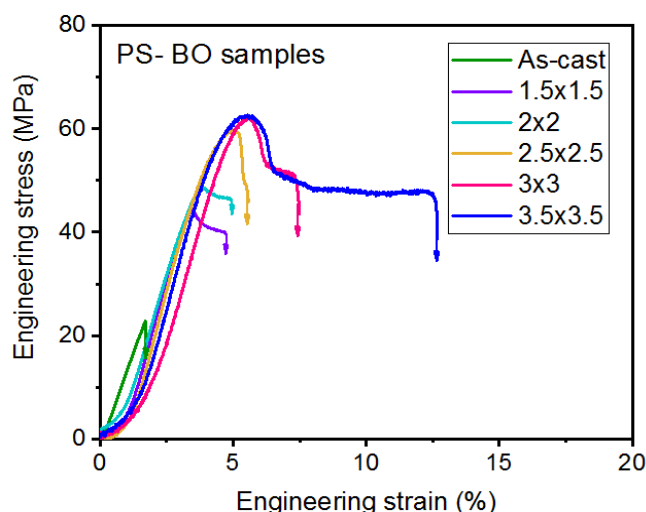
Figure V. 8. Engineering stress-strain curves of as-cast and BO PS samples of various draw ratios upon uniaxial stretching at room temperature at $\dot{\varepsilon}=10^{-3}/s$.

The as-cast isotropic PS film is extremely brittle and breaks very quickly from the early stages of deformation. Contrary to as-cast PLA and as-cast PEF samples, PS seems even fail to develop a non-linear viscoelastic domain, indicating a more pronounced intrinsic brittleness for this polymer. Regarding the BO samples, a B-D transition can be detected from a critical draw ratio above 2.5x2.5 is reached. For lower draw ratios, breaking of PS occurs before the yield point. One can observe that the stress at break increases steadily until reaching a yield around 65MPa. Starting from 2.5x2.5, the yield point is well-defined with a slight enhancement of stretchability with increasing of BO ratio. For the most ductile BO PS samples, the strain at break value is around 12% which is in the same order than what was reported by Matsumoto and his coworkers (Matsumoto et al., 1981; Xiaomin Zhang & Ajji, 2003). However this value is fairly lower than the ones reported by Choi et al. (Choi et al., 1989) where a BO PS was able to deform as much as 100% upon uniaxial stretching.

Regarding the yield stress, for samples exhibiting a well-defined yield point, it is observed that the values remain constant around 65MPa and does not seem to evolve with increasing draw ratios. This insensitivity of yield stress to orientation is in agreement with former results obtained for PLA (set-70ºC) and for PEF.

In summary, the mechanical behavior of BO PS samples confirms the possibility to induce a B-D transition by macromolecular orientation, as observed for PLA. The quantification of the orientation functions of BO-PS films will be illustrated in next section and compared to the results of PLA.

V.2.2. Molecular orientation characterization

As performed for PLA, the molecular orientation of BO films are quantified thanks to trichroic FTIR analyses. The orientation functions were calculated using the characteristic parallel band at 906 cm^{-1} (Lefebvre et al., 1981; Olmos et al., 2014; Yuan et al., 2011). The orientation function of the chain axis along MD (f_{cM}) is plotted as a function of the draw ratios and compared to the ones determined for NC-PLA. Only selected draw ratio are presented in the Wilchinski diagram (*Figure V. 9*).
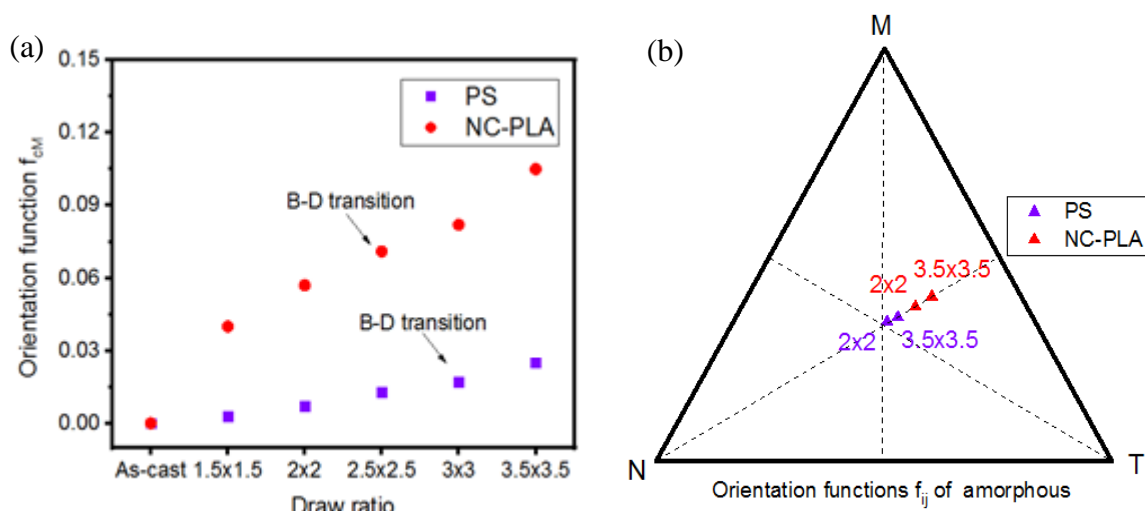
Figure V. 9. Orientation function quantified by trichroic FTIR of BO-PS and BO-PLA samples: (a) orientation function f_{cM} plotted as a function of the draw ratio and (b) representation in a Wilchinski diagram.

It can be concluded from the above figures the following points:

- As expected, chains become more and more oriented in the (MT) plane when the draw ratio is increased.

- However, for the same draw ratio, the values of orientation for BO-PS are lower as compared to the ones of BO PLA even if comparable biaxial stretching parameters were used. This means that PS chains orient less rapidly during stretching, which can be explained by the less entangled network of PS ($M_e \sim 19500$ g/mol) as compared to the one of PLA ($M_e \sim 5800$ g/mol).

- For $f_{cM}=f_{cT} \approx 0.03$ a distinct B-D transition can be observed for BO PS. This critical value is lower than the one determined for PLA ($f_{cM}=f_{cT} \approx 0.07$), indicating that the critical value for B-D transition may vary with the type of polymer.

The value of the critical orientation required to induce a ductile behavior, (i.e. $f_{cM}=f_{cT} \approx 0.03$) is close to the ones reported in the literature (Choi et al., 1989; Matsumoto et al., 1981; Xiaomin Zhang & Ajji, 2003). For instance, Zhang et al. (Xiaomin Zhang & Ajji, 2003) reported that above $f_{cM}=f_{cT} \approx 0.04$, the strain at break values of BO PS films can be improved to 6-8%. (Choi et al., 1989) also reported that a value of $f_{cM} \times f_{cT} \approx 0.0025$ is needed to observe a B-D transition.

Despite the different orientation kinetics between PS, PLAs and PEF, the main conclusion is that for these three polymers **a critical orientation factor of the amorphous phase is the key parameter to induce a B-D transition**. In the next section, the structural characterization at the microscopic scale will be carried out to reveal the evolution of the deformation mechanisms with orientation.

V.2.3.   Deformation mechanisms characterization

A post-mortem study using the same methodology than previously carried out on PLA and on PEF has been applied to the as-cast and BO PS samples to characterize the deformation mechanisms involved during the stretching. Note that "Pseudo in-situ" analysis will not be applied as such experimental set-up is not adapted to this type of polymer due to its too high brittleness.

The characteristic SAXS patterns recorded at a position close to the breaking point of the as-cast and biaxially stretched samples of various BO ratios are summarized in *Figure V. 10.*
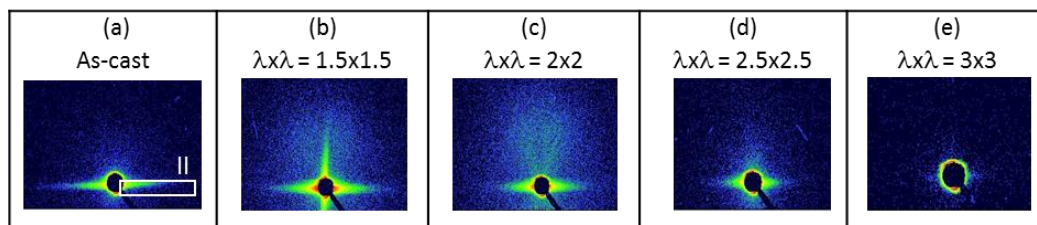
Figure V. 10. Representative SAXS patterns taken near from the break point for as-cast and BO samples (post-mortem scanning analyses, the draw axis is horizontal).

As-cast and low-BO-ratio samples reveal the presence of crazes unlike the sample stretched at 3x3. In order to better analyze the deformation mechanisms involved, *Figure V. 11* depicts the scattering intensities extracted from craze walls (zone II) of *Figure V. 10* and *Figure V. 12* shows the optical microscopic observations of the breaking zone of as-cast and a few typical BO samples.
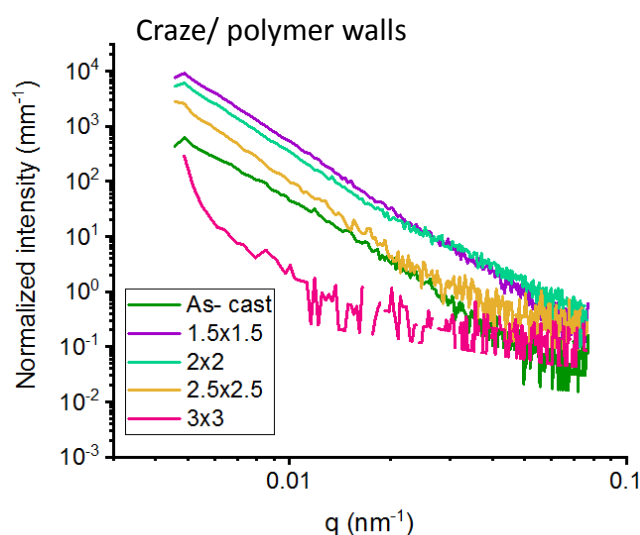
Figure V. 11. Normalized scattering intensities extracted from craze walls (zone II) of as-cast and samples of various BO samples.
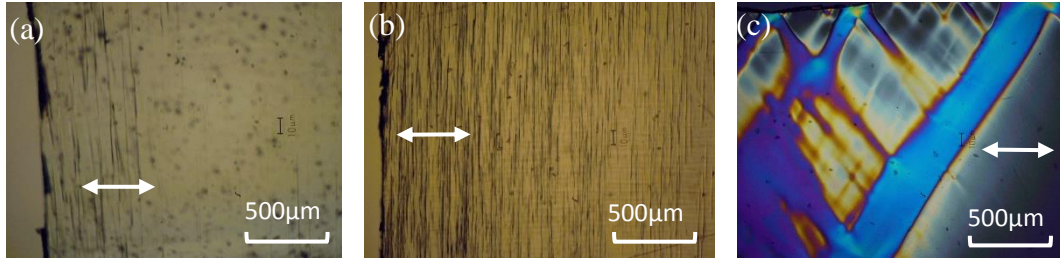
Figure V. 12. Optical microscopy observations of few PS samples after breaking upon uniaxial stretching: (a) as-cast sample; pre-oriented BO samples at (b) 1.5x1.5 and (c) 3.5x3.5.

For the as-cast sample, only few crazes located near the rupture zone are observed. Such observation is in good agreement with the low normalized scattering intensity extracted from the crazes walls. This suggests that cast PS failed to form stabilized crazes probably due to a rapid craze-crack transition.

For low BO ratio sample (1.5x1.5), a considerable amount of thin and elongated crazes are observed perpendicularly to the draw axis. For this material, the crazes density is significantly higher than for as-cast sample giving a higher normalized scattering intensity extracted from the crazes walls.

Finally for BO sample presenting ductile behavior, only shear bands are detected on the sample surface. Both coarse and thin bands are observed: the coarse bands appear to propagate into large and diffuse deformation zones while in between, a number of thin, well defined intersecting slips are observed.

Despite the particular evolution of craze density observed in case of as-cast and low BO PS, the global change of craze-to-shear band transition with orientation is in accordance with PLA and PEF: **one can associate the origin of B-D transition of mechanical behavior to a transition of elementary deformation mechanisms**.

Influence of orientation on the craze/yield initiation stresses

The critical stress for craze initiation (σ_{cr}) calculated from post-mortem scanning analyses and the yield stress determined from the engineering stress-strain curves were plotted as a function of draw ratios (*Figure V. 13*).
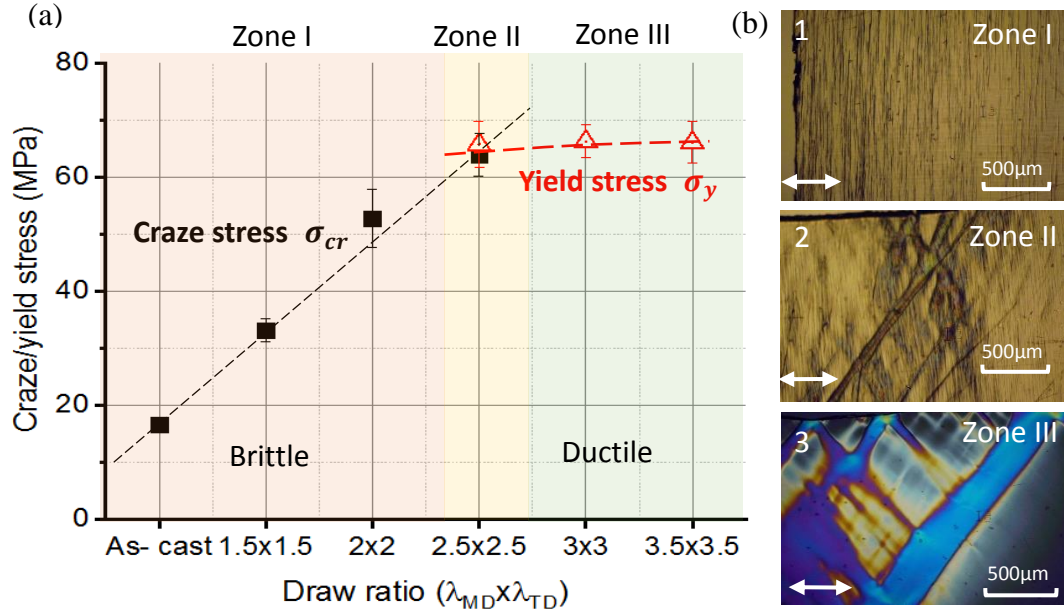
Figure V. 13. (a) Critical craze initiation stress calculated from post-mortem scanning analysis and the yield stress determined from engineering stress-strain curves as function of BO draw ratios (b) characteristic optical microscopy observation of samples in the different zones.

The different sensitivity of craze/yield stress to molecular orientation for PS is in agreement with former results obtained with PLA and PEF. Three kinds of behaviors can be encountered depending of the chain orientation:

- <u>Zone I: brittle behavior.</u> At low BO ratios, the value of σ_{cr} is lower than σ_y (considering that the value of yield stress remains constant with orientation). As a consequence, crazing is initiated as the dominant deformation mechanism (image 1).

- <u>Zone II: transient behavior.</u> The σ_{cr} and σ_y are similar leading to a coexistence of the two deformation mechanisms (image 2). Crazes are largely suppressed and some localized shear bands begin to appear. In this zone, sample begins to show a ductile behavior upon stretching.

- <u>Zone III: ductile behavior.</u> The extrapolation of the curve of σ_{cr} to higher BO ratios leads to values well above σ_y. Shear banding becomes the "easier"

mechanism and the only one activated (image 3). A "full" B-D transition is completed and an improvement of stretchability is observed.

The transition of deformation mechanisms is globally in line with that determined for PLA and for PEF. In next section, authors will try to present a generalization of the main observations obtained for these three polymers.

V.3.   Generalization of studies of PLA, PEF and PS

In previous sections of this chapter, PEF and PS, as complementary materials, have been investigated through the same methodology than for PLA in order to compare their behaviors. At this stage, the structure-property relationships of these different amorphous polymers were studied regarding three main aspects: mechanical behavior, molecular orientation quantification and deformation mechanisms characterization.

As a result, it is established for these three amorphous polymers that molecular orientation can induce a B-D transition. The key parameter inducing this transition behavior is the achievement of a critical chain orientation of amorphous phase, whose value depends of the considered material. The origin of this transition is linked to a change of elementary plastic deformation mechanisms from crazing to shear banding. Such a change lies in a different sensitivity of the critical initiation stress of craze/shear band to molecular orientation. The craze initiation stress increases while the initiation stress of shear bands, i.e. the yield stress, was found to remain roughly constant when increasing chain orientation. Consequently as soon as the applied stress is under the stress of craze initiation, shear bands will be activated as the only preferable deformation mechanism leading to a ductile mechanical response.

The study on chain-orientation-induced B-D transition is of prime interest from both academic and industrial points of view since it proposes a simple route to drastically improve the end use properties of this type of materials.

The last question addressed in this PhD work is: what is the origin increase of the critical stress for craze initiation with molecular orientation? The last section will try to give insights about this question on the basis of theoretical considerations.

V.4.   Complementary discussion on the increase of the critical craze initiation stress with molecular orientation

It has been shown in previous sections that the brittle-to-ductile transition is related to a change of the crazing deformation mode to the shear deformation mechanism with molecular orientation. Particularly it has been evidenced that the critical stress for craze initiation σ_{cr} increases with the orientation factor.

Basically, crazes are initiated when the external stretch causes a microscopic void to open up at a stress concentration created by a heterogeneity in the molecular network. This microscopic void will propagate in a plane perpendicular to the highest principal stress and will be stabilized temporarily by fibrils inside the craze. Eventually, the stabilization by fibrils will fail and a craze-crack transition occurs (Kramer, 1983). The macroscopic stress required for the craze initiation is the so-called critical craze stress (σ_{cr}). It was observed in this study that increasing orientation involves an increase of σ_{cr}. In other words, in an oriented molecular network it appears that the essential step of forming crazes, i.e. opening up new surfaces, will cost more energy as compared to an isotropic material.

(Argon, 1973; Kramer, 1983; Kramer & Berger, 1990) have developed some models for craze initiation for isotropic amorphous polymers, particularly in the case of PS. They propose that the crazing stress is dependent of different material parameters such as the flow stress of the fluid at a strain rate, surface energy…..etc. When dealing with isotropic amorphous polymers, authors have shown that the key parameter governing the craze stress is the craze surface energy Γ. Also, within this framework, we will consider in a first approximation that the surface energy Γ is the only parameter which

influences the craze initiation stress σ_{cr} for both isotropic and anisotropic samples, as described by following expression (Kramer & Berger, 1990):

$$\sigma_{cr} \propto \sqrt{\Gamma(\gamma, \vartheta_e, \mathrm{d})} \qquad (\mathrm{V.1})$$

Where Γ, the energy needed to create new surface, can be written as sum of two contributions:

$$\Gamma = \gamma + \frac{1}{4}\vartheta_e U d \qquad (\mathrm{V.2})$$

The first term γ is the surface free energy characterizing the van der Waals cohesive energy between molecules. The second term, $\frac{1}{4}\vartheta_e U d$, is related to the chain scission of the strands: ϑ_e is the effective entanglement density, U the energy needed to fracture a covalent chain and d the end-to-end distance between effective entanglements.

Case of isotropic materials

According to (Kramer, 1983) the contribution of the entanglements-related energy term , $\frac{1}{4}\vartheta_e U d$, to the total surface energy Γ is much more significant than that of γ. Moreover, for the term $\frac{1}{4}\vartheta_e U d$ the most dominant parameter is the entanglement density ϑ_e. For instance these authors have compared two polymers possessing extremely different ϑ_e: poly(p-tert-butyl styrene) (PTBS) and PC and found that due to the difference of their entanglement densities, the predicted craze stress value are quite different (~27 and ~74MPa for PTBS and PC respectively). This allows crazes to be more easily initiated and propagated in PTBS than in PC.

(S. Wu, 1990) have proposed a relation $\sigma_{cr} \propto \sqrt{\vartheta_e}$ to show the dependency of craze stress on entanglement density. Thus, in this thesis work, authors have examined this relation on cast samples of PS, PLA, PEF where the values of ϑ_e (mmol/cm^3) is calculated using the expression (S. Wu, 1990)

$$\vartheta_e = \frac{\rho}{M_e} \qquad (\mathrm{V.3})$$

With ρ the polymer density and M_e the mass between entanglements determined from DMA analyses (cf chapter II). The results are summarized in *Table V. 1.*

Table V. 1. Entanglement characteristics and experimental craze initiation stress values determined for as-cast polymers of study.

As-cast sample	M_e (g/mol)	ϑ_e (mmol/cm^3)	σ_{cr} measured from SAXS results (MPa)
PS	~19500	~0.06	~18
PLA	~5800	~0.2	~40
PEF	~3500	~0.4	~55

Authors have plotted σ_{cr} versus ϑ_e in a log-log plot (*Figure V. 14 (a)*). In addition, the values $(\sigma_{cr}, \vartheta_e)$ were placed in the reference plot proposed by (S. Wu, 1990) for comparisons as illustrated in *Figure V. 14(b).*
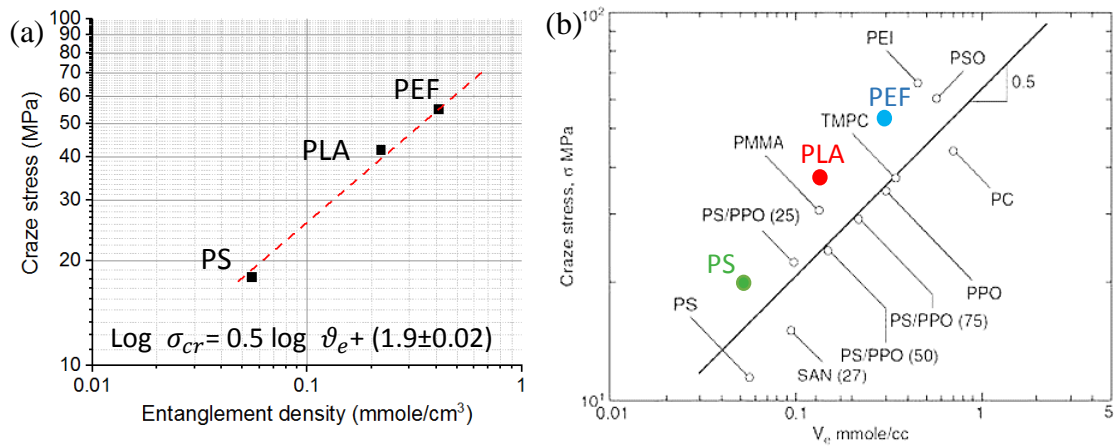
Figure V. 14. (a)Craze initiation stress plotted as a function of entanglement density for as-cast PS, PLA and PEF (b) Comparison of results of this work (colored points) to (S. Wu, 1990).

As can be seen from the figures, the regression line of $\log(\sigma_{cr})$ versus $\log(\vartheta_e)$ exhibits a slope of 0.5 which confirms relation $\sigma_{cr} \propto \sqrt{\vartheta_e}$. Also, the pairs $\sigma_{cr}(\vartheta_e)$ determined for the three types of amorphous polymers all follow the main evolution trend determined by (S. Wu, 1990). The increasing of ϑ_e (in the order of PS, PLA and PEF)

results in an increase of the surface energy Γ (eq V.2), leading to an easier craze initiation in PS and more difficultly in PLA and PEF. Important to note that the rather good accordance of correlations $\sigma_{cr}(\vartheta_e)$ determined in this work with that of (S. Wu, 1990) validates our experimental approach to assess the craze initiation stress values.

Influence of orientation on surface energy

For a given entanglement density, i.e. for a given polymer, the increasing of σ_{cr} with orientation should be linked to an increase of surface energy $\Gamma(\gamma, \vartheta_e, d)$. In fact, it is known that the fibril diameter D is linked to σ_{cr} and Γ by expression (Kramer & Berger, 1990):

$$D \propto \frac{\Gamma(\gamma, \vartheta_e, d)}{\sigma_{cr}} \qquad (V.4)$$

As formerly obtained with modeling results from our SAXS analysis, the fibril diameter D does not significantly change with orientation. Considering that σ_{cr} increases with orientation, the value of $\Gamma(\gamma, \vartheta_e, d)$ should also increase to insure the constancy of fibril diameter.

Considering the expression of $\Gamma(\gamma, \vartheta_e, d)$ (Eq. V.2), two origins should be considered to explain the increase of $\Gamma(\gamma, \vartheta_e, d)$ with orientation:

1) Term related to cohesion between molecules: γ

The surface free energy, γ, was measured for PLA, PEF and PS as a function of the BO ratio by means of the contact angle technique (cf chapter II). The results are depicted in *Figure V. 15*.
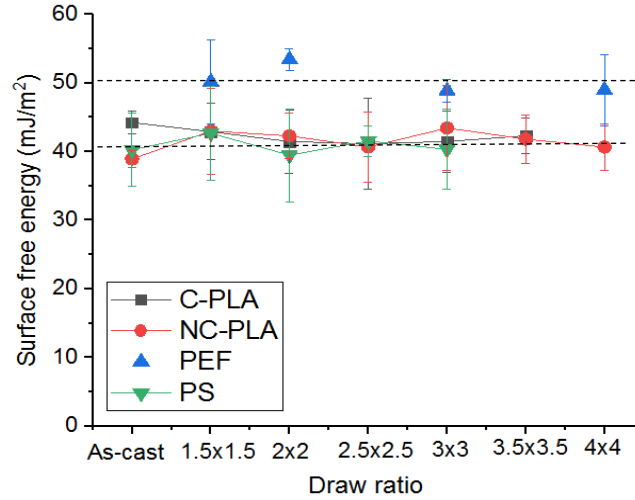
Figure V. 15. Surface free energy plotted as function of draw ratios for C-PLA, NC-PLA, PS and PEF.

It can be seen from the figure that whatever the materials, the surface free energy γ remains roughly constant around 40 and 50 mJ/m^2 respectively, showing no dependency on molecular orientation. This determined value of γ is close to what was reported in (Kramer & Berger, 1990) for glassy polymers and does not seem to evolve significantly with the polymer type. Therefore, surface energy in terms of van der Waals cohesive contribution should not be the essential factor that influences the evolution of craze stress with orientation.

2) Term related to entanglements: $\vartheta_e U d / 4$

One can consider that during stretching in the rubbery state the entanglement density, ϑ_e, remains constant or slightly decreases if disentanglements occurred at-high level of orientation. Unfortunately, the determination of ϑ_e for oriented samples via viscoelastic measurements was not applicable since the results are strongly affected by the contraction/recovery of the sample during the test. However, one can reasonably suspect that disentanglements do not significantly occur during stretching, otherwise the craze initiation stress would decrease as function of orientation.

The other parameter to consider in the entanglement energy term is the end-to-end distance between effective entanglements *d*. With biaxial stretching, this parameter increases as schematically presented in *Figure V. 16*.
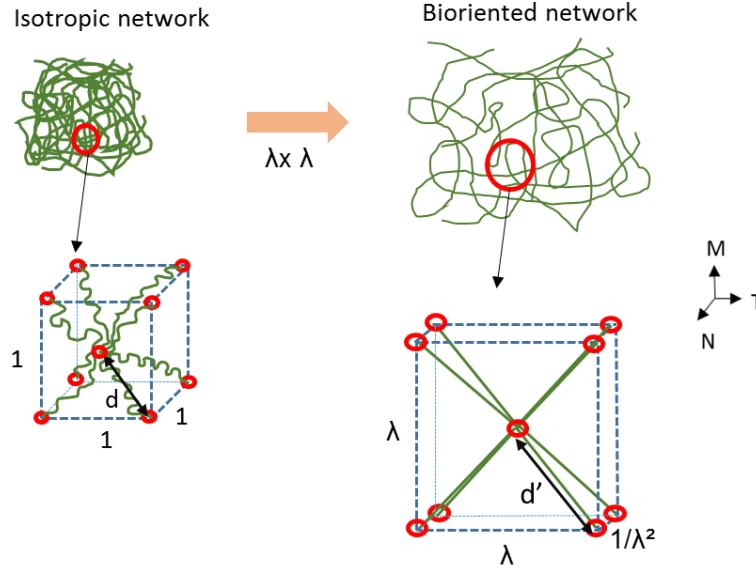
Figure V. 16. A schematic presentation of extension of polymer network and the evolution of end-to-end distance d between entanglements during biaxial stretching (draw axis along MD and TD).

The value of *d* in the considered volume unit of a randomly coiled network equals to $\frac{\sqrt{3}}{2}$. Assuming that the "average" chain segments between two entanglements points deform affinely under biaxial stretching, *d* could then be written as $\frac{1}{2}\sqrt{2\lambda^2 + \frac{1}{\lambda^4}}$. One could then estimate the ratio of *d'/d* by equation:

$$d'/d = \sqrt{\frac{1}{3}\left(2\lambda^2 + \frac{1}{\lambda^4}\right)} \qquad (V.5)$$

One can then estimate a theoretical evolution of σ_{cr} from the increase of *d* for that $\sigma'_{cr}/\sigma_{cr} \propto \sqrt{d'_c/d}$ combining eq (V.5) with eq (V.1) and eq (V.2). For example, at λ x λ=1.5x1.5, the corresponding $\sqrt{d'_c/d}$ is around 1.1 whatever the type of materials. However experimental results have shown a more pronounced increase of σ_{cr} with orientation (experimental value of σ'_{cr}/σ_{cr} is around 1.4 when λxλ= 1.5x1.5). This suggests that other parameters, besides d, should also contribute to the increase of

surface energy. To address this point, further theoretical modeling analysis is envisaged as a perspective of this thesis work. Particularly it should be more relevant to consider the orientation factor than the draw ratio considering the different orientation kinetics depending on type of material of study. Moreover, the influence of molecular network anisotropy induced by orientation should also be taken into account in future theoretical analysis.

Conclusions of chapter

Complementary structure-property study on other glassy polymers

⭐   **Confirmation of findings on PLA**

Complementary biaxial stretching above Tg on:

| PEF | PS |

| B-D transition | A remarkable gain of strain up to 150% | A limited gain of strain to 10-15% |

| Molecular orientation | The critical orientation function depends on the considered material |

| Deformation mechanism | With increasing of orientation a change of crazing to shear banding occurs |

◇ Generalization of methodology of thesis: by stretching brittle glassy polymers above Tg: a B-D transition occurs when reaching a critical molecular orientation of amorphous phase.

◇ Confirmation of origin of macroscopic B-D transition of mechanical behavior: change of elementary deformation mechanism from crazing to shear bands.

◇ Confirmation of influence of molecular orientation on initiation stress of craze/shear bands: σ_c increases systematically with orientation function whereas σ_y remains constant. When reaching a critical orientation function value, shear bands will be activated as a more favorable deformation mechanism which leads to a ductile mechanical response.

◇ The increase of craze stress with orientation could be originated at an increase of surface energy in oriented films. The increase of end-to-end distance between entanglements during stretching is one of the elements which contribute to this increase of surface energy.

Appendix-V

It has been previously shown that BO PLA and BO PEF films are able to present a remarkable enhancement of stretchability once a critical level of orientation is reached. For these two materials a maximum strain at break value is detected in the region of 100-150% upon uniaxial stretching at room temperature. This suggests biaxial stretching could be a generalized method to improve the ductility of brittle bio-based polymers.

Then question remains that if this improvement of deformability can truly compete with the performance of industrialized petro-chemically resourced polymers, for instance with PET the most dominant polymer applied in production of films/ bottles. Indeed, it has already been discussed that PLA and PEF are both seen as potential counterparts of PET. Thus, to compare the influence of biaxial stretching on mechanical behavior of PLA/PEF to that of PET, initially amorphous PET films (kindly provided by Indorama®) were biaxially drawn at 110ºC (Tg+20 ºC) at various ratios and tested upon uniaxial stretching at room temperature.

The stress-strain curves of as-cast and BO PET are depicted in *Figure AV. 1(a)*. A comparison of stretchability with PLA and PEF is summarized in *Figure AV. 1(b)*.
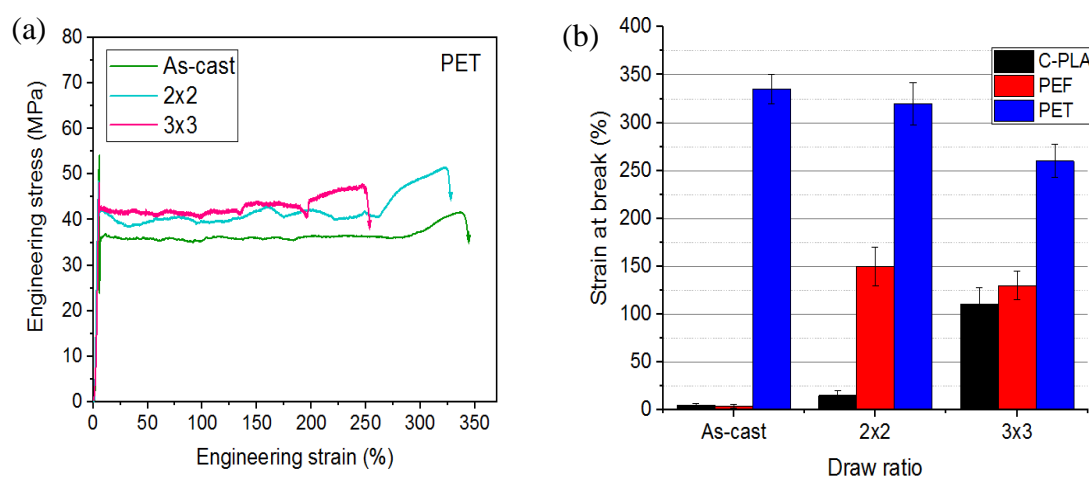
Figure AV. 1. (a) Stress-strain curves of as-cast and BO PET films tested upon uniaxial stretching at $\dot{\varepsilon}=4x10^3$, 23ºC. (b) Comparison of stretchability of as-cast and BO C-PLA, PEF with PET.

The as-cast PET, unlike PLA or PEF, presents already a ductile behavior before being biaxially oriented. Under same solliciation parameters, PET shows a more extraordinary stretchability (over 300%) than PLA/ PEF.

Regarding the behavior of BO PET samples, it can be seen that the maximum stretchability decreases with draw ratio. Similar behavior has already been discussed in case of PLA, PEF and PC that due to chain orientation in biaxial stretching process the chains cannot be over-stretched upon uniaxial deformation. In addition, for draw ratio where all three materials are ductile, e.g. $\lambda x \lambda = 3x3$, the stretchability detected for BO PET is almost twice the value determined for BO PLA and BO PEF. However in terms of yield stress, the value determined for PET ($\sim$50 MPa) appears to be less important than PLA/ PEF ($\sim$80 MPa).

To conclude, biaxial stretching proves to be an effective method to improve the intrinsic brittleness of bio-based polymers. Nevertheless this enhancement of ductility induced by macromolecular orientation seems still less significant compared to the performance of petro-chemical derived materials. In order to meet with industrial requirement of mechanical properties, it appears that more complex solutions besides pure mechanical modification should be proposed, for instance involving physico-chemistry routes like crosslinking, blending nanocomposites..etc.

Conclusions& perspectives

<u>*Conclusions*</u>

The main goal of this PhD thesis was to understand the influence of molecular orientation on mechanical properties of glassy polymers. Two grades of Polylactide (PLA) exhibiting an ability to crystallize or not, and two others complementary polymers, Polyethylene furandicarboxylate (PEF) and Polystyrene (PS) have been selected for this work.

Biaxial stretchings at temperature just above the glass transition temperature using different stretching parameters (temperature, strain rate, draw ratios) have been performed on all materials to obtain films with different orientation degrees. Then, structural and uniaxial tensile behavior at room temperature of such oriented samples have been systematically investigated. A Brittle-to-Ductile (B-D) transition occurs for all studied polymers from a critical value of amorphous chain orientation function depending of the material.

For both grades of PLA, an improvement of strain at break around 100% has been shown. Through an orientation-mechanical property correlation analysis, it has been found that the achievement of a critical orientation function of amorphous chain is the key parameter to induce the ductile behavior. We have clearly shown that the presence of an induced ordered phase during stretching, whether being mesomorphic or crystalline, is not required to obtain a ductile behavior, contrary to what was previously proposed in literature. The induced mesophase/crystalline phase will rather play a similar role as physical entanglement points that improve the stiffness of network and increase the yield strength at the expense of stretchability. In addition, the complementary study of physical ageing effect on BO PLA samples has revealed that the gained ductility with molecular orientation decreases with increasing of aging time. However the overall transition nature will still be kept and the ductile oriented sample will not return to as brittle as a cast sample.

Then the origin of B-D transition behavior has been investigated by characterizing the deformation mechanisms involved for as-cast and oriented samples through in-situ and post-mortem SAXS experiments. It was found that it is a change of elementary deformation mechanisms, i.e. from crazing to shear banding, that is at the origin of the B-D transition. To better address this point, a detailed orientation-deformation mechanism study was conducted to illustrate the influence of orientation function on critical initiation stresses of crazing/ shear banding. As a result, it was found that the critical stress for initiation crazes, σ_{cr}, increases systematically with orientation function whereas the yield stress for activation of shear bands, σ_y, appears to remain quasi-constant. Three different behaviors were then identified as the orientation function is increased: the first one (low orientation function) corresponds to the "brittle" behavior zone ($\sigma_{cr} < \sigma_y$) where only crazes are initiated. In this zone the craze density decreases substantially with the orientation increase while the geometry of the crazes remains unaffected. Then, a transient behavior zone ($\sigma_{cr} \approx \sigma_y$) develops at intermediate orientation function, characterized by the coexistence of crazes and shear bands. Finally at higher orientation function, crazes are completely inhibited and a "ductile" behavior zone ($\sigma_{cr} > \sigma_y$) manifests where shear bands act as the more favorable deformation mechanism, leading to a ductile mechanical response.

The last part of this PhD lies in an attempt of generalization of the important conclusions and findings obtained from PLA by using the same approach for the two complementary materials: PEF and PS. Again, a B-D transition is observed with chain orientation. Like for PLA this one is originates from a change of elementary deformation mechanism from crazing to shear bands due to an increase of the craze initiation stress with orientation. Then, based on theoretical considerations, authors have attempted to explain the σ_{cr} increase with orientation and they show that the increase of the end-to-end distance between effective entanglements can partially explain this behavior.

Perspectives

Several remaining questions of this thesis worth to be further studied. From an experimental point of view, it will be interesting to study more specifically the effect of physical aging on the B-D transition on both PLA grades. Besides, a similar ageing investigation should be conducted on PEF to compare the observations. Also, this study revealed that the gain brought by orientation in terms of stretchability is lost with time. Thus, it could be interesting to determine it some treatments, for example short annealing, could allow to preserve these benefits. In addition to various properties that have already been studied in this work, the barrier properties of as-cast and oriented films should also be studied, e.g. against oxygen for that this property is also essential for packaging applications.

Concerning the elementary deformation mechanisms study, the morphology observations were conducted in a post-mortem manner after sample rupture. It will be essential to complete this study by an in-situ study of the deformation mechanism to confirm the result regarding the initiation of crazes in isotropic material and the suppression of crazing/ activation of shear banding in an oriented polymer matrix.

From theoretical point of view, we have shown that the increase of the end-to-end distance between effective entanglements is not the only parameter which contributes to the σ_{cr} increase. Another parameter which seems to be more relevant than the draw ratio to be considered is the orientation function. This factor should be taken into account in the future works. To go further regarding this part, simulation/modeling studies should bring precious complementary information. For example, molecular dynamics simulation studies could allow to better assess the evolution of the macromolecular network upon deformation. Finally, a collaboration with physicists should be also valuable in order to define how the formalism initially developed for isotropic materials could be adapted to oriented ones.

Bibliography

Abou-Kandil, A. I., Goldbeck-Wood, G., & Windle, A. H. (2007). Molecular modeling of the intermediate smectic mesophase in polyethylene terephthalate. *Macromolecules*, *40*(18), 6448–6453. https://doi.org/10.1021/ma070604o

Al-Itry, R., Lamnawar, K., Maazouz, A., Billon, N., & Combeaud, C. (2015). Effect of the simultaneous biaxial stretching on the structural and mechanical properties of PLA, PBAT and their blends at rubbery state. *European Polymer Journal*, *68*, 288–301. https://doi.org/10.1016/j.eurpolymj.2015.05.001

Allison, S. W., & Ward, I. M. (1967). The cold drawing of polyethylene terephthalate. *British Journal of Applied Physics*, *18*(8), 1151.

Andrews, E. H., & Bevan, L. (1972). Mechanics and mechanism of environmental crazing in a polymeric glass. *Polymer*, *13*(7), 337–346.

Araujo, C. F., Nolasco, M. M., Ribeiro-Claro, P. J. A., Rudić, S., Silvestre, A. J. D., Vaz, P. D., & Sousa, A. F. (2018). Inside PEF: Chain Conformation and Dynamics in Crystalline and Amorphous Domains. *Macromolecules*, *51*(9), 3515–3526. https://doi.org/10.1021/acs.macromol.8b00192

Argon, A. S. (1973). Physical basis of distortional and dilational plastic flow in glassy polymers. *Journal of Macromolecular Science, Part B*, *8*(3–4), 573–596.

Argon, A. S., & Hannoosh, J. G. (1977). Initiation of crazes in polystyrene. *Philosophical Magazine*, *36*(5), 1195–1216.

Arnoult, M., Dargent, E., & Mano, J. F. (2007). Mobile amorphous phase fragility in semi-crystalline polymers: Comparison of PET and PLLA. *Polymer*, *48*(4), 1012–1019. https://doi.org/10.1016/j.polymer.2006.12.053

Arruda, E. M., Boyce, M. C., & Quintus-Bosz, H. (1993). Effects of initial anisotropy on the finite strain deformation behavior of glassy polymers. *International Journal of Plasticity*, *9*(7), 783–811.

Auras, R. A., Harte, B., Selke, S., & Hernandez, R. (2003). Mechanical, physical, and barrier properties of poly(lactide) films. *Journal of Plastic Film and Sheeting*, *19*(2), 123–135. https://doi.org/10.1177/8756087903039702

Auras, R., Harte, B., & Selke, S. (2004). An overview of polylactides as packaging materials. *Macromolecular Bioscience*, *4*(9), 835–864. https://doi.org/10.1002/mabi.200400043

Awaja, F., Gilbert, M., Kelly, G., Fox, B., & Pigram, P. J. (2009). Adhesion of polymers. *Progress in Polymer Science (Oxford)*, *34*(9), 948–968. https://doi.org/10.1016/j.progpolymsci.2009.04.007

Berger, L. L. (1990). On the mechanism of craze fibril breakdown in glassy polymers. *Macromolecules*, *23*(11), 2926–2934.

Bonnebat, C., Roullet, G., & De Vries, A. J. (1981). Biaxially oriented poly (ethylene terephthalate) bottles: effects of resin molecular weight on parison stretching behavior. *Polymer Engineering & Science*, *21*(4), 189–195.

Brown, H. R., Mills, P. J., & Kramer, E. J. (1985). Saxs Study of a Single Crack and Craze in Plasticized Polystyrene. *Journal of Polymer Science. Part A-2, Polymer Physics*, *23*(9), 1857–1867. https://doi.org/10.1002/pol.1985.180230910

Brown, H R, Sindoni, Y., Kramer, E. J., & Mills, P. J. (1984). Diffraction studies of craze structure. *Polymer Engineering & Science*, *24*(10), 825–832.

Brown, Hugh R, & Kramer, E. J. (1981). Craze microstructure from small-angle X-ray scattering (SAXS). *Journal of Macromolecular Science, Part B: Physics*, *19*(3), 487–522.

Bucknall, C. B. (1997). Rubber toughening. In *The physics of glassy polymers* (pp. 363–412). Springer.

Burgess, S. K., Leisen, J. E., Kraftschik, B. E., Mubarak, C. R., Kriegel, R. M., & Koros, W. J. (2014). Chain mobility, thermal, and mechanical properties of poly(ethylene furanoate) compared to poly(ethylene terephthalate). *Macromolecules*, *47*(4), 1383–1391. https://doi.org/10.1021/ma5000199

Cansfield, D. L. M., Patel, R., & Ward, I. M. (1993). Tensile drawing of high and low molecular weight polyethylene terephthalate. *Journal of Macromolecular Science, Part B: Physics*, *32*(4), 373–393.

Carr, P. L., Nicholson, T. M., & Ward, I. M. (1997). Mesophase structures in poly(ethylene terephthalate), poly(ethylene naphthalate) and poly(ethylene naphthalate bibenzoate). *Polymers for Advanced Technologies*, *8*(10), 592–600. https://doi.org/10.1002/(SICI)1099-1581(199710)8:10<592::AID-PAT713>3.0.CO;2-H

Cartier, L., Okihara, T., Ikada, Y., Tsuji, H., Puiggali, J., & Lotz, B. (2000). Epitaxial crystallization and crystalline polymorphism of polylactides. *Polymer*, *41*(25), 8909–8919.

Cavrot, J.P., Haussy, J., Lefebvre, J.M., Escaig, B. (1978). Thermally activated deformation of glassy polystyrene. *Materials Science and Engineering*, *36*(1), 95–103.

Celli, A., & Scandola, M. (1992). Thermal properties and physical ageing of poly (l-lactic acid). *Polymer*, *33*(13), 2699–2703. https://doi.org/10.1016/0032-3861(92)90440-8

Chandran, P., & Jabarin, S. (1993). Biaxial orientation of poly (ethylene terephthalate). Part II: The strain–hardening parameter. *Advances in Polymer Technology*, *12*(2), 133–151. https://doi.org/10.1002/adv.1993.060120203

Chang, C. L., Chiu, W. Y., Hsieh, K. H., & Ma, C. ‑ C M. (1993). The molecular orientation and mechanical properties of poly(ethylene terephthalate) under uniaxial extension. *Journal of Applied Polymer Science*, *50*(5), 855–862. https://doi.org/10.1002/app.1993.070500513

Chapleau, N., Huneault, M. A., & Li, H. (2007). Biaxial orientation of polylactide/thermoplastic starch blends. *International Polymer Processing*, *22*(5), 402–409.

Choi, K.-J., Spruiell, J. E., & White, J. L. (1989). Structure development in biaxially stretched polystyrene film: Part I. Property-orientation correlation. *Polymer Engineering & Science*, *29*(21), 1516–1523.

Claudy, P., Létoffé, J. M., Camberlain, Y., & Pascault, J. P. (1983). Glass transition of polystyrene versus molecular weight. *Polymer Bulletin*, *9*(4–5), 208–215. https://doi.org/10.1007/BF00283709

Cole, K. C., Depecker, C., Jutigny, M., Lefebvre, J. M., & Krawczak, P. (2004). Biaxial Deformation of Polyamide-6: Assessment of Orientation by Means of Infrared Trichroism. *Polymer Engineering and Science*, *44*(2), 231–240. https://doi.org/10.1002/pen.20022

De Focatiis, D. S. A., & Buckley, C. P. (2011). Craze initiation in glassy polymers: Quantifying the influence of molecular orientation. *Polymer*, *52*(18), 4045–4053. https://doi.org/10.1016/j.polymer.2011.06.044

De Francesco, A., & Duckett, R. A. (2004). Development of orientation with drawing in polystyrene films: Effects of time and temperature. *Polymer*, *45*(12), 4297–4306. https://doi.org/10.1016/j.polymer.2004.04.007

Delpouve, N., Stoclet, G., Saiter, A., Dargent, E., & Marais, S. (2012). Water barrier properties in biaxially drawn poly(lactic acid) films. *Journal of Physical Chemistry B*, *116*(15), 4615–4625. https://doi.org/10.1021/jp211670g

Di Lorenzo, M. L., & Androsch, R. (2018). *Synthesis, Structure and Properties of Poly (lactic acid)*. Springer.

Doi, M., & Edwards, S. (1986). *The theory of polymer dynamics*. Oxford University Press.

Donald, A M. (1985). The effect of temperature on crazing mechanisms in polystyrene. *Journal of Materials Science*, *20*(7), 2630–2638.

Donald, Athene M., & Kramer, E. J. (1982a). Deformation zones and entanglements in glassy polymers. *Polymer*, *23*(8), 1183–1188. https://doi.org/10.1016/0032-3861(82)90376-7

Donald, Athene M., & Kramer, E. J. (1982b). The competition between shear deformation and crazing in glassy polymers. *Journal of Materials Science*, *17*(7), 1871–1879. https://doi.org/10.1007/BF00540402

Donald, Athene M., Kramer, E. J., & Kambour, R. P. (1982). Interaction of crazes with pre-existing shear bands in glassy polymers. *Journal of Materials Science*, *17*(6), 1739–1744. https://doi.org/10.1007/BF00540802

Eerhart, A. J. J. E., Faaij, A. P. C., & Patel, M. K. (2012). Replacing fossil based PET with biobased PEF; Process analysis, energy and GHG balance. *Energy and Environmental Science*, *5*(4), 6407–6422. https://doi.org/10.1039/c2ee02480b

Eling, B., Gogolewski, S., & Pennings, A. J. (1982). Biodegradable materials of poly (l-lactic acid): 1. Melt-spun and solution-spun fibres. *Polymer*, *23*(11), 1587–1593.

ESRF1. (n.d.). https://www.esrf.eu/about/synchrotron-science/synchrotron

ESRF2. (n.d.). https://www.esrf.eu/about/synchrotron-science/beamline

Faivre, J. P., Jasse, B., & Monnerie, L. (1985). Orientation and relaxation in uniaxially stretched poly(vinyl methyl ether)-atactic polystyrene blends. *Polymer*, *26*(6), 879–883. https://doi.org/10.1016/0032-3861(85)90131-4

Farah, S., Anderson, D. G., & Langer, R. (2016). Physical and mechanical properties of PLA, and their functions in widespread applications — A comprehensive review. *Advanced Drug Delivery Reviews*, *107*, 367–392. https://doi.org/10.1016/j.addr.2016.06.012

FDA notification no.178. (2002).

Fereydoon, M., Tabatabaei, S. H., & Ajji, A. (2014). X-ray and trichroic infrared orientation analyses of uniaxially stretched PA6 and MXD6 nanoclay composite films. *Macromolecules*, *47*(7), 2384–2395. https://doi.org/10.1021/ma402466c

Ferry, J. D. (1980). *Viscoelastic properties of polymers*. John Wiley & Sons.

G'Sell, C., Hiver, J. M., Dahoun, A., & Souahi, A. (1992). Video-controlled tensile testing of polymers and metals beyond the necking point. *Journal of Materials Science*, *27*(18), 5031–5039.

Garlotta, D. (2001). A literature review of poly(lactic acid). *Journal of Polymers and the Environment*, *9*(2), 63–84. https://doi.org/10.1023/A:1020200822435

Ge, T., & Robbins, M. O. (2010). Anisotropic plasticity and chain orientation in polymer glasses. *Journal of Polymer Science Part B: Polymer Physics*, *48*(13), 1473–1482.

Gogolewski, S., Jovanovic, M., Perren, S. M., Dillon, J. G., & Hughes, M. K. (1993). The effect of melt-processing on the degradation of selected polyhydroxyacids: polylactides, polyhydroxybutyrate, and polyhydroxybutyrate-co-valerates. *Polymer Degradation and Stability*, *40*(3), 313–322. https://doi.org/10.1016/0141-3910(93)90137-8

Gomes, M., Gandini, A., Silvestre, A. J. D., & Reis, B. (2011). Synthesis and characterization of poly (2, 5-furan dicarboxylate) s based on a variety of diols. *Journal of Polymer Science Part A: Polymer Chemistry*, *49*(17), 3759–3768.

Gordon, D. H., Duckett, R. A., & Ward, I. M. (1994). A study of uniaxial and constant-width drawing of poly(ethylene terephthalate). *Polymer*, *35*(12), 2554–2559. https://doi.org/10.1016/0032-3861(94)90378-6

Gorlier, E., Haudin, J. M., & Billon, N. (2001). Strain-induced crystallisation in bulk amorphous PET under uni-axial loading. *Polymer*, *42*(23), 9541–9549. https://doi.org/10.1016/S0032-3861(01)00497-9

Guigo, N., van Berkel, J., de Jong, E., & Sbirrazzuoli, N. (2017). Modelling the non-isothermal crystallization of polymers: Application to poly(ethylene 2,5-furandicarboxylate). *Thermochimica Acta*, *650*, 66–75. https://doi.org/10.1016/j.tca.2017.02.008

Gupta, A. P., & Kumar, V. (2007). New emerging trends in synthetic biodegradable polymers - Polylactide: A critique. *European Polymer Journal*, *43*(10), 4053–4074. https://doi.org/10.1016/j.eurpolymj.2007.06.045

Halary, J. L., Lauprêtre, F., & Monnerie, L. (2011). *Polymer materials: macroscopic properties and molecular interpretations*. John Wiley & Sons.

Hammouda, B. (2010). A new Guinier-Porod model. *Journal of Applied Crystallography*, *43*(4), 716–719. https://doi.org/10.1107/S0021889810015773

Hasan, O. A., & Boyce, M. C. (1993). Energy storage during inelastic deformation of glassy polymers. *Polymer*, *34*(24), 5085–5092. https://doi.org/10.1016/0032-3861(93)90252-6

Hassan, M. K., & Cakmak, M. (2013). Mechano optical behavior of polyethylene terephthalate films during simultaneous biaxial stretching: Real time measurements with an instrumented system. *Polymer*, *54*(23), 6463–6470.

Haward, R. N. (1993). Strain Hardening of Thermoplastics. *Macromolecules*, *26*(22), 5860–5869. https://doi.org/10.1021/ma00074a006

191

Heffelfinger, C. J., & Schmidt, P. G. (1965). Structure and properties of oriented poly (ethylene terephthalate) films. *Journal of Applied Polymer Science*, *9*(8), 2661–2680.

Hu, J., Zhang, T., Gu, M., Chen, X., & Zhang, J. (2012). Spectroscopic analysis on cold drawing-induced PLLA mesophase. *Polymer*, *53*(22), 4922–4926. https://doi.org/10.1016/j.polymer.2012.09.012

Huang, J., Lisowski, M. S., Runt, J., Hall, E. S., Kean, R. T., Buehler, N., & Lin, J. S. (1998). Crystallization and microstructure of poly (L-lactide-co-meso-lactide) copolymers. *American Chemical Society, Polymer Preprints, Division of Polymer Chemistry*, *39*(2), 88–89. https://doi.org/10.1021/ma9714629

Hui, C. Y., Ruina, A., Creton, C., & Kramer, E. J. (1992). Micromechanics of crack growth into a craze in a polymer glass. *Macromolecules*, *25*(15), 3948–3955.

Hutchinson, J. M. (1995). Physical aging of polymers. *Progress in Polymer Science*, *20*(4), 703–760.

Hutchinson, M. H., Dorgan, J. R., Knauss, D. M., & Hait, S. B. (2006). Optical properties of polylactides. *Journal of Polymers and the Environment*, *14*(2), 119–124. https://doi.org/10.1007/s10924-006-0001-z

Ikada, Y., Jamshidi, K., Tsuji, H., & Hyon, S. H. (1987). Stereocomplex formation between enantiomeric poly (lactides). *Macromolecules*, *20*(4), 904–906.

Ilavsky, J., & Jemian, P. R. (2009). Irena: Tool suite for modeling and analysis of small-angle scattering. *Journal of Applied Crystallography*, *42*(2), 347–353. https://doi.org/10.1107/S0021889809002222

Jain, A. K., & Gupta, V. B. (1990). Effect of molecular orientation on the melting behavior of heat-set poly (ethylene terephthalate) fibers. *Journal of Macromolecular Science, Part B: Physics*, *29*(1), 49–62.

Jariyasakoolroj, P., Tashiro, K., Wang, H., Yamamoto, H., Chinsirikul, W., Kerddonfag, N., & Chirachanchai, S. (2015). Isotropically small crystalline lamellae induced by high biaxial-stretching rate as a key microstructure for super-tough polylactide film. *Polymer*, *68*, 234–245. https://doi.org/10.1016/j.polymer.2015.05.006

Jones, T. T. (2013). *The Effect of Molecular Orientation on the Mechanical Properties of Polystyrene: Macromolecular Division*. Elsevier.

Kahar, N., Duckett, R. A., & Ward, I. M. (1978). Stress optical studies of oriented poly(methyl methacrylate). *Polymer*, *19*(2), 136–144. https://doi.org/10.1016/0032-3861(78)90029-0

Kambour, R. P. (1973). A review of crazing and fracture in thermoplastics. *Journal of Polymer Science: Macromolecular Reviews*, *7*(1), 1–154.

Kausch, H. H. (1978). *Polymer Fracture*. Springer.

Kawakami, D., Hsiao, B. S., Burger, C., Ran, S., Avila-Orta, C., Sics, I., Kikutani, T., Jacob, K. I., & Chu, B. (2005). Deformation-induced phase transition and superstructure formation in poly(ethylene terephthalate). *Macromolecules*, *38*(1), 91–103. https://doi.org/10.1021/ma049333x

Knoop, R. J. I., Vogelzang, W., Van Haveren, J., & Van Es, D. S. (2013). High molecular weight poly(ethylene-2,5-furanoate); Critical aspects in synthesis and mechanical property determination. *Journal of Polymer Science, Part A: Polymer Chemistry*, *51*(19), 4191–4199. https://doi.org/10.1002/pola.26833

Kramer, E. J. (1975). The growth of shear bands in polystyrene. *Journal of Polymer Science: Polymer Physics Edition*, *13*(3), 509–525.

Kramer, E. J. (1983). Microscopic and molecular fundamentals of crazing. In *Crazing in polymers Vol.1* (pp. 1–56). Advances in polymer science, 51/52

Kramer, E. J., & Berger, L. L. (1990). Fundamental processes of craze growth and fracture. In *Crazing in Polymers Vol. 2* (pp. 1–68). Advances in polymer science, 91/92.

le Bourvellec, G., Monnerie, L., & Jarry, J. P. (1987). Kinetics of induced crystallization during stretching and annealing of poly(ethylene terephthalate) films. *Polymer*, *28*(10), 1712–1716. https://doi.org/10.1016/0032-3861(87)90014-0

LeBourvellec, G., Monnerie, L., & Jarry, J. P. (1986). Amorphous orientation and induced crystallization in uniaxially stretched poly(ethylene terephthalate glycol). *Polymer*, *27*(6), 856–860. https://doi.org/10.1016/0032-3861(86)90294-6

Lee, S. C., Han, J. Il, & Heo, J. W. (2013). Endotherm just above glass transition in uniaxially drawn poly(lactic acid)s films with various d-isomer contents. *Polymer*, *54*(14), 3624–3632. https://doi.org/10.1016/j.polymer.2013.04.063

Lefebvre, D., Jasse, B., & Monnerie, L. (1981). Fourier transform infra-red study of uniaxially oriented poly(2,6-dimethyl 1,4-phenylene oxide)-atactic polystyrene blends. *Polymer*, *22*(12), 1616–1620. https://doi.org/10.1016/0032-3861(81)90374-8

Lefebvre, D., Jasse, B., & Monnerie, L. (1983). Orientation and relaxation in uniaxially stretched atactic polystyrene. *Polymer*, *24*(10), 1240–1244.

Lefebvre, D., Jasse, B., & Monnerie, L. (1984). Orientation and relaxation in uniaxially-stretched poly (2, 6-dimethyl 1, 4-phenylene oxide)-atactic polystyrene blends. *Polymer*, *25*(3), 318–322.

Li, J. C. M. (1984). Behavior and properties of shear bands. *Polymer Engineering & Science*, *24*(10), 750–760. https://doi.org/10.1002/pen.760241005

Li, J. C. M., & Wu, J. B. C. (1976). Pressure and normal stress effects in shear yielding. *Journal of Materials Science*, *11*(3), 445–457. https://doi.org/10.1007/BF00540925

Li, Z., Ye, L., Zhao, X., Coates, P., Caton-Rose, F., & Martyn, M. (2017). Structure and biocompatibility of highly oriented poly(lactic acid) film produced by biaxial solid hot stretching. *Journal of Industrial and Engineering Chemistry*, *52*, 338–348. https://doi.org/10.1016/j.jiec.2017.04.008

Lindner, W. L. (1973). Characterization of the crystalline, intermediate and amorphous phase in poly (ethylene terephthalate) fibres by X-ray diffraction. *Polymer*, *14*(1), 9–15.

Lode, U., Pomper, T., Karl, A., von Krosigk, G., Cunis, S., Wilke, W., & Gehrke, R. (1998). Development of crazes in polycarbonate, investigated by ultra small angle X-ray scattering of synchrotron radiation. *Macromolecular Rapid Communications*, *19*(1), 35–39.

Lunn, A. C., & Yannas, I. V. (1972). Chain-Backbone Motion in Glassy Polycarbonate Studied By Polarized Infrared Spectroscopy. *J Polym Sci Part A-2 Polym Phys*, *10*(11), 2189–2208. https://doi.org/10.1002/pol.1972.180101107

Lunt, J. (1998). Large-scale production, properties and commercial applications of poly lactic acid polymers. *Polymer Degradation and Stability*, *59*(1–3), 145–152. https://doi.org/10.1016/s0141-3910(97)00148-1

Mahendrasingam, A., Blundell, D. J., Martin, C., Fuller, W., MacKerron, D. H., Harvie, J. L., Oldman, R. J., & Riekel, C. (2000). Influence of temperature and chain orientation on the crystallization of poly(ethylene terephthalate) during fast drawing. *Polymer*, *41*(21), 7803–7814. https://doi.org/10.1016/S0032-3861(00)00129-4

Maini, L., Gigli, M., Gazzano, M., Lotti, N., Bikiaris, D. N., & Papageorgiou, G. Z. (2018). Structural investigation of poly(ethylene furanoate) polymorphs. *Polymers*, *10*(3). https://doi.org/10.3390/polym10030296

Mano, J. F. (2007). Structural evolution of the amorphous phase during crystallization of poly (l-lactic acid): A synchrotron wide-angle X-ray scattering study. *Journal of Non-Crystalline Solids*, *353*(26), 2567–2572.

Mao, Y., Kriegel, R. M., & Bucknall, D. G. (2016). The crystal structure of poly(ethylene furanoate). *Polymer*, *102*, 308–314. https://doi.org/10.1016/j.polymer.2016.08.052

Maruhashi, Y., & Asada, T. (1996). Structure and properties of biaxially stretched Poly (ethylene terephthalate) sheets. *Polymer Engineering & Science*, *36*(4), 483–494.

Matsumoto, K., Fellers, J. F., & White, J. L. (1981). Uni- and Biaxial Orientation Development and Mechanical Properties of Polystyrene Films. *Annual Technical Conference - Society of Plastics Engineers*, *26*, 105–109.

Mayo, F. R. (1943). Chain Transfer in the Polymerization of Styrene: The Reaction of Solvents with Free Radicals. *Journal of the American Chemical Society*, *65*(12), 2324–2329. https://doi.org/10.1021/ja01252a021

Meaurio, E., López-Rodríguez, N., & Sarasua, J. R. (2006). Infrared spectrum of poly(L-lactide): Application to crystallinity studies. *Macromolecules*, *39*(26), 9291–9301. https://doi.org/10.1021/ma061890r

Michler, G. H. (1989). Crazes in amorphous polymers I. Variety of the structure of crazes and classification of different types of crazes. *Colloid & Polymer Science*, *267*(5), 377–388. https://doi.org/10.1007/BF01410182

Michler, Goerg H. (2008). *Electron microscopy of polymers*. Springer Science & Business Media.

Mills, P. J., Kramer, E. J., & Brown, H. R. (1985). Real time small-angle X-ray scattering from polystyrene crazes during fatigue. *Journal of Materials Science*, *20*(12), 4413–4420. https://doi.org/10.1007/BF00559330

Mulligan, J., & Cakmak, M. (2005). Nonlinear mechanooptical behavior of uniaxially stretched poly(lactic acid): Dynamic phase behavior. *Macromolecules*, *38*(6), 2333–2344. https://doi.org/10.1021/ma048794f

Nielsen, L. E., & Buchdahl, R. (1950). Mechanical Properties of Oriented Polystyrene Film. *Journal of Applied Physics*, *21*(6), 488–493.

Nunes, R. W., Martin, J. R., & Johnson, J. F. (1982). Influence of molecular weight and molecular weight distribution on mechanical properties of polymers. *Polymer Engineering & Science*, *22*(4), 205–228. https://doi.org/10.1002/pen.760220402

O'connell, P. A., Duckett, R. A., & Ward, I. M. (2002). Brittle-ductile transitions in polyethylene. *Polymer Engineering & Science*, *42*(7), 1493–1508.

Oh, M. O., & Kim, S. H. (2014). Conformational development of polylactide films induced by uniaxial drawing. *Polymer International*, *63*(7), 1247–1253. https://doi.org/10.1002/pi.4630

Olmos, D., Martín, E. V., & González-Benito, J. (2014). New molecular-scale information on polystyrene dynamics in PS and PS-BaTiO3 composites from

FTIR spectroscopy. *Physical Chemistry Chemical Physics*, *16*(44), 24339–24349. https://doi.org/10.1039/c4cp03516j

Ou, X., & Cakmak, M. (2008). Influence of biaxial stretching mode on the crystalline texture in polylactic acid films. *Polymer*, *49*(24), 5344–5352. https://doi.org/10.1016/j.polymer.2008.09.053

Ou, X., & Cakmak, M. (2010). Comparative study on development of structural hierarchy in constrained annealed simultaneous and sequential biaxially stretched polylactic acid films. *Polymer*, *51*(3), 783–792. https://doi.org/10.1016/j.polymer.2009.11.058

Ouchiar, S., Stoclet, G., Cabaret, C., Addad, A., & Gloaguen, V. (2016). Effect of biaxial stretching on thermomechanical properties of polylactide based nanocomposites. *Polymer*, *99*, 358–367. https://doi.org/10.1016/j.polymer.2016.07.020

Pan, P., Liang, Z., Zhu, B., Dong, T., & Inoue, Y. (2008). Roles of physical aging on crystallization kinetics and induction period of poly(L-lactide). *Macromolecules*, *41*(21), 8011–8019. https://doi.org/10.1021/ma801436f

Pan, P., Zhu, B., Dong, T., Yazawa, K., Shimizu, T., Tansho, M., & Inoue, Y. (2008). Conformational and microstructural characteristics of poly(L-lactide) during glass transition and physical aging. *Journal of Chemical Physics*, *129*(18). https://doi.org/10.1063/1.3010368

Pan, P., Zhu, B., & Inoue, Y. (2007). Enthalpy Relaxation and Embrittlement of Poly(l -lactide) during Physical Aging . *Macromolecules*, *40*(26), 9664–9671. https://doi.org/10.1021/ma071737c

Papageorgiou, G. Z., Tsanaktsis, V., & Bikiaris, D. N. (2014). Synthesis of poly(ethylene furandicarboxylate) polyester using monomers derived from renewable resources: Thermal behavior comparison with PET and PEN. *Physical Chemistry Chemical Physics*, *16*(17), 7946–7958. https://doi.org/10.1039/c4cp00518j

Perego, G., Cella, G. D., & Bastioli, C. (1996). Effect of molecular weight and crystallinity on poly(lactic acid) mechanical properties. *Journal of Applied Polymer Science*, *59*(1), 37–43. https://doi.org/10.1002/(sici)1097-4628(19960103)59:1<37::aid-app6>3.3.co;2-7

Perena, J. M., Duckett, R. A., & Ward, I. M. (1980a). A study of the drawing behavior of poly(ethylene terephthalate). *Journal of Applied Polymer Science*, *25*(7), 1381–1390. https://doi.org/10.1002/app.1980.070250712

Perena, J. M., Duckett, R. A., & Ward, I. M. (1980b). A study of the drawing behavior of poly (ethylene terephthalate). *Journal of Applied Polymer Science*, *25*(7), 1381–1390.

Quinson, R., Perez, J., Rink, M., & Pavan, A. (1997). Yield criteria for amorphous glassy polymers. *Journal of Materials Science*, *32*(5), 1371–1379.

Rao, Y., Greener, J., Avila-Orta, C. A., Hsiao, B. S., & Blanton, T. N. (2008). The relationship between microstructure and toughness of biaxially oriented semicrystalline polyester films. *Polymer*, *49*(10), 2507–2514.

Razavi, M., & Wang, S.-Q. (2019). Why Is Crystalline Poly (lactic acid) Brittle at Room Temperature? *Macromolecules*, *52*(14), 5429–5441.

Rietsch, F., Duckett, R. A., & Ward, I. M. (1979). Tensile drawing behaviour of poly(ethylene terephthalate). *Polymer*, *20*(9), 1133–1142. https://doi.org/10.1016/0032-3861(79)90306-9

Rong, W., Fan, Z., Yu, Y., Bu, H., & Wang, M. (2005). Influence of entanglements on glass transition of atactic polystyrene. *Journal of Polymer Science, Part B: Polymer Physics*, *43*(16), 2243–2251. https://doi.org/10.1002/polb.20513

Saeidlou, S., Huneault, M. A., Li, H., & Park, C. B. (2012). Poly(lactic acid) crystallization. *Progress in Polymer Science*, *37*(12), 1657–1677. https://doi.org/10.1016/j.progpolymsci.2012.07.005

Sallem-Idrissi, N., Miri, V., Elkoun, S., Krawczak, P., Lacrampe, M. F., Lefebvre, J. M., & Seguela, R. (2009). Trichroic infrared analysis of the strain-induced structural changes in the PA6 layer of PA6/PE multilayer films under biaxial drawing. *Polymer*, *50*(24), 5812–5823. https://doi.org/10.1016/j.polymer.2009.09.052

Salomons, G. J., Singh, M. A., Bardouille, T., Foran, W. A., & Capel, M. S. (1999). Small-angle X-ray scattering analysis of craze-fibril structures. *Journal of Applied Crystallography*, *32*(1), 71–81. https://doi.org/10.1107/S0021889898010486

Sarasua, J. R., Arraiza, A. L., Balerdi, P., & Maiza, I. (2005a). Crystallinity and mechanical properties of optically pure polylactides and their blends. *Polymer Engineering & Science*, *45*(5), 745–753.

Sarasua, J. R., Arraiza, A. L., Balerdi, P., & Maiza, I. (2005b). Crystallinity and mechanical properties of optically pure polylactides and their blends. *Polymer Engineering and Science*, *45*(5), 745–753. https://doi.org/10.1002/pen.20331

Sauer, J. A., & Hara, M. (1990). Effect of molecular variables on crazing and fatigue of polymers. In *Crazing in Polymers Vol. 2* (pp. 69–118). Springer.

Scheirs, J., & Priddy, D. (2003). *Modern styrenic polymers: polystyrenes and styrenic copolymers* (Vol. 6). John Wiley & Sons.

Schmidt, P. G. (1963). Polyethylene terephthalate structural studies. *Journal of Polymer Science Part A: General Papers*, *1*(4), 1271–1292.

Senden, D. J. A., Krop, S., van Dommelen, J. A. W., & Govaert, L. E. (2012). Rate- and temperature-dependent strain hardening of polycarbonate. *Journal of Polymer Science Part B: Polymer Physics*, *50*(24), 1680–1693.

Shimomura, Y., Spruiell, J. E., & White, J. L. (1982). Orientation development in the tubular film extrusion of polypropylene. *Journal of Applied Polymer Science*, *27*(7), 2663–2674. https://doi.org/10.1002/app.1982.070270733

Sin, L. T., Rahmat, A. R., & Rahman, W. A. W. A. (2013). Overview of Poly(lactic Acid). In *Polylactic Acid*. https://doi.org/10.1016/b978-1-4377-4459-0.00001-9

Stoclet, G., Gobius Du Sart, G., Yeniad, B., De Vos, S., & Lefebvre, J. M. (2015). Isothermal crystallization and structural characterization of poly(ethylene-2,5-furanoate). *Polymer*, *72*, 165–176. https://doi.org/10.1016/j.polymer.2015.07.014

Stoclet, G., Lefebvre, J. M., Séguéla, R., & Vanmansart, C. (2014). In-situ SAXS study of the plastic deformation behavior of polylactide upon cold-drawing. *Polymer*, *55*(7), 1817–1828. https://doi.org/10.1016/j.polymer.2014.02.010

Stoclet, G., Lefebvre, J. M., Yeniad, B., Gobius du Sart, G., & de Vos, S. (2018). On the strain-induced structural evolution of Poly(ethylene-2,5-furanoate) upon uniaxial stretching: An in-situ SAXS-WAXS study. *Polymer*, *134*, 227–241. https://doi.org/10.1016/j.polymer.2017.11.071

Stoclet, G., Seguela, R., Lefebvre, J. M., Elkoun, S., & Vanmansart, C. (2010). Strain-induced molecular ordering in polylactide upon uniaxial stretching. *Macromolecules*, *43*(3), 1488–1498. https://doi.org/10.1021/ma9024366

Stoclet, G., Séguéla, R., Lefebvre, J. M., Li, S., & Vert, M. (2011). Thermal and strain-induced chain ordering in lactic acid stereocopolymers: Influence of the composition in stereomers. *Macromolecules*, *44*(12), 4961–4969. https://doi.org/10.1021/ma200469t

Stoclet, G., Seguela, R., Lefebvre, J. M., & Rochas, C. (2010). New insights on the strain-induced mesophase of poly(d, l-lactide): In situ WAXS and DSC study of the thermo-mechanical stability. *Macromolecules*, *43*(17), 7228–7237. https://doi.org/10.1021/ma101430c

Stoclet, Grégory. (2009). *Etude de la structuration à différents niveaux d'échelle et du comportement thermomécanique d'un polymère issu de ressources renouvelables:l'acide Poly(lactique)*. Université de Lille.

Tábi, T., Wacha, A. F., & Hajba, S. (2019). Effect of D-lactide content of annealed poly (lactic acid) on its thermal, mechanical, heat deflection temperature, and creep properties. *Journal of Applied Polymer Science*, *136*(8), 47103.

Tanabe, Y., & Kanetsuna, H. (1978). Structure of oriented polystyrene monofilaments and its relationship to brittle‐to‐ductile transition. *Journal of Applied Polymer Science*, *22*(6), 1619–1630. https://doi.org/10.1002/app.1978.070220613

Tassin, J. F., & Monnerie, L. (1988). Molecular weight effects in the relaxation of orientation of polystyrene chains as revealed by infrared dichroism. *Macromolecules*, *21*(6), 1846–1854.

Taylor, G. I. (1950). The instability of liquid surfaces when accelerated in a direction perpendicular to their planes. I. *Proceedings of the Royal Society of London. Series A. Mathematical and Physical Sciences*, *201*(1065), 192–196.

Terada, T., Sawatari, C., Chigono, T., & Matsuo, M. (1982). Oriented Crystallization of Poly(ethylene terephthalate) under Uniaxial Stretching. *Macromolecules*, *15*(4), 998–1004. https://doi.org/10.1021/ma00232a010

Thomas, L. S., & KJ, C. (1972). Gaging benefits of biaxial orientation. 1. General purpose of polystyrene. *SPE JOURNAL*, *28*(4), 61.

Tsai, C.-C., Wu, R.-J., Cheng, H.-Y., Li, S.-C., Siao, Y.-Y., Kong, D.-C., & Jang, G.-W. (2010). Crystallinity and dimensional stability of biaxial oriented poly (lactic acid) films. *Polymer Degradation and Stability*, *95*(8), 1292–1298.

Tsanaktsis, V., Papageorgiou, D. G., Exarhopoulos, S., Bikiaris, D. N., & Papageorgiou, G. Z. (2015). Crystallization and Polymorphism of Poly(ethylene furanoate). *Crystal Growth and Design*, *15*(11), 5505–5512. https://doi.org/10.1021/acs.cgd.5b01136

Uchiyama, A., & Yatabe, T. (2003). Molecular orientation of aromatic polycarbonates containing fluorene side chains by polarized infrared spectroscopy and birefringence analysis. *Journal of Polymer Science, Part B: Polymer Physics*, *41*(13), 1554–1562. https://doi.org/10.1002/polb.10505

Urayama, H., Kanamori, T., & Kimura, Y. (2001). Microstructure and thermomechanical properties of glassy polylactides with different optical purity of the lactate units. *Macromolecular Materials and Engineering*, *286*(11), 705–713. https://doi.org/10.1002/1439-2054(20011101)286:11<705::AID-MAME705>3.0.CO;2-Q

van Berkel, J. G., Guigo, N., Kolstad, J. J., & Sbirrazzuoli, N. (2018). Biaxial Orientation of Poly(ethylene 2,5-furandicarboxylate): An Explorative Study. *Macromolecular Materials and Engineering*, *303*(3), 1–9. https://doi.org/10.1002/mame.201700507

Van Melick, H. G. H., Govaert, L. E., & Meijer, H. E. H. (2003). On the origin of strain hardening in glassy polymers. *Polymer*, *44*(8), 2493–2502. https://doi.org/10.1016/S0032-3861(03)00112-5

Velazquez-Infante, J. C., Gamez-Perez, J., Franco-Urquiza, E. A., Santana, O. O., Carrasco, F., & Ll Maspoch, M. (2013). Effect of the unidirectional drawing on the thermal and mechanical properties of PLA films with different L -isomer content. *Journal of Applied Polymer Science*, *127*(4), 2661–2669. https://doi.org/10.1002/app.37546

Vorselaars, B., Lyulin, A. V., & Michels, M. A. J. (2009). Deforming glassy polystyrene: Influence of pressure, thermal history, and deformation mode on yielding and hardening. *Journal of Chemical Physics*, *130*(7), 1–16. https://doi.org/10.1063/1.3077859

Ward, I. M. (2012). *Structure and properties of oriented polymers*. Springer Science & Business Media.

Ward, I. M., & Sweeney, J. (2012). *Mechanical properties of solid polymers*. John Wiley & Sons.

Wellinghoff, S. T., & Baer, E. (1978). Microstructure and its relationship to deformation processes in amorphous polymer glasses. *Journal of Applied Polymer Science*, *22*(7), 2025–2045. https://doi.org/10.1002/app.1978.070220723

Wendlandt, M., Tervoort, T. A., & Suter, U. W. (2005). Non-linear, rate-dependent strain-hardening behavior of polymer glasses. *Polymer*, *46*(25), 11786–11797. https://doi.org/10.1016/j.polymer.2005.08.079

Wu, J. B. C., & Li, J. C. M. (1976). Slip processes in the deformation of polystyrene. *Journal of Materials Science*, *11*(3), 434–444. https://doi.org/10.1007/BF00540924

Wu, J. H., Yen, M. S., Wu, C. P., Li, C. H., & Kuo, M. C. (2013). Effect of Biaxial Stretching on Thermal Properties, Shrinkage and Mechanical Properties of Poly (Lactic Acid) Films. *Journal of Polymers and the Environment*, *21*(1), 303–311. https://doi.org/10.1007/s10924-012-0523-5

Wu, S. (1990). Chain structure, phase morphology, and toughness relationships in polymers and blends. *Polymer Engineering & Science*, *30*(13), 753–761. https://doi.org/10.1002/pen.760301302

Wu, W., & Turner, A. P. L. (1973). Shear bands in polycarbonate. *Journal of Polymer Science: Polymer Physics Edition*, *11*(11), 2199–2208.

Yuan, C., Wang, J., Chen, G., Zhang, J., & Yang, J. (2011). Orientation studies of uniaxial drawn syndiotactic polystyrene/carbon nanotube nanocomposite films. *Soft Matter*, *7*(8), 4039–4044. https://doi.org/10.1039/c0sm01475c

Zafeiropoulos, N. E., Davies, R. J., Schneider, K., Burghammer, M., Riekel, C., & Stamm, M. (2006). The Relationship between Craze Structure and Molecular

Weight in Polystyrene as Revealed by $μ$SAXS Experiments. *Macromolecular Rapid Communications*, *27*(19), 1689–1694.

Zhang, J., Duan, Y., Sato, H., Tsuji, H., Noda, I., Yan, S., & Ozaki, Y. (2005). Crystal modifications and thermal behavior of poly(L-lactic acid) revealed by infrared spectroscopy. *Macromolecules*, *38*(19), 8012–8021. https://doi.org/10.1021/ma051232r

Zhang, J., Tashiro, K., Tsuji, H., & Domb, A. J. (2008). Disorder-to-order phase transition and multiple melting behavior of poly(L-lactide) investigated by simultaneous measurements of WAXD and DSC. *Macromolecules*, *41*(4), 1352–1357. https://doi.org/10.1021/ma0706071

Zhang, Xiaomin, & Ajji, A. (2003). Biaxial orientation behavior of polystyrene: Orientation and properties. *Journal of Applied Polymer Science*, *89*(2), 487–496. https://doi.org/10.1002/app.12268

Zhang, Xiuqin, Schneider, K., Liu, G., Chen, J., Brüning, K., Wang, D., & Stamm, M. (2011). Structure variation of tensile-deformed amorphous poly(l-lactic acid): Effects of deformation rate and strain. *Polymer*, *52*(18), 4141–4149. https://doi.org/10.1016/j.polymer.2011.07.003

Zhou, C., Li, H., Zhang, W., Li, J., Huang, S., Meng, Y., DeClaville Christiansen, J., Yu, D., Wu, Z., & Jiang, S. (2016). Direct investigations on strain-induced cold crystallization behavior and structure evolutions in amorphous poly(lactic acid) with SAXS and WAXS measurements. *Polymer*, *90*, 111–121. https://doi.org/10.1016/j.polymer.2016.03.014